FACULTY OF ENGINEERING
AND ARCHITECTURE

Quantitative Assessment of Reinforced Concrete Buildings Subjected to Column Removal Scenarios Taking into Account Dynamic Response Behaviour

Luchuan Ding

Doctoral dissertation submitted to obtain the academic degree of
Doctor of Civil Engineering

Supervisors

Prof. Robby Caspeele, PhD - Prof. Ruben Van Coile, PhD

Department of Structural Engineering and Building Materials
Faculty of Engineering and Architecture, Ghent University

December 2021

GHENT
UNIVERSITY

FACULTY OF ENGINEERING AND ARCHITECTURE

Quantitative Assessment of Reinforced Concrete Buildings Subjected to Column Removal Scenarios Taking into Account Dynamic Response Behaviour

Luchuan Ding

Doctoral dissertation submitted to obtain the academic degree of
Doctor of Civil Engineering

Supervisors
Prof. Robby Caspeele, PhD - Prof. Ruben Van Coile, PhD

Department of Structural Engineering and Building Materials
Faculty of Engineering and Architecture, Ghent University

December 2021

GHENT UNIVERSITY

ISBN 978-94-6355-553-1
NUR 955, 956
Wettelijk depot: D/2021/10.500/101

Members of the Examination Board

Chair

Prof. Em. Luc Taerwe, PhD, Ghent University

Other members entitled to vote

Prof. Jan Belis, PhD, Ghent University
Wouter Botte, PhD, Ghent University
Prof. Jianbing Chen, PhD, Tongji University, China
Prof. Jean-François Demonceau, PhD, Université de Liège
Prof. Geert Lombaert, PhD, KU Leuven

Supervisors

Prof. Robby Caspeele, PhD, Ghent University
Prof. Ruben Van Coile, PhD, Ghent University

ACKNOWLEDGEMENTS

After almost four years of intensive work, my PhD dissertation is finally lying in front of me. There are so many people who contributed directly or indirectly to this research and my graduate studies. I would like to take this opportunity to sincerely thank them.

First and foremost I wish to sincerely thank my two supervisors Prof. Robby Caspeele and Prof. Ruben Van Coile who gave me the opportunity to execute my PhD study with them at the Department of Structural Engineering and Building Materials of Ghent University. I appreciated every discussion and helpful suggestion related to my research in the past years. I am very grateful for their support, trust and guidance throughout my doctoral research. I will truly miss the time in their teams. I would also like to express special acknowledgements to Prof. Jianbing Chen and Prof. Yongbo Peng who recommended me as a PhD researcher to study at UGent.

I would like to express my large gratitude to the members of the jury for their detailed review of my work, for their many valuable comments and suggestions, and for their time to take part in my defence. Their efforts enabled me to further improve this dissertation. Further, my research has been made possible thanks to the funding provided by the China Scholarship Council.

My research was conducted at the Department of Structural Engineering and Building Materials of Ghent University. The department provided me a great environment to meet nice colleagues and conduct my research work. I would like to express my thanks to all the other colleagues, for their kind help and different kinds of nice snacks in the kitchen which made my stay at the Magnel-Vandepitte Laboratory so unique.

Appreciations are also delivered to the many colleagues and friends who were very kind to me and did me a lot of favors in past years: Wouter Botte, Dider Droogné, Nicky Reybrouck, Tim Van Mullem, Cheng Xing, Lijie Wang, Thomas Thienpont, Eline Vereecken, Balša Jovanović, Mirko Pejatovic, Shamseldin Abdo, Antonella Cosentino, Stef Helderweirt, Karel Van Den Hende, Lien Saelens, Constantijn Martens, Dan Wang, Dengwu Jiao, Yaxin Tao, Weixi Zhang, Qiang Ren, Xiaodi Dai, Beibei Sun, Yubo Sun, Zhiyuan Liu, Xuejiao Zhu, Xiujiao Qiu, Kai Yang, Changyuan Chen, Tianlong Mei, Hongwei He, Jianyun Wang, Yu Liang, Xiliang Ning, Fanghui Han, Sumei Liu, Xiaoyun Wang, Heng Fang, Wenhao Xiao, Bo Zhang, Jingbin Yang, Yiyuan Zhang, Yilin Wang, Kenny Martens, Bart Van

Weyenberge, Dider Snoeck, Laurence De Meyst, Philip Van Den Heede, Mohammad Ali Yazdi, Robin De Schryver, Chizya Chibulu, Natalia Maria Alederete, Manu Mohan, Shahryar Nategh, Evelien Symoens, Decheng Feng, Jingran He, Hao Zhou, Yanqiong Ding, Zhiqiang Wan, Mengze Lv, Weifeng Tao, Jun Xu, Xueping Lu, Qingming Deng, Yunzhu Wang, Wenjing Tian, Weikang Guo, Rong Wang, and Huan Teng. Special thanks to Ranjit Kumar Chaudhary and Luiza Miranda with whom I shared the office, as well as Christal Malfait, Marijke Reunes, and Jens Mortier for the administrative help during and at the end of my PhD study.

Finally, sincere thanks go to my family for the immense support and encouragement. Without your understanding and warm care, I would never have been where I am today. Your encouragement has been my source of strength to finish this work.

Luchuan Ding
Ghent, November 2021

TABLE OF CONTENTS

LIST OF SYMBOLS

Roman symbols

A_c	Cross-sectional area of concrete (Chapters VII & VIII)
A_s	Cross-sectional area of reinforcement (Chapters V & VIII)
A_{sw}	Cross-sectional area of the transverse reinforcement (Chapters VII & VIII)
A_{sl}	Cross-sectional area of the tensile reinforcement (Chapters VII & VIII)
ΔA_s	Cross-sectional area reduction due to corrosion (Chapter VIII)
b	- Harding ration of reinforcement (Chapter IV) - Width (Chapters VII & VIII)
b_0	Initial section width (Chapter VIII)
b_w	Smallest width of the cross-section in the tensile area (Chapters VII & VIII)
c	Concrete cover (Chapters V & VII)
C_c	A factor related to shear strength (Chapters VII & VIII)
$C(.)$	Consequences (Chapters II & VI)
C_{DAP}	Consequences in case of failure of the DAP (Chapter VII)
C_{Dir}	Direct consequences (Chapters II & VII)
C_{IAP}	Consequences in case of failure of the IAP (Chapter VII)
C_{Ind}	Indirect consequences (Chapters II & VII)
C_{tot}	Total building costs (Chapter VII)
$C_{\mathrm{res\&cle}}$	Cost from rescue & clean-up (Chapter VII)
C_{stru}	Cost from structure (Chapter VII)
C_{inv}	Cost from inventory of building (Chapter VII)
C_{fat}	Cost from fatalities (Chapter VII)
C_{env}	Cost from environmental and cultural aspects (Chapter VII)
C_{eco}	Cost from impact to economy (Chapter VII)
d	Effective depth of cross section (Chapters VII & VIII)
d_c	Concrete cover (Chapter VIII)
D	Damage state (Chapters II, VI & VII)
D_{EBM}	Maximum displacement according to EBM (Chapter V)
D_{IDA}	Maximum displacement according to IDA (Chapter V)

DL	Dead load (Chapters VI & VII)
E	Exposure (Chapters II, VI & VII)
E_{ci}	Young's modulus of concrete (Chapters IV, V & VII)
E_h	Harding modulus of reinforcement (Chapter IV)
E_s	Young's modulus of reinforcement (Chapters IV, V & VII)
EX	Exposure (Chapter II)
F	Failure (Chapters II & VII)
f	- Load (Chapter II) - Frequency (Chapter IV)
f_c	Concrete compressive strength (Chapters VII & VIII)
f_{cm}	Mean concrete compressive strength (Chapters IV, V, VII & VIII)
$f_{c,cor}$	Confined core concrete compressive strength (Chapter VIII)
f_c^*	Reduced concrete compressive strength (Chapter VIII)
f_{ck}	Characteristic cylinder concrete compressive strength (Chapters IV, V, VII & VIII)
f_{ctm}	Mean concrete tensile strength (Chapters IV, V & VII)
f_{ctms}	Mean concrete tensile strength at quasi-static condition (Chapter IV)
f_{yt}	Yield stress of corroded transverse reinforcement (Chapter VIII)
f_y	Yield stress of reinforcement (Chapters IV & VIII)
f_{yw}	Yield stress of shear reinforcement (Chapters VII & VIII)
f_{ym}	Mean yield stress of reinforcement (Chapters IV, V, VII & VIII)
f_{yk}	Characteristic yield stress of reinforcement (Chapters IV, V, VII & VIII)
$f_{ym,d}$	Mean yield stress of reinforcement at an evaluated strain rate (Chapter IV)
$f_{ym,s}$	Mean yield stress of reinforcement at quasi-static condition (Chapter IV)
f_{uk}	Characteristic ultimate stress of reinforcement (Chapters IV, V & VII)
f_{um}	Mean tensile strength of reinforcement (Chapters IV, V & VII)
$f_{um,d}$	Mean tensile strength of reinforcement at an evaluated strain rate (Chapter IV)
$f_{um,s}$	Mean tensile strength of reinforcement at quasi-static condition (Chapter IV)

G_{fc}	Compressive fracture energy of concrete (Chapter IV)
G_{f1}	Fracture energy of concrete (Chapter IV)
h	Height (Chapter VII)
H	Height of first storey (Chapter VII)
H_i	Hazard i (Chapter II)
i_{corr}	Corrosion rate (Chapter VIII)
I_R	Robustness index (Chapter II)
I_{Rob}	Risk-based robustness index (Chapters II & VII)
$I_{Rob}\|D_l, E_k$	Conditional risk-based robustness index (Chapters II & VII)
k	- Stiffness of horizontal spring (Chapter V) - Slope (Chapter VII) - A factor related to shear strength (Chapters VII & VIII)
k_1	A factor related to shear strength (Chapters VII & VIII)
K	- Stiffness matrix (Chapter II) - Confinement ratio (Chapter VIII)
K_H	Horizontal spring constant (Chapter VII)
K_L	Model uncertainty factor for the load (Chapters V, VI & VII)
K_R	- Model uncertainty factor for the resistance (Chapters V, VI & VII) - Rotational spring constant (Chapter VII)
K_{EBM}	Model deviation for the EBM comparing to the IDA (Chapters V & VI)
L	- Span length (Chapters IV & VII) - Load effect (Chapters V, VI & VII)
$L_{damaged}$	Collapse load of the damaged structure (Chapter II)
L_{intact}	Overall collapse load of the intact structure (Chapter II)
LL	Live load (Chapters VI & VII)
M	- Mass matrix (Chapter II) - Moment (Chapters IV & VII)
M_{Eq}	Moment of the equivalent DAP model (Chapter VII)
M_{Ent}	Mean moment of the entire system (Chapter VII)
$M_{pl,Ci}$	Plastic moment of column i (Chapter VII)
M_u	Ultimate moment (Chapter VII)
M_y	Yield moment (Chapter VII)
MF	Membrane force (Chapter VII)
MF_{DAP}	Membrane force from DAP (Chapter VII)
MF_{Eq}	Membrane force of the equivalent DAP model (Chapter VII)
MF_{Ent}	Mean membrane force of the entire system (Chapter VII)
$MF_{pushdown}$	Membrane force from static analysis (Chapter VII)

$MF_{IDA-peak}$	Peak membrane force from dynamic analysis (Chapter VII)
$MF_{IDA-residual}$	Residual membrane force from dynamic analysis (Chapter VII)
n	- Number of samples (Chapters V & VI) - Number of columns (Chapter VII)
n_{bar}	Number of bars (Chapter VIII)
N	- Axial force (Chapter IV) - Number of floors (Chapter VII)
N_{peak}	Peak axial force (Chapter VII)
$N_{residual}$	Residual axial force (Chapter VII)
N_D	Number of damage scenarios (Chapter II)
N_E	Axial force (Chapters VII & VIII)
N_H	Number of hazard scenarios (Chapter II)
N_S	Number of adverse states (Chapter II)
P	Point load (Chapter IV)
$P[A]$	Probability of an event A (Chapters II, VI & VII)
$P[A\|B]$	Probability of an event A conditional on the occurrence of event B (Chapters II, VI & VII)
P_f	Failure probability (Chapter VII)
$P_{f,damaged}$	Failure probability of a damaged system (Chapters II & VI)
$P_{f,dam}$	Failure probability associated with any first member failure (Chapter II)
$P_{f,intact}$	Failure probability of an intact structural system (Chapters II & VI)
$P_{f,sys}$	Failure probability of an intact structural system (Chapter II)
$P_{f,IDA}$	Failure probability in dynamic situation (Chapter VII)
$P_{f,pushdown}$	Failure probability in static situation (Chapter VII)
q	Uniform load (Chapter VII)
Q_d	Load according to dynamic capacity curve (Chapter IV)
Q_s	Load according to static capacity curve (Chapter IV)
R	- Total risk (Chapter II) - Resistance (Chapters IV, V, VI, VII & VIII)
R^2	Coefficient of determination (Chapters V & VIII)
R_{Case}	Resistance for different cases (Chapter IV)
R_{EBM}	Resistance according to EBM (Chapters IV & V)
R_{IDA}	Resistance according to IDA (Chapters IV & V)
R_{Ii}	Resistance of the intact system (Chapter VI)
R_{Di}	Resistance of the damaged system (Chapter VI)
R_{direct}	Direct risks (Chapters II & VII)
$R_{direct,con}$	Conditional direct risks (Chapter II)

$R_{indirect}$	Indirect risks (Chapters II & VII)
$R_{indirect,con}$	Conditional indirect risks (Chapter II)
R_c	Characteristic value of the base shear capacity (Chapter II)
$R_{pushdown}$	- Resistance according to EBM pushdown analysis (Chapters IV & V) - Load in pushdown curve (Chapter VII) - Mean resistance from pushdown analyses (Chapter VII)
R_{IDA}	Mean resistance from IDA (Chapter VII)
$R_{IDA-peak}$	Load in IDA curve (Chapter VII)
R_{Eq}	Static resistance of the equivalent DAP model (Chapter VII)
R_{Ent}	Static resistance of the entire system (Chapter VII)
R_{IAP}	Resistance of the IAP (Chapter VII)
$R_{steel,yield}$	Mean resistance considering yield reinforcement strain (Chapter VII)
$R_{steel,ultimate}$	Mean resistance considering ultimate reinforcement strain (Chapter VII)
RI	Robustness index (Chapter II)
s	- Displacement (Chapter II) - Stirrup spacing (Chapters VII & VIII)
S	Adverse structural performance state (Chapter II)
S_c	Design load corresponding to collapse (Chapter II)
t	Time (Chapter VIII)
T	Time (Chapter IV)
T_n	The first natural vibration period (Chapter II)
u_d	Maximum dynamic deflection (Chapter IV)
u_s	Static deflection (Chapter IV)
V	Shear capacity of RC component (Chapters VII & VIII)
V_c	Shear capacity from concrete (Chapters VII & VIII)
V_s	Shear capacity corresponding to transverse reinforcement (Chapters VII & VIII)
V_{tot}	Total building volume (Chapter VII)
V_J	Volume of joint panel (Chapter IV)
W	Distance between two adjacent frames (Chapter VI)
x	Corrosion penetration depth (Chapter VIII)
w/c	Water cement ratio (Chapter VIII)
$Y_{2,j}$	Model uncertainty for concrete tensile strength (Chapters V & VII)
z	The inner lever arm (Chapters VII & VIII)
Z	Limit state function (Chapters V & VI)
Z_1	Limit state function (Chapter VII)

Z_2	Limit state function for IAP (Chapter VII)

Greek symbols

α	- Mass proportional coefficient (Chapter IV) - Corrosion level (Chapter VIII)
α_{cw}	A coefficient taking into account the state of the stress in the compression chord (Chapters VII & VIII)
α_{max}	Percentage of corrosion level with complete loss of ductility (Chapter VIII)
β	- Reliability index (Chapters II, VI & VII) - Stiffness proportional coefficient (Chapter IV)
β_R	Redundancy factor (Chapters II & VI)
β_{intact}	Reliability index of an intact structural system (Chapters II & VI)
$\beta_{damaged}$	Reliability index of a damaged structural system (Chapters II & VI)
$\beta_{f,sys}$	Reliability index of an intact structural system (Chapter II)
$\beta_{f,dam}$	Reliability index associated with any first member failure (Chapter II)
μ	Mean of variable (Chapter V)
ξ_i	Damping ratio (Chapter IV)
$\dot{\varepsilon}$	Strain rate of reinforcement (Chapter IV)
$\dot{\varepsilon}_0$	Quasi-static strain rate of reinforcement (Chapter IV)
$\dot{\varepsilon}_{ct}$	Tensile strain rate of concrete (Chapter IV)
$\dot{\varepsilon}_{ct0}$	Quasi-static strain rate of concrete (Chapter IV)
ε_{c1}	Compressive peak strain of concrete (Chapters IV, V, VII & VIII)
ε_{cr}	Average (smeared) tensile strain in cracked concrete (Chapter VIII)
$\varepsilon_{c,cor}$	Peak strain of confined core concrete (Chapter VIII)
ε_y	Yield strain of reinforcement (Chapter IV)
ε_u	Ultimate strain of reinforcement (Chapters IV, V & VII)
ε_{sy}	Yield strain of non-corroded reinforcement (Chapter VIII)
ε_{su}	Ultimate strain of non-corroded reinforcement (Chapter VIII)
$\varepsilon_{su,c}$	Ultimate strain of corroded reinforcement (Chapter VIII)
ε	Strain (Chapter IV)
ρ	Dimensionless performance index (Chapter II)
ρ_c	Density of concrete (Chapter V)

ρ_l	Reinforcement ratio in the tensile area (Chapters VII & VIII)
ρ_{st}	Volume corroded transverse reinforcement ratio (Chapter VIII)
σ	- Stress (Chapter IV) - Standard deviation of variable (Chapters IV, V & VIII)
σ_{cp}	Stress on the concrete cross-section (Chapters VII & VIII)
λ_i	The i^{th} eigenvalue (Chapter II)
λ_u^i	Normalized ultimate capacity (Chapter II)
ν_1	Strength reduction factor for concrete crack in shear (Chapters VII & VIII)
$\nu_{\min}$	A factor related to shear stregnth (Chapters VII & VIII)
γ	Shear strain (Chapter IV)
γ_{rs}	Ratio of volumetric expansion (Chapter VIII)
τ	Shear stress (Chapter IV)
ϕ	- Stored energy (Chapter II) - Diameter (Chapter VII)
$\Phi[.]$	The cumulative standard normal distribution function (Chapter VI)
ω	Natural frequency (Chapter IV)
ω_{cr}	Total crack width (Chapter VIII)
θ_i	Input variable *i* (Chapters V & VI)
θ	- Rotation angle (Chapters IV & VII) - The angle between the concrete compression strut and the beam axis perpendicular to the shear force (Chapters VII & VIII)
κ	Coefficient related to bar roughness and diameter (Chapter VIII)

Abbreviations

ABCB	Australian Building Codes Board
ALP	Alternate load path
ASCE	American Society of Civil Engineers
CA	Catenary action
CC	Consequence Class
CDP	Concrete damage plasticity
CECS	China Association of Engineering and Construction Standardization
CEN	European Committee for Standardization
COST	European Cooperation in Science and Technology
COV	Coefficient of variation
DAF	Dynamic amplification factor

DAP	Directly affected part
DIF	Dynamic increase factor
DL	Dead load
DoD	Department of Defense
DR	Damping ratio
EBM	Energy-based method
FE	Finite element
fib	International Federation for Structural Concrete
FSP	Fourier amplitude spectra
FORM	First-order reliability method
F6B6	6-storey and 6-bay RC frame
F3B12	3-storey and 12-bay RC frame
GSA	General Services Administration
IAP	Indirectly affected part
IBC	International building code
IDA	Incremental dynamic analysis
JCSS	Joint Committee on Structural Safety
KE	Kinetic energy
LDA	Linear dynamic analysis
LHS	Latin Hypercube sampling
LL	Live load
LN	Lognormal distribution
LPHC	Low-probability high-consequence
LSA	Linear static analysis
MCFT	Modified compression-field theory
MCS	Monte Carlo simulation
MF	Membrane force
NBCC	National Building Code of Canada
NCC	National Construction Code
NDA	Nonlinear dynamic analysis
NRCC	National Research Council of Canada
NTHA	Nonlinear time history analysis
NSA	Nonlinear static analysis
OpenSees	Open System for Earthquake Engineering Simulation
PC	Precast concrete
PDF	Probabilistic density function
PE	Potential energy
RC	Reinforced concrete
RD	Rayleigh damping
RSR	Reserve strength ratio
SDOF	Single-degree-of-freedom
SEI	Structural Engineering Institute
SE	Strain energy

SORM	Second-order reliability method
SRF	Strength redundancy factor
St.D.	Standard deviation
SPD	Stiffness-proportional damping
TMA	Tensile membrane action
UFC	United Facilities Criteria
WR	Without strain rate effect
YP	Yield point

SAMENVATTING

Constructieve veiligheid is een belangrijk onderwerp in het vakgebied bouwkunde. Een van de aspecten om constructieve veiligheid te bereiken is de constructies zodanig te ontwerpen dat zij voldoende robuust zijn om het risico van voortschrijdende of disproportionele instorting als gevolg van lokale constructieve schade tot een minimum te beperken. Een voortschrijdende of disproportionele instorting is een gedeeltelijk of volledig falen van de constructie als gevolg van een gebeurtenis die plaatselijke schade aan de constructie heeft veroorzaakt en die niet kon worden opgevangen door de samenhang en ductiliteit van het constructiesysteem. De plaatselijke schade of het plaatselijke falen brengt een kettingreactie op gang die zich door het structurele systeem voortplant en tot een gedeeltelijke of volledige instorting leidt.

Het belang van constructieve robuustheid om weerstand te bieden aan voortschrijdende of disproportionele instorting werd algemeen erkend na de voortschrijdende instorting van het Ronan Point gebouw in Londen (1968). Nadien hebben instortingen zoals de instorting van het A.P. Murrah Federal Building in Oklahoma (1995) en de terroristische aanslagen op het World Trade Centre in New York (2001), de onderzoeksinteresse in dit verband nog verder aangewakkerd. Bovendien benadrukken recente instortingen zoals de instorting van de Morandi-brug in Genua (2018) en de gedeeltelijke instorting van het Champlain Towers South Condominium in Florida (2021), de hedendaagse relevantie van verder onderzoek naar de kwetsbaarheid van bouwkundge constructies met betrekking tot lokale schade. Deze gebeurtenissen benadrukken ook de dringende noodzaak om de ontwerpeisen van constructies te verbeteren, teneinde voortschrijdende of disproportionele instorting tegen te gaan en efficiëntere beoordelingsmethoden te ontwikkelen met betrekking tot de robuustheid van constructies.

Regels met betrekking tot robuustheid van constructies zijn opgenomen in internationale bouwkundige normen en richtlijnen, zoals Eurocodes (EN 1991-1-7 en EN 1992-1-1) en UFC 4-023-03. Er is echter geen algemene consensus over criteria met betrekking tot de kwantificering van robuustheid. Verder onderzoek op dit gebied is nog steeds vereist.

De voortschrijdende of disproportionele instorting van gewapende betonconstructies die worden onderworpen aan scenario's waarbij kolommen worden verwijderd, is bovendien een dynamisch fenomeen. De

oorzaakonafhankelijke methode van de alternatieve draagweg wordt veel gebruikt om numerieke analyses uit te voeren in het kader van voortschrijdende of disproportionele instorting. De beschikbare numerieke analysebenaderingen omvatten lineaire statische analyse, lineaire dynamische analyse, niet-lineaire statische analyse, niet-lineaire dynamische analyse, en de zogenaamde *energy-based method* (EBM). De lineaire analysebenaderingen kunnen geen rekening houden met de niet-lineaire eigenschappen en de verkregen resultaten kunnen dientengevolge te conservatief zijn. De niet-lineaire statische analyse wordt vaak gebruikt voor de analyse van voortschrijdende instortingen. Dynamische effecten kunnen echter niet in aanmerking worden genomen bij de niet-lineaire statische analyse en er is een dynamische versterkingsfactor nodig om rekening te houden met dynamische effecten, indien men van oordeel is dat deze een significante invloed hebben. Met de niet-lineaire dynamische analyse kunnen nauwkeurigere resultaten worden verkregen, maar de rekenintensiteit kan als gevolg hiervan zeer hoog worden. De EBM kan de maximale dynamische respons benaderend berekenen op basis van het principe van energiebehoud, waarbij dan geen niet-lineaire dynamische analyses en dynamische versterkingsfactoren vereist zijn. Wanneer de EBM wordt toegepast om de robuustheid van constructies te evalueren – waarbij rekening wordt gehouden met dynamische effecten – kan de berekeningsbehoefte aanzienlijk worden beperkt. De EBM is derhalve een veelbelovende benadering om een evaluatie van de maximale dynamische respons te bekomen. Aangezien de dynamische effecten (bijvoorbeeld reksnelheidseffecten, dempingseffecten en de snelheid van kolomverwijdering) in de EBM niet in aanmerking kunnen worden genomen, kunnen dergelijke effecten de prestatie van de EBM beïnvloeden en moeten ze worden onderzocht.

In het licht van het bovenstaande is een van de doelstellingen van dit proefschrift het evalueren van de prestaties van de EBM zowel op deterministische als op probabilistische wijze, met het oog op het verder toepassen van de EBM als een efficiënte benadering voor het bepalen van dynamische capaciteiten in het kader van de beoordeling van de robuustheid van constructies. Daartoe worden de resultaten van de EBM vergeleken met die van directe dynamische analyses. Wat de deterministische evaluatie betreft, wordt in de dynamische analyses rekening gehouden met de invloed van de dynamische effecten (d.w.z. reksnelheidseffecten, dempingseffecten en snelheden van kolomverwijdering). Bovendien wordt ook de aanname van een systeem met één vrijheidsgraad in de dynamische respons geëvalueerd, aangezien aan deze aanname in een scenario met hoekkolomverwijdering mogelijk niet wordt voldaan. Wat de probabilistische evaluatie betreft, wordt rekening gehouden met de onzekerheden in de materiaaleigenschappen en worden afwijkingen tussen resultaten bekomen met de EBM en de directe dynamische analyses gebruikt om een modelonzekerheid te kwantificeren. Deze modelonzekerheid houdt louter verband met het gebruik van EBM in plaats van het gebruik van directe dynamische analyses. De evaluatie van

de verschillende analyses wordt uitgevoerd op basis van een gewapende betonvloerplaat op reële schaal en een vlak gewapend betonraamwerk.

Voor de gewapende betonvloerplaat is de invloed van dynamische effecten (d.w.z. reksnelheidseffecten, dempingseffecten, en snelheid van kolomverwijdering) onderzocht. De reksnelheidseffecten met betrekking tot zowel de wapening als het beton blijken een beperkte invloed te hebben op de dynamische respons in scenario's waarbij de kolom plotseling wordt verwijderd. Dit kan worden toegeschreven aan het feit dat de optredende vervormingssnelheden van de eindige elementen over het algemeen klein zijn en dat alleen gelokaliseerde elementen grote vervormingssnelheden ervaren en dit slechts voor een korte duur. In een situatie met grote vervormingen blijkt de invloed van de reksnelheid van de wapening iets groter te zijn dan die van het beton, aangezien de weerstand in de trekfase sterk beïnvloed wordt door de capaciteit van het wapeningsstaal. In het algemeen, blijkt de invloed van de reksnelheidseffecten echter beperkt te zijn en levert de EBM ook in deze situatie een goede benadering.

In de elastische fase blijkt de invloed van dempingseffecten op de dynamische respons niet significant te zijn. In situaties met grote vervorming is de invloed van dempingseffecten groter, aangezien grote schade in de gewapende betonconstructie optreedt. Bij een hogere belasting en een grotere dempingsratio, wordt een grotere invloed op de dynamische respons waargenomen, aangezien de energiedissipatie door de demping tot een grotere capaciteit leidt, hetgeen niet in de EBM is rekening kan worden gebracht. Het is van belang op te merken dat de stijfheid van de plaat verschillend is bij verschillende beschadigde toestanden. Rayleigh-demping, die evenredig is met de massa en de initiële stijfheidsmatrices, wordt toegepast in de directe dynamische analyses. In dit geval worden echter ongewenste kunstmatige dempingskrachten waargenomen en deze krachten resulteren in een onrealistisch groot draagvermogen. Rayleigh-demping, die evenredig is met de massamatrix en de initiële stijfheidsmatrix, blijkt dus ongeschikt te zijn in situaties met grote vervorming. Aan de andere kant blijken de resultaten van de EBM enigszins conservatief te zijn als geen rekening wordt gehouden met dempingseffecten.

In het algemeen leidt een abrupte verwijdering (kortere verwijderingsduur) tot een grotere piekwaarde van de doorbuiging in de directe dynamische analyse. Dit heeft een invloed op de prestaties van de EBM. Indien echter de aanbeveling van het DoD wordt gevolgd (t.t.z. de verwijderingsduur dient minder dan een tiende van de eerste natuurlijke periode in de dynamische analyse te bedragen), blijken de situaties met een dergelijke korte verwijderingsduur door de EBM accuraat te worden voorspeld.

Voor het gewapend betonraamwerk worden de dempingseffecten en verschillende scenario’s van kolomverwijdering onderzocht. Rayleigh demping die evenredig is

met de massamatrix en de tangens stijfheidsmatrix wordt gebruikt in de dynamische analyses. Aangezien de tangens stijfheidsmatrix wordt gebruikt, wordt het bovengenoemde ongewenste kunstmatige dempingseffect vermeden, aangezien de stijfheidsmatrix wordt geüpdated in functie van het schadeniveau. Ook voor deze situatie vertoont de EBM een goed resultaat in vergelijking met de directe dynamische analyse die rekening houdt met dempingseffecten.

Verder gaat de EBM ervan uit dat een constructie die wordt onderworpen aan een kolomverwijdering, vervormt in een vervormingsmodus met één vrijheidsgraad. Een scenario waarbij hoekkolommen worden verwijderd, blijkt van invloed te zijn op de prestaties van de EBM, aangezien de dynamische respons niet wordt gekenmerkt door een vervormingsmodus met één vrijheidsgraad. Toch blijkt de invloed over het algemeen beperkt te zijn. Anderzijds lijkt de veronderstelling van een vervormingsmodus met één vrijheidsgraad te voldoen wanneer een gewapende betonconstructie wordt onderworpen aan een scenario waarbij interne kolommen worden verwijderd, waarvoor de EBM zeer goede prestaties levert.

Er wordt een benaderend resultaat verkregen met behulp van de EBM in de context van gewapende betonconstructies die worden onderworpen aan kolomverwijderingen. Aangezien het om een benaderende werkwijze gaat, is het van belang de prestaties van de EBM te kwantificeren, t.t.z. de modelonzekerheid te kwantificeren door vergelijking van de bekomen resultaten met de nauwkeurigere resultaten bekomen via de directe dynamische analyse. Deze kwantitatieve beoordeling van de modelonzekerheid van de EBM is bovendien van belang om in rekening te brengen wanneer de EBM wordt toegepast om de betrouwbaarheid of robuustheid van een gewapende betonconstructie na kolomverwijdering te berekenen.

Op basis van de ontwikkelde eindige elementenmodellen (FE) en probabilistische modellen en parameters voor de veranderlijken worden stochastische FE simulaties uitgevoerd om de capaciteiten voor zowel EBM als directe dynamische analyses te bepalen. Door de resultaten van de EBM te vergelijken met de resultaten van de directe dynamische analyses, worden distributies voor de modelonzekerheid voorgesteld. Een lognormale verdeling blijkt de modelonzekerheid goed weer te geven. De waarden van de modelonzekerheden in verband met de maximale belastingen blijken dicht bij de eenheid te liggen en de standaardafwijkingen zijn klein. Dit wijst er opnieuw op dat de EBM een goede nauwkeurigheid heeft voor het berekenen van de dynamische invloed. Anderzijds zijn de prestaties van de EBM met betrekking tot de berekening van de bijbehorende verplaatsingen iets minder, aangezien – hoewel de bias nog steeds klein is – de standaardafwijkingen veel groter zijn.

Het tweede doel van dit proefschrift betreft de evaluatie van de prestaties van constructieve robuustheidsindicatoren voor gewapende betonconstructies, rekening houdend met dynamische effecten, en de ontwikkeling van een efficiënte rekenmethodiek daarvoor. De voortschrijdende of disproportionele instorting ten gevolge van extreme gebeurtenissen is een gebeurtenis met een lage waarschijnlijkheid en grote gevolgen. Het is belangrijk om de structurele robuustheid van de gewapende betonconstructies op de juiste wijze te bepalen. De bovengenoemde EBM kan worden toegepast ter vervanging van de directe dynamische analyses, hetgeen een aanzienlijk rekenvoordeel oplevert. Bijgevolg wordt een op EBM gebaseerde redundantie- of robuustheidskwantificatie voorgesteld. Om de redundantie-index van gewapende betonraamwerken te berekenen, worden eerst de betrouwbaarheidsindices van zowel intacte als beschadigde constructies berekend met behulp van zogenaamde *Latin Hypercube* simulaties. Voor drie verschillende types van kolomverwijdering worden zowel statische als dynamische redundantie-indices berekend. Het blijkt dat de redundantie-indices bekomen met dynamische analyses significant lager zijn dan die bekomen met statische analyses. Wat de dynamische berekeningen betreft, worden zowel de EBM-methode als directe dynamische analyses gebruikt om de dynamische redundantie-indices te berekenen. In vergelijking met de resultaten die zijn verkregen met de meer rekenintensieve kwantificering (t.t.z. de directe dynamische analyses), blijkt de op EBM gebaseerde redundantie- of robuustheidskwantificatie een goed resultaat neer te zetten.

Een rekenkundig nog efficiëntere benadering wordt bekomen door voor de risico-gebaseerde robuustheidskwantificering een meerlagige berekeningsprocedure toe te passen, die goed blijkt te presteren in vergelijking met een meer volledige analyse van de betonnen raamwerken. In deze meerlagige berekeningsprocedure wordt een constructiesysteem verdeeld in een direct beïnvloed deel (DAP), t.t.z. de portieken direct boven de verwijderde kolom, en een indirect beïnvloed deel (IAP), t.t.z. het resterende deel van de constructie. De berekeningen op de verschillende delen worden onafhankelijk van elkaar uitgevoerd, t.t.z. er wordt een soort hybride model opgesteld dat bestaat uit een gedetailleerd FE-model voor het DAP en een vereenvoudigd model voor het IAP. Zodoende wordt de robuustheid gekwantificeerd op verschillende niveaus van structurele idealisering, met aanzienlijk minder rekenwerk, maar met voldoende nauwkeurigheid.

Het DAP met meerdere verdiepingen wordt vereenvoudigd tot een gelijkwaardig DAP-model met één verdieping, t.t.z. met slechts twee liggers en de bijbehorende balk-kolomverbindingen. Voor het gelijkwaardige DAP-model met één verdieping wordt een gedetailleerd FE-model gemaakt, waarin materiaal- en geometrische niet-lineariteiten in aanmerking worden genomen. Bovendien worden translatie- en rotatieveren gebruikt als randvoorwaarden om de zijdelingse randvoorwaarden van het DAP te modelleren. Ook wordt een benadering voorgesteld om de

veerconstanten te bepalen. In het meerdere verdiepingen tellende DAP wordt ter hoogte van elke verdieping een kracht versus verplaatsing (of moment-rotatie) kromme bepaald met betrekking tot de balkuiteinden door middel van een statische pushdown analyse. Vervolgens worden secansstijfheden m.b.t. de verschillende verdiepingen berekend en de gemiddelde waarden van de secansstijfheden worden toegewezen aan de veren. Vergeleken met de resultaten van het volledige constructiesysteem, wordt een goede overeenkomst gevonden en deze aanpak blijkt dus efficiënt te zijn. Het rekenkundig veel efficiëntere equivalente DAP-model voor één verdieping wordt verder gebruikt om stochastische dynamische analyses uit te voeren, en er worden redelijk nauwkeurige resultaten verkregen in vergelijking met de resultaten van stochastische dynamische analyses van het volledige constructiesysteem. Dit bevestigt opnieuw de goede prestaties van het equivalente DAP-model.

Bij lage tot gemiddelde doorbuigingen blijken dynamische effecten een aanzienlijke invloed te hebben op de capaciteit van het DAP. De dynamische curve blijkt altijd lager te zijn dan de statische curve. Het verschil tussen de statische en dynamische curves (t.t.z. de dynamische versterkingsfactor) neemt af met toenemende doorbuiging. Bovendien wordt geconstateerd dat dynamische effecten de krachten in de translatieveren (t.t.z. de membraankrachten) aanzienlijk versterken. Wat het IAP betreft, blijken dynamische effecten weinig invloed te hebben op de capaciteit van het IAP, aangezien dynamische versterkingsfactoren voor de axiale belastingen in de kolommen de eenheid benaderen. Over het algemeen blijken dynamische effecten een significante invloed te hebben op de faalkans en de constructieve robuustheid van de gewapende betonconstructies die aan een kolomverwijdering worden blootgesteld. In vergelijking met de resultaten van statische analyses zijn de robuustheidsindices (faalkansen) van dynamische analyses significant kleiner (hoger). Daarom is het van belang om dynamische effecten mee in rekening te brengen bij de beoordeling van gewapende betonconstructies onderhevig aan voortschrijdende instorting.

De derde en laatste doelstelling van het proefschrift is het onderzoeken van het (dynamisch) voortschrijdend instortingsgedrag van bestaande gewapende betonconstructies, aangezien wapeningscorrosie de prestaties van de constructie aanzienlijk kan verminderen. Wapeningsstaal wordt beschouwd te zijn onderworpen aan uniforme corrosie, t.t.z. de dwarsdoorsnede van alle staven wordt uniform verminderd. De uiterste rek van het wapeningsstaal wordt verminderd afhankelijk van het corrosieniveau, terwijl de vloeispanning en treksterkte niet verminderen. Vier verschillende empirische modellen worden gebruikt om de vermindering van de uiterste rek van de wapening ten gevolge van corrosie te modelleren. Eerst worden niet-lineaire statische analyses uitgevoerd, waarbij een gewapend betonraamwerk als numeriek voorbeeld wordt genomen. De draagkracht van de wapening blijkt af te nemen met toenemend corrosieniveau voor alle vier

de modellen. Er wordt vastgesteld dat verschillende modellen met betrekking tot de verminderde uiterste rek van de wapening resulteren in een verschillend gedrag. Bovendien wordt een zeer conservatief uiterste belastingsniveau waargenomen als de uiterste rek van de wapening afneemt tot de waarde bij de vloeispanning. Anderzijds wordt de invloed van degradatie van het beton onderzocht. De sterkte van het betondekking wordt verminderd in functie van de wapeningscorrosie, terwijl het effect van de insluiting van de centrale betonmassa wordt berekend in functie de gecorrodeerde dwarswapening. De aantasting van het beton blijkt een beperkte invloed te hebben op het draagvermogen van het gewapend betonraamwerk.

Zowel statische als dynamische analyses worden uitgevoerd met betrekking tot het gewapend betonraamwerk onderworpen aan verschillende kolomverwijderingsscenario's. Eerst wordt wapeningscorrosie in het DAP (de portieken direct boven de verwijderde kolom) en in het IAP (het resterende deel) onderzocht. Uit het onderzoek blijkt dat wapeningscorrosie in de liggers van het DAP in hoge mate de uiteindelijke draagcapaciteit bepaalt in geval van degradatie. Verder is de invloed de locatie van de wapeningscorrosie onderzocht. Het blijkt dat meer vloeren die onderhevig zijn aan wapeningscorrosie resulteren in een lagere draagkracht.

Wanneer berekend via dynamische analyses, blijkt de weerstand tegen voortschrijdende instorting van de bestaande constructies aanzienlijk lager te zijn dan de statische weerstand en de daling wordt sterker naarmate het corrosieniveau toeneemt. Dit onderstreept opnieuw het belang van het in aanmerking nemen van dynamische effecten, zelfs nog meer in geval van bestaande constructies onderhevig aan degradatie. Als alternatieve manier om de maximale dynamische respons te berekenen, blijkt de EBM ook voor deze situaties goed te presteren.

SUMMARY

Structural safety is an important topic in the structural engineering community. One of the aspects to achieve structural safety is to design the structures to be sufficiently robust in order to minimize the risk of progressive or disproportional collapse resulting from local structural damage. A progressive collapse or disproportional collapse is a catastrophic partial or total structural failure that results from an event that causes local structural damage that cannot be absorbed by the inherent continuity and ductility of the structural system. The local damage or failure initiates a chain reaction of failures that propagates through the structural system, leading to an extensive partial or total collapse.

The importance of structural robustness in order to resist progressive or disproportional collapse was widely recognized after the progressive collapse of the Ronan Point building in London (1968). Afterwards, more collapse events, such as the collapse of the A. P. Murrah Federal Building in Oklahoma (1995) and the terrorist attacks on the World Trade Centre in New York (2001), have further highlighted the research interest in this field. Moreover, recent collapse events such as the collapse of the Morandi bridge in Genoa (2018) and the partial collapse of the Champlain Towers South Condominium in Florida (2021), emphasize the contemporary relevance of continued investigation into the vulnerability of civil engineering structures to local damage. These events also stress the urgent need to improve design requirements of structures to resist progressive or disproportional collapse, and develop efficient assessment methods in relation to structural robustness.

Nowadays, the concept of structural robustness has been adopted in structural codes and guidelines around the world, such as Eurocodes (EN 1991-1-7 and EN 1992-1-1) and UFC 4-023-03. However, no uniform criteria with regard to the structural robustness quantification have been accepted. Further research in this field is still required.

The progressive collapse or disproportional collapse of RC building structures subjected to sudden column removal scenarios is moreover a dynamic phenomenon. The threat-independent alternate load path method is widely used to perform numerical analyses in the context of progressive or disproportional collapse. Available numerical analysis approaches include linear static analysis, linear dynamic analysis, nonlinear static analysis, nonlinear dynamic analysis, and

the energy-based method (EBM). The linear analysis approaches cannot take the nonlinear properties into account and the obtained results may be too conservative. The nonlinear static analysis approach is widely used for progressive collapse analysis. However, dynamic effects cannot be considered in the nonlinear static analysis approach and a dynamic amplification factor is required to consider dynamic effects, if these are deemed to have a significant influence. The nonlinear dynamic analysis enables to give more accurate response results, but the computational demand may be very high. The EBM is able to approximately calculate the maximum dynamic responses on the basis of the principle of energy conservation, in which no nonlinear dynamic analyses and dynamic amplification factors are required. When the EBM is adopted to evaluate the structural robustness in which dynamic effects are considered, the calculation demand can be significantly reduced. Hence, the EBM is a promising approach to obtain an approximate evaluation of the maximum dynamic responses. As the dynamic effects (e.g. strain rate effects, damping effects, and column removal durations) cannot be considered in the EBM, such effects may affect the performance of the EBM and should be investigated.

According to the background above, one of the objectives of this thesis is to evaluate the performance of the EBM both in a deterministic way and in a probabilistic way, envisaging that the EBM could be further adopted as an efficient approach to determine dynamic capacities in the context of structural robustness assessment. In order to do so, results of the EBM are compared with those of direct dynamic analyses. With regard to the deterministic evaluation, the influence of the dynamic effects (i.e. strain rate effects, damping effects, and column removal durations) are considered in the dynamic analyses. Moreover, the assumption of the single deformation mode in the dynamic response is also evaluated, as this assumption may not be satisfied in an exterior column removal scenario. In terms of the probabilistic evaluation, the uncertainties in the material properties are taken into account and deviations of the results between the EBM and the direct dynamic analyses are used to quantify a model uncertainty in relation to the use of EBM instead of the use of direct dynamic analyses. The evaluation of the different analyses is performed considering a real-scale one-way RC slab and a planar RC frame.

For the RC slab, the influence of dynamic effects (i.e. strain rate effects, damping effects, and column removal durations) is investigated. Strain rate effects with regard to both the reinforcement and the concrete are found to have a limited influence on the dynamic response in sudden support removal scenarios. This can be attributed to the fact that the occurring strain rates of most finite elements are in general small and only localized elements experience large strain rates and only for a short duration. In a large deformation situation, the influence of the reinforcement strain rate effect is observed to be slightly larger than that of the concrete, since the

resistance in the tensile membrane action stage is heavily influenced by the capacity of the reinforcing steel. Overall, the influence of the strain rate effects is however found to be limited and the EBM exhibits overall a good performance, also in this situation.

In the elastic stage, the influence of damping effects on the dynamic responses is found to be not significant. In the large deformation situation, the influence of damping effects are larger, as large damage in the RC structures occurs. A more significant influence on the dynamic response under a high load and large damping ratio is observed, since the energy dissipation by the damping leads to a larger capacity and this is not accounted for in the EBM. It is worth noting that the stiffness of the slab is different at different damage states. Rayleigh damping which is proportional to mass and initial stiffness matrices (the associated coefficients are not updated in the dynamic analyses) is adopted in the direct dynamic analyses. In this case, unwanted artificial damping forces are observed and these forces result in unrealistic large load-carrying capacity. Hence, Rayleigh damping which is proportional to mass matrix and initial stiffness matrix is found to be unsuitable in the large deformation situation. On the other hand, results resulting from EBM are found to be slightly conservative if no damping effects are considered.

In general a more abrupt removal (shorter removal duration) results in a larger peak displacement in the direct dynamic analysis. This has an influence on the performance of the EBM. However, if the recommendation by the DoD (i.e. the removal duration must be less than one tenth of the first natural period in the dynamic analysis) is followed, cases with such short support removal time prove to be accurately predicted by the EBM.

For the RC frame, damping effects and different column removal scenarios are investigated. Rayleigh damping which is proportional to mass matrix and tangent stiffness matrix (the associated coefficients are updated accordingly) is used in dynamic analyses. As the tangent stiffness matrix is adopted, the aforementioned unwanted artificial damping effect is avoided, as the stiffness matrix is updated according to its damage state. In this situation, a good performance is found for the EBM, in comparison with the direct dynamic analysis considering damping effects.

Further, the EBM assumes that a structure subjected to a column removal scenario deforms in a single deformation mode. An exterior column removal scenario is observed to affect the performance of the EBM, since its dynamic response is not represented by a single deformation mode. Nonetheless, the influence is overall found to be limited. On the other hand, the single deformation mode assumption seems to be adequate when a RC structure is subjected to an interior column removal scenario, for which the EBM has a very good performance.

An approximate result is obtained using the EBM in the context of RC building structures subjected to sudden column removal scenarios. Considering it is an approximate approach, it is therefore important to quantitatively assess the performance of the EBM, i.e. quantifying its model uncertainty through comparison to the more accurate direct dynamic analysis results. Moreover, the quantitative assessment of the model uncertainty associated to the EBM becomes important when the EBM is applied to quantify the reliability or robustness of a RC building structure following a sudden column removal scenario.

On the basis of the developed finite element (FE) models and selected input random variables, stochastic FE simulations are carried out to determine the capacities for both EBM and direct dynamic analyses. Comparing the results of EBM to the results of the direct dynamic analyses, model uncertainty distributions for the EBM are proposed. A lognormal distribution is found to represent the model uncertainty well. The values of the model uncertainties associated with the resistances are found to be close to unity and the standard deviations are small. This again indicates that the EBM has a good accuracy in calculating the dynamic resistances. On the other hand, a slightly worse performance is found for the EBM in relation to the computation of the corresponding displacements, as – although the bias is still small – the standard deviations are much larger.

The second objective of this thesis is to evaluate the performance of structural robustness indicators for RC building structures, taking into account dynamic effects, and to develop a computationally efficient quantification approach for that. The progressive or disproportional collapse resulted from extreme events is a low-probability high-consequence event. It is important to appropriately determine the structural robustness of the RC building structures. The aforementioned EBM can be adopted to replace direct dynamic analyses involved in the structural robustness analyses, providing a significant computational benefit. Consequently, an EBM-based redundancy or robustness quantification approach is proposed. In order to calculate the redundancy index of RC frames, reliability indices of both intact and damaged structures are first calculated using the Latin Hypercube sampling technique. For three different column removal cases, both static and dynamic redundancy indices are calculated. It is found that the redundancy indices from dynamic analyses are significantly lower than those from static analyses. Regarding the dynamic calculations, both the EBM method and direct dynamic analyses are adopted to calculate the dynamic redundancy indices. Comparing to the results obtained with the more computationally intensive quantification (i.e. the direct dynamic analyses), a good performance for the EBM-based redundancy or robustness quantification approach is found.

Further, a multilevel calculation scheme in combination with the risk-based robustness quantification approach for the structural robustness quantification,

establishes a computationally efficient quantification approach that proves to have a good performance compared to a more complete analysis of the concrete frames. In this multilevel calculation scheme, a structural system is divided into a directly affected part (DAP), i.e. the bays immediately above the removed column, and an indirectly affected part (IAP), i.e. the remaining part. The calculations on different parts are carried out independently, i.e. establishing a kind of hybrid model composed of a detailed FE model for the DAP and a simplified model for the IAP. As such the robustness quantification is carried out at different levels of structural idealization, with significantly less computational efforts, although providing sufficient accuracy.

The multi-storey DAP is simplified into a one-storey equivalent DAP model, i.e. only two beams and the associated beam-column joints. A detailed FE model is created for the one-storey equivalent DAP model, in which material and geometric nonlinearities are considered. Moreover, translational and rotational springs are used as boundary conditions to reflect restraint effects from the IAP. Also an approach to determine the spring constants is proposed. In the multi-story DAP, a force vs. displacement (or moment - rotation) curve is recorded at a beam end in each floor through a static pushdown analysis. Subsequently, secant slopes at different floors are calculated and the mean values of the secant slopes are assigned to the boundary springs. Comparing to the results from the entire structural systems in cases of two RC frames, a good agreement is found and this approach hence proved to be efficient. The much more computationally efficient one-storey equivalent DAP model is further adopted to carry out stochastic dynamic analyses, and reasonably accurate results are obtained comparing to results from stochastic dynamic analyses of the entire structural systems. This further confirms the good performance of the one-storey equivalent DAP model.

In low to medium displacement levels, dynamic effects are observed to have a significant influence on the capacity of the DAP. The dynamic capacity curve is observed to be always lower than static capacity curve. The difference between the static and dynamic capacity curves (i.e. dynamic amplification factor) decreases with increasing displacement. Moreover, dynamic effects are observed to significantly amplify the forces in the translational springs (i.e. membrane forces). With regard to the IAP, dynamic effects are found to have little influence on the capacity of the IAP, as dynamic amplification factors for the axial loads in the columns corresponding to the ultimate load-carrying capacity approach unity. Overall, dynamic effects are found to have a significant influence on the failure probability and the structural robustness of the RC structures subjected a sudden column loss. Comparing to the results from static analyses, the structural robustness indices (failure probabilities) from dynamic analyses are significantly smaller (higher). Therefore, it is of paramount importance to include dynamic

effects when assessing the performance of RC building structures subjected to progressive collapse.

The third and last objective of the thesis is to investigate the (dynamic) progressive collapse behaviour of existing RC building structures, as reinforcement corrosion can significantly reduce the performance of the structures. Reinforcing steel subjected to uniform corrosion is considered, i.e. cross-sectional area of all bars is reduced uniformly. Meanwhile, the ultimate tensile strain of the reinforcing steel is reduced depending on the corrosion level, while yield stress and tensile strength are not reduced. Four different empirical models are used to model the reduction of the reinforcement ultimate tensile strain due to corrosion. Nonlinear static analyses are first carried out, where a RC frame is adopted as a numerical example. The load-carrying capacity of the reinforcement is observed to decrease with increasing corrosion level for all the four models. It is found that different models in relation to the reduced reinforcement ultimate tensile strain result in different responses. Moreover, a very conservative load-carrying capacity is observed if the reinforcement ultimate strain decreases to yield strain. On the other hand, the influence of deterioration of concrete is investigated. The strength of the cover concrete is reduced depending on the influence of reinforcement corrosion level, while the confinement of the core concrete is calculated according to properties of corroded transverse reinforcement. Concrete deterioration is found to have limited influence on the load-carrying capacity of the RC frame.

Both static and dynamic analyses are performed with regard to the RC frame subjected to different column removal scenarios. First, reinforcement corrosion in the DAP (the bays immediately above the removed column) and in the IAP (the remaining part) is investigated. From the investigations, reinforcement corrosion in the beams of the DAP is found to heavily determine the ultimate capacity in case of deterioration. Further, the influence of reinforcement corrosion occurring at different floors is investigated. It is found that more floors subjected to reinforcement corrosion result in a lower load-carrying capacity.

The progressive collapse resistances obtained by dynamic analyses are significantly lower than the static resistances and the decrease is intensified with increasing corrosion levels, stressing the importance of the inclusion of dynamic effects even more in case the structure is subjected to deterioration. As an alternative way to calculate maximum dynamic responses, the EBM is found to also have a good performance in case of deterioration.

PART A

INTRODUCTION AND STATE OF THE ART

CHAPTER I

General introduction

I.1 Introduction

Progressive or disproportional collapse is a major threat to buildings. Once it occurs, very high consequences may be induced with huge casualties and property losses. During the past decades several structural failures brought the issue of progressive or disproportional collapse to the attention of the structural engineering community.

In 1968 an accidental gas explosion destroyed one load-bearing wall at a corner of the 18th floor of a precast concrete building at Ronan Point (UK), which resulted in the loss of one part of the structure as shown in Figure I.1 (Choi and Chang, 2009; Agarwal *et al.*, 2012). Following this collapse event, the engineering community became aware of the issue and regulations therefore were developed to tackle it. These regulations required to provide minimum levels of structural robustness to enable multi-storey buildings to redistribute and withstand gravity loads after the loss of one or more load-bearing members (Ellingwood, 2006; Adam *et al.*, 2018).

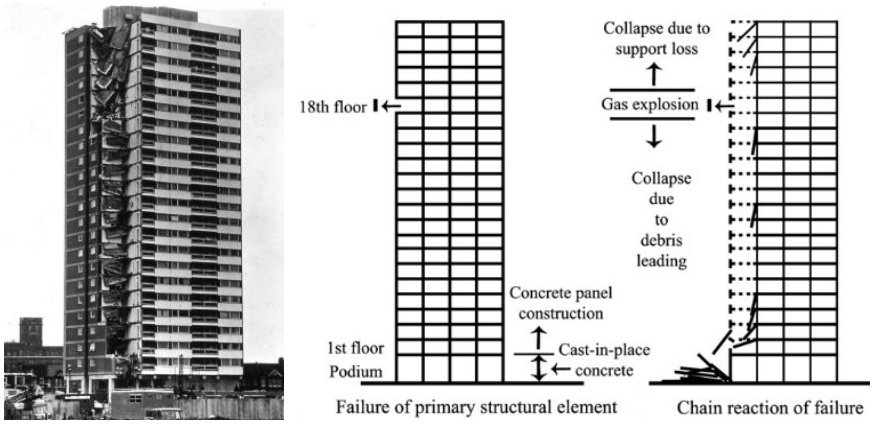

Figure I.1. (a) Progressive collapse at Ronan Point 1968 (Gouverneur, 2014); and (b) local damage and progressive collapse (Choi and Chang, 2009).

Other well-known failures such as the collapse of the A.P. Murrah Federal building due to bombing (Oklahoma City, 1995) and the collapse of the WTC towers due to the 9/11 terrorist attacks (New York, 2001; see Figure I.2a), renewed the interest in topics on progressive or disproportionate collapse and resulted in modifications and new developments of the design regulations (Ellingwood and Dusenberry, 2005; Byfield *et al.*, 2014; Qian *et al.*, 2016). Nowadays, strategies to mitigate the risk of disproportionate damage and progressive collapse in case of an unforeseen event can be found in most codes and guidelines worldwide (Adam *et al.*, 2018; Russell *et al.*, 2019b).

Although strategies against progressive or disproportional collapse are provided in most current design standards, an objective quantifying method to prove the effectiveness of current guidelines to improve structural robustness is lacking (Adam *et al.*, 2018). In literature, numerous robustness indices can be found to quantify the robustness of a structural system. However currently these robustness indices can be used for comparative purposes only, since no target values are available (Droogné, 2019).

(a) (b)

Figure I.2. (a) Progressive collapse of the WTC towers in 2001; and (b) truck impact on Wemmel bridge over the ring road around Brussels in 2007 (Botte, 2017).

The traditional design of reinforced concrete (RC) structures is usually based on small deformation theories. Basic principles and calculation methods adopted by current design codes and guidelines are commonly available for the traditional design of structural elements (Botte, 2017). However, in order to assess the ultimate load-bearing capacities against progressive collapse significant deformations should be taken into account, in which the potential secondary load resisting mechanisms for RC structures are commonly observed, such as Vierendeel action, compressive arch action and tensile catenary action (Qian *et al.*, 2016; Alshaikh *et al.*, 2020). For example, Figure I.2b shows the truck impact on an intermediate pier of a multi-span concrete bridge over the ring road around Brussels in 2007 (Botte, 2017). Although the bridge was not explicitly designed for truck impact and the consequent loss of (part of) the intermediate support, no collapse occurred due to the inherent robustness provided by the activation of membrane action in the deck under large deformations. With regard to numerical simulations of such events, material and geometrical nonlinearities need to be considered (Byfield and Paramasivam, 2007; Byfield *et al.*, 2014; Zheng *et al.*, 2020), as well as dynamic effects (Izzuddin *et al.*, 2008; DoD, 2016; Russell *et al.*, 2019a). Moreover, the aforementioned important favourable aspects such as the development of

membrane action are wrongfully neglected by current design codes and guidelines (Droogné, 2019).

Furthermore, practicing engineers are more and more confronted with the assessment of existing structures due to ageing of the building structures (Biondini and Frangopol, 2016; Botte, 2017). However, the assessment of existing structures is still a challenging problem. Many uncertainties related to existing structures need to be appropriately accounted for (Biondini and Frangopol, 2016). Consequently, the assessment of existing structures is quite different from that of new structures as the model uncertainties related to existing structures (e.g. corrosion rate of reinforcing bars) and the assessment of their robustness are significantly different from those considered for the design of new structures (Botte, 2017). Figure I.3 (right side) shows the partial collapse of the Champlain Towers South Condominium in Florida on 24 June 2021, in which 98 people had been confirmed dead (Lu *et al.*, 2021). It is a 12/13-storey RC building which was built in 1981. The Champlain Towers collapse illustrates the importance to comprehensively assess the performance of existing structures. Moreover, a structural progressive collapse may occur at any time during the design lifetime of a structure, as well as at any location. Thus, the progressive collapse behaviour of existing structures still needs further investigation.

Progressive collapse is an inherently dynamic phenomenon (Izzuddin *et al.*, 2008; DoD, 2016; Russell *et al.*, 2019a), such as shown in Figure I.3 in which a comparison is visualized between simulated and actual progressive collapse processes (Lu *et al.*, 2021). However, dynamic experimental tests may be extremely expensive, while dynamic numerical simulations are complex and time-consuming. Therefore, most of the current studies are carried out in a quasi-static manner. However, only a direct dynamic analysis allows to account for dynamic effects (e.g. inertial effects, damping and strain-rate effects), which is more accurate and comprehensive for a progressive collapse analysis. Hence, for high-risk buildings EN 1991-1-7 (CEN, 2006) suggests it may be required to use refined methods such as dynamic analyses and nonlinear models. It is of great value if some efficient tools with less calculation cost can be developed to assess the structural robustness, in which nonlinearities, dynamic effects, and uncertainties (e.g. uncertainties from material properties and loads) can be incorporated.

Despite the importance of structural robustness, the knowledge to investigate in depth the progressive collapse resistance of important structures under realistic conditions is still lacking. In order to proceed towards a general set of design rules and a standardization of the design or verification procedure for structural robustness, the aspects discussed previously should be investigated properly and corresponding calculation methods and procedures should be developed.

Accordingly, the aim of the present research is to investigate the structural robustness of both new and existing RC building structures with a particular emphasis on the consideration of dynamic effects. The outcomes will help enhance the understanding of structural robustness in a more comprehensive way.

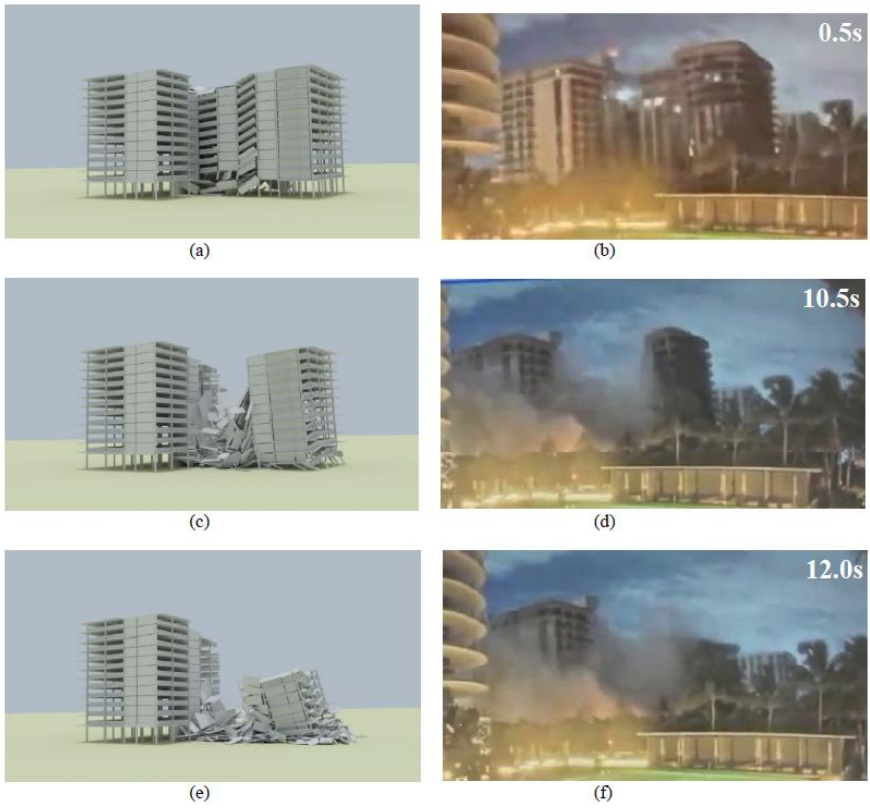

Figure I.3. Comparison between simulated and actual collapse processes of the Champlain Towers South Condominium in Florida in 2021: (a) simulated collapse process 1; (b) actual collapse process 1; (c) simulated collapse process 2; (d) actual collapse process 2; (e) simulated collapse process 3; and (f) actual collapse process 3 (Lu et al., 2021).

I.2 Research scope and methodology

I.2.1 Research scope

The aim of the research is the evaluation of progressive collapse behaviour of both new and existing RC building structures taking into account nonlinearities, uncertainties and in particular dynamic effects, using efficient numerical methods. Moreover, different numerical modelling methods are investigated as well.

I.2.2 Research methodology

For this purpose, numerical models are developed to investigate the development of threat-independent alternate load paths in both new and existing RC building structures. Based on the numerical models, on one hand different robustness indices in both static and dynamic situations are calculated to quantitatively assess the progressive collapse performance of RC frames, using efficient approaches for the dynamic situation. On the other hand, also the progressive collapse behaviour of deteriorated RC frames is investigated.

At first, a scientific survey is executed with respect to the current state-of-the-art on (1) structural robustness and robustness indices, (2) current structural strategies and design guidelines to increase the robustness in structural systems, and (3) experimental and numerical research regarding the development of alternate load paths in RC building structures.

Secondly, in this dissertation numerical simulation techniques are adopted to investigate the progressive collapse behaviour of RC structures. In this context two types of finite element (FE) modelling techniques are adopted, each having its field of application. On the one hand a detailed continuum model (or micro-based FE model) is used which uses plane stress elements and truss-elements to model the concrete and steel reinforcement respectively. On the other hand, detailed FE models (or macro-based FE models) are considered for large-scale building structural systems. After a validation study for these numerical models, the influence of various design parameters on the progressive collapse performance of RC elements and structures is investigated. Moreover, the verified FE models are adopted to execute both static and dynamic analyses. In addition, an energy-based method (EBM) is adopted to approximately calculate the maximum dynamic response without the need to perform the more computationally demanding direct dynamic analyses.

Next, different robustness indices are calculated for RC frames subjected to the accidental removal of a column, i.e. the reliability-based redundancy index and risk-based robustness index. The influence of uncertainties related to parameters, such as uncertainties in material properties and imposed loads, are taken into account. To include the effects of these uncertainties, the Latin Hypercube Sampling (LHS) technique or Monte Carlo simulation (MCS) technique is considered. The reliability or robustness indices of RC frames subjected to column removal scenarios are calculated in both static and dynamic situations.

Finally, progressive collapse performances of deteriorated RC building structures are investigated in both static and dynamic situations. Similarly, the threat-

independent alternate load path (ALP) method is adopted to model the column loss. Some empirical models are adopted to reflect the deteriorated mechanical properties of both concrete and reinforcement in RC structures.

I.3 Thesis layout

This thesis consists of nine chapters, divided in four main parts:

- **Part A** provides an overview of some general aspects related to structural robustness, current design methods for robustness, and the current state-of-the-art with regard to both experimental and numerical research on the progressive collapse performance of RC building structures;
- **Part B** focuses on the evaluation of the performance of the energy-based method (EBM) and quantification of the model uncertainty of the EBM, as the latter is critical in the context of probabilistic assessments of progressive collapse performances of RC building structures when the EBM is adopted as an alternative approach to approximate maximum dynamic responses;
- **Part C** is aimed at quantitatively calculating structural robustness indices using efficient approaches for dynamic situations. On the one hand, the EBM is further adopted to calculate the redundancy index for a RC frame. On the other hand, an efficient hybrid numerical simulation technique for risk-based robustness assessment is evaluated considering dynamic effects;
- **Part D** studies the progressive collapse performances of deteriorated RC frames in function of the degree of reinforcement corrosion.

Following the general introduction in the current **Chapter I**, an overview of the terminology related to structural robustness, a literature survey of current design methods for robustness and different approaches to quantify structural robustness is presented in **Chapter II**.

In **Chapter III** an overview is given of the major experimental and numerical studies regarding progressive collapse in RC building structures.

Chapter IV investigates the performance of the EBM in a deterministic way for both a RC slab and a RC frame. In order to verify the effectiveness of the EBM, both the EBM and direct dynamic analyses are carried out.

In **Chapter V** stochastic analyse are carried out and the model uncertainty occurring due to the use of the EBM relative to direct dynamic analyses is quantified for both a RC slab and a RC frame.

Chapter VI applies the EBM to assess the redundancy or robustness of the RC frame through calculating a redundancy index, where the model uncertainty information obtained in the previous chapter is considered.

In **Chapter VII** a more comprehensive risk-based robustness index is adopted through using an efficient multilevel calculation scheme to evaluate the progressive collapse behaviour of RC frames subjected to sudden column removal scenarios.

Chapter VIII extends the investigations on the progressive collapse behaviour of RC frames to structures subjected to degradation. The performance of deteriorated RC frame is investigated in function of the corrosion level of reinforcing bars, where both static and dynamic calculations are carried out.

Eventually, general conclusions and a summary of the research presented in this thesis are given in **Chapter IX**. Based on the results of this thesis some recommendations are given, together with suggestions for further research.

I.4 References

Adam JM, Parisi F, Sagaseta J, et al. (2018) Research and practice on progressive collapse and robustness of building structures in the 21st century. Engineering Structures 173:122-149.

Agarwal J, Haberland M, Holický M, et al. (2012) Robustness of structures: Lessons from failures. Structural Engineering International 22:105-111.

Alshaikh IMH, Abu Bakar BH, Alwesabi EAH, et al. (2020) Experimental investigation of the progressive collapse of reinforced concrete structures: An overview. Structures 25:881-900.

Biondini F, Frangopol DM (2016) Life-cycle performance of deteriorating structural systems under uncertainty: Review. Journal of Structural Engineering 142:F4016001.

Botte W (2017) Quantification of structural reliability and robustness of new and existing concrete structures considering membrane action. PhD diss. Ghent University.

Byfield M, Mudalige W, Morison C, et al. (2014) A review of progressive collapse research and regulations. Proceedings of the Institution of Civil Engineers-Structures and Buildings 167:447-456.

Byfield M, Paramasivam S (2007) Catenary action in steel-framed buildings. Proceedings of the Institution of Civil Engineers-Structures and Buildings 160:247-257.

CEN (2006) Eurocode 1: Actions on structures, part 1—7: General actions—Accidental actions. Comité Européen de Normalisation Brussels.

Choi J-h, Chang D-k (2009) Prevention of progressive collapse for building structures to member disappearance by accidental actions. Journal of Loss Prevention in the Process Industries 22:1016-1019.

DoD (2016) Design of buildings to resist progressive collapse. Unified Facilities Criteria (UFC) 4-023-03.
Droogné D (2019) Reliability-Based design for robustness: evaluation of progressive collapse in concrete structures taking into account membrane action. PhD diss. Ghent University.
Ellingwood BR (2006) Mitigating risk from abnormal loads and progressive collapse. Journal of Performance of Constructed Facilities 20:315-323.
Ellingwood BR, Dusenberry DO (2005) Building design for abnormal loads and progressive collapse. Computer-Aided Civil and Infrastructure Engineering 20:194-205.
Gouverneur D (2014) Experimental and numerical analysis of tensile membrane action in reinforced concrete slabs in the framework of structural robustness. PhD diss. Ghent University.
Izzuddin BA, Vlassis AG, Elghazouli AY, et al. (2008) Progressive collapse of multi-storey buildings due to sudden column loss - Part I: Simplified assessment framework. Engineering Structures 30:1308-1318.
Lu X, Guan H, Sun H, et al. (2021) A preliminary analysis and discussion of the condominium building collapse in surfside, Florida, US, June 24, 2021. Frontiers of Structural and Civil Engineering.
Qian K, Li B, Tian Y (2016) Recent progress in understanding of load resisting mechanisms for mitigating progressive collapse. Special Publication 309:1-18.
Russell JM, Owen JS, Hajirasouliha I (2019a) Dynamic column loss analysis of reinforced concrete flat slabs. Engineering Structures 198:109453.
Russell JM, Sagaseta J, Cormie D, et al. (2019b) Historical review of prescriptive design rules for robustness after the collapse of Ronan Point. Structures 20:365-373.
Zheng Z, Tian Y, Yang ZB, et al. (2020) Hybrid framework for simulating building collapse and ruin scenarios using finite element method and physics engine. Applied Sciences-Basel 10:4408.

CHAPTER II

Structural robustness and progressive collapse

II.1 Introduction

In conventional design situations, structural components are designed against specified limit states, in order to provide sufficient safety to a structure. However, it has been recognized that this approach may not be sufficient to prevent the collapse risk when a structure is subjected to some localised damage introduced by extreme events (Arup Group, 2011). As it is difficult to predict the probability of occurrence and the magnitude of the extreme events, it is neither practical nor possible to design a structure against them through the traditional methods for conventional loads (Adam *et al.*, 2018). The design concept of robustness incorporated in codes and guidelines is that the structure should be insensitive to local damage. Note that most often no action is taken against the undefined extreme events itself, since its occurrence most often cannot be eliminated. Contrary, the aim is to control its consequences through designing structures to be robust. However, after many years of research and applications on the assessment and mitigation of consequences from adverse abnormal loads on structures, a general consensus on terminology and procedures (e.g. structural robustness quantification) is still lacking. This section provides the major conceptual definitions and quantitative measures with regard to structural robustness, as well as relevant provisions in codes.

In this chapter first definitions of structural robustness and relevant concepts are provided in section II.2. Subsequently, section II.3 provides a brief overview of design approaches for robustness. Section II.4 summarizes different approaches which can be used to quantify structural robustness. Finally, a brief summary is provided in section II.5.

II.2 Concepts and definitions related to robustness

II.2.1 Progressive and disproportionate collapse

Although the two terms ‘progressive collapse’ and ‘disproportionate collapse’ usually are closely related with each other, they describe the phenomenon of collapse in different aspects. There is no unique definition of what constitutes a progressive or disproportionate collapse (Starossek and Haberland, 2010). A selection of relevant definitions from different sources is presented in Table II.1.

In summary, progressive collapse is a collapse that starts with a localised damage of one or more structural components, where the localized damage results in the successive damage to other components, i.e. a chain reaction. Progressive collapse is associated with the failure progression or mechanism, i.e. the manner in which it occurs.

On the other hand, disproportionate collapse is a collapse characterized between cause and consequence, where there is a significant disproportion in damage size between a minor localised damage (cause) and the subsequent final damage or collapse which may involve failure of a major part or even complete collapse of a structural system (consequence).

Table II.1. Definition of progressive collapse and disproportionate collapse according to different sources.

Progressive collapse	
Source	**Definition**
GSA (2016)	An extent of damage or collapse that is disproportionate to the magnitude of the initiating event.
Ellingwood (2006)	A progressive collapse initiates as a result of local structural damage and develops, in a chain reaction mechanism, into a failure that is disproportionate to the initiating local damage.
COST (2011)	Progressive collapse, where the initial failure of one or more components results in a series of subsequent failures of components not directly affected by the original action is a mode of failure that can give rise to disproportionate failure.
ASCE (2016) & DoD (2016)	Progressive collapse is defined as the spread of an initial local failure from element to element, eventually resulting in the collapse of an entire structure or a disproportionately large part of it.
Starossek and Haberland (2010)	A collapse that commences with the failure of one or a few structural components and then progresses over successively affected other components.
Disproportionate collapse	
Source	**Definition**
Starossek and Haberland (2010)	A collapse that is characterized by a pronounced disproportion between a relatively minor event and the ensuing collapse of a major part or the whole of a structure.
Fascetti *et al.* (2016)	Disproportionate collapse state is an unstable configuration which can degenerate in a loss of stability if a small perturbation occurs.

Generally, a progressive collapse can result in a disproportionate collapse if the successive failures spread over a major part or the whole system of a structure. However, a disproportionate collapse can be either immediate or progressive, e.g. immediate collapse of statically determinate systems (Adam *et al.*, 2018). Moreover, progressive collapse can be qualitatively described, whereas disproportionate collapse may need to be quantitatively described. In spite of different meanings, the terms disproportionate collapse and progressive collapse are often used interchangeably because disproportionate collapse often occurs in a

progressive manner and progressive collapse can be disproportionate. The term disproportionate collapse is more appropriate in the context of design and performance because a precise definition of disproportionate requires reference to design objectives. For instance, the definition by GSA (see Table II.1) focuses on the relative consequence or magnitude of the collapse rather than the manner in which it occurs, which is often referred to in the industry as 'disproportionate' rather than 'progressive' collapse (GSA, 2016). The term progressive collapse is more suitable when referring to the physical phenomenon and mechanism of collapse (Starossek and Haberland, 2010). A progressive collapse can involve different mechanisms of collapse that depend on the type and form of a structure and its orientation in space, as well as on the type and magnitude of the triggering abnormal event. There is also research in which the progressive collapse is regarded as a special case of disproportional collapse in which failure occurs in a progressive way (Kiakojouri *et al.*, 2020).

II.2.2 Robustness

The term 'robustness' is used in many fields of application, such as software engineering (Shahrokni and Feldt, 2013) and control theory (Bhattacharyya *et al.*, 2018). The definitions of robustness vary greatly in different fields (Faber *et al.*, 2006). Generally, robustness is related to the degree to which the system performance characteristics are affected by perturbations. Robustness is also a measure of the sensitivity of certain qualitative features in a system with regard to changes in system composition, system state, fundamental assumptions regarding the system and generally unexpected systemic disturbances (Faber *et al.*, 2006).

This thesis is related to the topic of structural robustness. There is no consistent definition of structural robustness up to date. The definition varies considerably and a selection of definitions is given in Table II.2. In general, a structure should be designed to be robust to resist progressive or disproportionate collapse, i.e. the ability of a structure to avoid consequences disproportional to the initiating damage events. Regarding these definitions, a measure of robustness should usually arise by comparing the system performance in the original state, where the structure is completely intact, to the performance in a perturbed state, in which a prescribed damage scenario is considered. Moreover, depending on the damage mechanism, ageing and progressive deterioration may also involve disproportionate effects (Biondini and Frangopol, 2016).

From the definitions presented in Table II.2, it can be concluded that robustness is a property relating causes, events and damage with consequences and structural functions. If the relation is proportionate, the structure is considered robust, if not, the structure is not robust, as illustrated in Figure II.1a (Cavaco, 2009). Given a structure built in a specified environment subjected to an event, some damage may arise depending on the type and magnitude of the event. Depending on the damage,

consequences may arise to both structure and environment leading to progressive loss in structural function and in some cases to full collapse. Some researchers define robustness as only a property of the structure, while others account for both the structure and the environment, as can be seen in Figure II.1b (Cavaco, 2009). Consequently, different robustness indices have been proposed in literature (Frangopol and Curley, 1987; Cavaco, 2009; Starossek and Haberland, 2009; Sørensen *et al.*, 2012; Bao *et al.*, 2017; Adam *et al.*, 2018; Praxedes and Yuan, 2021). More details in relation to the structural robustness indices can be found in section II.4.

Table II.2. Definition of structural robustness according to different sources.

Source	**Definition**
CEN (2006)	The ability of a structure to withstand events like fire, explosions, impact or the consequences of human error, without being damaged to an extent disproportionate to the original cause.
Biondini and Frangopol (2016)	Structural robustness can be viewed as the ability of the system to suffer an amount of damage not disproportionate with respect to the causes of the damage itself.
JCSS (2009)	The robustness of a system is defined as the ratio between the direct risks and the total risks (total risks is equal to the sum of direct and indirect risks), for a specified time frame and considering all relevant exposure events and all relevant damage states for the constituents of the system.
Starossek and Haberland (2010)	Robustness is defined as insensitivity of a structure to initial damage. A structure is robust if an initial damage does not lead to disproportionate collapse.
fib (2013)	Robustness is a specific aspect of structural safety that refers to the ability of a system subject to accidental or exceptional loadings (such as fire, explosions, impact or consequences of human errors) to sustain local damage to some structural components without experiencing a disproportionate degree of overall distress or collapse.

II.2.3 Redundancy

The term ‘redundancy’ is generally defined as the ability of a system to redistribute among its members the loading that can no longer be sustained by damaged members after the occurrence of a local failure (Starossek and Haberland, 2010; Biondini and Frangopol, 2016). The load redistribution capacity is a desirable structural feature to ensure suitable system performance under accidental actions, e.g. sufficient alternate load paths. Research indicates redundancy does not only

depends on the degree of static indeterminacy, but also on many other factors including material behaviour, loading condition, topology, continuity, ductility and damage scenario (Frangopol and Curley, 1987; Biondini *et al.*, 2008).

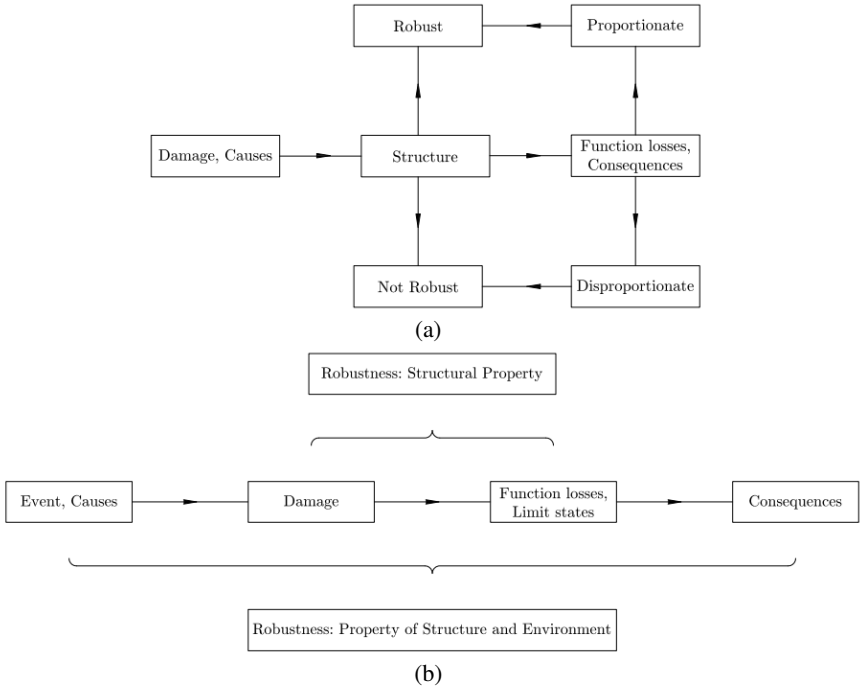

Figure II.1. Robustness: (a) defining robustness; and (b) robustness as a structural property vs. robustness as a property of both structure and environment (Cavaco, 2009).

The concept of structural redundancy can be extended over time to consider the time-evolution of the redistribution mechanism owing to deterioration processes, e.g. reinforcement corrosion (Biondini and Frangopol, 2015; Feng *et al.*, 2021). In such cases, redundancy is closely related to the durability of the structure.

Although redundancy is a key factor to provide robustness to a structure, the two terms represent different properties of a structure (Starossek and Haberland, 2010). The difference between redundancy and robustness lies on whether the index is associated with the amount of damage, i.e. the amount of damage is taken into account in the latter but not in the former (Feng *et al.*, 2021). Moreover, using them as synonyms obscures the fact that redundancy is not the only means to achieve robustness (Starossek and Haberland, 2010). Adam *et al.* (2018) indicates that a robust structure does not imply an over-designed structure but a structure which is

able to activate latent resisting mechanisms to mitigate the consequence of a damage event.

II.2.4 Vulnerability

The term 'vulnerability' is regarded as an antonym to robustness by several authors (Starossek and Haberland, 2010). However, in JCSS (2009) the vulnerability accounts for the direct consequences of an extreme or abnormal event affecting a structure. The direct consequences are related to the component behaviour following an event. Hence, vulnerability refers to the initial damage susceptibility of a structure when subjected to abnormal events. It is related to local conditions, which depend on the level of protection and the strength and resistance of the structural components. However, robustness accounts for both direct and indirect consequences, where indirect consequences are related to the system behaviour, that is, the possible disproportionate collapse of the structure or its impaired functionality. More specifically, vulnerability is associated with the local conditions, while robustness refers to global system behaviour, see Figure II.2.

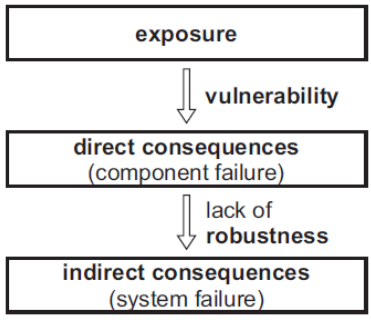

Figure II.2. Difference between vulnerability and robustness (JCSS, 2009).

II.3 Current design methods for robustness

II.3.1 Structural robustness in international codes

The timeline of some well-known progressive collapse events and the development of design codes and guidelines is shown in Figure II.3 (Kiakojouri *et al.*, 2020). The lack of robustness of structures was recognized after the 1968 Ronan Point collapse in UK. The 1995 collapse of the Murrah Federal Building in Oklahoma and the 2001 collapse of the World Trade Centre towers (9/11 attacks) resulted in a new interest in progressive collapse and robust design. Subsequently, a number of codes and guidelines implemented provisions to address disproportionate collapse (GSA, 2003; DoD, 2005; DoD, 2009). Nowadays, this concept has been adopted in the structural codes around the world, such as in Europe (CEN, 2002;

CEN, 2006), UK (HMG, 2013), USA (ICC, 2009; ASCE, 2016; DoD, 2016; GSA, 2016), Canada (NRCC, 1995), Australia (ABCB, 2016) and China (CECS, 2014).

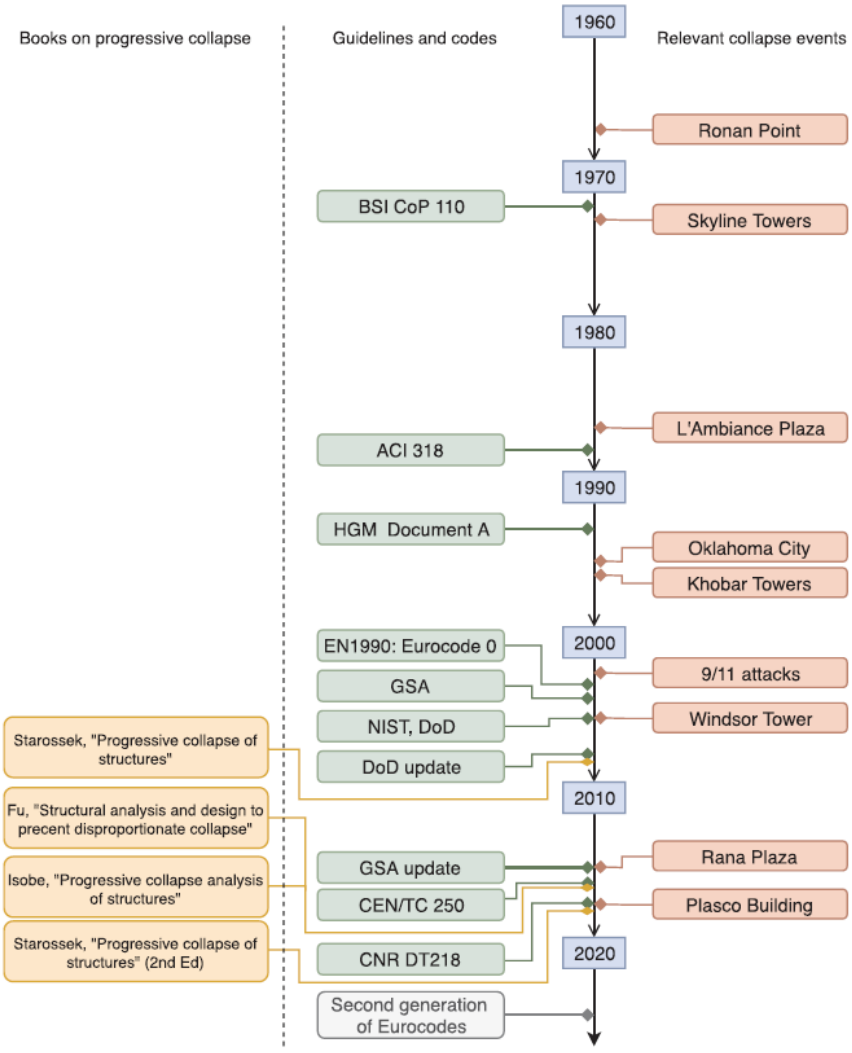

Figure II.3. Timeline of the main progressive collapse events and the developments of design provisions (Kiakojouri et al., 2020).

Further background associated with the development of current design codes and guidelines for structural robustness can be found in (Moore, 2003; Gulvanessian

and Vrouwenvelder, 2006; Arup Group, 2011; Stevens *et al.*, 2011; Byfield *et al.*, 2014; Droogné, 2019).

II.3.2 Design methods against progressive collapse

It is clear that there are no universal rules to design against progressive collapse in the aforementioned various codes and guidelines (Adam *et al.*, 2018). In general, two types of approaches can be adopted: an indirect design approach or a direct design approach (Agarwal *et al.*, 2012; Byfield *et al.*, 2014; DoD, 2016; Qian *et al.*, 2016; Alshaikh *et al.*, 2020). The indirect design approach implicitly considers resistance to progressive collapse by providing minimum levels of continuity, redundancy, ductility and energy dissipation capacity, e.g. the tying force approach. Direct design comprises two methods: the alternate load path (ALP) method or the specific (or enhanced) local resistance method (or key element design method). As the specific local resistance method requires each member to be designed to resist a specific threat, the assumed threat affects the design. Local failure is considered in the tying force and ALP approaches, while the key element design method prevents local failure of key elements and is adopted as a method of last resort when ALP approaches are unable to demonstrate sufficient load redistribution ability of the structure (Adam *et al.*, 2018; Russell *et al.*, 2019b).

The alternate load path method is the major direct design method and it can be implemented in both threat-independent and threat-dependent ways (Qian *et al.*, 2016). Moreover, the ALP method is widely investigated in both experimental tests (Yi *et al.*, 2008; Russell *et al.*, 2015; Xiao *et al.*, 2015; Shan *et al.*, 2016) and numerical simulations (Xu and Ellingwood, 2011; Brunesi and Parisi, 2017; Parisi *et al.*, 2019; Russell *et al.*, 2019a) in the context of progressive collapse. Also in this dissertation, the alternate load path method is considered in relation to the investigation of progressive collapse behaviour of RC building structures subjected to sudden column removal scenarios.

According to the review on the design codes by Adam *et al.* (2018), there are mainly four recognised approaches across the different international codes:

1) Tying force methods;
2) Alternate load path (ALP) methods;
3) Key element design methods; and
4) Risk-based methods.

Table II.3 summarises the general codes currently available with respect to these four widely recognised groups of design approaches (Adam *et al.*, 2018). The risk-based methods compare the type of extreme event, its likelihood and severity of the consequences against the cost of protection and assumed potential losses (Adam *et al.*, 2018). Moreover, the risk-based method is developed more recently compared to the others.

Table II.3. Summary of design methods considered by international codes (Adam et al., 2018).

Area	Code	1. Tying	2. ALP	3. Key	4. Risk
UK	Building Reg. 2010 (HMG, 2013)	√	√	√	~
Europe	EN 1991-1-7 (CEN, 2006)	√	√	√	√
USA (Civil)	ASCE/SEI 7-16 (ASCE, 2016)	√	√	√	~
USA (Civil)	IBC 2009 (ICC, 2009)	√	×	×	×
USA (Government)	UFC 4-023-03 (DoD, 2016)	√	√	√	~
USA (Federal)	GSA 2016 (GSA, 2016)	×	√	×	~
China	CECS 392:2014 (CECS, 2014)	√	√	√	×
Canada	NBCC 1995 (NRCC, 1995)	√	√	√	~
Australia	NCC 2016 (ABCB, 2016)	×	√	√	√

√: method considered; ×: method not considered; ~: method implicitly considered.

II.3.2.1 Tying force method

Tying force approaches are often recommended for structures with low risk of progressive collapse, which are aimed at providing minimum levels of tying, continuity and ductility (Adam *et al.*, 2018). In this approach, the structural elements are assumed to be mechanically tied together, thereby enhancing the continuity, ductility, and development of alternate load paths. Tie forces are typically provided by the existing structural elements and connections, which are designed using conventional procedures to carry the standard loads imposed upon the structure (Li *et al.*, 2011). However, the obtained performance is not normally checked explicitly. The tying force method is adopted in many codes (Table II.3), e.g. EN 1991-1-7 (CEN, 2006) and UFC 4-023-03 (DoD, 2016). Both horizontal and vertical ties by prescribing a minimum tying force requirement can be designed to enhance the progressive collapse performance of the structures. However, research shows that the rotations required in the connections to form a pure tensile membrane that arrests progressive collapse may be unachievable in some cases (Moore, 2003; Byfield and Paramasivam, 2007; Li *et al.*, 2011). Although it is difficult to quantify the enhancement in the minimum levels of robustness provided by the different tying force approaches, it is generally accepted that tying has a

beneficial effect on robustness (Byfield and Paramasivam, 2007; Arup Group, 2011; Li *et al.*, 2011; Adam *et al.*, 2018).

II.3.2.2 Alternate load path method

The ALP method based on the notional member removal concept is widely accepted by all codes (Table II.3), except for IBC 2009. Moreover, as mentioned before this method is widely considered as a subject in experimental investigations and in numerical simulations in the context of progressive collapse. The ALP method aims at assessing the ability of the structures to redistribute the additional or unbalanced loads from the area subjected to local damage. In other words, the ability of the structures to develop alternate load paths if they are subjected to accidental loads.

In practice several assumptions and simplifications may be adopted in the ALP method. This can result into a large number of potential assumption combinations, which can lead to different levels of robustness with respect to the design/assessment solution (Adam *et al.*, 2018). For instance, these considerations include whether or not to take into account the source of local damage, refinements in the dynamic assessment (direct consideration from nonlinear dynamic analysis or indirectly considerations using static methods with dynamic amplification factors), material nonlinearities and large deformations of members (Arup Group, 2011). Moreover, the suitable level of refinement in the ALP method would depend on the building classification given by risk considerations or other performance-based criteria (Adam *et al.*, 2018). For examples, for structures with the consequence class 3 in EN 1991-1-7 (CEN, 2006), it is indicated that a risk analysis may be required to be carried out, possibly in combination with refined methods such as dynamic analysis, nonlinear models and interaction between the load and the structure.

Considering the difficulty of the identification of probability of the accidental loads or the local damage (e.g. a column or wall removal), the ALP method is more often implemented in a threat-independent manner, e.g. (CEN, 2006; Lu *et al.*, 2013; Brunesi and Nascimbene, 2014; DoD, 2016; GSA, 2016; Bao *et al.*, 2017; Chen *et al.*, 2018b). It aims to provide a minimum level of robustness covering different unspecified extreme events. On the other hand, threat-dependent approaches may be needed when the likelihood, consequences of failure, and acceptable levels of risk need to be considered.

II.3.2.3 Key element design method

The key element design approach (or enhanced/specific local resistance approach) is adopted as a method of last resort when ALP approaches are unable to demonstrate sufficient load redistribution ability of the structure (Adam *et al.*, 2018). If failure of a structural member activates a progressive collapse, the

member is identified as a key element and designed to resist specified accidental loads. It is clear that in this approach the emphasis is on avoiding local failure of each key element (i.e. a direct design method), which is strongly threat-dependent. However, in some codes a specified load value intended to cover different unspecified extreme events is adopted in the key element design (Adam *et al.*, 2018; Russell *et al.*, 2019b). For example, the Building Regulations (HMG, 2013) use a notional static load pressure of 34.0 kPa, where this value is an estimation of the explosion of pressure on the flank wall at Ronan Point and is debated (Russell *et al.*, 2019b).

II.3.2.4 Risk-based method

Risk is considered implicitly in design by most codes, see Table II.3, by means of the building classification and design methods recommended for each class (Adam *et al.*, 2018). A major drawback in many codes is that risk is not considered in a very transparent nor systematic way (Adam *et al.*, 2018), e.g. only on the basis of the occupancy of the building or the likelihood of the event or the consequences of the failure.

EN 1991-1-7 (CEN, 2006) includes explicit guidelines for implementing a systematic risk-based assessment for high-risk structures (Annex B), with background and the theoretical method in (Vrouwenvelder *et al.*, 2005; COST, 2011; IStructE, 2013). In EN 1991-1-7 (CEN, 2006), measures to mitigate the risk of the accidental action include (a) reducing the probability of the hazard occurrence, (b) reducing the probability of significant damage given the hazard, and (c) providing minimum robustness by designing the structure for the hazard. In addition, tolerance levels for risk of collapse are provided by the Building Regulations (HMG, 2013) and EN 1991-1-7 (CEN, 2006), based on relative area of collapse. The limitation of the area at risk of collapse in the Building Regulations (HMG, 2013) is 70 m^2 or 15% of the floor area, while it increases to 100 m^2 or 15% of the floor area in EN 1991-1-7 (CEN, 2006).

Probabilistic approaches to consider the uncertainty in relevant variables to improve the accuracy in the structural robustness assessment have been suggested in among others (Alexander, 2004; Le and Xue, 2014; Li *et al.*, 2016; Adam *et al.*, 2018; Feng *et al.*, 2020; Feng *et al.*, 2021).

II.3.3 Eurocodes

According to the review above, it is clear that there are no universally accepted rules to design against disproportionate collapse. Since the design of structures in Europe is based on the Eurocodes, an overview of the rules in the Eurocodes related to robustness is given below. Note that the second generation of the Eurocodes is in preparation. The review is now on the basis of the current version of the

Eurocodes. The guidelines related to structural robustness are mainly covered by two Eurocodes, i.e. 'EN 1990: Eurocode: Basis of Structural Design' (CEN, 2002), which provides the high level principles for achieving robustness and 'EN 1991-1-7 Eurocode 1: Part 1-7: Accidental actions' (CEN, 2006), which provides strategies and methods to obtain robustness and the actions to consider.

II.3.3.1 EN 1990: Basis of Structural Design

Eurocode EN 1990 states the following provisions for structural robustness:

(4)P - A structure shall be designed and executed in such a way that it will not be damaged by events such as:

- *explosion,*
- *impact, and*
- *the consequences of human errors,*

*to an extent **disproportionate** to the original cause.*

NOTE 1 The events to be taken into account are those agreed for an individual project with the client and the relevant authority.
*NOTE 2 Further information is given in **EN 1991-1-7**.*

*(5)P - **Potential damage** shall be avoided or **limited** by appropriate choice of one or more of the following:*

- *avoiding, eliminating or reducing the hazards to which the structure can be subjected;*
- *selecting a structural form which has low sensitivity to the hazards considered;*
- *selecting a structural form and design that can survive adequately the accidental removal of an individual member or a limited part of the structure, or the occurrence of acceptable localised damage;*
- *avoiding as far as possible structural systems that can collapse without warning;*
- *tying the structural members together.*

(6) The basic requirements should be met:

- *by the choice of suitable materials,*
- *by appropriate design and detailing, and*
- *by specifying control procedures for design, production, execution, and use relevant to the particular project.*

(7) The provisions of [..] should be interpreted on the basis that due skill and care appropriate to the circumstances is exercised in the design, based on such knowledge and good practice as is generally available at the time that the design of the structure is carried out.

Clause (4)P indicates which exposure conditions should be considered during the structural robustness assessment. Although the evaluation of the term depends on the individual interpretation of the designer, the use of the term disproportionate in clause (4)P makes the design concept clear. Moreover, the events to be taken into account are those agreed for an individual project with the client and the relevant authority, which means that the events that can be considered are not only limited to explosions, impact or human errors. Actually, EN 1991-1-7 (CEN, 2006) gives more relevant information and will be reviewed later. Moreover, it implicitly indicates that some local damage/failure may be accepted, e.g. the limitation of the area at risk of collapse in EN 1991-1-7 (CEN, 2006) is 100 m^2 or 15% of the floor area. Clause (5)P gives different strategies which can be adopted in the design for structural robustness.

For the purpose of reliability differentiation, three consequences classes (CC) are established by considering the consequences of failure or malfunction of the structure as given in Table II.4 (CEN, 2002).

Table II.4. Definition of consequence classes according to EN 1990 (CEN, 2002).

Consequence Class	Description	Examples of buildings and civil engineering works
CC3	**High** consequence for loss of human life, or economic, social or environmental consequences **very great**	Grandstands, public buildings where consequences of failure are high (e.g. a concert hall)
CC2	**Medium** consequence for loss of human life, economic, social or environmental consequences **considerable**	Residential and office buildings, public buildings where consequences of failure are medium (e.g. an office building)
CC1	**Low** consequence for loss of human life, and economic, social or environmental consequences **small or negligible**	Agricultural buildings where people do not normally enter (e.g. storage buildings), greenhouses

II.3.3.2 EN 1991-1-7: Actions on Structures - Accidental Actions

II.3.3.2.1 General

In addition to EN 1990, EN 1991-1-7 provides strategies and application rules for the assessment of accidental actions on buildings and other civil engineering structures. Compared to EN 1990, EN 1991-1-7 adds exposures from unidentifiable causes to the list specified in EN 1990. In this regard a clear distinction is made

between strategies applicable for identified accidental actions and for unidentified accidental actions (Figure II.4). These are situations where the designer knows (identified accidental actions) or does not know (unidentified accidental actions) the possible hazards a particular structure might be exposed to.

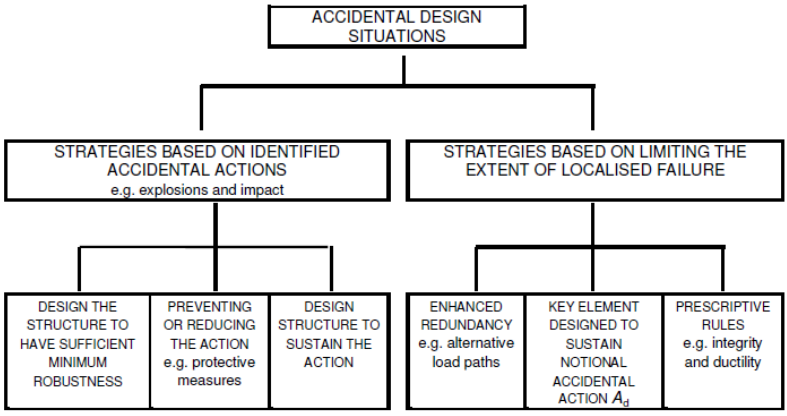

Figure II.4. Design strategies for identified and unidentified accidental actions (CEN, 2006).

The strategy used for accidental design situations may be based on the three consequence classes as set out in EN 1990 (i.e. CC1, CC2 and CC3 in Table II.4):

- CC1 (low consequences of failure): no specific consideration is necessary for accidental actions except to ensure that the robustness and stability rules in EN 1990 to EN 1999, as applicable, are met;
- CC2 (medium consequences of failure): depending upon the specific circumstances of the structure, a simplified analysis by static equivalent action models may be adopted or prescriptive design/detailing rules may be applied;
- CC3 (high consequences of failure): an examination of the specific case should be carried out to determine the level of reliability and the depth of structural analyses required. This may require a risk analysis to be carried out and **the use of refined methods such as dynamic analysis, nonlinear models and interaction between the load and the structure**.

Typical examples of identified accidental actions are fire, explosions, earthquakes, impact, floods, landslides and so on. Once an accidental action is defined, this identified action can be dealt with by classical (advanced) structural analysis, i.e. considering appropriate partial factors and load combinations. However, it is important to indicate that for the verification of accidental design situations, no target reliability levels are specified. Moreover, for the structures with high

consequences of failure, the use of refined method such as dynamic analysis and nonlinear models are suggested.

II.3.3.2.2 Annex A: Design for consequences of localised failure in buildings from an unspecified cause

For unidentified accidental actions or unspecified causes, e.g. human errors, terrorist attacks and aircraft crashes (Gulvanessian and Vrouwenvelder, 2006), Annex A gives rules and methods for designing buildings to sustain an extent of localised failure from an unspecified cause without disproportionate collapse. However due to the occurrence of extreme and unexpected events, no design can be made risk free. Hence, localized failure is acceptable to a certain extent as long as the global structural stability is not endangered. To limit the extent of localised failure due to unidentified accidental actions three strategies are given in EN 1991-1-7 (right branch in Figure II.4):

1) Designing the structure so that in the event of a localised failure (e.g. failure of a single member) the stability of the whole structure or of a significant part of it would not be endangered;
2) Designing key elements, on which the stability of the structure depends, to sustain the effects of a notional accidental action;
3) Applying prescriptive design/detailing rules that provide acceptable robustness for the structure (e.g. three-dimensional tying for additional integrity, or a minimum level of ductility of structural members subject to impact).

The design for accidental situations is of particular importance where a collapse may result in consequences in terms of injury to human beings, or may have significant economic, social or environmental consequences. A convenient approach to decide which structures should be designed for accidental actions, is to arrange the structures or structural components in categories according to the consequences of an accident. As such EN 1991-1-7 makes a distinction between the strategies to be applied for unidentified accidental design situations, on the basis of the three consequence classes defined in EN 1990 (Table II.4).

In Annex A of EN 1991-1-7, the consequence classes in EN 1990 (Table II.4) are further extended. Consequence Class 2 is subdivided into two subclasses, i.e. Consequence Class 2a (lower risk group) and Consequence Class 2b (upper risk group). However, this table is not exhaustive and can be adjusted by national annexes. Subsequently, in EN 1991-1-7 the strategy to be adopted for accidental design situations is based on the Consequence Classes and can be summarized as follows:

- **CC1:** Provided a building has been designed and constructed in accordance with the rules given in EN 1990 to EN 1999 for satisfying

stability in normal use, no further specific consideration is necessary with regard to accidental actions from unidentified causes;

- **CC2a:** In addition to the recommended strategies for Consequences Class 1, the provision of effective horizontal ties, or effective anchorage of suspended floors to walls should be provided;
- **CC2b:** In addition to the recommended strategies for Consequences Class 1, the provision of:
    - horizontal ties should be provided together with vertical ties in all supporting columns and walls; or alternatively,
    - the building should be checked to ensure that upon the notional removal of each supporting column and each beam supporting a column, or any nominal section of load-bearing wall the building remains stable and that any local damage does not exceed a certain limit. Where the notional removal of such columns and sections of walls would result in a damage extent in excess of the agreed limit, or other such limit specified, then such elements should be designed as a 'key element';
- **CC3:** A systematic risk assessment of the building should be undertaken taking into account both foreseeable and unforeseeable hazards. As stated before, an examination of the specific case should be carried out to determine the level of reliability and the depth of the structural analyses required. This may require **the use of refined methods such as dynamic analyses and nonlinear models**. Guidance on the preparation of the risk analysis is given in Annex B of EN 1991-1-7 (CEN, 2006).

II.3.3.3 Annex B: Information on risk assessment

For buildings in Consequence Class 3 (CC3), EN 1991-1-7 recommends a formal quantitative risk analysis. Annex B gives guidance for the planning and execution of risk assessment in the field of buildings and civil engineering structures, where a general overview is presented in Figure II.5. The recommended steps for this assessment are:

1) Definition of scope and limitations
2) Qualitative risk analysis (inventory and description)
3) Quantitative risk analysis (modelling and calculations)
4) Risk evaluation and mitigation measures
5) Risk communication

In case of a formal quantitative risk analysis of structures subjected to accidental actions according to Annex B of EN 1991-1-7, three analysis steps can be distinguished (Figure II.6) as follows:

1) Identification and modelling of relevant accidental hazards. Assessment of the probability of occurrence of different hazards with different intensities;
2) Assessment of damage states to the structure from different hazards. Assessment of the probability of different states of damage and corresponding consequences for given hazards;
3) Assessment of the performance of the damaged structure. Assessment of the probability of inadequate performance(s) of the damaged structure together with the corresponding consequence(s).

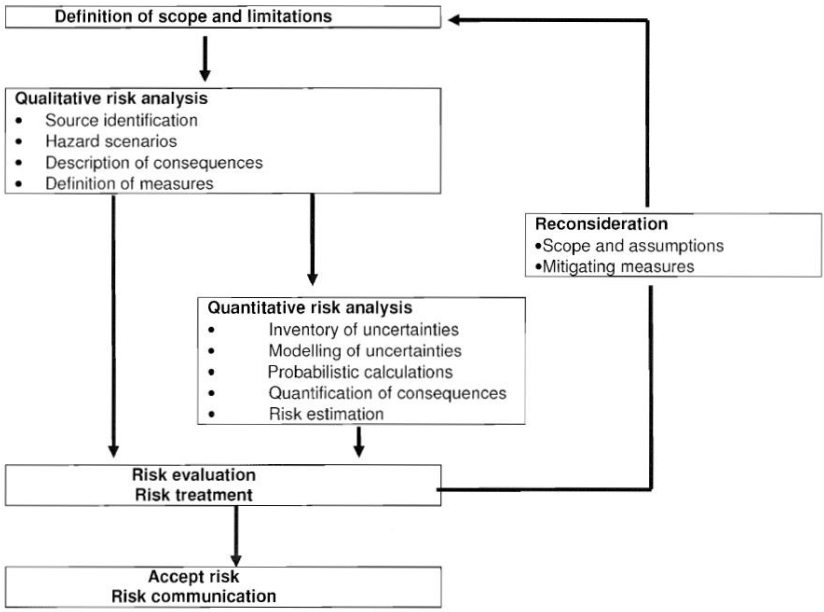

Figure II.5. Overview of risk analysis according to EN 1991-1-7 (CEN, 2006).

According to Annex B of EN 1991-1-7, the following formula is given to evaluate the total risk:

$$R = \sum_{i=1}^{N_H} P[H_i] \sum_{j}^{N_D} \sum_{k=1}^{N_S} P\left[D_j \middle| H_i\right] \cdot P\left[S_k \middle| D_j\right] \cdot C[S_k] \qquad \text{(II.1)}$$

where it is assumed that the structure is subjected to N_H different hazards that may damage the structure in N_D different ways (can be dependent on the considered hazards) and that the performance of the damaged structure can be discretised into

N_S adverse states S_k with corresponding consequences $C[S_k]$. $P[H_i]$ is the probability of occurrence (within a reference time interval) of the i^{th} hazard, $P[D_j|H_i]$ is the conditional probability of the j^{th} damage state of the structure given the i^{th} hazard, and $P[S_k|D_j]$ is the conditional probability of the k^{th} adverse overall structural performance S_k given the j^{th} damage state.

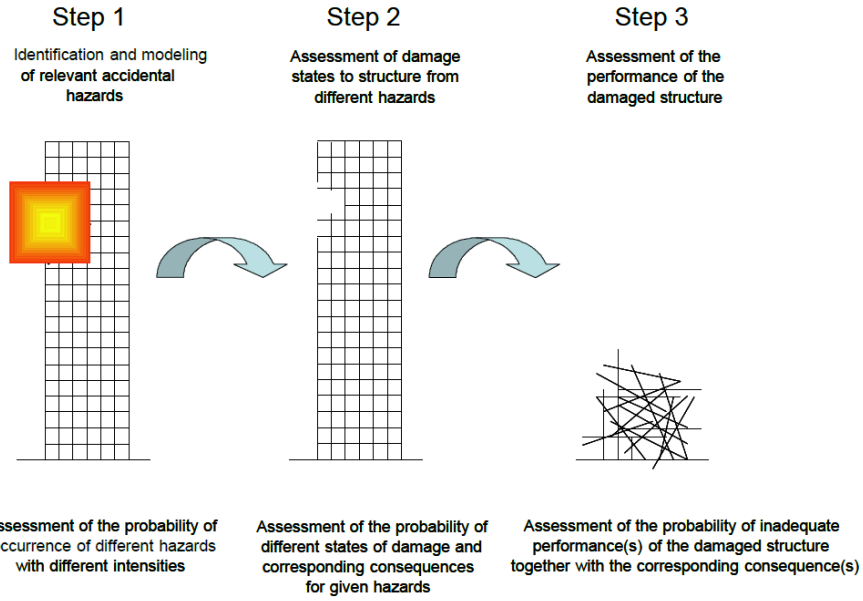

Figure II.6. Illustration of the steps in risk analysis for structures subject to accidental actions according to EN 1991-1-7 (CEN, 2006).

Based on Eq. (II.1) the following strategies are identified to mitigate the risk, i.e. risk mitigation measures (CEN, 2006):

- Reducing the probability of the hazard occurrence (i.e. reducing $P[H_i]$);
- Reducing the probability of significant damage given the hazard (i.e. reducing $P[D_j|H_i]$). This is related to the vulnerability of the structure (see section II.2.4);
- Reducing the probability of adverse structural performance (i.e. reducing $P[S_k|D_j]$). This might be undertaken by designing the structures with sufficient degree of redundancy thus allowing for alternate load transfer should the static system change due to damage.

II.4 Quantitative measure of structural robustness

Robustness has been recognized as a desirable property of structures to minimise the probability of disproportionate collapse. Therefore, it is of great importance to be able to quantify it so one can compare the level of robustness with certain target values or compare among different design solutions. Despite significant theoretical and methodical advances over the last decades, quantification of structural robustness is still an issue of controversy (Droogné, 2019). In general, approaches to quantify a robustness index can be divided into the following three approaches with increasing complexity (Sørensen *et al.*, 2012; Li *et al.*, 2016; Feng *et al.*, 2020):

- Deterministic-based measures derived from structural properties or characteristics;
- Probabilistic-based measures based on probabilities of failure or the reliability indices of the structural system for an undamaged structure and a damaged structure;
- Risk-based measures based on a complete risk analysis of the system, where both probabilities and consequences are taken into account.

In the following, some robustness measures or indices are summarized.

II.4.1 Deterministic-based robustness indices

The deterministic-based measures do not taken into account any uncertainties (e.g. material uncertainty). They are based on the deterministic structural characteristics of the considered system. Hence, this type of indices is simple and practical.

A deterministic index for structural robustness used in the offshore industry is the residual influence factor (Sørensen *et al.*, 2012). This index is based on the reserve strength ratio (RSR) which is defined as:

$$RSR = \frac{R_c}{S_c} \tag{II.2}$$

where R_c is the characteristic value of the base shear capacity of an off-shore platform, and S_c is the design load corresponding to ultimate collapse. Other indices have been proposed as well in (Sørensen *et al.*, 2012).

Frangopol and Curley (1987) proposed a series of deterministic redundancy measures in terms of the load bearing capacities of both damaged and undamaged structures. For instance, one is the strength redundancy factor (SRF) which takes into account the overall collapse load of the intact structure (L_{intact}) and the collapse load of the damaged structure ($L_{damaged}$):

$$SRF = \frac{L_{intact}}{L_{intact} - L_{damaged}} \tag{II.3}$$

the SRF varies between unity (for structures without strength reserve) and infinity (for structures where the initial local damage has no influence on the reserve strength of the structure).

The effectiveness of several dimensionless performance indices $0 \leq \rho \leq 1$ related to the structural deterministic behaviour is investigated by Biondini and Restelli (2008). It is found that indices associated with the properties of the first natural variation period, displacements and stored energy are suitable and recommended to describe the structural performance:

$$\rho_T = \frac{T_{n0}}{T_{n1}} \qquad T_n = 2\pi \sqrt{\max_i \lambda_i \left(\mathbf{K}^{-1}\mathbf{M}\right)} \tag{II.4}$$

$$\rho_s = \frac{s_0}{s_1} \qquad s = \|\mathbf{s}\| = \|\mathbf{K}^{-1}\mathbf{f}\| \tag{II.5}$$

$$\rho_\phi = \frac{\phi_0}{\phi_1} \qquad \phi = \frac{1}{2}\mathbf{s}^T\mathbf{K}\mathbf{s} = \frac{1}{2}\mathbf{s}^T\mathbf{f} \tag{II.6}$$

where T_n is the first natural vibration period associated with the stiffness matrix $\mathbf{K}$ and mass matrix $\mathbf{M}$, $\lambda_i(\mathbf{A})$ denotes the i^{th} eigenvalue of a square matrix $\mathbf{A}$, $\mathbf{s}$ is the displacement vector, $\mathbf{f}$ is the load vector, ϕ is the stored energy, $\|\cdot\|$ denotes the Euclidean scalar norm, and the subscripts 0 and 1 refer to the intact and damaged states, respectively.

A metric for structural robustness is proposed by Bao *et al.* (2017), calculated through normalizing the ultimate capacities of the structural system under sudden column loss by the applicable service-level gravity loading and by evaluating the minimum value of this normalized ultimate capacity over all column removal scenarios. The minimum value is adopted as the robustness index, I_R, as follows:

$$I_R = \min_i (\lambda_u^i | i \in \text{column removal scenarios}) \tag{II.7}$$

where λ_u^i is the normalized ultimate capacity for the i^{th} sudden column loss. This procedure is applied to two prototype 10-storey RC buildings (with different seismic designs and detailings) each subjected to seven single-column-removal scenarios. $I_R > 1$ indicates that collapse would not occur under any of the sudden column removal scenarios in case of gravity loading.

II.4.2 Probabilistic-based robustness indices

Comparing to the deterministic-based indices, the probabilistic-based indices can take uncertainties about the variables into account, e.g. the uncertainties in material properties and loads (Biondini and Frangopol, 2016; Chen *et al.*, 2018a; Jovanović *et al.*, 2020). Some probabilistic-based measures related to structural redundancy

have been proposed, which also indicate the level of robustness. Sørensen *et al.* (2012) presents the following redundancy index RI_1:

$$RI_1 = \frac{P_{f,damaged} - P_{f,intact}}{P_{f,intact}} \tag{II.8}$$

where $P_{f,intact}$ is the probability of failure of an intact system, while $P_{f,damaged}$ is the probability of failure of a damaged structural system. Reliability analysis methods (e.g. Monte Carlo simulation) can be used to calculate these failure probabilities. The index takes values between zero and infinity, where smaller values indicating larger robustness.

Frangopol and Curley (1987) proposed the redundancy factor $\beta_{R,1}$ with regard to the reliability indices, which is defined as:

$$\beta_{R,1} = \frac{\beta_{intact}}{\beta_{intact} - \beta_{damaged}} \tag{II.9}$$

where β_{intact} is the reliability index of the intact structural system and $\beta_{damaged}$ is the reliability index of the damaged structural system. This index takes values between zero and infinity, with larger values indicating larger redundancy.

Fu and Frangopol (1990) proposed a redundancy index RI_2 for the probabilistic representation of system redundancy as follows:

$$RI_2 = \frac{P_{f,dam} - P_{f,sys}}{P_{f,sys}} \tag{II.10}$$

where $P_{f,sys}$ is the probability of failure of an intact system, while $P_{f,dam}$ is the probability of damage occurrence (e.g. first component failure) to the system. This index represents the availability of system warning before failure. For non-redundant systems it is equal to zero, i.e. damage results in the system failure. It takes positive values for systems that possess some redundancy. It is worth highlighting the distinction between the failure probability of the damaged system $P_{f,damaged}$, i.e. in Eqs. (II.8) and (II.9), and the probability of damage occurrence $P_{f,dam}$, i.e. in Eq. (II.10).

Alternatively, similar indices have been defined (Frangopol and Okasha, 2008; Decò *et al.*, 2011; Zhu and Frangopol, 2012):

$$\beta_{R,2} = \beta_{f,sys} - \beta_{f,dam} \tag{II.11}$$

$$RI_3 = P_{f,dam} - P_{f,sys} \tag{II.12}$$

$$\beta_{R,3} = \frac{\beta_{f,sys} - \beta_{f,dam}}{\beta_{f,sys}} \tag{II.13}$$

where $\beta_{f,sys}$ is the reliability index of the intact system and $\beta_{f,dam}$ is the reliability index associated with any first component failure; $P_{f,sys}$ is the probability of failure of an intact system, while $P_{f,dam}$ is the probability of damage occurrence (e.g. first component failure) to the system.

All the indices here are conditional to the specific damage. As the reliability-based index can take uncertainties into account (Feng *et al.*, 2020; Feng *et al.*, 2021), this kind of indices can be used to quantify the structural robustness (adopted in Chapter VI of this dissertation).

II.4.3 Risk-based robustness indices

The risk-based analysis is the basic and most general one among the three approaches, since both probabilities and consequences are taken into account. For instance, an event tree as shown in Figure II.7 (Sørensen *et al.*, 2012) is presented as a graphical tool for evaluating event scenarios that could occur to the system incorporating its associated probability and consequence. First, an exposure EX_{BD} occurs which has the potential of damaging components in the system. If no damge occurs ($\overline{D}$), then the analysis is finished. Otherwise, a damage state (D) occurs. For each of these states, there is a probability that system failure (F) results. Consequences are associated with each of the possible damage and failure scenarios, and are classified as either direct (C_{Dir}) or indirect (C_{Ind}).

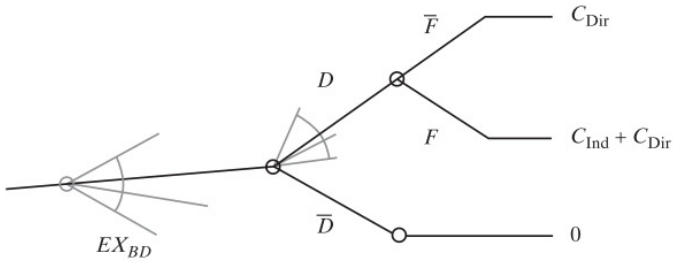

Figure II.7. An event tree for robustness quantification (Sørensen et al., 2012).

Incorporating the exposure resulting to damage and the related consequences of failure, a risk-based robustness index was introduced by Baker *et al.* (2008). In this risk-based approach a comprehensive model is presented which can include both the probability of structural collapse and the potential economic, political or societal related consequences. The consequences are separated into two contributions: direct consequences associated with the damage of elements directly affected by the hazardous event (initial damage), and indirect consequences associated to the subsequent partial or total system failure. Risk is calculated by the product of probability of occurrence of disproportionate collapse and

corresponding consequences. To quantify the risk of a total collapse, the following equation is used:

$$R = \sum P[F|D] \cdot P[D|E] \cdot P[E] \cdot C \tag{II.14}$$

where R denotes the total risk related to collapse of the structure; $P[F|D]$ is the probability of failure F given a certain damage D; $P[D|E]$ is the probability of a certain damage D given a certain exposure E; $P[E]$ is the probability of exposure E; and C are the costs resulting from collapse or failure F.

Related to the distinction between the direct and indirect consequences, the direct risks (R_{direct}) and indirect risks (R_{indirect}) can be computed (JCSS, 2008):

$$R_{\text{direct}} = \sum_{k=1}^{n_{\text{exp}}} \sum_{l=1}^{n_{\text{D}}} C_{\text{Dir}} \cdot P[D_l|E_k] \cdot P[E_k] \tag{II.15}$$

$$R_{\text{indirect}} = \sum_{k=1}^{n_{\text{exp}}} \sum_{l=1}^{n_{\text{D}}} C_{\text{Ind}} \cdot P[F|D_l, E_k] \cdot P[D_l|E_k] \cdot P[E_k] \tag{II.16}$$

where C_{Dir} and C_{Ind} are the direct and indirect consequences respectively, $P[E_k]$ is the probability of exposure E_k, $P[D_l|E_k]$ is the probability of having some damage D_l given the exposure E_k and $P[F|D_l, E_k]$ is the failure probability given a certain damage D_l and exposure E_k.

Once the direct and indirect risks are quantified, the risk-based robustness index is expressed as follows (Baker *et al.*, 2008):

$$I_{\text{Rob}} = \frac{R_{\text{direct}}}{R_{\text{direct}} + R_{\text{indirect}}} \tag{II.17}$$

the index varies between zero and one, with larger values representing larger robustness. This index measures only the relative risk due to indirect consequences, e.g. $I_{\text{Rob}} = 1$ if the system failure does not involve indirect consequences.

Considering the probability of a certain exposure and damage is sometimes difficult to assess, the robustness index I_{Rob} in Eq. (II.17) can also be expressed conditionally on the exposure E_k and the damage D_l as indicated in Baker *et al.* (2008) and applied in JCSS (2009):

$$I_{\text{Rob}}|D_l, E_k = \frac{R_{\text{direct,con}}}{R_{\text{direct,con}} + R_{\text{indirect,con}}} = \frac{C_{\text{Dir}}}{C_{\text{Dir}} + P[F|D_l, E_k]C_{\text{Ind}}} \tag{II.18}$$

in this expression the probabilities corresponding to exposure and damage events are no longer required as they are fixed.

As shown above, the risk-based index is comprehensive, as both probabilities and consequences are taken into account. This index is adopted in Chapter VII of this dissertation. More applications of such kind of indices can be found in (Faber, 2008; Izzuddin *et al.*, 2012; Droogné *et al.*, 2018).

II.5 Summary

In this chapter, some general background on structural robustness has been provided, including concepts, available design methods, and different indices. Generally, robustness is the ability of the structure to avoid consequences disproportionate to the event causing failure. Although structural robustness has been widely investigated in the last decades, no consensus is yet found on the definitions of basic concepts related to structural robustness.

Many design codes and guidelines have been developed worldwide in the past decades in order to provide structural robustness to mitigate the collapse risk. Among different methods, the alternate load path method is the major direct design method and it can be implemented in both threat-independent and threat-dependent manners. The threat-independent ALP method based on the notional member removal concept enables to investigate the ability of a structure to redistribute the unbalanced loads resulted from accidental loads, although not specifying the threats directly. Hence, the alternate load path method can be implemented to investigate the progressive collapse behaviour of RC building structures subjected to sudden column removal scenarios.

Different approaches can be found in literature in order to provide a quantitative indication about the structural robustness. Generally, these indices can be attributed to the following three different types: deterministic-based, probabilistic-based (or reliability-based) and risk-based indices. Usually, it is accepted that a comprehensive assessment in terms of structural robustness should consider the exposures or causes, damages, and consequences. Therefore, the risk-based index is the most comprehensive one. However, it may be subjective in relation to the definition of consequences. In this regard the reliability-based index is more objective, as no consequences are taken into account. Both the reliability-based and risk-based robustness indices are able to consider the uncertainties, i.e. provide an evaluation in a probabilistic way. The deterministic-based indices cannot consider the uncertainties, although the uncertainties may significantly affect the responses.

It should be mentioned that no target values have been calibrated yet to decide between robust or not robust in current design codes and guidelines. For instance, EN 1990 and EN 1991-1-7 provide deemed-to-satisfy provisions and proposed strategies in order to obtain robustness. However, it does not explicitly indicate how to quantify the robustness, or which robustness index should be considered

(and neither are target robustness index values specified). Consequently, robustness indices can only be adopted to compare different structural solutions with each other and are currently still not used to verify acceptable robustness levels.

II.6 References

ABCB (2016) National Construction Code 2016. Australian Building Codes Board.

Adam JM, Parisi F, Sagaseta J, et al. (2018) Research and practice on progressive collapse and robustness of building structures in the 21st century. Engineering Structures 173:122-149.

Agarwal J, Haberland M, Holický M, et al. (2012) Robustness of structures: Lessons from failures. Structural Engineering International 22:105-111.

Alexander S (2004) New approach to disproportionate collapse. The Structural Engineer 82:14-18.

Alshaikh IMH, Abu Bakar BH, Alwesabi EAH, et al. (2020) Experimental investigation of the progressive collapse of reinforced concrete structures: An overview. Structures 25:881-900.

Arup Group L (2011) Review of international research on structural robustness and disproportionate collapse. Department for Communities and Local Government.

ASCE (2016) Minimum design loads and associated criteria for buildings and other structures. American Society of Civil Engineers.

Baker JW, Schubert M, Faber MH (2008) On the assessment of robustness. Structural safety 30:253-267.

Bao Y, Main JA, Noh SY (2017) Evaluation of structural robustness against column loss: Methodology and application to RC frame buildings. Journal of Structural Engineering 143:04017066.

Bhattacharyya SP, Datta A, Keel LH (2018) Linear control theory: structure, robustness, and optimization. CRC press.

Biondini F, Frangopol DM (2015) Life-cycle robustness of deteriorating concrete structures.

Biondini F, Frangopol DM (2016) Life-cycle performance of deteriorating structural systems under uncertainty: Review. Journal of Structural Engineering 142:F4016001.

Biondini F, Frangopol DM, Restelli S (2008) On structural robustness, redundancy, and static indeterminacy Structures Congress 2008: Crossing Borders. pp. 1-10.

Biondini F, Restelli S (2008) Damage propagation and structural robustness Life-Cycle Civil Engineering: Proceedings of the International Symposium on Life-Cycle Civil Engineering, IALCCE'08. Varenna, Lake Como, Italy, pp. 131.

Brunesi E, Nascimbene R (2014) Extreme response of reinforced concrete buildings through fiber force-based finite element analysis. Engineering Structures 69:206-215.
Brunesi E, Parisi F (2017) Progressive collapse fragility models of European reinforced concrete framed buildings based on pushdown analysis. Engineering Structures 152:579-596.
Byfield M, Mudalige W, Morison C, et al. (2014) A review of progressive collapse research and regulations. Proceedings of the Institution of Civil Engineers-Structures and Buildings 167:447-456.
Byfield M, Paramasivam S (2007) Catenary action in steel-framed buildings. Proceedings of the Institution of Civil Engineers-Structures and Buildings 160:247-257.
Cavaco ES (2009) Robustness of corroded reinforced concrete structures.
CECS (2014) CECS 392: Code for Anti-collapse Design of Building Structures. China Planning Press Beijing, China. Beijing.
CEN (2002) Basis of Structural design. EN 1990: 2002.
CEN (2006) Eurocode 1: Actions on structures, part 1—7: General actions—Accidental actions. Comité Européen de Normalisation Brussels.
Chen JB, He JR, Ren XD, et al. (2018a) Stochastic harmonic function representation of random fields for material properties of structures. Journal of Engineering Mechanics 144:04018049.
Chen XX, Xie W, Xiao YF, et al. (2018b) Progressive collapse analysis of SRC frame-rc core tube hybrid structure. Applied Sciences-Basel 8:2316.
COST (2011) Theoretical framework on structural robustness. European Cooperation in the field of Scientific and Technical Research (COST).
Decò A, Frangopol DM, Okasha NM (2011) Time-variant redundancy of ship structures. Journal of Ship Research 55.
DoD (2005) Unified facilities criteria: Design of buildings to resist progressive collapse (ufc 4-023-03). Department of Defense Washington, DC, USA.
DoD (2009) Unified facilities criteria: Design of buildings to resist progressive collapse. UFC 4-023-03. United States Department of Defense.
DoD (2016) Design of buildings to resist progressive collapse. Unified Facilities Criteria (UFC) 4-023-03.
Droogné D (2019) Reliability-Based design for robustness: evaluation of progressive collapse in concrete structures taking into account membrane action. PhD diss. Ghent University.
Droogné D, Botte W, Caspeele R (2018) A multilevel calculation scheme for risk-based robustness quantification of reinforced concrete frames. Engineering Structures 160:56-70.
Ellingwood BR (2006) Mitigating risk from abnormal loads and progressive collapse. Journal of Performance of Constructed Facilities 20:315-323.
Faber MH (2008) Risk assessment in engineering: principles, system representation & risk criteria. ETH Zurich.

Faber MH, Maes MA, Straub D, et al. (2006) On the quantification of robustness of structures. pp. 79-87.
Fascetti A, Kunnath SK, Nisticò N (2016) Disproportionate collapse simulations. 847:87-94.
Feng D, Xie S, Xu J, et al. (2020) Robustness quantification of reinforced concrete structures subjected to progressive collapse via the probability density evolution method. Engineering Structures 202:109877.
Feng DC, Xie SC, Li Y, et al. (2021) Time-dependent reliability-based redundancy assessment of deteriorated RC structures against progressive collapse considering corrosion effect. Structural safety 89:102061.
fib (2013) fib model code for concrete structures 2010.
Frangopol DM, Curley JP (1987) Effects of damage and redundancy on structural reliability. Journal of Structural Engineering 113:1533-1549.
Frangopol DM, Okasha NM (2008) Life-cycle performance and redundancy of structures. pp. 1-14.
Fu G, Frangopol DM (1990) Balancing weight, system reliability and redundancy in a multiobjective optimization framework. Structural safety 7:165-175.
GSA (2003) GSA guidelines for progressive collapse analysis. General Services Administration. Office of the Chief Architect Washington, DC.
GSA (2016) Alternate path analysis and design guidelines for progressive collapse resistance. General Services Administration. Office of the Chief Architect Washington, DC.
Gulvanessian H, Vrouwenvelder T (2006) Robustness and the Eurocodes. Structural Engineering International 16:167-171.
HMG (2013) The Building Regulations 2010 - Structure: Approved Document A. NBS London, UK.
ICC (2009) International building code (IBC 2009) Cengage Learning.
IStructE (2013) Manual for the Systematic Risk Assessment of High-risk Structures Against Disproportionate Collapse. Institution of Structural Engineers.
Izzuddin BA, Pereira MF, Kuhlmann U, et al. (2012) Application of probabilistic robustness framework: risk assessment of multi-storey buildings under extreme loading. Structural Engineering International 22:85-79.
JCSS (2009) Risk assessment in engineering: Principles, System representation and Risk criteria. Joint Committee on Structural Safety (JCSS).
Jovanović B, Van Coile R, Hopkin D, et al. (2020) Review of current practice in probabilistic structural fire engineering: permanent and live load modelling. Fire Technology 57:1-30.
Kiakojouri F, De Biagi V, Chiaia B, et al. (2020) Progressive collapse of framed building structures: Current knowledge and future prospects. Engineering Structures 206:110061.
Le JL, Xue B (2014) Probabilistic analysis of reinforced concrete frame structures against progressive collapse. Engineering Structures 76:313-323.

Li Y, Lu X, Guan H, et al. (2016) Probability-based progressive collapse-resistant assessment for reinforced concrete frame structures. Advances in Structural Engineering 19:1723-1735.
Li Y, Lu X, Guan H, et al. (2011) An improved tie force method for progressive collapse resistance design of reinforced concrete frame structures. Engineering Structures 33:2931-2942.
Lu X, Lu XZ, Guan H, et al. (2013) Collapse simulation of reinforced concrete high-rise building induced by extreme earthquakes. Earthquake engineering & structural dynamics 42:705-723.
Moore DB (2003) The UK and European regulations for accidental actions Workshop on Prevention of Progressive Collapse, National Institute of Building Sciences.
NRCC (1995) National building code of Canada. National Research Council.
Parisi F, Scalvenzi M, Brunesi E (2019) Performance limit states for progressive collapse analysis of reinforced concrete framed buildings. Structural Concrete 20:68-84.
Praxedes C, Yuan X-X (2021) Robustness assessment of reinforced concrete frames under progressive collapse hazards: Novel risk-based framework. Journal of Structural Engineering 147:04021119.
Qian K, Li B, Tian Y (2016) Recent progress in understanding of load resisting mechanisms for mitigating progressive collapse. Special Publication 309:1-18.
Russell JM, Owen JS, Hajirasouliha I (2015) Experimental investigation on the dynamic response of RC flat slabs after a sudden column loss. Engineering Structures 99:28-41.
Russell JM, Owen JS, Hajirasouliha I (2019a) Dynamic column loss analysis of reinforced concrete flat slabs. Engineering Structures 198:109453.
Russell JM, Sagaseta J, Cormie D, et al. (2019b) Historical review of prescriptive design rules for robustness after the collapse of Ronan Point. Structures 20:365-373.
Shahrokni A, Feldt R (2013) A systematic review of software robustness. Information and Software Technology 55:1-17.
Shan S, Li S, Xu S, et al. (2016) Experimental study on the progressive collapse performance of RC frames with infill walls. Engineering Structures 111:80-92.
Sørensen JD, Rizzuto E, Narasimhan H, et al. (2012) Robustness: theoretical framework. Structural Engineering International 22:66-72.
Starossek U, Haberland M (2009) Evaluating measures of structural robustness. pp. 1-8.
Starossek U, Haberland M (2010) Disproportionate collapse: terminology and procedures. Journal of Performance of Constructed Facilities 24:519-528.

Stevens D, Crowder B, Sunshine D, et al. (2011) DoD research and criteria for the design of buildings to resist progressive collapse. Journal of Structural Engineering 137:870-880.
Vrouwenvelder A, Stieffel U, Harding G (2005) Eurocode 1, part 1.7 accidental actions, background document. pp. 3311-3317.
Xiao Y, Kunnath S, Li FW, et al. (2015) Collapse test of three-story half-scale reinforced concrete frame building. ACI Structural Journal 112.
Xu GQ, Ellingwood BR (2011) An energy-based partial pushdown analysis procedure for assessment of disproportionate collapse potential. Journal of Constructional Steel Research 67:547-555.
Yi WJ, He QF, Xiao Y, et al. (2008) Experimental study on progressive collapse-resistant behavior of reinforced concrete frame structures. ACI Structural Journal 105:433-439.
Zhu B, Frangopol DM (2012) Reliability, redundancy and risk as performance indicators of structural systems during their life-cycle. Engineering Structures 41:34-49.

CHAPTER III

Progressive collapse of reinforced concrete building structures

III.1 Introduction

The issues and challenges in modelling structural progressive collapse can be quite different between a steel building and a RC building (El-Tawil *et al.*, 2014; Kunnath *et al.*, 2018). This dissertation focuses on the investigation of RC building structures only.

Estimation of the capacity of flexural RC structural elements is based on the yielding of reinforcing bars in the conventional design, where the flexural limit state is attained when the longitudinal bars yield and plastic hinges form at the beam ends and/or mid-sections (small deformation theories). However, when an accidental situation occurs, e.g. loss of a column or wall, large deformations are expected and the bending behaviour may be shifted towards membrane behaviour in slabs and catenary effects in both beams and slabs (Botte, 2017). These effects can significantly enhance the capacity of RC buildings. It is crucial to taking these potential secondary load resisting mechanisms into account when estimating the true strength and deformation capacity of the buildings near collapse. The potential secondary load resisting mechanisms for RC structures include Vierendeel (frame) action, tensile catenary action, compressive arch action, tensile membrane action and compressive membrane action (Qian *et al.*, 2016). Moreover, the progressive collapse of RC building structures is a dynamic phenomenon (Izzuddin *et al.*, 2008; Byfield *et al.*, 2014; DoD, 2016; Bao *et al.*, 2017; Adam *et al.*, 2020; Parisi and Scalvenzi, 2020). Therefore, both dynamic effects and the aforementioned strongly nonlinear responses need to be considered.

The investigations from both experimental tests and numerical simulations have made significant contributions to progressive collapse studies of RC buildings subjected to column loss scenarios (Kunnath *et al.*, 2018). The experimental studies in this field have made huge advances to improve existing codes and design recommendations and calibrate numerical models (Adam *et al.*, 2018). A review in relation to existing experimental tests is presented in section III.2.

Currently, available commercial and open-source software packages provide the user with a variety of choices for modelling and simulation, e.g. Abaqus (Abaqus, 2014), OpenSees (OpenSees, 2006), LS-DYNA (Hallquist, 2007) and Diana (Diana, 2017). Some of the modelling considerations in relation to progressive collapse analyses are summarized as follows:

- Threat-dependent vs. threat-independent modelling: The imposed loading (accidental loads) is modelled explicitly in the threat-dependent modelling, while the initiating loading event leading to initial structural damage is not modelled but the effects of the damage are evaluated in the threat-independent modelling (Kunnath *et al.*, 2018). Considering the uncertainty in accurately defining the loading (or accidental loads), threat-independent approaches are more commonly used to evaluate the

progressive collapse resistance of RC buildings (Kunnath *et al.*, 2018), such as the applications in (Bao *et al.*, 2012; Cai *et al.*, 2012; Brunesi and Nascimbene, 2014; Brunesi *et al.*, 2015; Biagi *et al.*, 2020). The alternate load path method is a threat-independent approach (El-Tawil *et al.*, 2014; DoD, 2016; Alshaikh *et al.*, 2020);

- Static vs. dynamic modelling: the static methods to assess the collapse potential of structures aim at providing simplified, economical approaches (Izzuddin *et al.*, 2008; Tsai, 2011; Brunesi and Nascimbene, 2014; Russell *et al.*, 2015). However, static approaches are limited in their ability to realistically simulate the sudden load redistribution when a structure is subject to a sudden column removal scenario, while only dynamic analysis methods can account for such an event (Kunnath *et al.*, 2018). Thus, both static and dynamic methods can be used to investigate progressive collapse mechnisms, but the dynamic methods can be used to consider the worst conditions in case of sudden column removal scenarios. Nonlinear dynamic analysis may be carried out using either implicit or explicit schemes. An implicit scheme may encounter severe convergence problems (Kunnath *et al.*, 2018; Feng *et al.*, 2019). Therefore, the explicit schemes are more often used, e.g. (Bao *et al.*, 2012; Russell *et al.*, 2019). One of the disadvantages of explicit schemes is that the time step is sometimes controlled by one or a few elements with small mass or small element sizes (e.g. springs) (Abaqus, 2014). Alternatively, it has also recently been demonstrated that the nonlinear static pushdown analysis can approximately reproduce results obtained from a nonlinear dynamic analysis through an energy-balance concept (Izzuddin *et al.*, 2008; Herraiz *et al.*, 2015);
- Micro-based FE models (or detailed models) vs. macro-based FE models (or reduced-order models): FE models of a RC structure can be developed using continuum elements (detailed models), macro-level elements (reduced-order models) or a hybrid combination of different types. Examples of the micro-based FE models are solid and shell elements, e.g. (Bao *et al.*, 2012; Li *et al.*, 2016; Russell *et al.*, 2019), while examples of the macro-based FE models are beam-column elements with fibre sections and discrete spring elements, e.g. (Bao *et al.*, 2008; Shan *et al.*, 2016; Parisi and Scalvenzi, 2020; Zheng *et al.*, 2020).
- Two-dimensional (2D) vs. three-dimensional (3D) modelling: 3D models are more realistic, as 3D and slab effects are taken into account. However, the computational cost of 3D models are much higher (Adam *et al.*, 2018; Kunnath *et al.*, 2018). 2D models are computational efficient and the validation of the numerical models is possible through the existing experimental test results. Moreover, 2D models can be useful for primary assessment and for comparison of different scenarios (Kunnath *et al.*, 2018).

A review with regard to numerical simulations is presented in section III.3. Finally, a brief summary is provided in section III.4.

III.2 Experimental tests

Research based on the experimental tests has made a big contribution in the field of progressive collapse. Moreover, the obtained data have made it possible to improve existing codes and design recommendations and calibrate numerical models (Adam *et al.*, 2018). The threat-independent ALP method has been used in most of these tests, through simulating the failure of one or more columns, e.g. (Qian and Li, 2012a; Gouverneur *et al.*, 2013; Yu and Tan, 2013a; Russell *et al.*, 2015; Ren *et al.*, 2016; Qian and Li, 2017b; Qian *et al.*, 2018). Although the tests on several kinds of structures, e.g. concrete and steel structures, have been investigated, only the tests in relation to the RC building structures are reviewed in this section as this dissertation focuses on the progressive collapse behaviour of RC building structures. In general, the tests have been carried out on four different levels (Adam *et al.*, 2018):

a) RC subassemblies such as beam-column or beam-slab specimens;
b) RC planar frames formed by beams and columns;
c) RC building structures constructed for experimental purposes; and
d) actual (existing) buildings awaiting demolition.

In general two types of experimental tests have been applied: quasi-static loading and dynamic loading (Alshaikh *et al.*, 2020). The quasi-static loading is conducted by releasing the support of the column and increasing the vertical displacement until complete failure occurs, see Figure III.1a. The dynamic loading is implemented by simulating the gravity loads as stacked (concrete and sand) blocks. The dynamic loading effects are simulated by instantaneous removal of the support of the column, see Figure III.1b. The dynamic tests with uniformly distributed loads are reported to be the most realistic conditions to simulate the damages of the progressive collapses (Alshaikh *et al.*, 2020).

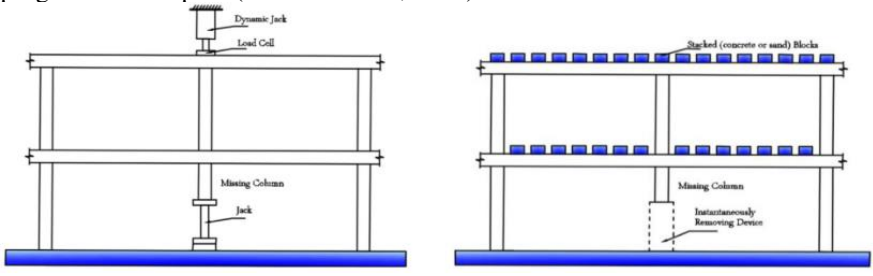

(a) Quasi-static loading (b) Dynamic loading

Figure III.1. The schematic diagram of different loading types (Alshaikh et al., 2020).

III.2.1 Tests on RC subassemblies

As the tests on subassemblies are much less expensive compared to those on frames and entire building structures, they are used more often. Numerous quasi-static pushdown tests have been carried out on RC or precast concrete (PC) beam-column subassemblies (Yap and Li, 2011; Qian and Li, 2012b; Qian and Li, 2012a; Qian and Li, 2013b; Yu and Tan, 2013a; Yu and Tan, 2013b; Qian *et al.*, 2014; Ren *et al.*, 2016; Elsanadedy *et al.*, 2017; Weng *et al.*, 2017; Qian *et al.*, 2021). Other research tested RC or PC beam-column subassemblies with the presence of slabs to quantify how slabs contribute to resist against progressive collapse (Qian and Li, 2012c; Qian and Li, 2013a; Qian and Li, 2014; Qian *et al.*, 2014; Lu *et al.*, 2017; Pham *et al.*, 2017a; Qian and Li, 2019). Among these subassemblies, the substructure composed of two span beams and one or three columns (one middle column is removed) as illustrated in Figure III.2a (Alshaikh *et al.*, 2020) are usually tested and the general results have been summarized as follows by Alshaikh *et al.* (2020): in general three stages can be observed in the curve shown in Figure III.2d (which is adopted to investigate the progressive collapse resistance of RC beams subjected to middle column removal scenarios in a static manner), a flexural action stage (A-B), a compressive arch action stage (B-D) and a catenary action stage (D-E) can be distinguished. In the AB segment, the behaviour of the beams can be considered elastic. However, the inelastic stage occurs from point B onwards and the compressive arch action is developed in the beams due to beam-column connections assisting in the horizontal restraint of beams (see Figure III.2a). Compressive arch action can enhance the flexural capacity of beams and redistribute loads to the neighbouring elements. The load is increased from B to C in Figure III.2d. Subsequently, in the CD segment the load-bearing capacity gradually diminishes due to concrete crushing in the compression zone (Figure III.2b). At point D, the catenary action is activated in the beams and the additional load-bearing capacity is developed in the DE segment, where the axial force in the beams switches from compressive to tensile due to the large vertical deflections (Figure III.2c). Consequently, both compressive arch action and catenary action can significantly enhance the progressive collapse resistance of the beams. Catenary action is the final defence mechanism to mitigate or prevent the progressive collapse of the RC beams. The activation of compressive arch action and catenary action in RC beams depends on many factors, such as cross-section, concrete strength, and longitudinal reinforcing ratio (Gouverneur *et al.*, 2013; Yu and Tan, 2013b; Qian *et al.*, 2014; Pham *et al.*, 2017a; Pham *et al.*, 2017b).

In addition to the quasi-static experimental tests, dynamic experimental tests with regard to RC beam-column or beam-slab assemblies have been carried out (Qian and Li, 2012a; Qian and Li, 2014; Yu *et al.*, 2014; Qian and Li, 2017a). This kind of test can more realistically reflect the progressive collapse behaviour of RC structures subjected to sudden column removal scenarios, since the progressive collapse is a dynamic phenomenon. Moreover, this kind of tests are not usually

loaded to failure (i.e. one dynamic test for each specimen and not a destructive test). Comparing to the results from quasi-static tests, the structures are usually subjected to more severe plastic damage in a dynamic test.

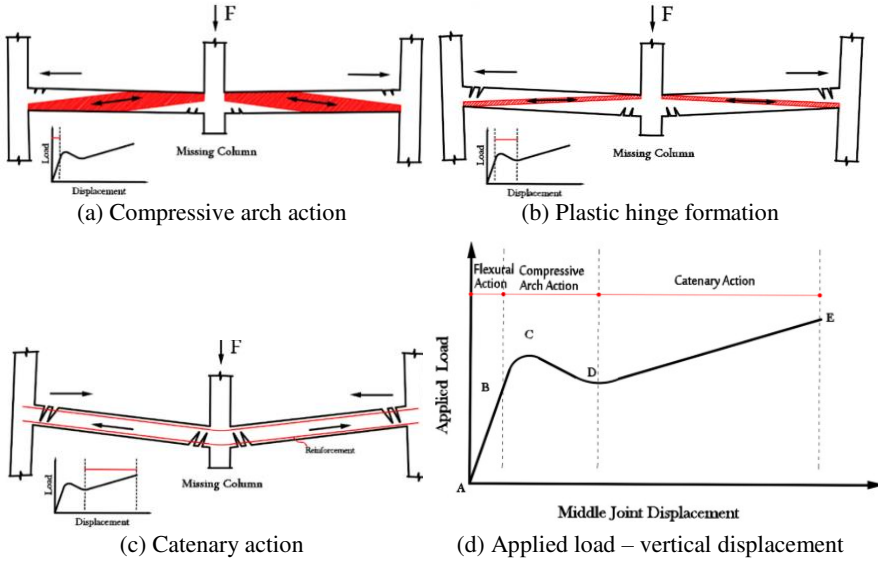

(a) Compressive arch action (b) Plastic hinge formation

(c) Catenary action (d) Applied load – vertical displacement

Figure III.2. Transformation of load resistance mechanisms during the collapse of RC beams subjected to middle column removal scenarios (Alshaikh et al., 2020).

For example, Qian and Li (2017a) conducted a series of dynamic tests to study the dynamic behaviour of multi-bay beam-column-slab substructures subjected to the sudden column removal scenario. Three 1/4-scaled slab-beam-column RC specimens were tested. These three specimens had identical dimensions and reinforcement details. The control specimen Con-1 (Figure III.3a) was tested subjected to a pushdown loading regime. One of the specimens (designated as D-0.91) was tested dynamically with externally applied pressure (Figure III.3b). Another dynamically tested specimen was designated D-1.16 and subjected to a higher externally applied pressure (Figure III.3c). According to the results, the displacement amplification factors of specimen D-0.91 and D-1.16 were 2.5 and 4.5, respectively. A larger value was obtained for specimen D-1.16 due to its more severe plastic damage during dynamic tests. It was found that the load imposed in D-0.91 only resulted in relatively little plastic deformation due to compressive arch action and compressive membrane action. The specimen D-1.16 did not collapse thanks to the load resistance from catenary action and tensile membrane action in the large deformation stage. The displacement amplification factor was close to 2.0 when the specimen had elastic behaviour. As the substructures could survive after sudden removal of the column, their residual behaviour was also captured by

conducted subsequent pushdown tests by applying multiple point loads on the slab. The experimental results indicated that the damage caused by the dynamic response might significantly degrade the initial stiffness and detriment the efficiency of compressive arch action and compressive membrane action even if the specimens actually only experienced a small plastic dynamic response. However, when the specimens undergoes a considerable plastic dynamic response, no compressive arch action and compressive membrane action were able to develop. The load resisting capacity would derive mainly from tensile membrane action and catenary action in large deformation stage.

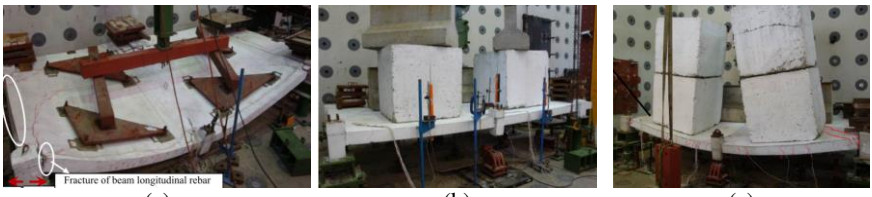

(a) (b) (c)

Figure III.3. Dynamic test on beam-column-slab substructures: (a) Con-1; (b) D-0.91; and (c) D-1.16 (Qian and Li, 2017a).

The behaviour of RC flat slabs have also been studied in both static (Foster *et al.*, 2004; Gouverneur *et al.*, 2013; Qian and Li, 2013a; Yi *et al.*, 2014) and dynamic manners (Russell *et al.*, 2015; Peng *et al.*, 2017; Peng *et al.*, 2018; Qian *et al.*, 2018; Ma *et al.*, 2019; Ma *et al.*, 2020). In the context of progressive collapse in accidental situations, the RC slabs may provide considerable secondary load-carrying mechanisms (or alternate load paths) to resist the progressive collapse. For example, Gouverneur *et al.* (2013) conducted quasi-static tests on real-scale RC one-way slabs subjected to a central support removal scenario (see Figure III.4), to investigate the development of catenary action or tensile membrane action associated with the formation of large displacements. The results demonstrated that the slab strip exhibited three different distinct stages: elastic, plastic and catenary stages. Both the development of the displacements and the horizontal forces confirmed a load transfer process from an elastic bending mechanism to a catenary mechanism controlled by tension. The catenary action was found to considerably increase the load-carrying capacity, where the obtained ultimate load-bearing capacity was found to be three times the service load that was specified for the design situation with the central support. Figure III.4b shows the deformation of the slab specimen just before collapse. The results highlight that a sufficient horizontal restraint is necessary to ensure that the tensile strength of the reinforcing rebars would develop catenary action. Note: no compressive membrane action was observed in these experiments, since only inward movement at the end of the slab was restrained (i.e. outward movement was free).

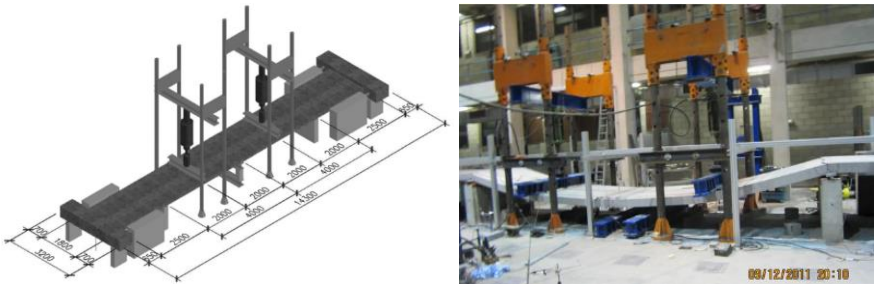

(a) Test set-up (b) Slab at a central deformation of 640 mm

Figure III.4. Experimental test on real-scale RC slab (Gouverneur et al., 2013).

The dynamic effects involved in suddenly removing a support for RC slabs were observed to have a significant influence on the force redistributions and the damage in the structural system. In such cases sufficient ductility is required in order to avoid brittle failures, such as punching shear which may potentially result in progressive collapse (Qian *et al.*, 2018). For instance, Russell *et al.* (2015) carried out experimental tests on seven 1/3-scale RC flat slabs subjected to different column removal scenarios (corner, penultimate and middle column removal scenarios). This study aimed to experimentally study the behaviour of flat slabs after a sudden column loss, especially considering nonlinear and dynamic effects. Dynamic results under different loading levels were compared to static tests to assess the additional damage sustained due to inertial effects. From the tests, it was found that the ability of the flat slabs to efficiently span in two directions provided sufficient alternate load paths after a single column loss. The cracking patterns after the tests are shown in Figure III.5a,b for the corner and penultimate column loss cases, respectively. Although flexural cracks were observed, they did not lead to ultimate failure. All observed failures were due to punching shear. The slabs were found to have significant additional capacity in the inelastic stage due to material and geometric nonlinearities. The dynamic effects involved in suddenly removing a column were observed to have a significant influence in relation to the force redistributions and the damage in the structural system. In the dynamic situation the level of loading changed the response of the system due to two aspects: the increase in load (or additional mass) changed the natural frequency of the system and higher loading resulted in damage to the structure. The dissipation of energy due to the damage altered the peak displacement and level of damping, as well as reducing the stiffness, and therefore natural frequency. From all the tests the maximum strain rate of the reinforcing steel was less than 0.35 s^{-1}. A high strain rate would change the material properties. However, the influence of the strain rate was observed to be less significant, since the high strain rate only occurred at very

localised points and in a short duration. Moreover, the peak strain occurred in a period of time after the peak strain rate, which further limited its influence.

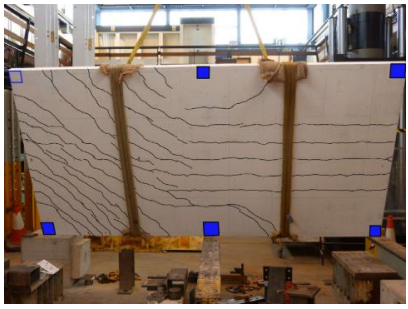

(a) Corner column loss

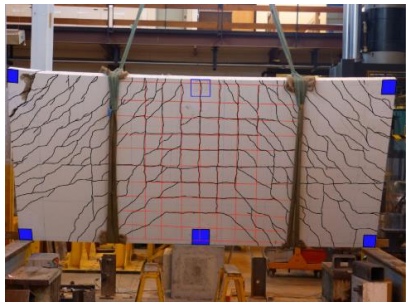

(b) Penultimate column loss

Figure III.5. Annotated cracking pattern for the flat RC slabs (Russell et al., 2015).

III.2.2 Tests on RC planar frames

Although the studies on subassemblies enable the study of the behaviour of the beams (such as arch and catenary actions) and the beam-column connections affected by a column failure, research on RC frames focuses further on the general behaviour of the connection, the Vierendeel action and how a column failure affects beam and column elements and neighbouring joints. After the failure of a column, the loads originally carried by the removed column are redistributed to neighbouring columns. These loads change the bending moments in the beams over the missing column from negative to positive as shown in Figure III.6 (Alshaikh *et al.*, 2020). It is easy to see that the bending moments are very large due to the double span, which may result in the progressive collapse of the entire structure or a large part of it.

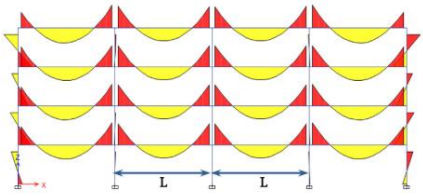

(a) Before column loss

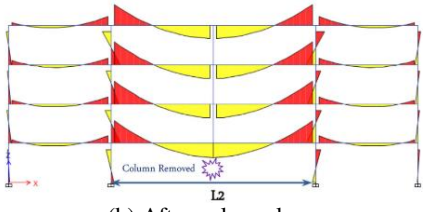

(b) After column loss

Figure III.6. Diagram of the change in bending moment due to column loss (Alshaikh et al., 2020).

In terms of framed buildings, five resisting mechanisms can provide alternate load paths and minimise the risk of progressive collapse as summarized by (Adam *et al.*, 2018):

a) Bending of the beams where the column has failed;
b) Vierendeel behaviour of the frame over the failed column;
c) Arch effect of the beams where the column has failed (effective mechanism when horizontal displacement of the neighbouring columns is small);
d) Catenary/membrane behaviour of beams/slabs, bridging the damaged column by means of large rotations and displacements; and
e) Contribution of non-structural elements such as infill walls and partitions.

Yi *et al.* (2008) carried out one of the first laboratory tests on progressive collapse resistance of RC frame structures. The experimental test was conducted on a 1/3-scale and four-bay-by-three-storey RC frame subjected to the loss of the central column removal at the ground floor, see Figure III.7a. A quasi-static loading procedure was adopted in the test. Experimental observations evidenced a redistribution and transition of load resisting mechanism from beam behaviour to arch and catenary actions. The fracture of the reinforcement occurred (Figure III.7b) when the vertical displacement and rotation reached 456 mm. Moreover, when catenary action is considered, the capacity of the RC frame was 1.4 times the capacity calculated according to the plastic limit state.

(a) Failure mode (b) Rupture of reinforcing bar

Figure III.7. Test-setup and final failure mode (Yi et al., 2008).

Dynamic effects are found to have a significant influence on the responses, such as internal forces and strains. For example, Stinger and Orton (2013) experimentally tested three 1/4-scale and two-bay-by-two-storey RC frames. In order to simulate the interaction with the remaining part of the prototype structure, the specimen was axially restrained to a lateral reaction frame at beam ends. Loss of the column between the two bays was simulated by a pushdown test. Both compressive arch action and catenary action resistance mechanisms were observed in frames under a collapse loading. Further, using the same specimen design, Orton and Kirby (2014)

performed dynamic tests. Dead loads were applied to the beams. The central column was suddenly removed by a special device (a kickstand constructed from wood). Analysis of the test data showed a consistent dynamic amplification factor for the vertical deflection of approximately 1.09. The amplification factor for the horizontal load and strain in the reinforcement was much greater, as much as 4.49, possibly due to the impact effect of dynamic loading. Catenary action response was observed in these tests.

These RC planar frames are simple but more comprehensive than the RC sub-structures in relation to the understanding of the global behaviour of the RC structures. Such experimental test results are of great value with regard to the validation of numerical models. Moreover, dynamic effects are found to have significant influence on internal forces and strains in the RC structures. When the specimens in dynamic tests are used to validate FE models, information, such as natural frequencies, dampings, and column removal durations, are needed.

III.2.3 Tests on RC building structures purpose-built for research

Previous tests have been mainly limited to smaller-scale or 2D frames without slab effects. Static tests of 3D RC structures can be found in (Wang *et al.*, 2016a; Wang *et al.*, 2016b; Zhang *et al.*, 2016). Zhang *et al.* (2016) carried out experimental tests on the progressive collapse behaviour of 3D RC structures with special columns subjected to middle and corner column removal scenarios. The results indicated that the redistribution of internal force was mainly realized through the beam mechanism and the compressive arch action played an important role to enhance the collapse capacity. Limited studies in relation to the large-scale 3D RC structures subjected to the sudden column removal scenarios have been done (Qing-Feng *et al.*, 2009; Kokot *et al.*, 2012; Xiao *et al.*, 2015; Adam *et al.*, 2020). Especially for corner column loss situations, these are the most vulnerable columns in the structures according to the experimental results in (Adam *et al.*, 2020).

Qing-Feng *et al.* (2009) conducted tests on a four-storey (two-bay and two-span) 1/3-scale RC frame to investigate the building progressive collapse response. First, the structure was subjected to sudden column removal scenarios under blast loading, followed by a quasi-static test in which the middle column deflection was increased until complete failure. After the loss of a column, the loads carried by the removed column were redistributed into alternate load paths due to the participation of both longitudinal and transverse frames (Vierendeel action) and floor slabs. Catenary action was not observed to increase the capacity of the frame because the frame was discontinuous, thus limiting the lateral restraints of the beam–column joints.

A three-storey, three-bay-by-three-bay (in two directions) and 1/2-scale RC building (see Figure III.8a) was built and experimentally tested in (Xiao *et al.*,

2013; Xiao *et al.*, 2015). In order to investigate the dynamic response, failure mechanism and changes in the load-transfer paths, the RC structure was subjected to a series of sudden column failures. In the test, five column removal scenarios were investigated: corner column, column adjacent to the corner column, two exterior columns, two middle exterior columns, and one interior column. The slabs were loaded with concrete and steel blocks. Columns were suddenly removed by a hydrogen gas cannon. The results show that the structure did not collapse in case of a corner or inner column loss. The slabs and beams that directly connect the failed column provide the most effective resisting mechanism against disproportionate structural collapse. When the two middle-side first-floor beam-column joints exhibited a vertical displacement greater than the depth of the beam due to loss of two middle exterior columns (with the final failure mode shown in Figure III.8a), the frame behaviour exhibited a transition from moment-resisting frame mechanism to catenary mechanism. The crushing of concrete was observed in the bottom compressive zone at the first-floor beam end in the longitudinal frame, see Figure III.8b. However, the buckling of the compression steel bars was less evident because they were likely straightened once catenary action developed. The through-cracks near the beam end shown in Figure III.8b provided additional evidence of the formation of catenary action. Meantime, damage to the first-floor transverse beams was significant, with the full formation of plastic hinges and eventual concrete crushing and bar buckling, see Figure III.8c. They also pointed out that a sufficient anchorage capacity was required at each end of the beams in order to fully develop the catenary action.

(a) (b) (c)

Figure III.8. Collapse test of the RC structure after two side column removal: (a) failure mode; (b) damage at the end of one longitudinal beam; and (c) damage at the end of one transverse beam (Xiao et al., 2015).

Recently, Adam *et al.* (2020) tested a full-scale RC cast-in-place building structure subjected to a sudden corner column failure scenario, as shown in Figure III.9. It was the first study of a corner column removal on a full-scale building specially built for the purpose subjected to representative loading used in design. Based on the experimental measurements, real-time strain, displacement, accelerations, alternate load paths and dynamic amplification factors were analysed. The structure was able to find effective alternate load paths after the sudden removal of the

corner-column. The time-history test results showed that the peak dynamic values were significantly higher than the stabilized residual values after the test. The predominant alternate load paths in the test were the flexural and Vierendeel beam actions, while slab membrane action was not a significant alternate load path for the investigated case. The load initially carried by the removed column was redistributed through the entire building system (not just the neighbouring columns). For the vertical displacements, the values obtained for the dynamic amplification factor were around 2.6 which was within the recommended values of DoD (DoD, 2016). For the axial load amplification, the values obtained for the dynamic amplification factor were around 1.24.

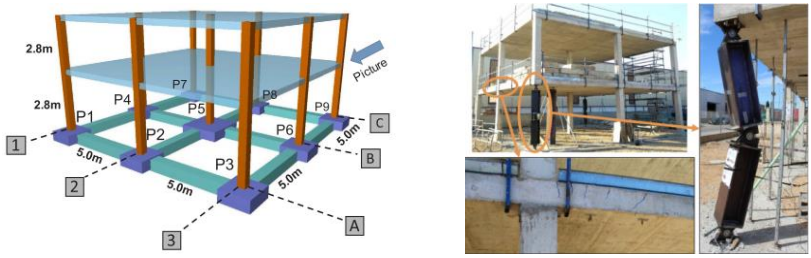

(a) (b)

Figure III.9. Full-scale RC building structure: (a) 3D view; and (b) final state (Adam *et al.*, 2020).

III.2.4 Tests on existing RC buildings

Several actual buildings, which were scheduled to be demolished, have been experimentally tested. Considering the limitations for such tests in the laboratory, e.g. very high costs, laboratory conditions and crucial safety procedures (Alshaikh *et al.*, 2020), it is difficult to investigate these cases in the laboratory. These tests show the possibility of investigating the overall interaction between the structural elements within multi-storey structures to resist the progressive collapse. From the tests described in (Matthews *et al.*, 2007; Sasani *et al.*, 2007; Sasani, 2008; Sasani and Sagiroglu, 2008; Sasani and Sagiroglu, 2010; Sasani *et al.*, 2011), Vierendeel action in both longitudinal and transverse frames was the major resistance mechanism against progressive collapse.

Sasani and Sagiroglu (2010) experimentally evaluated the dynamic gravity-load redistribution of the Baptist Memorial Hospital in Memphis following the removal of an interior ground-floor column. The building, completed in 1967, was a 20-story RC structure including a core and four wings, see Figure III.10a. The obtained maximum and permanent vertical displacements approximate 9.7 and 8.6 mm directly above the removed column, respectively. No signs of damage were observed on the floors above, since the structure responded to the column removal

with a small maximum vertical displacement. The experimental data show that the maximum and permanent vertical displacements on the seventh floor were approximately 60% smaller than those on the second floor due to the axial deformations of the columns. The elongation of the columns above the removed columns and the shortening of the neighbouring columns due to the change in their axial forces led to smaller deformations of the beams and slabs on higher floors compared to lower floors. The axial forces of columns above the removed column dropped significantly faster than the vertical displacement of the structure. This was due to the higher speed of axial wave (i.e. axial forces) propagation compared to that of the flexural wave (i.e. flexural deformations at beam-column interfaces) propagation. The capacity of structural systems to redistribute gravity loads and to provide alternate load paths increases as the number of floors increases. The increase in capacity was due to the system-level response to resist progressive collapse and the reserve capacity of elements farther up in the structure and away from the location of the local damage.

(a) (b)

Figure III.10. Experimental tests on actual buildings: (a) Baptist Memorial Hospital (Sasani and Sagiroglu, 2010); and (b) Crowne Plaza Hotel (Sasani et al., 2011).

Sasani *et al.* (2011) also experimentally studied the progressive collapse resistance of an 11-story structure (see Figure III.10b) with discontinued columns on the first storey. The building was constructed in 1973 in Houston. The initial damage was intended to represent the effects of a severe explosion causing the loss of four adjacent columns and two beam segments. The maximum recorded permanent vertical displacement following the imposed initial damage at the top of the first floor exploded columns was only about 56.0 mm. Two primary gravity load redistribution paths were observed. One was the flexural-axial response of the second-floor deep beams. The other was Vierendeel action of the flat plate structural system in floors above, which reduced the axial compressive force of the columns (in the vicinity of initial damage) to about two-thirds of that before the

initial damage. The other one-third was transferred through Vierendeel frame action away from the damaged region.

III.3 Numerical simulations

III.3.1 Progressive collapse analysis procedures

Considering the limitations of experimental tests, a suitable numerical simulation procedure can also be adopted to investigate the progressive collapse performance of RC building structures subjected to column removal scenarios. The advantages of numerical simulations in this field include making cost savings and avoiding the possible dangers in relation to experimental tests. The threat-independent alternate load path method (similar to experimental tests) is the most widely used approach for the assessment of the capability of a structural system to redistribute load away from damaged members, e.g. (Tsai and Lin, 2008; Russell *et al.*, 2019). In general, five procedures can be adopted to perform such an analysis (Byfield *et al.*, 2014):

a) LSA: a linear static analysis using dynamic amplification factor;
b) NSA: a nonlinear static analysis using dynamic amplification factor;
c) LDA: a linear dynamic analysis;
d) NDA: a nonlinear dynamic analysis; and
e) EBM: an energy-based method on the basis of a nonlinear static pushdown analysis.

All of these analysis approaches have their advantages and disadvantages. A comparison among them is summarized in Table III.1 as summarized in (Byfield *et al.*, 2014). In general the simpler procedures produce conservative designs but are easily to be implemented and verified (Brunesi and Nascimbene, 2014). Conversely the more complicated methods allow a more comprehensive understanding of the real behaviour and often provide more economical designs (Tsai, 2011), but require significant expertise of the users (Izzuddin *et al.*, 2008).

Since progressive collapse is inherently a dynamic phenomenon and may be accompanied by large deformations (Tsai, 2010; DoD, 2016; Adam *et al.*, 2020), all approaches should need to account for both dynamic effects and nonlinearities. Linear approaches require the material response to remain in the elastic range and second-order effects and instabilities are ignored. Therefore, they can only be used for small displacement conditions and often lead to conservative design in order to prevent invalidating the assumptions (Byfield *et al.*, 2014). However, large deformations are usually expected in progressive collapse analyses. A dynamic amplification factor can be used to reflect material and geometric nonlinearities and dynamic effects (DoD, 2016; GSA, 2016). However, the dynamic amplification factor (or load increase factor) is influenced by the level of damage which in turn depends on the stiffness and the level of gravity loading applied in the structure (Izzuddin and Nethercot, 2009; Pujol and Smith-Pardo, 2009;

Kwasniewski, 2010; Tsai, 2010; Russell *et al.*, 2015; Adam *et al.*, 2020). Moreover, Tsai (2011) pointed out that mathematical regression formulas for the dynamic amplification factor usually rely on the trend of their database and thus may lack some physical backgrounds. This was also discussed in (Qian and Li, 2012a), in which it is stated that the data pool for fitting the dynamic amplification factor needs to be improved. This issue also occurs in cases of the nonlinear static analysis, as a dynamic amplification factor (or dynamic increase factor) is still required to reflect the dynamic effects despite nonlinear approaches are able to account for both material and geometric nonlinearities.

Table III.1. Capability in relation to different procedures (Byfield et al., 2014).

	LSA	**NSA**	**LDA**	**NDA**	**EBM**
Include material plasticity	×	√	×	√	√
Account for strain hardening	×	√	×	√	√
Include second-order effects	×	√	×	√	√
Avoid using dynamic amplification factor	×	×	√	√	√
Explicitly account for strain-rate material effects	×	×	×	√	×
Account for damping	×	×	×	√	×

Note: LSA: linear static analysis; NSA: nonlinear static analysis; LDA: linear dynamic analysis; NDA: nonlinear dynamic analysis; and EBM: energy-based method.

In a direct dynamic analysis the equations of motion are solved over discrete time steps with allow the complete time history response of the structure to be calculated, i.e. linear or nonlinear time history analysis. Since the dynamic effects are explicitly considered there is no requirement to define a dynamic amplification factor. It is uncommon to perform a linear dynamic analysis because of the inability to account for material and geometric nonlinearities and the requirement to stay in the elastic regime, although dynamic effects such as damping can be considered. Nonlinear dynamic analyses have the highest level of complexity but they allow considering the dynamic effects, such as damping (Tsai and Lin, 2008; Xu and Ellingwood, 2011) and strain-rate effects (Stoddart *et al.*, 2013; Olmati *et al.*, 2017; Russell *et al.*, 2019). Therefore, the nonlinear dynamic procedure is currently the most accurate way to perform an analysis for a sudden column removal scenario. However, the nonlinear dynamic analyses are time consuming and require detailed information in order to achieve accurate results (Russell *et al.*, 2015).

Alternatively, the energy-based method (EBM) can be adopted to approximate the maximum dynamic response on the basis of the nonlinear static analysis result. This technique is based on the energy balance of the system, where the potential energy released by the column removal is compared against the energy absorption

capability of the structure. The method allows analysis at various levels of structural idealisation, from substructures (Tsai, 2010; Pham *et al.*, 2017b; Qian and Li, 2017b) to entire structural systems (Tsai and Lin, 2008; Xu and Ellingwood, 2011; Yu *et al.*, 2017). The nonlinear static load-deflection curve (pushdown curve in Figure III.11) is obtained by gradually applying the gravitational loads in a nonlinear static analysis. Based on the pushdown curve, a simplified dynamic assessment (as shown in Figure III.11) is conducted to transform the nonlinear static response into the maximum dynamic response by considering the energy balance between the work done by the load and the internal energy stored within the structure (Izzuddin *et al.*, 2008; Herraiz *et al.*, 2015). It should be noted that although the static capacity curve and the EBM curve are frequently illustrated in the same graph further in this work, their background is different and hence one should be careful with its interpretation, e.g. when considering loads corresponding to a specific value of displacement.

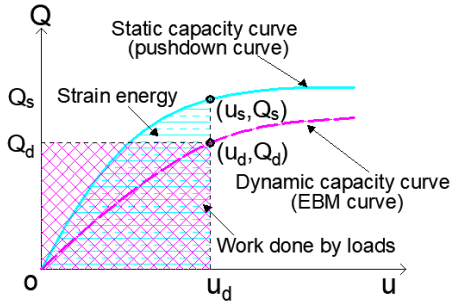

Figure III.11. EBM: energy balance (The static capacity curve is obtained from a static pushdown analysis, and the dynamic capacity curve is calculated from the EBM).

The EBM does not require an estimation of the dynamic amplification factor to predict the dynamic response (Table III.1), i.e. the use of dynamic amplification factor is avoided. Moreover, no nonlinear dynamic analyses are required and therefore it requires much less computational demand. The EBM is becoming a more and more used tool in progressive collapse analyses. For example, in order to evaluate the structural robustness of two 10-storey RC buildings subjected to different column loss scenarios in (Bao *et al.*, 2017), the NSA, EBM and NDA were adopted. The EBM (derived from the load-displacement curve obtained from NSA) and NDA were applied to calculate the dynamic capacities. The results showed that a good agreement between EBM and NDA was obtained, although the ultimate capacities estimated using the EBM were found to be slightly conservative. Some more studies in relation to the use of the EBM can be found in (Marjanishvili, 2004; Marjanishvili and Agnew, 2006; Izzuddin *et al.*, 2008; Tsai and Lin, 2008; Tsai, 2011; Herraiz *et al.*, 2015; Liu and Pirmoz, 2016; Yu *et al.*, 2017; Huang *et al.*, 2021).

As shown in Table III.1, the dynamic effects such as strain rate effects and damping effects cannot be considered in the EBM. Therefore, the EBM results in an approximate result. On the other hand, the EBM may not be suitable to calculate the dynamic response if the response does not satisfy a single deformation mode. Although the EBM has been widely used, a systematic investigation on the performance of the EBM is still lacking. However, the calculation demand can be significantly reduced if the EBM is adapted to replace the direct dynamic analyses for structural robustness quantification. Hence, the evaluation of the performance of the EBM, as a promising approach to calculate the maximum dynamic response, is one of the topics of this thesis.

III.3.2 Numerical FE modelling approaches

The progressive collapse of building structures involves nonlinearities and dynamic effects, which is a complex phenomenon. Different numerical modelling techniques have been developed. The following numerical modelling techniques are used in literature: finite element (FE) method (Bao *et al.*, 2017; Russell *et al.*, 2019), discrete element method (Masoero *et al.*, 2010; Masoero *et al.*, 2012), applied element method (Sasani, 2008; Zheng *et al.*, 2020), and cohesive element method (Le and Xue, 2014).

The FE method technique is the most widely used approach in relation to the simulation of progressive collapse of RC building structures (Adam *et al.*, 2018; Kiakojouri *et al.*, 2020). The FE method includes micro-based FE modelling techniques (with continuum solid elements), macro-based FE modelling techniques (with beam/shell elements and macro-level beam-column joints), and hybrid models. Considering this technique will be adopted in this dissertation, the following review will focus on the FE modelling method with respect to progressive collapse studies.

III.3.2.1 Micro-based FE model and macro-based FE model

The micro-based FE modelling technique (or detailed model) with continuum solid elements are very powerful, and can be used to simulate complex geometries with high accuracy. For example, the detailed response of concrete cracking and crushing, reinforcement yielding and fracture, and the bond behaviour between reinforcement and neighbouring concrete can be taken into account. However, this approach usually has a very high computational cost. Hence, it is frequently adopted to simulate parts of structures (or subassemblies) but not often used to simulate entire structural systems, e.g. (Li *et al.*, 2016; Peng *et al.*, 2017; Pham *et al.*, 2017a; Pham *et al.*, 2017b; Russell *et al.*, 2019; Qian *et al.*, 2020; Yu *et al.*, 2020).

The macro-based FE modelling technique (or reduced model) with beam/shell elements are more suitable to be adopted to simulate entire RC buildings. The beam-type elements with fibre sections are often used to simulate beams and columns, while the shell elements are employed to model floor slabs or shear walls. Moreover, different types of macro-level joint models have also been developed and can be applied to simulate the structural progressive collapse together with the beam/shell elements. This approach has high computational efficiency and therefore is frequently adopted for the progressive collapse and robustness calculations, e.g. (Marjanishvili and Agnew, 2006; Bao *et al.*, 2008; Tsai and Lin, 2008; Bao *et al.*, 2012; Lu *et al.*, 2013; Brunesi and Nascimbene, 2014; Brunesi *et al.*, 2015; Feng *et al.*, 2016; Bao *et al.*, 2017; Bermejo *et al.*, 2017; Yu *et al.*, 2017; Kunnath *et al.*, 2018; Parisi and Scalvenzi, 2020).

Both micro and macro-based FE approaches can accurately analyse the RC building structures subjected to column removal scenarios. Bao *et al.* (2012) investigated and compared the performance of the two types of FE modelling techniques (i.e. micro-based and macro-based FE models) for two RC beam-column assemblies subjected to monotonically increasing vertical displacement of the unsupported centre column simulating a column removal scenario. All analyses were carried out using explicit time integration in LS-DYNA (Hallquist, 2007). The detailed model - with high refined solid and beam elements to represent the nonlinear material behaviour of structural components - is shown in Figure III.12a, while the reduced-order models with significantly fewer beam and spring elements is shown in Figure III.12b. The former included over 60,000 solid and beam elements, while the latter was a reduced model with only around 80 beam and spring elements. The two specimens were analysed using both the detailed and reduced models and the experimental test results were adopted to validate the obtained results. The obtained results of both models shown that both detailed and reduced models were able to capture the primary response characteristics and failure modes. For example, in case of one specimen the obtained final deflected shapes and failure modes from the two models were almost identical, see Figure III.13, as well as consistent with those in the experimental test.

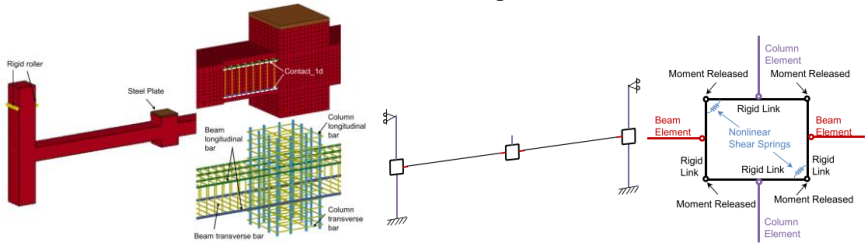

(a) Micro-based model (b) Macro-based model

Figure III.12. Comparison study between micro-based and macro-based FE models using LS-DYNA (Bao et al., 2012).

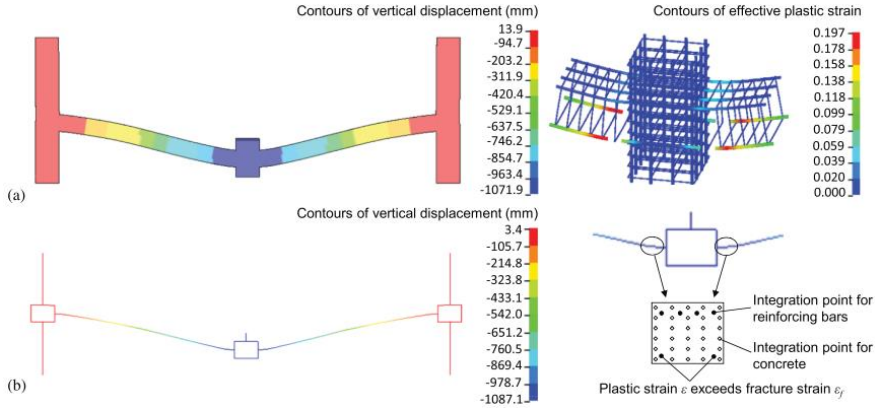

Figure III.13. Deflected shape and failure mode of one specimen: (a) micro-based FE model at a centre column vertical displacement of 1,072 mm; and (b) macro-based FE model at a centre column vertical displacement of 1,087 mm (Bao et al., 2012).

III.3.2.2 Hybrid FE model

Hybrid models (or multi-scale models) consider different parts of a structure on different scales (Droogné *et al.*, 2018) or use different solvers at different calculating stages (Xu *et al.*, 2013; Xu *et al.*, 2014; Zheng *et al.*, 2020). This approach is aimed at reducing the computational cost. Meanwhile, both the overall structural behaviour and local nonlinear damages can be well reflected. However, one of the critical issues in this approach is to appropriately model the interaction between the different types of elements or the different modelling scales, ensuring deformation compatibility and correct constraint conditions (Adam *et al.*, 2018). For example, a computational efficient calculation scheme, which considers different levels of structural idealization, has been developed in (Droogné *et al.*, 2018) to quantify the robustness of planar RC frames using a conditional risk-based robustness index. In the multilevel calculation scheme for structural reliability assessment, the structure subjected to a notional central column removal scenario was subdivided into the directly affected part (DAP) and indirectly affected part (IAP). The DAP consisted of the bay immediately above the removed column, while the IAP included the remainder of the frame. For the two parts, the robustness calculations were carried out at different levels of structural idealization in order to reduce the computational efforts. Detailed modelling using a nonlinear FE model (software package DIANA) was considered for low levels of structural idealization (i.e. DAP) in order to account accurately for the nonlinear response of the structural elements, where both geometrical and material nonlinear behaviours were considered, see the left branch in Figure III.14. On the other hand, simplified modelling based on a plastic analysis of an assumed failure mode was applied at

higher levels of structural idealizations (i.e. IAP), see the right branch in Figure III.14. As an implementation of the multi-level calculation scheme, the failure probabilities of progressive collapse of the structural frames were first calculated separately for the DAP and the IAP. Finally, the probabilities of progressive collapse in relation to the structural systems were calculated by combining previous obtained results, see Figure III.14.

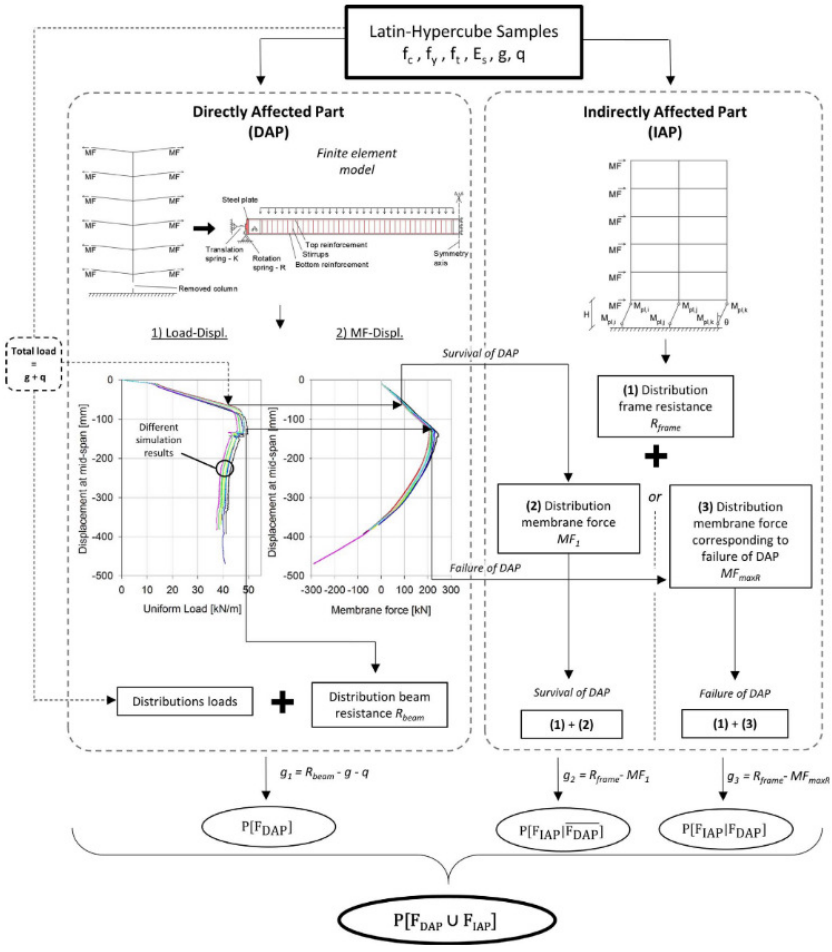

Figure III.14. Developed multi-level calculation scheme in (Droogné et al., 2018).

III.4 Summary and discussion

Both experimental tests and numerical simulations on RC building structures subjected to column removal scenarios have been reviewed. Considering the uncertainty in accurately defining the accidental loads, threat-independent alternate

load path approaches are more commonly used to evaluate the progressive collapse resistance of RC buildings. In this approach, the initiating loading event leading to initial structural damaged is not modelled but the effects of the damage are considered.

A limited amount of large-scale experimental tests have been carried out including mainly on the following structural idealization levels: RC subassemblies (e.g. beam-column, beam-column-slab and flat slab specimens); RC 2D planar frames; RC 3D building structures (purpose-built for research); and existing structures. The alternate load paths or secondary load-carrying mechanisms can be developed to provide additional load-bearing capacities to resist progressive collapse, e.g. Vierendeel (frame) action, tensile catenary (or membrane) action, and compressive arch action. Large deformations are observed and hence the material and geometrical nonlinearities are required to be considered in numerical simulations. In addition, the experimental tests are of great value for the validation of numerical models.

The experimental tests have been carried out in two manners: quasi-static loading and dynamic loading. Both approaches can be used to investigate progressive collapse mechanisms of RC building structures. Comparing to the static test results, the dynamic test results may show more damage. Moreover, static approaches are limited in their ability to realistically simulate the sudden load redistribution when a structure is subjected to a sudden column removal scenario. Apart from experimental tests, the numerical simulation approach is an efficient tool and will be used in this dissertation.

The numerical simulations can be conducted in either static or dynamic procedures. In general the following five procedures are reported: linear static analysis, nonlinear static analysis, linear dynamic analysis, nonlinear dynamic analysis, and the energy-based method (EBM). Dynamic effects are required to be considered for all the procedures. For the linear and nonlinear static analyses, a dynamic amplification factor is required to approximately account for the nonlinearities and/or dynamic effects. However, the dynamic amplification factor is a function of the structural damage level and imposed loading. This may result in conservative results. The linear dynamic analysis is less used, since the inability to consider the nonlinearities. The nonlinear dynamic analysis is the most accurate approach but the computational cost may be high. Alternatively, the EBM can be used to approximate the maximum dynamic response without the use of the dynamic amplification factor. Although it has been adopted in some studies, a systematic evaluation of the performance of the EBM is missing in literature. Moreover, the performance of the EBM in very large deformation situations is yet to be investigated in relation to progressive collapse analysis. If the EBM can be used

for dynamic calculations with regard to structural robustness quantification, the calculation demand can be significantly reduced.

The FE modelling technique is widely used to perform progressive collapse analyses. This approach can be implemented in three manners: micro-based FE models (with continuum elements), macro-based FE models (with beam/shell elements and macro-level beam-column joints), and hybrid models. All of the three approaches will be used for progressive collapse simulations in this dissertation. The micro-based FE models (detailed model) are more often used for the simulation of substructures, while the macro-based models (reduced-order model) are more suitable for the calculation of entire buildings as less elements are required. Also hybrid models can be adopted to reduce the computational cost. Considering the reduction of calculation demand, macro-based and hybrid FE models are considered as the most efficient tools for structural robustness evaluations in a probabilistic manner.

III.5 References

Abaqus (2014) ABAQUS user's manual. Version 6.14. ABAQUS Providence, RI.

Adam JM, Buitrago M, Bertolesi E, et al. (2020) Dynamic performance of a real-scale reinforced concrete building test under a corner-column failure scenario. Engineering Structures 210:110414.

Adam JM, Parisi F, Sagaseta J, et al. (2018) Research and practice on progressive collapse and robustness of building structures in the 21st century. Engineering Structures 173:122-149.

Alshaikh IMH, Abu Bakar BH, Alwesabi EAH, et al. (2020) Experimental investigation of the progressive collapse of reinforced concrete structures: An overview. Structures 25:881-900.

Bao Y, Kunnath SK, El-Tawil S, et al. (2008) Macromodel-based simulation of progressive collapse: RC frame structures. Journal of Structural Engineering 134:1079-1091.

Bao Y, Lew HS, Kunnath SK (2012) Modeling of reinforced concrete assemblies under column-removal scenario. Journal of Structural Engineering 140:04013026.

Bao Y, Main JA, Noh SY (2017) Evaluation of structural robustness against column loss: Methodology and application to RC frame buildings. Journal of Structural Engineering 143:04017066.

Bermejo M, Santos AP, Goicolea JM (2017) Development of practical finite element models for collapse of reinforced concrete structures and experimental validation. Shock and Vibration 2017:1-9.

Biagi VD, Kiakojouri F, Chiaia B, et al. (2020) A simplified method for assessing the response of RC frame structures to sudden column removal. Applied Sciences 10:3081.

Botte W (2017) Quantification of structural reliability and robustness of new and existing concrete structures considering membrane action. PhD diss. Ghent University.

Brunesi E, Nascimbene R (2014) Extreme response of reinforced concrete buildings through fiber force-based finite element analysis. Engineering Structures 69:206-215.

Brunesi E, Nascimbene R, Parisi F, et al. (2015) Progressive collapse fragility of reinforced concrete framed structures through incremental dynamic analysis. Engineering Structures 104:65-79.

Byfield M, Mudalige W, Morison C, et al. (2014) A review of progressive collapse research and regulations. Proceedings of the Institution of Civil Engineers-Structures and Buildings 167:447-456.

Cai J, Xu Y, Zhuang L, et al. (2012) Comparison of various procedures for progressive collapse analysis of cable-stayed bridges. Journal of Zhejiang University SCIENCE A 13:323-334.

Diana (2017) Diana User's Manual, Release 10.1. Delft The Netherlands.

DoD (2016) Design of buildings to resist progressive collapse. Unified Facilities Criteria (UFC) 4-023-03.

Droogné D, Botte W, Caspeele R (2018) A multilevel calculation scheme for risk-based robustness quantification of reinforced concrete frames. Engineering Structures 160:56-70.

El-Tawil S, Li HH, Kunnath S (2014) Computational simulation of gravity-induced progressive collapse of steel-frame buildings: Current trends and future research needs. Journal of Structural Engineering 140:A2513001.

Elsanadedy HM, Almusallam TH, Al-Salloum YA, et al. (2017) Investigation of precast RC beam-column assemblies under column-loss scenario. Construction and Building Materials 142:552-571.

Feng D-C, Xie S-C, Ning C-L, et al. (2019) Investigation of modeling strategies for progressive collapse analysis of RC frame structures. Journal of Performance of Constructed Facilities 33:04019063.

Feng D, Kolay C, Ricles JM, et al. (2016) Collapse simulation of reinforced concrete frame structures. The Structural Design of Tall and Special Buildings 25:578-601.

Foster SJ, Bailey CG, Burgess IW, et al. (2004) Experimental behaviour of concrete floor slabs at large displacements. Engineering Structures 26:1231-1247.

Gouverneur D, Caspeele R, Taerwe L (2013) Experimental investigation of the load-displacement behaviour under catenary action in a restrained reinforced concrete slab strip. Engineering Structures 49:1007-1016.

GSA (2016) Alternate path analysis and design guidelines for progressive collapse resistance. General Services Administration. Office of the Chief Architect Washington, DC.

Hallquist JO (2007) LS-DYNA keyword user's manual. Livermore Software Technology Corporation 970:299-800.
Herraiz B, Vogel T, Russell J (2015) Energy-based method for sudden column failure scenarios: theoretical, numerical and experimental analysis IABSE Workshop Helsinki 2015: Safety, Robustness and Condition Assessment of Structures. International Association for Bridge and Structural Engineering IABSE, pp. 70-77.
Huang M, Huang H, Hao R, et al. (2021) Studies on secondary progressive collapse - resistance mechanisms of reinforced concrete subassemblages. Structural Concrete:1-17.
Izzuddin BA, Nethercot DA (2009) Design-oriented approaches for progressive collapse assessment: Load-factor vs. Ductility-centred methods Structures Congress 2009: Don't Mess with Structural Engineers: Expanding Our Role. pp. 1-10.
Izzuddin BA, Vlassis AG, Elghazouli AY, et al. (2008) Progressive collapse of multi-storey buildings due to sudden column loss - Part I: Simplified assessment framework. Engineering Structures 30:1308-1318.
Kiakojouri F, De Biagi V, Chiaia B, et al. (2020) Progressive collapse of framed building structures: Current knowledge and future prospects. Engineering Structures 206:110061.
Kokot S, Anthoine A, Negro P, et al. (2012) Static and dynamic analysis of a reinforced concrete flat slab frame building for progressive collapse. Engineering Structures 40:205-217.
Kunnath SK, Bao YH, El-Tawil S (2018) Advances in computational simulation of gravity-induced disproportionate collapse of RC frame buildings. Journal of Structural Engineering 144:03117003.
Kwasniewski L (2010) Nonlinear dynamic simulations of progressive collapse for a multistory building. Engineering Structures 32:1223-1235.
Le JL, Xue B (2014) Probabilistic analysis of reinforced concrete frame structures against progressive collapse. Engineering Structures 76:313-323.
Li S, Shan S, Zhai C, et al. (2016) Experimental and numerical study on progressive collapse process of RC frames with full-height infill walls. Engineering Failure Analysis 59:57-68.
Liu M, Pirmoz A (2016) Energy-based pulldown analysis for assessing the progressive collapse potential of steel frame buildings. Engineering Structures 123:372-378.
Lu X, Lin K, Li Y, et al. (2017) Experimental investigation of RC beam-slab substructures against progressive collapse subject to an edge-column-removal scenario. Engineering Structures 149:91-103.
Lu X, Lu XZ, Guan H, et al. (2013) Collapse simulation of reinforced concrete high-rise building induced by extreme earthquakes. Earthquake engineering & structural dynamics 42:705-723.

Ma F, Gilbert BP, Guan H, et al. (2020) Experimental study on the progressive collapse behaviour of RC flat plate substructures subjected to edge-column and edge-interior-column removal scenarios. Engineering Structures 209:110299.

Ma F, Gilbert BP, Guan H, et al. (2019) Experimental study on the progressive collapse behaviour of RC flat plate substructures subjected to corner column removal scenarios. Engineering Structures 180:728-741.

Marjanishvili S, Agnew E (2006) Comparison of various procedures for progressive collapse analysis. Journal of Performance of Constructed Facilities 20:365-374.

Marjanishvili SM (2004) Progressive analysis procedure for progressive collapse. Journal of Performance of Constructed Facilities 18:79-85.

Masoero E, Wittel FK, Herrmann HJ, et al. (2010) Progressive collapse mechanisms of brittle and ductile framed structures. Journal of Engineering Mechanics 136:987-995.

Masoero E, Wittel FK, Herrmann HJ, et al. (2012) Hierarchical structures for a robustness-oriented capacity design. Journal of Engineering Mechanics 138:1339-1347.

Matthews T, Elwood KJ, Hwang S-J (2007) Explosive testing to evaluate dynamic amplification during gravity load redistribution for reinforced concrete frames. Structural Engineering Research Frontiers:1-14.

Olmati P, Sagaseta J, Cormie D, et al. (2017) Simplified reliability analysis of punching in reinforced concrete flat slab buildings under accidental actions. Engineering Structures 130:83-98.

OpenSees (2006) Open system for earthquake engineering simulation. University of California, Berkeley.

Orton SL, Kirby JE (2014) Dynamic Response of a RC Frame under Column Removal. Journal of Performance of Constructed Facilities 28:04014010.

Parisi F, Scalvenzi M (2020) Progressive collapse assessment of gravity-load designed European RC buildings under multi-column loss scenarios. Engineering Structures 209:110001.

Peng Z, Orton SL, Liu J, et al. (2017) Experimental study of dynamic progressive collapse in flat-plate buildings subjected to exterior column removal. Journal of Structural Engineering 143:04017125.

Peng ZH, Orton SL, Liu JR, et al. (2018) Experimental study of dynamic progressive collapse in flat-plate buildings subjected to an interior column removal. Journal of Structural Engineering 144:04018094.

Pham AT, Lim NS, Tan KH (2017a) Investigations of tensile membrane action in beam-slab systems under progressive collapse subject to different loading configurations and boundary conditions. Engineering Structures 150:520-536.

Pham AT, Tan KH, Yu J (2017b) Numerical investigations on static and dynamic responses of reinforced concrete sub-assemblages under progressive collapse. Engineering Structures 149:2-20.
Pujol S, Smith-Pardo JP (2009) A new perspective on the effects of abrupt column removal. Engineering Structures 31:869-874.
Qian K, Li B (2012a) Dynamic performance of RC beam-column substructures under the scenario of the loss of a corner column—Experimental results. Engineering Structures 42:154-167.
Qian K, Li B (2012b) Experimental and analytical assessment on RC interior beam-column subassemblages for progressive collapse. Journal of Performance of Constructed Facilities 26:576-589.
Qian K, Li B (2012c) Slab effects on response of reinforced concrete substructures after loss of corner column. ACI Structural Journal 109:845-855.
Qian K, Li B (2013a) Experimental study of drop-panel effects on response of reinforced concrete flat slabs after loss of corner column. ACI Structural Journal 110:319.
Qian K, Li B (2013b) Performance of three-dimensional reinforced concrete beam-column substructures under loss of a corner column scenario. Journal of Structural Engineering 139:584-594.
Qian K, Li B (2014) Quantification of slab influences on the dynamic performance of RC frames against progressive collapse. Journal of Performance of Constructed Facilities 29:04014029.
Qian K, Li B (2017a) Dynamic and residual behavior of reinforced concrete floors following instantaneous removal of a column. Engineering Structures 148:175-184.
Qian K, Li B (2017b) Effects of masonry infill wall on the performance of RC frames to resist progressive collapse. Journal of Structural Engineering 143:04017118.
Qian K, Li B (2019) Investigation into resilience of precast concrete floors against progressive collapse. ACI Structural Journal 116:171-182.
Qian K, Li B, Ma JX (2014) Load-carrying mechanism to resist progressive collapse of rc buildings. Journal of Structural Engineering 141:04014107.
Qian K, Li B, Tian Y (2016) Recent progress in understanding of load resisting mechanisms for mitigating progressive collapse. Special Publication 309:1-18.
Qian K, Liang S-L, Fu F, et al. (2021) Progressive collapse resistance of emulative precast concrete frames with various reinforcing details. Journal of Structural Engineering 147:04021107.
Qian K, Weng Y-H, Li B (2018) Impact of two columns missing on dynamic response of RC flat slab structures. Engineering Structures 177:598-615.
Qian LP, Li Y, Diao MZ, et al. (2020) Experimental and computational assessments of progressive collapse resistance of reinforced concrete

planar frames subjected to penultimate column removal scenario. Journal of Performance of Constructed Facilities 34:04020019.
Qing-Feng, HW-J Yi, Yan Xiao, et al. (2009) Experimental study of progressive collapse due to sudden column removal. The First International Conference on Computational Technologies in Concrete Structures(CTCS'09).
Ren P, Li Y, Lu X, et al. (2016) Experimental investigation of progressive collapse resistance of one-way reinforced concrete beam–slab substructures under a middle-column-removal scenario. Engineering Structures 118:28-40.
Russell JM, Owen JS, Hajirasouliha I (2015) Experimental investigation on the dynamic response of RC flat slabs after a sudden column loss. Engineering Structures 99:28-41.
Russell JM, Owen JS, Hajirasouliha I (2019) Dynamic column loss analysis of reinforced concrete flat slabs. Engineering Structures 198:109453.
Sasani M (2008) Response of a reinforced concrete infilled-frame structure to removal of two adjacent columns. Engineering Structures 30:2478-2491.
Sasani M, Bazan M, Sagiroglu S (2007) Experimental and analytical progressive collapse evaluation of actual reinforced concrete structure. ACI Structural Journal 104:731.
Sasani M, Kazemi A, Sagiroglu S, et al. (2011) Progressive collapse resistance of an actual 11-story structure subjected to severe initial damage. Journal of Structural Engineering 137:893-902.
Sasani M, Sagiroglu S (2008) Progressive collapse resistance of hotel San Diego. Journal of Structural Engineering 134:478-488.
Sasani M, Sagiroglu S (2010) Gravity load redistribution and progressive collapse resistance of 20-story reinforced concrete structure following loss of interior column. ACI Structural Journal 107:636-644.
Shan S, Li S, Xu S, et al. (2016) Experimental study on the progressive collapse performance of RC frames with infill walls. Engineering Structures 111:80-92.
Stinger SM, Orton SL (2013) Experimental evaluation of disproportionate collapse resistance in reinforced concrete frames. ACI Structural Journal 110:521-529.
Stoddart EP, Byfield MP, Davison JB, et al. (2013) Strain rate dependent component based connection modelling for use in non-linear dynamic progressive collapse analysis. Engineering Structures 55:35-43.
Tsai M-H (2011) Analytical load and dynamic increase factors for progressive collapse analysis of building frames AEI 2011: Building Integration Solutions. pp. 172-179.
Tsai MH (2010) An analytical methodology for the dynamic amplification factor in progressive collapse evaluation of building structures. Mechanics Research Communications 37:61-66.

Tsai MH, Lin BH (2008) Investigation of progressive collapse resistance and inelastic response for an earthquake-resistant RC building subjected to column failure. Engineering Structures 30:3619-3628.
Wang T, Chen Q, Zhao H, et al. (2016a) Experimental study on progressive collapse performance of frame with specially shaped columns subjected to middle column removal. Shock and Vibration 2016:1-13.
Wang T, Zhang L, Zhao H, et al. (2016b) Progressive collapse resistance of reinforced-concrete frames with specially shaped columns under loss of a corner column. Magazine of Concrete Research 68:435-449.
Weng J, Lee CK, Tan KH, et al. (2017) Damage assessment for reinforced concrete frames subject to progressive collapse. Engineering Structures 149:147-160.
Xiao Y, Kunnath S, Li FW, et al. (2015) Collapse test of three-story half-scale reinforced concrete frame building. ACI Structural Journal 112.
Xiao Y, Zhao YB, Li FW, et al. (2013) Collapse test of a 3-story half-scale RC frame structure Structures Congress 2013: Bridging Your Passion with Your Profession. pp. 11-19.
Xu GQ, Ellingwood BR (2011) An energy-based partial pushdown analysis procedure for assessment of disproportionate collapse potential. Journal of Constructional Steel Research 67:547-555.
Xu Z, Lu X, Guan H, et al. (2014) Seismic damage simulation in urban areas based on a high-fidelity structural model and a physics engine. Natural hazards 71:1679-1693.
Xu Z, Lu X, Guan H, et al. (2013) Physics engine-driven visualization of deactivated elements and its application in bridge collapse simulation. Automation in construction 35:471-481.
Yap SL, Li B (2011) Experimental investigation of reinforced concrete exterior beam-column subassemblages for progressive collapse. ACI Structural Journal 108:542-552.
Yi W-J, Zhang F-Z, Kunnath SK (2014) Progressive collapse performance of RC flat plate frame structures. Journal of Structural Engineering 140:04014048.
Yi WJ, He QF, Xiao Y, et al. (2008) Experimental study on progressive collapse-resistant behavior of reinforced concrete frame structures. ACI Structural Journal 105:433-439.
Yu J, Rinder T, Stolz A, et al. (2014) Dynamic progressive collapse of an RC assemblage induced by contact detonation. Journal of Structural Engineering 140:04014014.
Yu J, Tan K-H (2013a) Experimental and numerical investigation on progressive collapse resistance of reinforced concrete beam column sub-assemblages. Engineering Structures 55:90-106.

Yu J, Tan KH (2013b) Structural behavior of RC beam-column subassemblages under a middle column removal scenario. Journal of Structural Engineering 139:233-250.

Yu J, Tang J-h, Luo L-z, et al. (2020) Effect of boundary conditions on progressive collapse resistance of RC beam-slab assemblies under edge column removal scenario. Engineering Structures 225:111272.

Yu XH, Qian K, Lu DG, et al. (2017) Progressive collapse behavior of aging reinforced concrete structures considering corrosion effects. Journal of Performance of Constructed Facilities 31:04017009.

Zhang L, Zhao H, Wang T, et al. (2016) Parametric analysis on collapse-resistance performance of reinforced-concrete frame with specially shaped columns under loss of a corner column. The Open Construction & Building Technology Journal 10:466-480.

Zheng Z, Tian Y, Yang ZB, et al. (2020) Hybrid framework for simulating building collapse and ruin scenarios using finite element method and physics engine. Applied Sciences-Basel 10:4408.

PART B

THE ENERGY-BASED METHOD FOR DYNAMIC COLUMN REMOVAL SCENARIOS IN RC STRUCTURES

CHAPTER IV

Deterministic modelling of RC structures subjected to column removal scenarios

Partly redrafted after:

Ding L, Van Coile R, Botte W & Caspeele R, *"Quantification of model uncertainties of the energy-based method for dynamic column removal scenarios",* Engineering Structures, 237 (2021):112057

Ding L, Van Coile R, Botte W & Caspeele R, *"Performance assessment of an energy–based approximation method for the dynamic capacity of RC frames subjected to sudden column removal scenarios",* Applied Sciences, 11 (2021): 7492.

IV.1 Introduction

The alternate load path (ALP) method is a widely adopted method to evaluate the potential of progressive collapse due to the fact that it can represent a realistic structural response resulting from a local damage (Subki *et al.*, 2019; Parisi and Scalvenzi, 2020). Most often this method is implemented as a threat-independent method meaning that it does not explicitly consider the event that causes the initial damage, only its (conditional) consequences. This improves the practical applicability due to the fact that it is often difficult to identify and model the extreme events explicitly.

Dynamic effects (inertial effect, damping and strain rate effect etc.) should be taken into account in the threat-independent ALP method since the phenomenon of progressive collapse is a dynamic event in case of a sudden column removal scenario (DoD, 2016; Adam *et al.*, 2020; Parisi and Scalvenzi, 2020). However, a dynamic nonlinear time history analysis (NTHA) is computationally cumbersome as both nonlinearities and dynamic effects need to be included. Although the NTHA can provide a more accurate response prediction, it requires analysts to have significant numerical expertise to perform the analysis and has heavy computational demands. Such expertise is not commonly acquired by practicing engineers (Xu and Ellingwood, 2011; Subki *et al.*, 2019). Therefore, as an alternative, a static analysis considering a dynamic amplification factor (DAF) is often employed (DoD, 2009; Tsai, 2011; Byfield *et al.*, 2014; GSA, 2016), which can reduce the computational efforts. However, the DAF depends both on the loading level and the nature of the nonlinear behaviour (Izzuddin *et al.*, 2008; Xu and Ellingwood, 2011) and the use of DAF is associated with considerable model uncertainties as the empirical DAF equations are typically obtained from a curve-fitting process (Tsai, 2010; Liu, 2013; Liu and Pirmoz, 2016). The result may lead to a considerable bias (Izzuddin and Nethercot, 2009).

Alternatively, the energy-based method (EBM) has been developed as an alternative approach (Izzuddin *et al*., 2008; Xu and Ellingwood, 2011; Byfield *et al*., 2014). The EBM is based on the principle of energy conservation, where the resistance against progressive collapse is assessed based on the capability of absorbing and dissipating the energy introduced by the unbalanced loads (Izzuddin *et al.*, 2008; Xu and Ellingwood, 2011; Liu and Pirmoz, 2016). No dynamic analyses are needed and the use of DAF is avoided (Dusenberry and Hamburger, 2006; Izzuddin *et al.*, 2008; Liu and Pirmoz, 2016). In the early 1950's, Newmark (Newmark, 1953) formally described this concept for design in relation to blast loading. This kind of approach has since then been further developed and used for column removal scenarios (Powell, 2005; Dusenberry and Hamburger, 2006; Tsai and Lin, 2008; Szyniszewski and Krauthammer, 2012; Main, 2014; Herraiz *et al.*, 2015; Kim *et al.*, 2015; Yu *et al.*, 2017; Naji, 2019; Huang *et al.*, 2021), where good performance has been found for structural response predictions as obtained

from the EBM in comparison to direct dynamic response calculations (Izzuddin *et al*., 2008; Tsai and Lin, 2008; Xu and Ellingwood, 2011; Bao *et al*., 2017).

Although the EBM is based on several simplifications that lead to an approximate result, it is a compromise between accuracy and complexity. The NTHA is not carried out in the EBM, since it only consists of performing a static nonlinear pushdown analysis and subsequently predicts the maximum dynamic response through an energy balance. Therefore, dynamic effects are not explicitly taken into account in the EBM. Bao *et al.* (2017), for example, compared the results from the EBM to the results of direct dynamic analyses for two 10-storey RC frames subjected to middle column removal scenarios, and found a good agreement between both. Similarly, Xu and Ellingwood (2011) applied the EBM to approximate the maximum dynamic responses of two steel moment-resisting frames, where it was found that the EBM results were close to the results of nonlinear dynamic time history analyses. The influence of the dynamic effects on the performance of the EBM is however not yet well understood, and some studies directly apply the EBM without validation against nonlinear dynamic analyses. Yu *et al.* (2017), for example, used the EBM to calculate the time-dependent dynamic responses in relation to four ageing RC structures subjected to middle column loss scenarios, although the results of the EBM were not compared with any results from direct dynamic analyses. Herraiz *et al.* (2015) investigated the influence of dynamic effects on the performance of the EBM but only for some simplified models such as a single-degree-of-freedom (SDOF) system, see also (Herraiz and Vogel, 2014). Furthermore, the influence of damping effects on the performance of EBM is not clarified yet in literature, as the modelling of damping in the context of progressive collapse is still a controversial issue (Herraiz *et al*., 2015; Zheng *et al*., 2020). In addition, the existing studies in relation to the use of the EBM were only applied to the case of a structure subjected to a middle column removal scenario, such as (Izzuddin *et al*., 2008a; Tsai and Lin, 2008; Xu and Ellingwood, 2011; Bao *et al*., 2017; Parisi *et al*., 2019), where the assumption of a single deformation mode was usually satisfied. However, in case of an exterior column removal scenario which is more critical as less alternate load paths can be developed (Feng *et al.*, 2019b; Adam *et al.*, 2020; Biagi *et al.*, 2020), the effectiveness of the EBM has not yet been investigated comprehensively although the single deformation mode may be more difficult to be ensured.

Considering the above overview of the state of the art in this research field, the EBM can be a promising alternative to perform a dynamic analysis (through predicting maximum dynamic response) with significantly less calculation demand in the context of a sudden column removal scenario. The influences of dynamic effects i.e. strain rate dependency effects, damping effects, column removal durations, which are not taken into account in the EBM, need to be investigated to

evaluate the effectiveness of the EBM both in the bending mechanism stage (small deformation), in the compressive membrane/arching action stage, and in the tensile membrane/catenary action stage (large deformation). The performance of the EBM in relation to a structure subjected to an exterior column removal scenario requires to be investigated as the assumption of a single deformation may not be satisfied.

In the present thesis, the two types of finite element (FE) models, as mentioned in the previous chapter, are used to simulate the progressive collapse of RC structures: the highly detailed micro-based FE model (i.e. continuous solid elements) and the more efficient macro-based FE model (i.e. fibre beam elements). The former has the best adaptability and precision for investigating various kinds of behaviour. With regard to larger/more complex models such as multiple-storey and multiple-bay frames with a large number of degrees of freedom in which demands on computational resources and solution time make the use of the micro-based FE model impractical, the macro-based modelling approach is much more efficient for global-level structural performance evaluation with regard to progressive collapse simulations and has been adopted in several studies (Bao *et al.*, 2008; Brunesi and Nascimbene, 2014; Parisi *et al.*, 2019; Parisi and Scalvenzi, 2020). For the micro-based FE model developed in the present thesis, the Abaqus 6.14 (Abaqus, 2014) software package is used in order to get detailed responses, while for the macro-based FE model the open-source software package OpenSees (Open System for Earthquake Engineering Simulation) (OpenSees, 2006) is adopted in order to reduce calculation demands. Both numerical FE modelling techniques are adopted to evaluate the performance of the EBM approach in this chapter in a deterministic manner through two numerical examples of RC building structures:

- Numerical example A: a full-scale RC slab subjected to a notional sudden central support removal scenario using the highly detailed micro-based FE modelling technique; and
- Numerical example B: a RC frame subjected to different column removal scenarios (one exterior and two interior column removal scenarios), adopting the macro-based FE modelling technique.

In this chapter first the methodology of EBM is introduced (section IV.2). Subsequently section IV.3 investigates the performance of the EBM in the large deformation stage and in case of concentrated loading regarding the RC slab, while section IV.4 focuses on evaluating the performance of the EBM with regard to different column removal scenarios and in case of uniformly distributed loading for the RC frame. Finally, some concluding remarks and a brief summary are provided in section IV.5.

IV.2 The energy-based method

IV.2.1 Conservation of energy during collapse

Progressive collapse of structures is a dynamic process, for example caused by the sudden removal of a column in a building structure as shown in Figure IV.1a. The new unbalanced gravity loads result in a release of potential energy for the structural system. The release of potential energy in the first instance leads to dynamic motions and an increase of kinetic energy. In contrast, strain energy accumulating in the deforming structure dissipate the kinetic energy, counteracting the movement. Neglecting limited energy dissipated by other sources such as heat, throughout the structural movement three components of energy are taken into account when balancing the energy: released potential energy due to the downward movement of the structure, strain energy due to the structural deformation, and kinetic energy of the moving structure. When regarding the motion as a SDOF dynamic process, the change of the potential energy can be calculated by the product of the weight of the moving part and the corresponding displacement. The strain energy can be calculated by integrating the product of change in stress and the corresponding change in strain over the volume of the structural elements. Subsequently, the kinetic energy can be determined as the difference between the released potential energy and the strain energy, see Figure IV.1b.

If the kinetic energy attains a value of zero, the released potential energy can be absorbed by the strain energy and the structure can redistribute the unbalanced loads. Hence, collapse can be averted in this situation, see the curve 1 in Figure IV.1b. Otherwise, a collapse will occur, i.e. the curve 2 in Figure IV.1b.

IV.2.2 Principle of the energy-based method

The EBM is based on the principle of conservation of energy. Regarding the aforementioned energy balance during a typical column removal scenario, the EBM can be easily interpreted (Izzuddin *et al.*, 2008; Herraiz *et al.*, 2015). Consider a structure which is subjected to a sudden column removal at a certain moment in time. Before the column is removed, the structure is in equilibrium. Once the column is removed, released potential energy (PE) is transferred into kinetic energy (KE) and strain energy (SE). At the origin point in Figure IV.1b, the potential energy starts to be released along with the increase of downward displacement. In the meantime, the structural system starts to move (kinetic energy) and deform (strain energy) in order to absorb the released potential energy. As the kinetic energy is the difference between the released potential energy and the strain energy due to the principle of conservation of energy, the released potential energy is equal to the strain energy at the moment when the kinetic energy is zero. This enables to calculate the dynamic capacity curve. The above relates to situations in

which no collapse occurs, i.e. the curve 1 in Figure IV.1b. The kinetic energy becomes zero at the point of peak displacement, i.e. the intersection (KE = 0 in Figure IV.1b) in the curve 1.

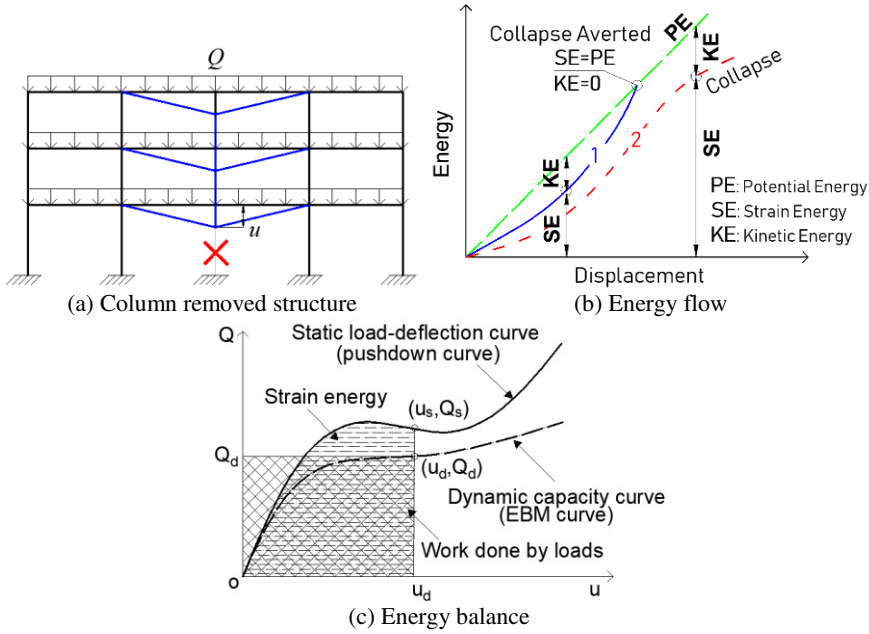

(a) Column removed structure

(b) Energy flow

(c) Energy balance

Figure IV.1. Concept of the energy-based method: (a) column removed building structure; (b) energy flow; and (c) energy balance. Figures redrafted and expanded after (Dusenberry and Hamburger, 2006; Izzuddin *et al.*, 2008; Herraiz *et al.*, 2015).

To apply the EBM, the strain energy stored in the deformed system can be calculated through a static nonlinear pushdown analysis. In that case, the strain energy is the hatched area under the static load-deflection curve up to a displacement u_s (Figure IV.1c). Moreover, the released potential energy generated by the unbalance loads is equal to the hatched rectangular area for a constant load level Q_d. Note that the self-weight is included. Considering that the internal stored strain energy and the released potential energy are equal at the same displacement level u_d ($u_s = u_d$), the dynamic load Q_d can be calculated as follows:

$$Q_d(u_d) = \frac{1}{u_d}\int_0^{u_s} Q_s(u)du \qquad \text{(IV.1)}$$

where Q_d is the load in the dynamic load-deformation curve, Q_s is the load in the static load-deformation curve, u_d is the peak dynamic deflection and u_s is the static deflection corresponding to the load Q_s. Hence, the application of Eq. (IV.1) leads

to the following analytical procedures for the EBM in case it is applied in the context of notional removal scenarios:

1) Preload the damaged structure (e.g. one column loss) with self-weight or external loads;
2) Perform a static nonlinear pushdown analysis on the damaged structure and record the output of the pushdown curve (u_s, Q_s); and
3) Convert the static pushdown curve into a dynamic load-bearing capacity curve (u_d, Q_d) through Eq. (IV.1), see Figure IV.1c as well.

The EBM approach is a compromise between accuracy and complexity. Following simplifications are incorporated:

- The moving sub-structure, subjected to a column failure, is assumed to behave like a SDOF system (Izzuddin *et al.*, 2008; Xu and Ellingwood, 2011; Herraiz *et al.*, 2015). The response is controlled by a single deformation mode and the mode keeps constant during the dynamic response. Therefore, the energy of the whole system can be linked to the energy of a point, i.e. every point in the system reaches its maximum displacement response at a same time. However, this never happens in a real structure, since the existing infinite number of deformation modes will reach their maximum response at different moments. Consequently, the stored strain energy counted by the EBM is overestimated as well as its calculated deflections (Herraiz *et al.*, 2015). For a structural system subjected to an exterior column removal scenario, a non-single deformation response may occur due to complex load redistribution mechanisms, such as observed in (Feng *et al.*, 2019b; Parisi *et al.*, 2019; Biagi *et al.*, 2020) in relation to RC frames subjected to an exterior or a side column removal scenario.
- All the energy introduced into a system by the loads is switched into pure strain energy. The EBM neglects the energy dissipated by damping or other mechanisms. Therefore, the maximum deflection response will be overestimated. Moreover, it is still a controversial issue how to model the damping mechanism for a sudden column removal scenario (Wang *et al.*, 2021), e.g. viscous damping or Coulomb damping (Herraiz *et al.*, 2015). For instance, studies have identified drawbacks associated with the use of Rayleigh damping based on initial stiffness (Hall, 2006; Zheng *et al.*, 2020). This is because the stiffness term and the associated coefficients involved in the Rayleigh damping should also be updated accordingly when the system responds in the inelastic stage (Charney, 2008).
- The strain energy storage capacities of a system for a given displacement in static and dynamic situations are different (Gao *et al.*, 2020). The EBM however cannot take this into account. However, the influence of strain rate is low according to both experimental results (Russell *et al.*, 2015)

and numerical studies (Herraiz *et al.*, 2015), since the maximum strain rates occur only in a small area and during a short time duration for sudden column removals.

IV.3 Performance evaluation of the EBM for a RC flat slab

IV.3.1 Micro-based FE model (numerical example A)

In this section, a micro-based FE model is used to assess the performance of the EBM in case of membrane action following column removal scenarios, i.e. in the large deformation stage. The FE model is validated based on an experimentally tested slab subjected to large deformations. The real-scale slab was tested by Gouverneur *et al.* (2013) to investigate the tensile membrane action after the removal of a support. The slab specimen had two inner spans of 4.0 m and two outer spans of 3.15 m, i.e. having a total length of 14.3 m. The width of the specimen was 1.8 m. The test set-up is illustrated in Figure IV.2a. The concrete was of class C30/37 as defined in EN 1992-1-1 (CEN, 2004), while the flexural reinforcement consisted of 16 bars of type S500 with a nominal diameter of 10 mm for both top and bottom reinforcing layers. The concrete cover was 20 mm. The material properties (mean values) are summarized in Table IV.1. Only the inward movements were restrained by heavily reinforced edge beams at two ends of the slab since the experiment aimed at investigating tensile membrane action only. Additional details can be found in the related paper (Gouverneur *et al.*, 2013).

A 2D plane stress FE model of the one-way RC slab is built using Abaqus 6.14 (Abaqus, 2014). Considering the symmetry in both geometry and loading, only one half of the slab is modelled (Figure IV.2c). For the concrete, 4-node bilinear plane stress elements (CPS4R) are used. As cracks are expected to occur all over the slab, and on the basis of a mesh analysis in which different mesh sizes have been investigated, a total of 8 elements through the slab depth is applied, i.e. a mesh size of 20 mm × 20 mm (Figure IV.2b,c). The concrete damaged plasticity (CDP) model (Abaqus, 2014) is employed, where the parabolic stress-strain relationship and the Hordijk tensile softening model (Hendriks *et al.*, 2017) are used for the compressive and tensile behaviour, respectively (see Figure IV.3a,b). Recommended parameters for the constitutive models are used as specified in (Hendriks *et al.*, 2017). The softening branch in compression is based on compressive fracture energy according to the *fib* Model Code 2010 (fib, 2013) and the fracture energy is divided by the equivalent length in order to reduce the sensitivity of mesh size (Hendriks et al., 2017). The tensile behaviour is governed by tensile strength and fracture energy, where the tensile strength is calculated according to EN 1992-1-1 (CEN, 2004), see Table IV.1. The Poisson ratio is take as 0.15. Finally, other default input values for the CDP model are based on the Abaqus user manual (Abaqus, 2014).

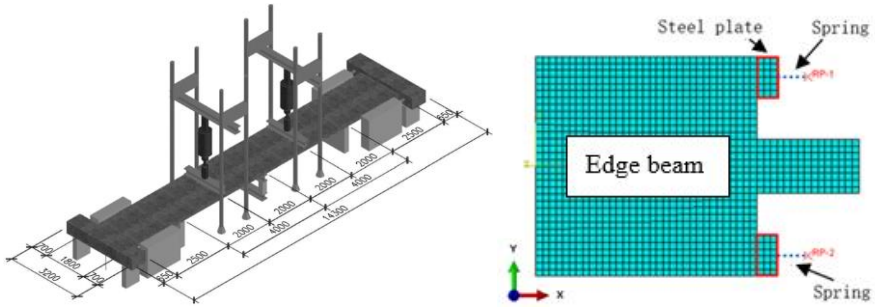

(a) Test set-up (b) Boundary condition

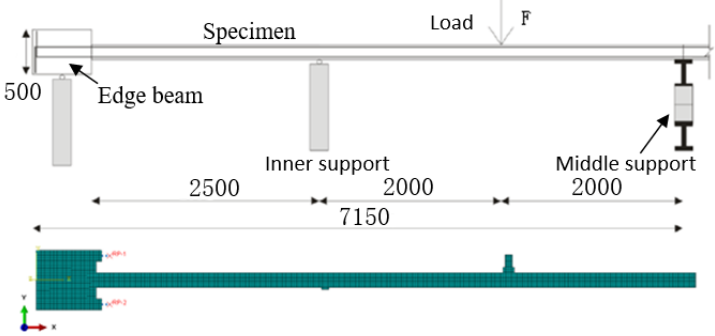

(c) FE model

Figure IV.2. Test set-up and FE model: (a) test set-up (Gouverneur *et al.*, 2013); (b) edge beam and lateral boundary condition; and (c) FE model in Abaqus.

For the reinforcing steel, 2-node linear truss elements (T2D2) are adopted. Perfect bond between the reinforcement elements and the neighbouring concrete elements is assumed. A multi-linear stress-strain relationship based on laboratory testing is employed, i.e. the strain hardening of reinforcing steel is taken into account (Figure IV.3c). A sudden decrease in strength after rupture of the reinforcing bars is used in order to enable the modelling of the observed failure phenomenon of the slab (Droogné *et al.*, 2018). Furthermore, the Poisson ratio for the reinforcement steel is taken as 0.3.

Since in the real test set-up the inward movement of the edge beams is restricted, two connector elements (Figure IV.2b) are adopted in Abaqus to simulate springs defining the relationship between the occurring horizontal force and the corresponding inward displacement. Based on the measured membrane forces versus the corresponding displacements of the edge beams and anchorage blocks, the spring stiffness is approximated as a constant value of 151.5 kN/mm for each spring.

Table IV.1. Material properties for concrete and reinforcement.

Material	Parameter	Units	Mean Value	Formula
Concrete	Compressive strength f_{cm}*	MPa	36.2	-
	Tensile strength f_{ctm} **	MPa	2.8	$f_{ctm} = 0.3 \cdot (f_{cm}\text{-}8)^{2/3}$
	Elastic Young's modulus E_{ci}*	GPa	31.97	-
	Tensile fracture energy G_{f1} ***	N/mm	0.074	$G_{f1} = 0.03 \cdot \left(\frac{f_{cm}}{10}\right)^{0.7}$
	Compressive fracture energy G_{fc} ***	N/mm	18.46	$G_{fc} = 250 \cdot G_{f1}$
Rebar	Yield stress f_{ym}*	MPa	555	-
	Tensile strength f_{um}*	MPa	605	-
	Ultimate strain ε_u*	%	8.31	-
	Elastic Young's modulus E_s*	GPa	207.9	-

Source: * Gouverneur *et al.* (2013); ** EN 1992 (CEN, 2004); *** (Droogné *et al.*, 2018).

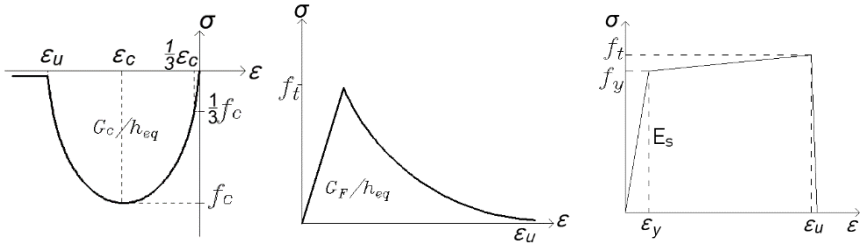

(a) Concrete in compression (b) Concrete in tension (c) Reinforcement

Figure IV.3. Stress-strain relationships for (a) concrete in compression; (b) concrete in tension (Hendriks *et al*., 2017); and (c) reinforcement.

IV.3.2 Validation of the developed finite element model

To validate the FE numerical model, a loading scheme is applied according to the loading procedure of the actual test performed by Gouverneur *et al.* (2013). The loading scheme consists of three loading phases. Initially, the self-weight and a service load of 60.0 kN are applied followed by the removal of the service load. Subsequently, the middle support is removed, where the two inner spans of 4.0 m then become one span of 8.0 m. Finally, a displacement-controlled vertical load is imposed on the slab until the failure of the slab. Abaqus/Standard is employed to

perform the static nonlinear pushdown analysis. Geometrical nonlinearity is taken into account.

Figure V.4 presents the vertical load–displacement curves obtained from both the test ('experiment' curve) and the numerical pushdown analysis ('pushdown curve'). Comparing with the experimental curve, a good agreement is observed for the pushdown curve until the first load peak. Similar as observed in the experiment (Gouverneur *et al.*, 2013), the slab experiences an elastic stage, an elastic-plastic stage, and a tensile membrane action (TMA) stage. Little difference is found between the values of the first load peak, which are 158.1 kN and 156.6 kN, obtained in the numerical analysis and the experiment respectively. This first load peak corresponds to rupture of the top layer of reinforcement over one of the inner support. The subsequent structural response is highly complex which is reflected by a significant discrepancy between experiment and numerical analysis. In the experiment the slab failed with the rupture of the bottom layer of reinforcement over the inner support. This is also predicted as such by the numerical model, although with an overestimation of the corresponding ultimate load. In case structural failure is defined as first rupture of reinforcement (a conservative criterion), it can be concluded that the FEM has a good performance. Although the FEM does not accurately predict the behaviour after the first load peak in the pushdown curve, in the following the performance of the EBM will also be evaluated beyond this load peak. The motivation is to evaluate the EBM performance for very large displacements and nonlinear behaviour.

IV.3.3 Assessment of the performance of the energy-based method

IV.3.3.1 EBM versus nonlinear dynamic analysis

Based on the numerical pushdown curve presented in Figure IV.4, a dynamic load-bearing curve is calculated according to the EBM by using Eq. (IV.1). The result is presented in Figure IV.4. Note that three curves are included in Figure IV.4: the experimental result (the curve 'experiment'), the result of the static pushdown analysis (the curve 'pushdown'), and the result of the EBM (the curve 'EBM'). It can be seen that the dynamic load-bearing curve is more smooth than the static pushdown curve. The ultimate dynamic load-bearing capacity is 100.4 kN, compared to a maximum load of 158.1 kN in the case of the static pushdown analysis. The sudden decrease in the load-displacement diagram of the pushdown curve is not observed in the dynamic capacity curve since the latter is calculated from the former based on the energy balance. However, a stage with slightly reduced slope on the dynamic capacity curve is observed between 80.0 kN and 100.0 kN. The dynamic capacity curve which exceeds the displacement of the first peak in the pushdown analysis should be treated with care, as the real post-peak behaviour after the rupture of the top reinforcement is highly complex and seems

to be overestimated by the FE analysis (see section IV.3.2), likely leading to also an overestimation in the range between 80.0 kN and 100.0 kN.

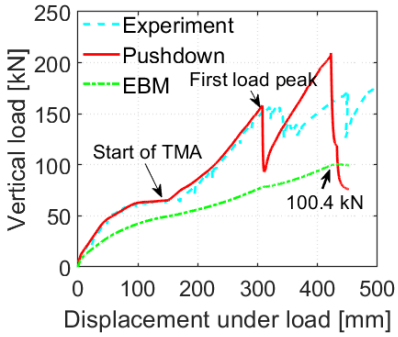

Figure IV.4. Vertical load – displacement relationship.

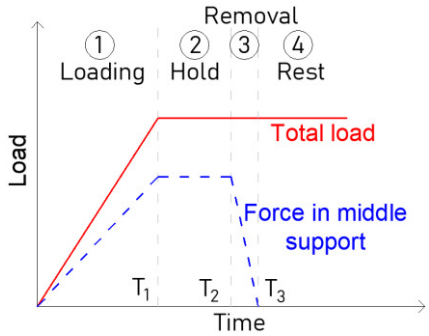

Figure IV.5. Loading scheme for dynamic analysis.

As the curve following from the EBM is directly derived from the pushdown curve without performing any nonlinear dynamic analyses, the effectiveness of the EBM should be validated by comparing it with results of direct nonlinear dynamic analyses. The incremental dynamic analysis (IDA) technique is used here to execute the dynamic nonlinear time history analysis (NTHA) on the same FE model. The IDA consists of performing a series of dynamic analyses from a lower load value to a higher load value until the collapse of the slab occurs.

A loading scheme with four phases is applied to every dynamic analysis (see Figure IV.5). First, self-weight and vertical loads are applied in phase 1 from 0 s to T_1 (1.5 s). Next, the loads are kept the same from T_1 to T_2 (1.5 s - 2.0 s). Subsequently, the middle support is removed by linearly reducing the force in the support in phase 3 in a time duration of 10^{-5} s from T_2 to T_3, where this short time duration is applied to simulate an instantaneous removal scenario. Following T_3, the structure oscillates together with the imposed loads, i.e. the loads imposed on the structure keep constant in the following time.

Abaqus/Explicit is employed to carry out the dynamic analyses to limit convergence problems. The stable time increment in the explicit analysis in Abaqus is kept smaller than 10^{-6}, allowing to model this short removal time duration.

The results of the IDA are presented in Figure IV.6a, where every star represents a peak displacement of the dynamic response under the corresponding vertical imposed load as shown in Figure IV.6b. A good agreement is observed between EBM and IDA, which indicates that the EBM predicts the maximum dynamic displacement well. Moreover, the ultimate dynamic load-bearing capacity is approximate 100.0 kN, which agrees well with the prediction through the EBM

with a value of 100.4 kN. For higher applied loads in the IDA, the structure fails in the dynamic analysis after removal of the middle support (Figure IV.6b). The tensile membrane effect is observed after 50.0 kN as shown in Figure IV.6c, where no horizontal force is found under 40.0 kN but it occurs at 50.0 kN and higher (Figure IV.6c). This can also be verified by the horizontal displacement in the upper spring as presented in Figure IV.6d, i.e. an inward displacement is observed only when the loading level reaches 50.0 kN. Note that an outward residual displacement can be observed when the load level is smaller than 50.0 kN as no outward restraint is applied to the edge beam.

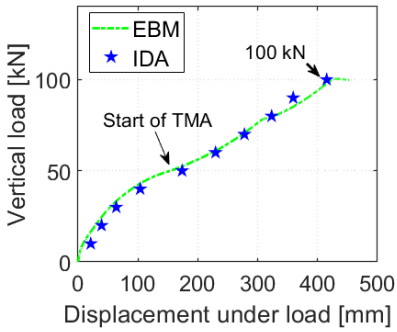

(a) Comparison for EBM to IDA

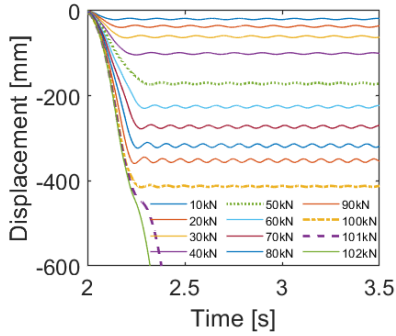

(b) Time history response of displacement

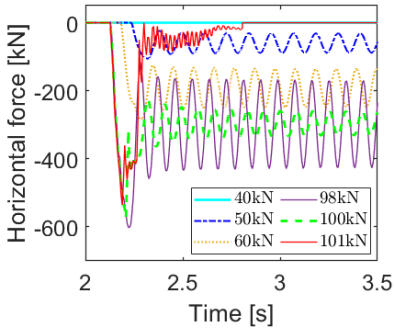

(c) Horizontal force in upper spring

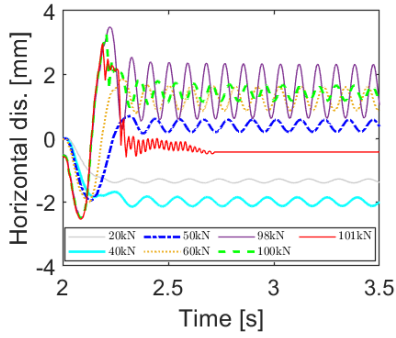

(d) Horizontal displacement in upper spring

Figure IV.6. Response of dynamic analysis (IDA): (a) load-displacement relationship; (b) time history response of displacement; (c) horizontal force in the upper spring; and (d) horizontal displacement in the upper spring.

It is important to emphasize that the failure mode observed in the dynamic case is different from the static case. For the latter, the top layer of reinforcement over the inner support in the slab firstly ruptured when the first load peak on the pushdown curve was reached. The slab however had a remaining load-bearing capability

resulting from the bottom layer of reinforcement until also the rupture of that reinforcement layer occurred (Gouverneur *et al.*, 2013). For the dynamic case, the slab directly fails when the imposed load reaches the ultimate load-bearing capacity of 101.0 kN, i.e. the two layers of reinforcement fail almost at the same time (i.e. going from 100.0 kN to 101.0 kN, see Figure IV.6).

It should be emphasized that different dynamic effects, i.e. the strain rate effects, damping and removal duration of the mid-support, cannot be taken into account in the EBM. Therefore, their influence is assessed in the following sub-sections.

IV.3.3.2 Influence of strain rate

The EBM assumes that the strain energy absorbed by the system for a given displacement is the same for both dynamic and static responses. However, in reality material properties of a system vary depending on the deformation rate, i.e. the so-called strain rate dependency. Different materials exhibit different strain rate properties. These properties are influenced by a large number of parameters, which makes it difficult to evaluate their impact on a structural system. For RC structures, the most critical parameters are the increase in yield stress of the reinforcement and the increase in tensile strength (or cracking stress) of concrete. Here, the recommendations in the *fib* Model Code (fib, 2013) are used to account for the increase of concrete tensile strength and the increase of the reinforcement yield stress and ultimate strength. The material properties are adjusted by dynamic increase factors (DIFs), i.e. the ratios of dynamic stresses to static stresses with regard to strain rates. For concrete, a two-step model, distinguishing between strain rates lower and higher than 10 s^{-1}, is used as follows:

$$DIF_t = f_{ctm} / f_{ctms} = \begin{cases} \left(\dot{\varepsilon}_{ct} / \dot{\varepsilon}_{ct0}\right)^{0.018} & for\ \dot{\varepsilon}_{ct} \le 10 s^{-1} \\ 0.0062\left(\dot{\varepsilon}_{ct} / \dot{\varepsilon}_{ct0}\right)^{1/3} & for\ \dot{\varepsilon}_{ct} > 10 s^{-1} \end{cases} \quad \text{(IV.2)}$$

$$\dot{\varepsilon}_{ct0} = 10^{-6}\, s^{-1} \quad \text{(IV.3)}$$

where DIF_t is the concrete tensile DIF at tensile strain rate $\dot{\varepsilon}_{ct}$. f_{ctm} and f_{ctms} are the mean tensile strengths at an evaluated strain rate $\dot{\varepsilon}_{ct}$ and at the quasi-static condition, respectively. $\dot{\varepsilon}_{ct0}$ is the quasi-static strain rate with a value of 10^{-6} s^{-1}.

Considering the range of applications in this contribution, however, applying a fixed value is preferred over the complex formulations (e.g. Eq. (IV.2)) and numerically much more efficient (Russell *et al.*, 2019a). Although a maximum stain rate up to 2.06 s^{-1} is observed in the FE calculations, strain rates larger than 0.6 s^{-1} are only observed in some elements in the top layer bar over the inner support. Therefore, peak strain rates in the range of 0.01 s^{-1} - 0.6 s^{-1} are expected for most of the elements. Consequently, two cases are considered, i.e. with fixed

DIFs of 1.2 and 1.3 applied to the tensile strength for all concrete elements during the entire dynamic simulation. These fixed DIFs are based on the following reasoning: the DIF value of 1.2 has been selected to avoid overestimating the strain rate effect by applying a fixed DIF according to Russell *et al.* (2019). Note that the value of 1.2 is the recommended value for normal RC slab structures, according to the results of different span to depth ratios and different support removal cases (Russell *et al.*, 2019b). The value of 1.3 is based on the maximum strain rate to determine the upper boundary of the response (the DIF for a strain rate of 2.06 s^{-1}). Actually, the results presented below show that the influence of strain rate effects of concrete on the displacement response is minor and can hence be adequately captured by this less cumbersome procedure.

DIFs for hot rolled reinforcing steel (CEB, 1988; fib, 2013), valid for strain rates up to 10 s^{-1}, are calculated as follows:

$$DIF_y = f_{ym,d} / f_{ym,s} = 1 + \left(6 / f_{ym,s}\right) \ln\left(\dot{\varepsilon} / \dot{\varepsilon}_0\right) \tag{IV.4}$$

$$DIF_u = f_{um,d} / f_{um,s} = 1 + \left(7 / f_{um,s}\right) \ln\left(\dot{\varepsilon} / \dot{\varepsilon}_0\right) \tag{IV.5}$$

$$\dot{\varepsilon}_0 = 5 \times 10^{-5}\,\mathrm{s}^{-1} \tag{IV.6}$$

where DIF_y and DIF_u are the DIFs for the yield stress and the ultimate strength of reinforcing steel, respectively. $f_{ym,d}$ and $f_{um,d}$ are the mean yield stress and the mean ultimate strength at an evaluated strain rate $\dot{\varepsilon}$, respectively. $f_{ym,s}$ and $f_{um,s}$ are the mean yield stress and the mean ultimate strength for a static condition, respectively. $\dot{\varepsilon}_0$ is the quasi-static strain rate with a value of 5×10^{-5} s^{-1}. According to the above formulas, stress-strain models at different strain rates can be updated during a dynamic analysis.

The influence of the strain rate effects is investigated based on the FE model with the same loading scheme as in section IV.3.3.1 for IDA (with a support removal duration of 10^{-5} s). Six cases are investigated: (1) without accounting for any strain rate effect (designated as 'Case 1'); (2) accounting only for the strain rate effect of reinforcing steel (designated as 'Case 2'); (3) accounting only for the strain rate effect of concrete with a DIF of 1.2 (designated as 'Case 3'); (4) accounting for the strain rate effects of both reinforcement and concrete with a DIF of 1.2 (designated as 'Case 4'); (5) accounting only for the strain rate effect of concrete with a DIF of 1.3 (designated as 'Case 5'); and (6) accounting for the strain rate effects of both reinforcement and concrete with a DIF of 1.3 (designated as 'Case 6'). The results are shown in Figure IV.7a. The results agree well with the result of EBM, except for responses corresponding to an imposed load higher than 80.0 kN, where the rupture of reinforcement results in softening of the EBM curve (as discussed in

section IV.3.3.1). Little difference is observed under small imposed loads. A slight influence is observed in case the strain rate effect of steel is considered (Case 2, Case 4 and Case 6). Although the differences are limited, the influence of the strain rate effect of reinforcement rather than concrete is higher under higher imposed loads (after 40.0 kN), i.e. when the reinforcement governs the structural response in the tensile membrane stage.

Little influence of the strain rate effect of concrete is observed. A similar conclusion is drawn by Russell *et al.* (2019). Note that four displacements (Figure IV.7a), i.e. corresponding to 90.0 kN in case of curve 'Case 3', 60.0 kN and 80.0 kN in case of curve 'Case 5', and 110.0 kN in case of curve 'Case 6' are considerably larger than those assumed for other strain rate effect assumptions. Analysis of the simulations indicates this is due to the rupture of the top layer reinforcement, as different stress/strain distributions at different strain rates are obtained.

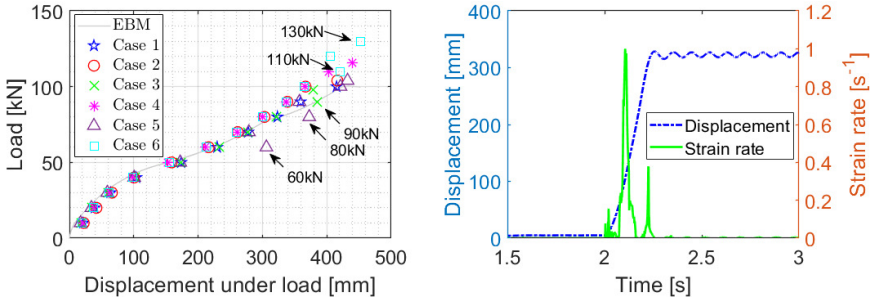

(a) Vertical load – displacement (b) Time-history response (80.0 kN)

Figure IV.7. Influence of strain rate effect: (a) load-displacement relationship; and (b) time-history response of strain rate and displacement.

Table IV.2. Ultimate load-bearing capacity (Units: kN) and the corresponding deviation.

Case	**EBM**	**Case 1**	**Case 2**	**Case 3**	**Case 4**	**Case 5**	**Case 6**
Resistance (R)	100.4	100.0	104.0	98.0	116.0	104.0	130.0
Deviation*	-	+0.4%	-3.5%	+2.5%	-13.5%	-3.5%	-22.8%

* The deviations are calculated as $(R_{EBM}-R_{Case})/R_{Case}$.

Differences for ultimate load-bearing capacities prove to be rather insignificant except in case of the curve 'Case 6' leading to a value of 130.0 kN. However, for the latter case, it should be emphasized that the fixed DIF of 1.3 may significantly overestimate the load-bearing response as the strain rates for most elements are much smaller than 2.06 s^{-1}. The ultimate load-bearing capacities are 100.0 kN,

104.0 kN, 98.0 kN, 116.0 kN, 104.0 kN and 130.0 kN for the six cases (Table IV.2), respectively. Comparing with the value of EBM, i.e. 100.4 kN, the corresponding deviations are 0.4%, -3.5%, 2.5%, -13.5%, -3.5%, and -22.8% (Table IV.2), respectively. As expected on the basis of previous observations, the deviations are higher in case the strain rate effects of both concrete and reinforcing steel are taken into account (curves 'Case 4' and 'Case 6').

Influences of the strain rate effects are hence considered not to be significant, which corresponds to the observations by Russell *et al.* (2019) and Pham *et al.* (2017b). This is due to the fact that large values of strain rate only occur in limited areas of the structure and for only a short duration. This can be observed in Figure IV.7b, where a typical time-history response of the strain rate at the element with maximum strain rate is illustrated (for the case relating to the curve 'Case 1' in Figure IV.7a). By comparing with the corresponding displacement under the vertical load, it is shown that the maximum strain rate only occurs for a quite short duration and reaches its peak value before the slab arrives to its peak displacement, limiting the effect of the strain rate.

IV.3.3.3 Influence of damping

In order to assess the influence of energy dissipated by damping, Rayleigh damping (viscous damping) (Yılmaz *et al.*, 2020) is employed to model the energy dissipation mechanism in the IDA. Considering to the first and second natural periods (0.141 s and 0.025 s) of the structural system, the mass proportional Rayleigh damping coefficient α and the stiffness proportional Rayleigh damping coefficient β can be calculated from

$$\xi_i = \frac{\alpha}{2\omega_i} + \frac{\beta\omega_i}{2} \tag{IV.7}$$

where ξ_i is the damping ratio for the i^{th} mode and ω_i is the i^{th} natural frequency.

Based on common damping ratios in structural engineering, the measured data from the experimental results of Russell *et al.* (2015) and the investigation by Xu and Ellingwood (2011), damping ratios of 1%, 2%, and 5% are investigated here. The results with different damping ratios are presented in Figure IV.8a. Although differences are not significant under small loads, damping is observed to have a significant influence on the dynamic response under high loads. Larger damping ratios result in larger capacities, which becomes more apparent at higher load levels. Ultimate dynamic capacities with damping are significantly higher than the ultimate capacity obtained based on the EBM or without damping. Note that the situations both without and with strain rate effects for the reinforcement strength have been investigated (designated as 'WR' and 'R', respectively).

The results confirm again that the EBM works well in the small deformation stage. However, the dynamic capacities can be significantly higher than predicted by the EBM in the tensile membrane action stage. For a commonly adopted damping ratio of 5% for RC structures, the obtained dynamic load capacities are almost as high as the capacities obtained in the quasi-static case and almost two times larger as compared to the case of zero damping. Furthermore, the peak displacement is observed to decay fast under a lower load level for the damping ratio of 5%. For instance, Figure IV.8b shows the time-history response of displacement considering a load of 40.0 kN (without TMA as shown in section IV.3.3.1), where a poor oscillation is observed for damping ratio 5%. The peak displacements are 98.0 mm, 90.4 mm and 74.4 mm for the considered damping ratios of 1%, 2% and 5%. Comparing with the peak displacement of 103.9 mm without damping, deviations are 5.7%, 12.9% and 28.4%, respectively.

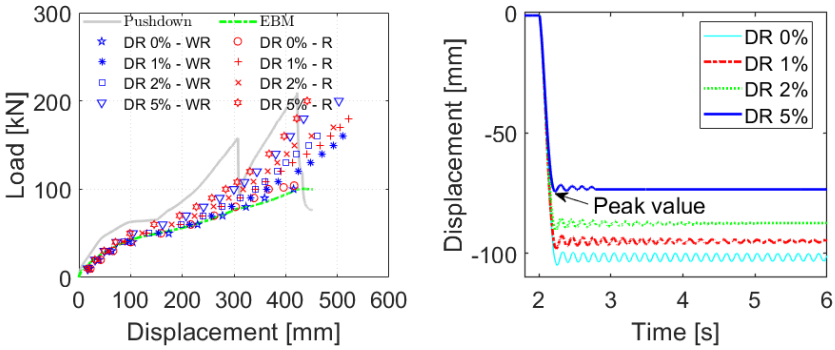

(a) Vertical load – displacement (b) Time-history response (40.0 kN)

Figure IV.8. Influence of damping: (a) load-displacement relationship; and (b) time history response of displacement. (Pushdown – the load-displacement curve from static pushdown analysis; EBM – the load-displacement curve from EBM; DR – damping ratio; WR – without strain rate effect; R – with strain rate effect)

However, it should be emphasized that assessing the appropriate damping ratio is not at all easy and highly controversial (Hall, 2006; Charney, 2008; Zheng *et al.*, 2020). Almost no test results are available to assess the result for these extreme loading situations. Herraiz *et al.* (2015) reported about a series of RC flat slabs subjected to loss of corner columns and penultimate columns, where a good agreement between the EBM and maximum dynamic response was found for the latter case, i.e. the loss of penultimate columns. However, this observation relates only to two data reads. On the other hand, a poor agreement was observed in case of corner column removal scenarios where the maximum dynamic responses were very similar to the static ones for the same loading levels (Herraiz *et al.*, 2015). However, other reasons such as incomplete similarity of the specimens, excessive support release times, etc. were believed to lie at the basis of the large deviations,

not larger damping ratios. Moreover, it was reported for these tests by Russell *et al.* (2015) that the damping ratios for the residual vibration for the elastic range were lower than 1%, while for the inelastic range damping ratios were up to 24%. These data were extracted from the residual vibrations, while maximum dynamic responses under sudden column removal scenarios were reached almost at one half of the first oscillation, i.e. before the residual vibration. It is not clear if this damping ratio was similar to the mean value before the peak response was reached. If they are similar, the use of Rayleigh damping is an incorrect assumption when the damping ratio is larger than 10% (Abaqus, 2014), i.e. the responses under large loading levels may not be reliable. This can be verified by the study of Hall (2006), where it is explicitly indicated that the damping forces can become unrealistically large compared to the restoring forces, resulting in an analysis being non-conservative under certain conditions, e.g. a nonlinear analysis with softening non-linearity.

Comparing with the total absorbed strain energy, energy dissipated through damping and cracking during such a short period should not be significant (Herraiz *et al.*, 2015). The investigation by Pham *et al.* (2017) indicates that the EBM is suitable for the analysis of structures under a threat-independent scenario of sudden column loss without considering damping. In this study, a maximum deviation of almost 22% was observed for the ultimate dynamic load-bearing capacity in case of a critical damping ratio of 5%. A very large deformation situation (780 mm) is observed in this case, following the development of catenary action. The deviation listed by Pham *et al.* (22%) is however much smaller than the value obtained here (almost 100% in case of DR = 5%). In addition, according to the investigation by Xu and Ellingwood (2011) where the stiffness-proportional damping was employed, a maximum difference of 10% was observed in case of damping ratios of 5%.

In the previous analyses Rayleigh damping was applied, combining mass-proportional damping (in case of lower frequency ranges) and initial stiffness-proportional damping (in case of higher frequency ranges) (Abaqus, 2014). However, the natural frequency decreases when a higher load is imposed due to the stiffness degradation (Russell *et al.*, 2015), which may lead to an overestimation of the dissipated energy by the mass-proportional component. As such, also simulations considering only stiffness-proportional damping (SPD) (Zheng *et al.*, 2020) are executed and compared with the simulations using Rayleigh damping (RD). The results are presented in Figure IV.9a,b. It is observed that considering stiffness-proportional damping leads to a considerable reduction of the load-displacement curve compared to the simulations employing Rayleigh damping.

Considering results reported in literature, the results obtained with stiffness-proportional damping are believed to lead to more reasonable results, as the energy disspated by damping should be limited in such a short duration. Moreover, it is also suggested by the Abaqus user' guide (Abaqus, 2014) that damping in an inelastic analysis can be neglected when material inelastic properties are taken into account, as the energy dissipated by damping should be limited. A further study is however necessary to investigate the influence of damping in detail, preferably supported by more extensive experimental data, which is currently lacking.

Considering all these observations, it is clear that the type of damping to apply as well as the values to consider are not univocal and still subject to discussion when relating to the extreme deformations associated with column removal scenarios in concrete structures. As such, applying for the time being calculations without damping proves to be a conservative approach and for those situations the EBM proves to provide a good approximation.

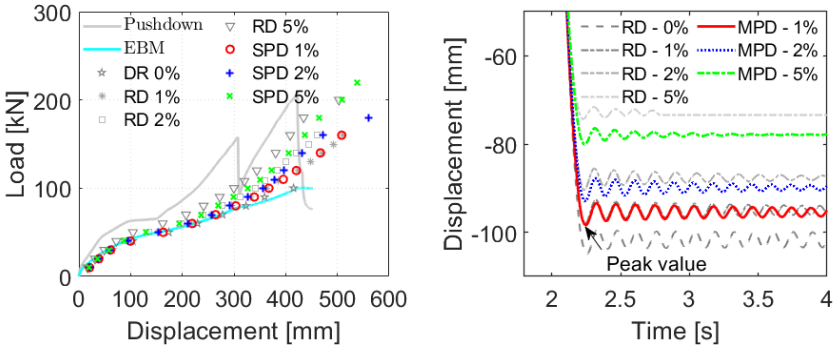

(a) Vertical load – displacement (b) Time-history response (40.0 kN)

Figure IV.9. Comparison of Rayleigh damping (RD) and stiffness proportional damping (SPD): (a) load-displacement relationship; and (b) time history response of displacement.

IV.3.3.4 Influence of column removal duration

As the speed of support removal can affect the dynamic response, the USA Department of Defense (DoD, 2009) stipulates that the duration of the column removal needs to be less than one-tenth of the first natural period of vertical oscillation. The natural period of the vertical vibration is approximately 0.141 s for the slab without the middle support (i.e. after column removal). Based on previous investigations (Qian and Li, 2012; Russell *et al.*, 2019a) on the influence of the support removal duration, a series of removal durations are selected, i.e. 10^{-2} ms (which is used in the previous analyses), 20 ms, 50 ms, and 100 ms. The IDA is executed by linearly reducing the force in the middle support with these assigned durations T_3 as shown in Figure IV.5. In order to investigate the influence of the

removal time only, both damping and strain rate effects are not considered in the dynamic analyses here.

Figure IV.10a shows that a more abrupt removal (shorter removal duration) usually results in a larger displacement. This can also be observed from the dynamic time-history responses of the vertical displacements for different removal durations, see Figure IV.10b. Figure IV.10a also shows that the influence between different removal durations is insignificant when the loads are smaller than 90.0 kN, and moreover the results are close to those predicted by the EBM. According to the guidelines of the DoD (DoD, 2009) the removal duration for this particular case must be less than 14.1 ms (i.e. one tenth of the first natural period), which is between 10^{-2} ms and 20 ms. The response of such a prescribed removal time is almost the same as when considering a sudden column removal scenario and is also accurately predicted by the EBM. More significant differences are observed under higher load levels, i.e. when the rupture of the top layer reinforcement results in larger displacements, see Figure IV.10a,c,d.

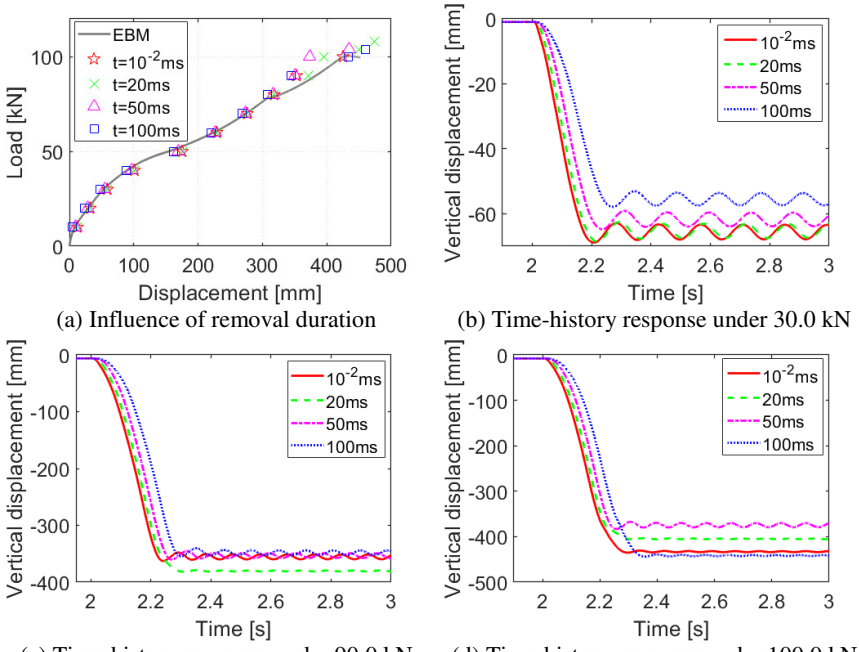

(a) Influence of removal duration

(b) Time-history response under 30.0 kN

(c) Time-history response under 90.0 kN

(d) Time-history response under 100.0 kN

Figure IV.10. Influence of support removal duration: (a) load-displacement relationship; (b) time history response of displacement under 30.0 kN; (c) time history response of displacement under 90.0 kN; and (d) time history response of displacement under 100.0 kN.

IV.3.4 Conclusions in relation to the investigated RC slab

To avoid cumbersome nonlinear dynamic analyses, the energy-based method (EBM) is a promising technique to predict the maximum dynamic responses of a structural system on the basis of a pushdown analysis. The accuracy and precision of the EBM was evaluated based on a validated FE model of a tested RC slab subjected to a sudden column removal scenario, in particular in relation to its performance for situations with tensile membrane action (TMA). After validation against experimental results of a quasi-static pushdown analysis, the model was employed to verify the accuracy and precision of the EBM in comparison to incremental dynamic analyses (IDA). The analyses indicated that the simple EBM efficiently predicted the maximum dynamic response for a concrete slab, even in the TMA stage. Note that the FE model was only validated up to the first load peak and the performance after partial rupture of the reinforcement should be further investigated by experimental data when this becomes available in the future. The post-peak behaviour after the rupture of the top reinforcement was highly complex and seemed to be overestimated. However, the performance of the EBM as an approximation of the NTHA was found to be very good also in this range, although for very large displacements with reinforcement rupture the FE model itself was not validated and the results needed to be treated with care. As the EBM neglected the influence of specific dynamic effects, such as strain rate effects, damping, and support removal duration, their influence on the dynamic capacity and the EBM's approximation was evaluated.

Based on the validated FE model, results of both EBM and IDA were obtained. A good performance in both flexural stage and TMA stage (large deformation stage) was found for the EBM when comparing with the IDA if damping and strain rate effects were not taken into account.

The strain rate effect was found to have limited influence on the dynamic response in sudden support removal scenarios. The occurring strain rates of most finite elements were in general small and only localized elements experienced large strain rates. The influence of the strain rate effect of reinforcement was slightly more significant than that of concrete, as in the TMA stage resistance was heavily influenced by the capacity of the reinforcing steel.

Damping had a slight influence in the elastic stage. However, a significant influence on the dynamic response under a high load and large damping ratio was observed, since the energy dissipation leaded to a larger capacity. It was however difficult to conclude whether that viscous damping (Rayleigh damping) was suitable in case of those extremely damaged states (Hall, 2006; Charney, 2008; Zheng *et al.*, 2020). In addition, it was not clear whether the damping mechanism for the residual oscillation was similar to that before the peak response was reached (Herraiz *et al.*, 2015). Moreover, different damping mechanisms leaded to different

results and more studies are needed to investigate which one was more realistic as there was no experimental result to compare with. Hence, damping needs to be further investigated, preferably in relation to experimental results which currently are lacking in relation to the applications under consideration. Neglecting damping however led to a conservative estimation of the load-bearing capacity and the associated displacements, and evaluations without damping were moreover approximated well by the simplified EBM calculations.

A series of support removal durations were selected in the IDA, i.e. 10^{-2} ms, 20 ms, 50 ms, and 100 ms. It was found that a more abrupt removal (shorter removal duration) could result in a larger displacement. Moreover, according to the guidelines of the DoD (DoD, 2009) the removal duration for this particular case must be less than 14.1 ms (i.e. one tenth of the first natural period), which was between 10^{-2} ms and 20 ms. The response of such a prescribed removal time was almost the same as when considering a sudden column removal scenario (i.e. 10^{-2} ms) and was also accurately predicted by the EBM.

IV.4 Performance evaluation of the EBM for a planar RC frame

IV.4.1 Description and numerical modelling

IV.4.1.1 Numerical modelling (macro-based model)

The modelling strategy for RC structures using OpenSees software package (OpenSees, 2006) is first introduced. Regarding the beam and column components, both displacement-based and the force-based fibre beam-column elements in OpenSees can be used. Nonetheless, the force-based fibre beam-column element was found to have a better performance for simulations of compressive arching action and catenary action in RC structures and with less calculation demand (less elements were required), according to a comparison study in (Feng *et al.*, 2019a). Shear deformation and shear failure are not accounted for, since the element is based on the Euler-Bernoulli beam theory. Nevertheless, an accurate prediction of the responses for slender flexure-dominated (large span-to-depth ratio) elements is possible, as the shear deformation is not significant in this situation (Ceresa *et al.*, 2007; Feng and Ren, 2021). Moreover, the shear capacity of both beams and columns can be checked to ensure no shear failure will occur. The cross-section of the fibre element is discretized into several fibres which are subjected to a uniaxial stress state. Different stress-strain relationships can be assigned to the different fibres, e.g. concrete fibres and steel fibres in a cross section as can be seen in Figure IV.11a. Finally, the mechanical behaviour of the section is obtained through integration over the entire section. Additionally, co-rotational transformation is adopted to consider geometrical nonlinearity (Mazzoni *et al.*, 2006; Brunesi and

Nascimbene, 2014; Yu *et al.*, 2017).

For beam-to-column connections, the Joint2D element in OpenSees is applied, which is idealized as a parallelogram-shaped shear panel with adjacent elements connected to its midpoints (Figure IV.11b). The Joint2D element consists of five rotational springs to simulate the shear behaviour of the joint panel (central spring) and the moment-rotation behaviour of the four sections at beam or column interfaces (interface connections). For the shear panel, the envelope of shear stress - shear strain relation τ-γ behaviour is determined by the modified compression-field theory (MCFT) (Vecchio and Collins, 1986). Subsequently, the shear stress - shear strain relation τ-γ is adopted to derive the shear-equivalent moment-rotation relation M-θ as follows: $M = \tau V_J$, and $\theta = \arctan\gamma$, where V_J is the volume of the panel. Eventually, the moment-rotation relation M-θ derived from the shear stress - shear strain relation is simplified into a multilinear relationship and then assigned to the central spring by the uniaxial Pinching 4 material model (Figure IV.11c) in OpenSees. Stiffness and strength are assumed to deteriorate due to the imposed loading history, where the parameters for cyclic behaviour are determined according to the recommendations by Lowes and Altoontash (2003). The four beam-column interface connections are assumed to be rigid (Bao *et al.*, 2017; Feng *et al.*, 2019b; Parisi and Scalvenzi, 2020), i.e. no moment-rotation relations are assigned to the four beam end and column end springs.

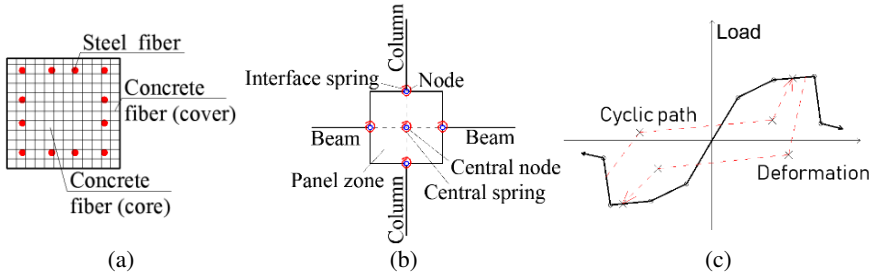

Figure IV.11. FE modelling using OpenSees: (a) fibre section; (b) Joint2D element; and (c) uniaxial Pinching 4 material model.

IV.4.1.2 Material models

The uniaxial plastic-damage model in OpenSees is adopted for concrete fibres, i.e. the ConcreteD material (Mazzoni *et al.*, 2006; Wu *et al.*, 2006). The confinement effect caused by the stirrups on the compressive behaviour is taken into account adopting the Mander model (Mander *et al.*, 1988) (curve 1 vs. curve 3 in Figure IV.12a). The tension stiffening effect is taken into account using the model by Stevens *et al.* (1991), considering the effect of longitudinal reinforcement (curve 2 vs. curve 4 in Figure IV.12a).

The uniaxial Giuffre-Menegotto-Pinto steel material model, i.e. the Steel02 material in OpenSees, is adopted for reinforcing bars (Esmaeiltabar *et al.*, 2019). The monotonic skeleton is as follows:

$$\sigma_s = \begin{cases} E_s \varepsilon_s & \text{for } \varepsilon_s \leq \varepsilon_y \\ f_y + E_h\left(\varepsilon_s - \varepsilon_y\right) = f_y + bE_s\left(\varepsilon_s - \varepsilon_y\right) & \text{for } \varepsilon_s > \varepsilon_y \end{cases} \quad \text{(IV.8)}$$

where σ_s and ε_s are the stress and strain, respectively. E_s and $E_h = b\,E_s$ are the elastic modulus and the hardening modulus, respectively. b is the hardening ratio and it is calculated according to mechanical properties of the reinforcement. f_y and ε_y are the yielding stress and strain of the steel, respectively. The typical hysteretic behaviour is presented in Figure IV.12b, where the recommended parameters (R0=20, cR1=0.925 and cR2=0.15 when applying the Steel02 materials) for the cyclic behaviour are adopted (Mazzoni *et al.*, 2006).

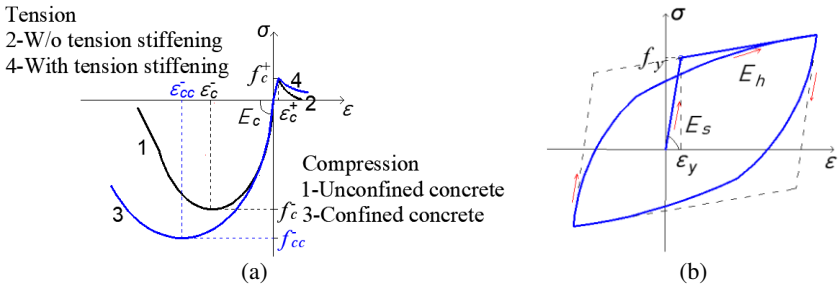

Figure IV.12. Stress-strain relationship: (a) concrete; and (b) steel.

Material failure may occur when a structure is undergoing progressive collapse, e.g. reinforcement fracture and concrete crushing. The min-max material model in OpenSees can be adopted to model the material failure (Mazzoni *et al.*, 2006). If the strain of the material exceeds the predefined minimum and maximum values, the material is assumed to have failed and zero stress and stiffness are returned. Specifically, the thresholds for reinforcement are ε_{min}= -0.01 (buckling) and ε_{max}= the ultimate strain (fracture); for unconfined concrete these are ε_{min} = -0.0035 (crushing) and ε_{max} = 0.001 (tensile failure); for confined concrete are ε_{min} = -0.03 (crushing) and ε_{max} = 0.001 (tensile failure) (fib, 2013; Lu *et al.*, 2013; Feng *et al.*, 2016; Feng *et al.*, 2019b).

IV.4.1.3 Validation of the modelling techniques

To validate the previously described modelling techniques, two RC structures are considered: a 1/4-scale RC beam-column assembly subjected to a middle column removal, and a 1/3-scale three-storey four-bay RC frame subjected to a middle column removal.

IV.4.1.3.1 A two-span beam-column assembly

The two-span beam-column assembly (designated as 'P2'which is similar to 'P1') subjected to a middle column removal was tested by Qian *et al.* (2014), see Figure IV.13a. The center to center span of P2 for the beam was 1.5 m. The specimen had a total length of 3.0 m (i.e. from two spans to one span) due to the middle column loss, see Figure IV.13b. The dimensions of the column were 200 mm × 200 mm. The cross-sectional dimension of the beam was 140 mm × 80 mm. Four continuous longitudinal reinforcements with a diameter of 10 mm were doubly reinforced in the beam. The yield stress and yield strain of the reinforcement were 437 MPa and 0.2273%, respectively. The ultimate strength of the reinforcement was 568 MPa. The average compressive strength of concrete was 20.8 MPa. More details can be found in the relevant reference (Qian *et al.*, 2014).

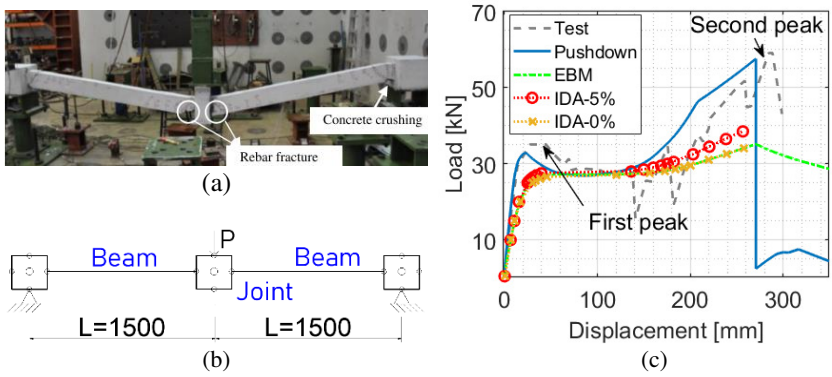

Figure IV.13. Beam-column assembly: (a) test specimen; (b) configuration of the specimen (dimensions in mm); and (c) load-displacement relationship (Test – the experimental result; Pushdown – the static pushdown analysis result; EBM – the result from EBM; IDA-5% - the dynamic capacity curve from IDA with damping ratio of 5%; IDA-0% - the dynamic capacity curve from IDA with no damping).

A displacement-controlled loading (identical to the test) is imposed at the top of the middle column (see Figure IV.13b). The vertical imposed load versus the recorded vertical displacement at the control point (i.e. at the top of the removed middle column) is shown in Figure IV.13c. Overall, a good agreement is observed between the test result (curve 'test') and simulated result (curve 'pushdown'),

where the flexural beam action stage, the compressive arch action stage and the tensile catenary action stage are well captured by the numerical FE model. The first and second load peaks in the pushdown curve are respectively 32.8 kN and 57.6 kN, while the first and second load peaks in the test curve are respectively 36.0 kN and 59.0 kN. The deviations for the two load peaks in the pushdown curve, comparing to those in the test curve, are -8.89% and -2.37%, respectively. Therefore, the FE modelling approaches described before is validated to be effective.

Furthermore, the predicted dynamic load-bearing capacity curve using the EBM is calculated based on the pushdown curve and the obtained EBM curve is presented in Figure IV.13c (curve 'EBM'). The ultimate dynamic load-bearing capacity is 35.2 kN in the EBM curve. To verify the effectiveness of the EBM, a series of NTHA, i.e. the incremental dynamic analysis (IDA) technique, are performed by progressively increasing the imposed load from a small intensity to the maximum load-bearing capacity. The load-displacement relationship between the imposed loads and the corresponding peak displacements at the top of middle column is recorded and plotted in Figure IV.13c (i.e. IDA curve). Two situations are considered to study the influence of damping effects, i.e. damping ratios DR = 0% and DR = 5%. Note that Rayleigh damping is adopted in which the involved stiffness matrix and coefficients are updated in each step. It is found that the EBM curve is identical to the IDA curve when DR = 0% is adopted in the IDA (curve 'IDA-0%' in Figure IV.13c). In terms of DR = 5%, the IDA curve (curve 'IDA-5%' in Figure IV.13c) is almost identical to the EBM curve in the small loading levels. However, a little difference is observed at the high loading levels approximating to the ultimate load-bearing capacity. Moreover, the ultimate dynamic load-bearing capacities are 34.0 kN and 38.5 kN for DR = 0% and DR = 5%, respectively. The EBM has a good performance in relation to the prediction of the dynamic load-bearing curve although a slight larger influence from the damping effect is observed at large displacement stage (i.e. tensile catenary action stage) for DR = 5%. Note that compressive arch action and the tensile catenary action are also observed in dynamic simulations. No load peaks corresponding to the compressive arch action stage are observed, as load-controlled loading is used in the dynamic analyses.

IV.4.1.3.2 A RC frame

A 1/3-scale three-storey four-bay RC frame tested by Yi *et al.* (2008) is considered in this section. The configuration of the frame is shown in Figure IV.14. The middle column at the ground floor was replaced by a hydraulic jack and a concentrated load was imposed at the top of the column in the third floor. Subsequently, the hydraulic jack in the first storey was gradually unloaded to simulate the progressive loss of the middle column, where the vertical displacement was recorded. More

details can be found in the article from Yi *et al.* (2008). Regarding the material mechanical properties, parameters obtained from testing are adopted (Yi *et al.*, 2008).

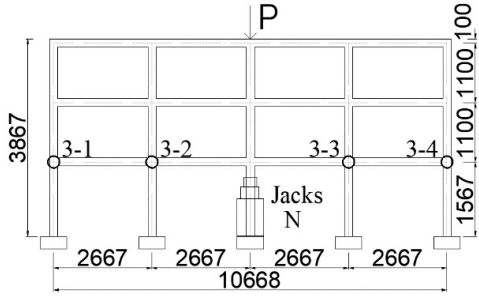

Figure IV.14. Layout of the RC frame (dimensions in mm).

The difference between the imposed load P and the axial load N at the top of the removed middle column, i.e. P-N, against the displacement is shown in Figure IV.15a, i.e. the pushdown curve. A good agreement is found between the test and the simulated pushdown curve, where both the beam mechanism and the catenary action (CA) are well captured. The ultimate load-bearing capacities are 106.1 kN and 107.3 kN for the test and simulated results, respectively. In addition, the horizontal displacements at the beam-column joints in the first floor ('3-1', '3-2', '3-3', and '3-4' in Figure IV.14) are plotted and compared to the test results (positive values correspond with a movement towards the central removed column), see Figure IV.15b. It can be seen that a good performance is obtained for the previously mentioned numerical modelling approach.

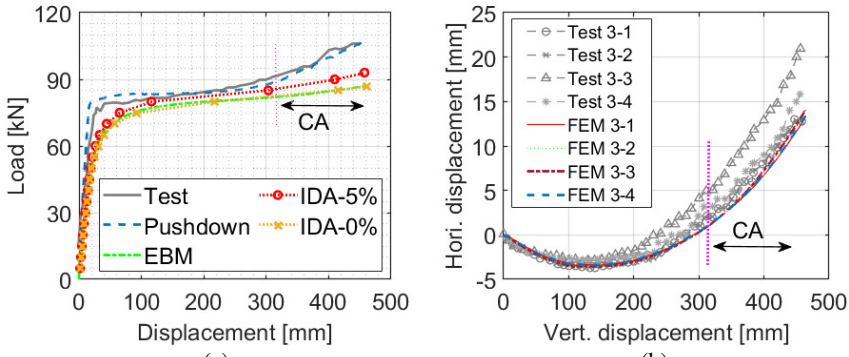

Figure IV.15. Comparison of the experimental and numerical results: (a) load-displacement relationship; and (b) horizontal displacement-vertical displacement.

Subsequently, the predicted dynamic capacity curve using the EBM is calculated and plotted in Figure IV.15a (curve 'EBM'). The ultimate dynamic capacity is 87.2 kN. To validate the EBM, a series of NTHA, i.e. the incremental dynamic analysis (IDA) technique, are carried out to determine the dynamic capacity curve by progressively increasing the imposed concentrate loads from a small value to the ultimate load-bearing capacity. The result is plotted in Figure IV.15a (curve 'IDA'). Again, two situations are considered to study the influence of damping effects (Rayleigh damping is adopted in which the tangent stiffness matrix is used as same as that in the previous section), i.e. damping ratios of DR = 0% and DR = 5%. The EBM curve is almost identical to the IDA curve in case DR = 0% (IDA-0%), where the resistance is 87.0 kN. In the case of DR = 5% (IDA-5%), the IDA curve is almost identical to the EBM curve in the small displacement stages, while some differences are found at the larger displacement levels. The ultimate capacity is 93.0 kN for that case. Overall, a good performance for the EBM can be observed.

IV.4.2 Description of the RC frame (numerical example B)

A 5-storey and 4-bay RC frame (inspired by (Feng *et al.*, 2020)) is designed according to the Eurocodes (CEN, 2002; CEN, 2004). The frame presented in Figure IV.16a is assumed to be a part of an office building. The height of the first storey is 4.5 m, while the height for the other four stories is 3.6 m each. The span for each bay is 6.0 m and the distance between two adjacent frames is also 6.0 m. The cross-sections and reinforcement layout of beams and columns are shown in Figure IV.16b. The shear reinforcement consists of stirrups with diameter of 10 mm and spacing of 150 mm. The dimensions of the beams and the columns are 250 mm × 500 mm and 500 mm × 500 mm, respectively. The concrete cover is 30 mm in all elements. Dead loads (*DL*) of both floors and roof are assumed to be 5 kN/m^2 (characteristic value), while the live loads (*LL*) on both floors and roof are 3 kN/m^2 (characteristic value) (CEN, 2002). The columns on the ground floor are labelled as A, B, C, D and E from left to right (Figure IV.16a).

Concrete of type C20/25 (CEN, 2004) is used, i.e. the characteristic cylinder compressive strength is f_{ck} = 20 MPa. According to *fib* Model Code 2010 (fib, 2013), the mean compressive strength of concrete is assumed to be $f_{cm} = f_{ck} + 8 = 28$ MPa, while the mean tensile strength is $f_{ctm} = 0.3\ (f_{ck})^{2/3} = 2.2$ MPa. The mechanical properties of the concrete are summarized in Table IV.3.

The characteristic yield stress and tensile strength of reinforcing steel are f_{yk} = 500 MPa and f_{uk} = 575 MPa (ductility class C), respectively (CEN, 2004). The mean yield stress of steel is assumed to be $f_{ym} = f_{yk} + 2\sigma_1 = 560$ MPa, where $\sigma_1 = 30$ MPa is the standard deviation (JCSS, 2001). The mean tensile strength is assumed to be $f_{um} = f_{uk} + 2\sigma_2 = 655$ MPa, where $\sigma_2 = 40$ MPa is the standard deviation (JCSS,

2001). The ultimate strain of the reinforcement is assumed to be 12% (Feng *et al.*, 2020). The Young's modulus E_s = 205 GPa is adopted. The mechanical properties of the reinforcing steel are summarized in Table IV.3.

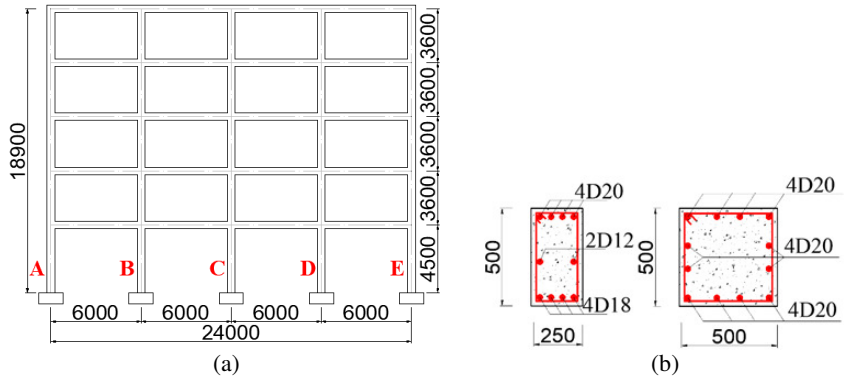

Figure IV.16. Layout of structural model: (a) RC frame; and (b) column and beam cross-sections (dimensions in mm).

Table IV.3. Mechanical properties of the materials.

Material	Parameter	Units	Mean value
Concrete	Compressive strength f_{cm}	MPa	28
	Compressive peak strain ε_{c1}	%	0.21
	Tensile strength f_{ctm}	MPa	2.2
	Young's modulus E_{ci}	GPa	30.3
Steel	Yield stress f_{ym}	MPa	560
	Tensile strength f_{um}	MPa	655
	Ultimate strain ε_u	%	12
	Young's modulus E_s	GPa	205

IV.4.3 Deterministic analysis

A 2D FE model of the RC frame is created in OpenSees using the previously introduced modelling techniques (section IV.4.1). On the basis of the FE model and the mean values of the previously mentioned material properties (section IV.4.2), deterministic analyses of both incremental dynamic analyses (IDA) and static pushdown analyses are carried out. Note that five integration points are used for the force-based fiber beam-column elements and the tolerance for convergence is set as 10^{-6} of the energy norm in OpenSees (OpenSees, 2006; Feng *et al.*, 2019a). Three cases of column removal scenarios (Figure IV.16a) are investigated:

- Case A: loss of the column A;

- Case B: loss of the column B; and
- Case C: loss of the column C.

IV.4.3.1 Dynamic nonlinear time history analysis (NTHA)

To determine the dynamic capacity curve, an IDA is carried out by successively increasing the vertical imposed loads on the structure by $P_{i+1} = P_i + \Delta P$, where ΔP is the load increment. A NTHA is applied for each load level, fully taking into account the dynamic effects. This gives the most accurate results, but one NTHA can only obtain the dynamic response for one imposed load case for a structural system, and thus a series of NTHA (i.e. an IDA) is needed to determine the dynamic capacity curve. Since the dynamic structural response becomes highly nonlinear when approaching the ultimate load-bearing capacity, the load increment ΔP of the IDA is gradually reduced. To accurately determine the resistance, a final load increment resolution of 0.05 kN/m is applied near the load for which failure occurs. Note that shear failure cannot be reproduced with the current model (fibre-based) and a check after analyses is implemented.

For every load level, one NTHA is executed, where uniform loads on all the beams are first applied followed by the instantaneous removal of column A, B or C (a removal time duration of 0.001 s). The explicit Kolay-Ricles-α algorithm (Kolay and Ricles, 2014; Kolay and Ricles, 2016) in OpenSees is employed to execute the dynamic column removal analysis, where the time step is set as 0.001 s (Feng *et al.*, 2019b). The dynamic response of the first 4.0 s for each NTHA is recorded at the top of column A, B or C (at the corresponding control point). Two different values for the damping ratio are investigated in the dynamic analyses (DR = 0% and DR = 5%, where 5% is a representative value for RC structures and Rayleigh damping is adopted) (Tsai and Lin, 2008; Brunesi *et al.*, 2015). Since the EBM cannot take into account any dynamic effects, DR = 0% in IDA is therefore investigated for a comparison purpose. Actually, following results show that almost identical results are obtained between EBM and IDA if DR = 0%.

The time-history displacement responses at the control points from the IDA when DR = 5% are presented in Figure IV.17a, Figure IV.19a and Figure IV.21a for Case A, Case B and Case C, respectively. The system oscillates around the equilibrium position and the oscillation decays due to the damping effect after the sudden column removal. Ultimate load-bearing capacities (and corresponding maximum displacements) of 35.5 kN/m (394.4 mm), 38.6 kN/m (356.9 mm), and 38.3 kN/m (341.4 mm) are obtained for Case A (Figure IV.17a), Cases B (Figure IV.19a), and C (Figure IV.21a), respectively. A summary of the results is presented in Table IV.4.

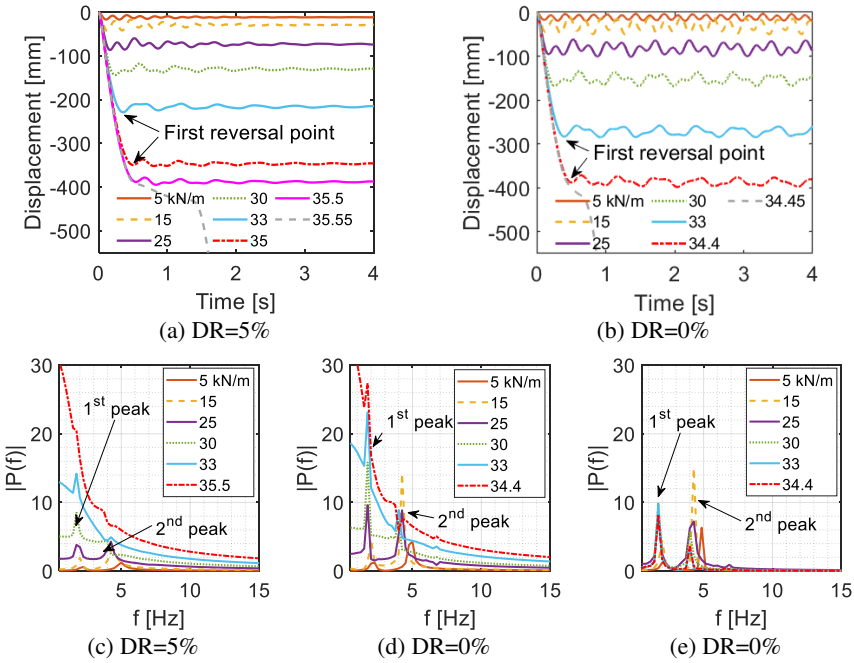

Figure IV.17. Responses for Case A (column A loss): (a) IDA with DR = 5%; (b) IDA with DR = 0%; (c) Fourier amplitude spectrum (FAS) of the displacement responses when DR = 5%; (d) FAS of the displacement responses when DR = 0%; and (e) FAS of the displacement responses with DR = 0% only after first reversal point.

It is found that the failure occurs due to concrete crushing at the beam ends. However, different failure locations and sequences are observed in the three cases. Regarding Case A, the first failure (at the ultimate load-bearing capacity of 35.5 kN/m) occurs at the beam end in the first floor, followed immediately by failures at the beam ends in the fourth, third and second floors. For Case B, the first failure (at the ultimate load-bearing capacity of 38.6 kN/m) is observed at the beam end in the first floor, followed immediately by failures at the beam ends in the fifth floor and then the other floors. In terms of Case C, the first (local) failure occurs at the beam end in the first floor with an imposed load (displacement) of 37.9 kN/m (279.2 mm) but the other floors are intact. However, the RC frame can survive this load (i.e. no collapse) and can still carry more load until the ultimate load-bearing capacity of 38.3 kN/m (341.4 mm) is reached. At this load level the first failure occurs in the first floor and then failures in the other floors occur.

The time-history displacement responses from the IDA when DR = 0% are presented in Figure IV.17b, Figure IV.19b and Figure IV.21b for Cases A, B and C, respectively. The system oscillates around the equilibrium position and the

oscillation does not decay since the damping ratio is set as 0%. A summary of the resistances is presented in Table IV.4, where the resistance in case DR = 0% is slightly lower than in case DR = 5%.

Table IV.4. Ultimate load-bearing capacity and discrepancy.

	Case A	**Case B**	**Case C**
$R_{\text{IDA-5\%}}$ [kN/m]	35.5	38.6	38.3
$R_{\text{IDA-0\%}}$ [kN/m]	34.4	37.6	37.2
R_{pushdown} [kN/m]	38.8	41.5	41.2
R_{EBM} [kN/m]	34.1	37.7	36.8
$(R_{\text{EBM}} - R_{\text{IDA-5\%}})/R_{\text{IDA-5\%}}$	-3.94%	-2.33%	-3.92%

From Figure IV.17a,b it can be seen that, the oscillations are irregular in Case A. The reason for this can be found in Figure IV.17c,d and e which show the Fourier amplitude spectra (FAS) of the time-history displacement responses using the Fourier transform technique (Peng *et al.*, 2019; Lee *et al.*, 2020; Peng *et al.*, 2020). It can be seen that there are two main frequency components in the frequency domain as shown in Figure IV.17c,d and e. Therefore, this configuration cannot be assumed as a single deformation mode, or a SDOF dynamic process, which may give rise to an error from this assumption as discussed in section IV.2. The oscillations may, on one hand, disappear in the time-history displacement when DR = 5% (Figure IV.17a) since the damping effects dissipate the kinetic energy, especially under the higher loading levels where the oscillations decay fast. On the other hand, there is little oscillation before the displacement response reaches its first reversal point, where a longer duration is needed to reach the first reversal point for a larger load level (Figure IV.17a,b). The two aspects result in a wide bond in the frequency domain, see Figure IV.17c,d. However, when only the responses once the system starts oscillating (after the first reversal point as shown in Figure IV.17b in case of DR = 0%) are considered, two peaks in the frequency domain (dominant frequencies) can be observed clearly, see Figure IV.17e.

Moreover, the frequencies associated with the two peaks (Figure IV.17c,d,e) are found to be around the first and second natural frequencies obtained from a linear elastic modal analysis, see Figure IV.18a,b. This means the two main frequency components in the responses may be linked to the first two modes (note that the former is obtained from the nonlinear dynamic analyses, while the latter is based on the linear modal analyses), i.e. evidently the response cannot be assumed as a single deformation mode.

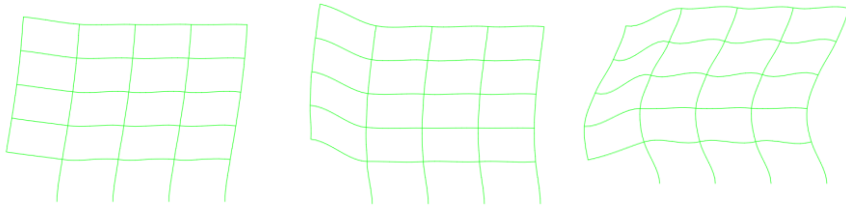

(a) f = 2.00 Hz (b) f = 5.54 Hz (c) f = 7.66 Hz

Figure IV.18. Mode shapes for Case A: (a) the first mode; (b) the second mode; and (c) the third mode.

Regarding the time-history displacement responses for Case B and Case C, the oscillations are more regular, since only one peak (i.e. a single deformation mode) is found in the corresponding FAS (calculated once the system starts oscillating from the first reversal point and DR = 0%), as shown in Figure IV.19c and Figure IV.21c, respectively. Moreover, the frequency peak (Figure IV.19c) is around the third natural frequency (obtained from a modal analysis) for Case B, see Figure IV.20c. This means the third mode may be associated with the response, since both its model shape and the displacement response in Case C are in vertical direction. Note that the first two modes are mainly in horizontal direction, although the second natural frequency is also close to the dominant frequency. Moreover the other natural frequencies are much higher than the dominant frequency. A similar phenomenon can be observed in Case C, i.e. a single deformation mode (Figure IV.21c) associated with the third mode (Figure IV.22c).

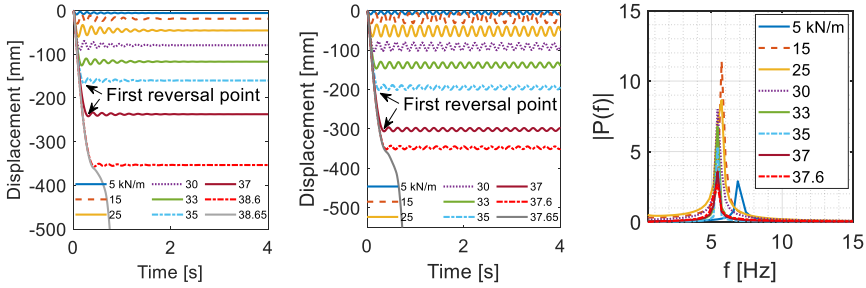

(a) DR=5% (b) DR=0% (c) FAS

Figure IV.19. Responses for Case B (column B loss): (a) IDA with DR = 5%; (b) IDA with DR = 0%; and (c) FAS of the displacement responses with DR = 0% only after first reversal point.

In order to construct the IDA curves (i.e. the envelope obtained from the series of NTHA), the vertical displacement peaks obtained in the NTHA (Figure IV.17a,b, Figure IV.19a,b, and Figure IV.21a,b) against the corresponding imposed loads are

presented in Figure IV.23 (IDA curve) for the three cases and for both DR = 5% and DR = 0%.

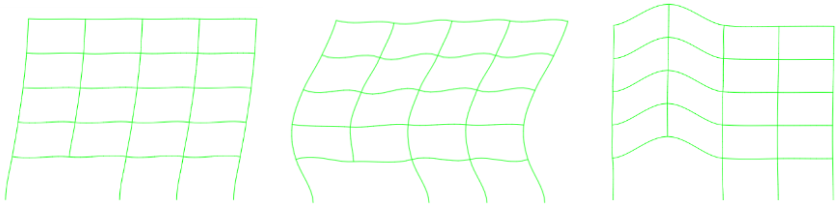

(a) f = 2.21 Hz (b) f = 7.29 Hz (c) f = 7.71 Hz

Figure IV.20. Mode shapes for Case B: (a) the first mode; (b) the second mode; and (c) the third mode.

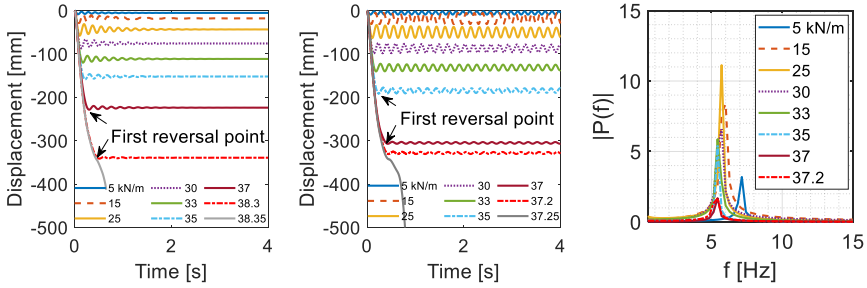

(a) DR=5% (b) DR=0% (c) FAS

Figure IV.21. Responses for Case C (column C loss): (a) IDA with DR = 5%; (b) IDA with DR = 0%; and (c) FAS of the displacement responses with DR = 0% only after first reversal point.

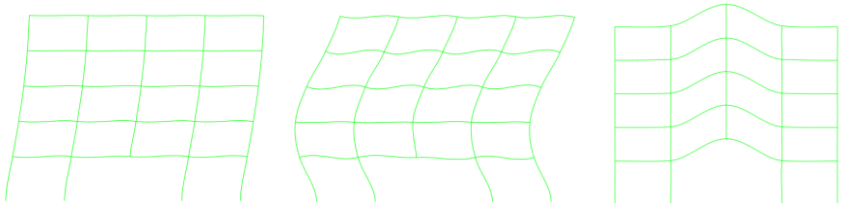

(a) f = 2.21 Hz (b) f = 7.30 Hz (c) f = 7.73 Hz

Figure IV.22. Mode shapes for Case C: (a) the first mode; (b) the second mode; and (c) the third mode.

IV.4.3.2 Nonlinear static analysis

Before applying the EBM, one pushdown analysis is carried out for each column removal case. Uniform loads are gradually increased on all beams. A displacement-controlled analysis is executed, where the displacement at the top of column A, B or C is controlled, depending on the column removal scenario that is considered. The displacements at the control points against the imposed loads are recorded, resulting in the pushdown curves in Figure IV.23a,b,c for Cases A, B and C, respectively. The static ultimate load-bearing capacities (and corresponding displacements) are 38.8 kN/m (392.8 mm), 41.5 kN/m (355.3 mm) and 41.2 kN/m (270.8 mm) for Cases A, B and C, respectively.

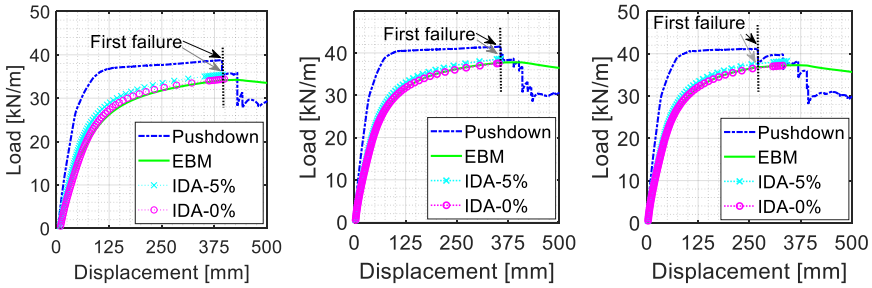

Figure IV.23. Load - displacement responses: (a) Case A; (b) Case B; and (c) Case C.

Moreover, the displacements at the first failure (concrete crushing at beam ends in the first floor at the first load peaks in the pushdown curves) according to the static analyses are almost identical to those of the IDA results for Cases A, B and C. The first failure in Case C corresponds with 37.9 kN/m (279.2 mm) for the IDA. The ultimate load-bearing capacity is however higher at 38.3 kN/m (341.4 mm). In Case C the maximum displacement following the IDA (corresponding to the dynamic ultimate load-bearing capacity) is more close to the displacement at the second load peak in the pushdown curve (when failure occurs at the beam ends in the second floor), see Figure IV.23c. This explains why the ultimate load-bearing capacities are obtained at different displacement levels, when comparing the static result to the dynamic results in Case C. For cases A and B, the static and dynamic ultimate load-bearing capacities are obtained at almost same displacement levels.

For all three cases, the second load peak in the pushdown curve is lower than the first load peak (failure only in the first floor). Consequently, only the first load peak is used here since it relates to the ultimate load-bearing capacity and the failure mode (first failure) is identical to the IDA. Furthermore, the first failure is a signal of a start of the system failure.

IV.4.3.3 Dynamic amplification factor

Typically, the DAF is defined as the ratio of the maximum dynamic displacement (u_d) to the static displacement (u_s) for an elastic SDOF system under an imposed loading (Q_d) (Tsai, 2010). Similarly, a displacement-based DAF_D can also be defined with regard to the IDA and pushdown curves:

$$DAF_D = \frac{u_d}{u_s} \tag{IV.9}$$

where u_d is the dynamic displacement in the dynamic capacity curve; and u_s is the static displacement under the same imposed load in the static capacity curve. Note that DAF_D can only be calculated up to the ultimate dynamic response, even if a higher portion still exists in the static capacity curve (see Figure IV.23).

A force-based DAF_F (Tsai, 2010; Brunesi and Nascimbene, 2014) can also be calculated by dividing the static load-bearing capacity by the dynamic load-bearing capacity at a same displacement:

$$DAF_F = \frac{Q_S}{Q_d} \tag{IV.10}$$

where Q_s is the load in the static capacity curve; and Q_d is the load in the dynamic capacity curve.

Based on the previous pushdown and IDA curves, the displacement-based DAF_D is calculated and presented in Figure IV.24a. Regarding Case A, the DAF_D increases from 1.74 to 4.11 when the imposed load increases. In terms of Case B and Case C, the DAF_D increases from 2.00 to 4.93 and 4.95 when the imposed load increases, respectively. It is worth noting that the results are obtained using a resolution of 0.05 kN/m for the imposed load increment in the IDA. A similar result is obtained for a bilinear SDOF model with different nonlinear parameters studied by (Tsai, 2010), where the DAF_D may increase from 2.00 to infinity as the applied loading increases. The values lower than 2.00 in Case A in Figure IV.24a can be attributed to the fact that the response in this case is not a single deformation mode as mentioned before. Additionally, yield points (YP), the moment when the reinforcement starts yielding, in the curves are marked (Figure IV.24a), where DAF_D are 2.10, 2.28, and 2.32 for the three cases.

The force-based DAF_F is calculated and shown in Figure IV.24b. For Case A, the DAF_F decreases from 2.23 (when the vertical imposed load is 4.0 kN/m in IDA curve) to 1.10 (at the displacement where first failure occurs) when the displacement increases. In terms of Cases B and C, the DAF_F decreases from 2.02

(at 4.0 kN/m) to 1.08 and 1.04 (at the displacement where first failure occurs), respectively. A similar result is obtained for a 5-storey RC frame subjected to a column removal scenario studied by Brunesi and Nascimbene (Brunesi and Nascimbene, 2014), where the DAF_F decreased from almost 2.70 to 1.11 with increasing the vertical displacement. Again, yield points (YP) in the curves are marked (Figure IV.24b), where DAF_F are 1.65, 1.73, and 1.72 for the three cases.

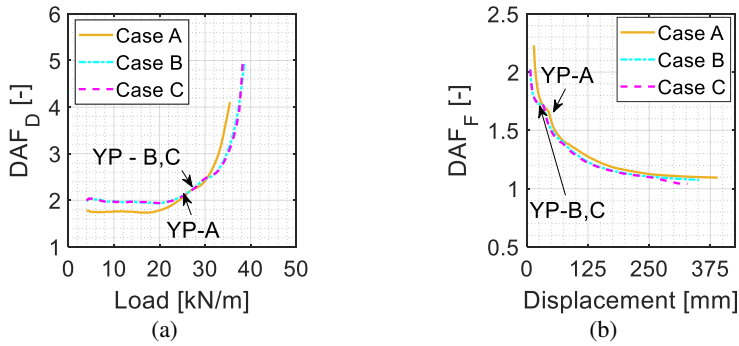

Figure IV.24. DAF: (a) displacement-based DAF vs. vertical imposed load; and (b) force-based DAF vs. displacement.

IV.4.4 Evaluation of the performance of the energy-based method

The EBM is subsequently applied to calculate the dynamic load-bearing capacity curve using Eq. (IV.1). The results for the different cases are presented in Figure IV.23. Generally, the EBM is observed to have a good performance in relation to predicting the maximum dynamic response, compared with the more accurate IDA results. Regarding the IDA curves with DR = 5%, a slight deviation is observed for the EBM curve, as the damping effect is taken into account in the IDA, which is not possible to account for in case of the EBM. However, the overall influence remains rather small. The deviation in Case A is slightly larger, which can be attributed to the fact that, as found before, this case is not a SDOF dynamic process. Nevertheless, an excellent performance is observed for all three cases when DR = 0% for which the EBM curves are almost identical to the IDA curves. A summary of the results can be found in Table IV.4 (see section IV.4.3.1).

IV.4.5 Conclusions in relation to the investigated RC frame

In this section, the effectiveness of an energy-based method (EBM) for the prediction of the dynamic resistance of RC frames was verified through comparing the approximation to more complex nonlinear dynamic analyses. The influences of damping effects and different column removal scenarios on the performance of the load-bearing capacity prediction were investigated. It was found that the response

was not a single deformation mode in the case of an exterior column removal scenario which may influence the performance of the EBM and the dynamic amplification factor.

Although no dynamic effects such as damping can be explicitly considered in the EBM, a good performance was found for the EBM to predict the dynamic capacity curve through comparison with results of IDA. Almost identical results were obtained between EBM and IDA curves if a damping ratio of 0% was considered, which indicated that the EBM could effectively calculate the maximum dynamic responses. Only a small difference was found between EBM and IDA results if the damping ratio was taken as 5%, which demonstrated that the damping effects had only a limited influence. Moreover, the EBM provided a conservative result for resistance assessment.

The EBM assumes that a structure subjected to a column removal scenario deforms in a single deformation mode. An external column removal scenario may influence the performance of the EBM and the dynamic amplification factor, since its dynamic response may not be represented by a single deformation mode according to the responses in the frequency domain. However, the internal column removal scenarios were found to behave like SDOF dynamic systems for which the EBM overall had a very good performance. A better performance for the EBM was observed in an internal column loss case than for an external column loss case.

Additionally, two kinds of DAF were calculated, denoting the ratio between the IDA results and the pushdown results. For the displacement-based DAF, the DAF_D increased from 1.74 to 4.11 with regard to Case A when the imposed load increased, while the DAF_D increased from 2.00 to 4.93 and 4.95 for Case B and Case C, respectively. Regarding the force-based DAF, the DAF_F decreased from 2.23 (when the vertical imposed load was 4.0 kN/m in IDA curve) to 1.10 (at the displacement where first failure occurs) for Case A, while the DAF_F decreased from 2.02 (at 4.0 kN/m) to 1.08 and 1.04 (at the displacement where first failure occurs) in terms of Cases B and C when the displacement increased.

IV.5 Summary and conclusions

As dynamic experimental studies on reinforced concrete structures are expensive and time-consuming, the development of numerical models provides a good solution. Nonetheless, the numerical dynamic simulations regarding progressive collapse may require high calculation demand. The simple energy-based method (EBM) is a promising approach to obtain an approximate evaluation of the maximum dynamic responses.

In order to validate the effectiveness of the EBM two numerical examples have been investigated in detail in this chapter, i.e. a RC slab and a RC frame. Two kinds of numerical modelling techniques, each with their fields of application, were adopted. First a detailed micro-based FE model (i.e. solid elements) was developed in Abaqus based on the experimental test of Gouverneur *et al.* (2013) to simulate tensile membrane action in a reinforced concrete slab. With this detailed model, localized damage can be simulated adequately and parametric studies were performed to evaluate the effectiveness of the EBM in relation to the one-way reinforced concrete slab. On the other hand, a macro-based FE model (i.e. fibre-based beam elements) was developed in OpenSees to evaluate the performance of the EBM as well. Further, this macro-based FE model was applied to simulate a more complex multi-storey reinforced concrete frame with a reasonable computational demand. According to the results of the two numerical case studies, the performance of the EBM has been found to be good.

Rayleigh damping proportional to the mass matrix and stiffness matrix was adopted. In the numerical example A with regard to the RC slab model in Abaqus, the Rayleigh damping was proportional to the initial stiffness matrix (the coefficients are not updated during the analysis) and a significant large artificial force was observed in the tensile membrane stage. In terms of the numerical example B using OpenSees, the Rayleigh damping was proportional to the tangent stiffness matrix (both the stiffness matrix and the coefficients are updated in the inelastic stage) and a reasonable deviation was observed through comparison to the results with zero damping. It is concluded that damping mechanisms require to be further investigated, preferably in relation to experimental results which currently are lacking in relation to the applications under consideration.

IV.5.1 Numerical example A: the RC slab

Based on the validated micro-based FE model with regard to the real-scale one-way RC slab, both nonlinear static (i.e. pushdown analyses) and nonlinear dynamic (i.e. IDA analyses) analyses were performed. Afterwards, responses for both EBM and IDA were obtained and compared with each other. A good performance in both flexural stage and tensile membrane action stage (large deformation stage) was found for the EBM when comparing with the IDA if damping and strain rate effects were not taken into account.

Overall, the strain rate effects with regard to both the reinforcement and the concrete materials have limited influence on the dynamic response in sudden support removal scenarios. The influence of the strain rate effect of reinforcement may be slightly more significant than that of concrete, since the resistance in tensile membrane action stage is heavily influenced by the behaviour of the reinforcing steel (i.e. tensile force in reinforcing bars).

Different damping mechanisms may lead to different results and it is difficult to say which one is more realistic as there is no experimental result to compare with. The Rayleigh damping proportional to the initial stiffness matrix might result in unwanted artificial forces in the responses and the tensile membrane action might significantly enlarge the structural stiffness. Neglecting damping however leads to a conservative estimation of the load-bearing capacity and the associated displacements, and the situation without damping can be predicted well also by the simplified EBM calculations.

A more abrupt removal (shorter removal duration) may result in a larger displacement. Moreover, according to the guidelines of the DoD (DoD, 2009), the removal duration must be less than one tenth of the first natural period. Cases with such short support removal time can be also accurately predicted by the EBM.

IV.5.2 Numerical example B: the RC frame

The performance of the EBM has been evaluated through a numerical example of a planar RC frame. In this numerical example, three different ground column removal cases were investigated: one exterior column removal case and two interior column removal cases.

The effectiveness of the EBM for the prediction of the dynamic resistance of RC frames has been verified with regard to the RC frame through comparing the approximation to more complex nonlinear dynamic analyses. It is concluded that the EBM has a good performance to predict the dynamic capacity curve through comparison with results of IDA, either in case of a damping ratio of 0% or 5%. Moreover, the EBM provides a conservative result for resistance assessment, since the damping effects are not included.

An exterior column removal scenario may influence the performance of the EBM, since its dynamic response may not be represented by a single deformation mode according to the responses in the frequency domain. On the other hand, an interior column removal scenario is more often found to behave like SDOF dynamic systems for which the EBM overall has a very good performance. Hence, a better performance for the EBM can be observed in an interior column loss case than for an exterior column loss case.

IV.6 References

Abaqus (2014) ABAQUS user's manual. Version 6.14. ABAQUS Providence, RI.

Adam JM, Buitrago M, Bertolesi E, et al. (2020) Dynamic performance of a real-scale reinforced concrete building test under a corner-column failure scenario. Engineering Structures 210:110414.

Bao Y, Kunnath SK, El-Tawil S, et al. (2008) Macromodel-based simulation of progressive collapse: RC frame structures. Journal of Structural Engineering 134:1079-1091.
Bao Y, Main JA, Noh SY (2017) Evaluation of structural robustness against column loss: Methodology and application to RC frame buildings. Journal of Structural Engineering 143:04017066.
Biagi VD, Kiakojouri F, Chiaia B, et al. (2020) A simplified method for assessing the response of RC frame structures to sudden column removal. Applied Sciences 10:3081.
Brunesi E, Nascimbene R (2014) Extreme response of reinforced concrete buildings through fiber force-based finite element analysis. Engineering Structures 69:206-215.
Brunesi E, Nascimbene R, Parisi F, et al. (2015) Progressive collapse fragility of reinforced concrete framed structures through incremental dynamic analysis. Engineering Structures 104:65-79.
Byfield M, Mudalige W, Morison C, et al. (2014) A review of progressive collapse research and regulations. Proceedings of the Institution of Civil Engineers-Structures and Buildings 167:447-456.
CEB (1988) Concrete structures under impact and impulsive loading: Synthesis report. Comite Euro-International Du Beton.
CEN (2002) Eurocode 1: Actions on structures-Part 1-1: General actions-Densities, self-weight, imposed loads for buildings. European Committee for Standardization Brussels. EN 1991-1-1.
CEN (2004) Eurocode 2: Design of concrete structures—Part 1-1: General rules and rules for buildings. EN 1992-1-1.
Ceresa P, Petrini L, Pinho R (2007) Flexure-shear fiber beam-column elements for modeling frame structures under seismic loading - state of the art. Journal of Earthquake Engineering 11:46-88.
Charney FA (2008) Unintended consequences of modeling damping in structures. Journal of Structural Engineering 134:581-592.
DoD (2009) Unified facilities criteria: Design of buildings to resist progressive collapse. UFC 4-023-03. United States Department of Defense.
DoD (2016) Design of buildings to resist progressive collapse. Unified Facilities Criteria (UFC) 4-023-03.
Droogné D, Botte W, Caspeele R (2018) A multilevel calculation scheme for risk-based robustness quantification of reinforced concrete frames. Engineering Structures 160:56-70.
Dusenberry DO, Hamburger RO (2006) Practical means for energy-based analyses of disproportionate collapse potential. Journal of Performance of Constructed Facilities 20:336-348.
Esmaeiltabar P, Vaseghi J, Khosravi H (2019) Nonlinear macro modeling of slender reinforced concrete shear walls. Structural Concrete 20:899-910.

Feng D-C, Xie S-C, Ning C-L, et al. (2019a) Investigation of modeling strategies for progressive collapse analysis of RC frame structures. Journal of Performance of Constructed Facilities 33:04019063.
Feng D, Kolay C, Ricles JM, et al. (2016) Collapse simulation of reinforced concrete frame structures. Structural Design of Tall and Special Buildings 25:578-601.
Feng D, Wang Z, Wu G (2019b) Progressive collapse performance analysis of precast reinforced concrete structures. Structural Design of Tall and Special Buildings 28:e1588.
Feng D, Xie S, Xu J, et al. (2020) Robustness quantification of reinforced concrete structures subjected to progressive collapse via the probability density evolution method. Engineering Structures 202:109877.
Feng DC, Ren XD (2021) Implicit gradient-enhanced force-based Timoshenko fiber element formulation for reinforced concrete structures. International Journal for Numerical Methods in Engineering 122:325-347.
fib (2013) fib model code for concrete structures 2010.
Gao X, Zhou L, Ren X, et al. (2020) Rate effect on the stress–strain behavior of concrete under uniaxial tensile stress. Structural Concrete 22:E815-E830.
Gouverneur D, Caspeele R, Taerwe L (2013) Experimental investigation of the load–displacement behaviour under catenary action in a restrained reinforced concrete slab strip. Engineering Structures 49:1007-1016.
GSA (2016) Alternate path analysis & design guidelines for progressive collapse resistance. General Services Administration.
Hall JF (2006) Problems encountered from the use (or misuse) of Rayleigh damping. Earthquake engineering & structural dynamics 35:525-545.
Hendriks MA, de Boer A, Belletti B (2017) Guidelines for nonlinear finite element analysis of concrete structures. Rijkswaterstaat Technisch Document (RTD), Rijkswaterstaat Centre for Infrastructure, RTD 1016-1:2012.
Herraiz B, Russell J, Vogel T (2015) Energy-based method for sudden column failure scenarios: theoretical, numerical and experimental analysis IABSE Symposium Report. International Association for Bridge and Structural Engineering, pp. 70-77.
Herraiz B, Vogel T (2014) Simplified approach for analysing building structures subjected to sudden column removal scenarios Proceedings of the 9th European Conference on Structural Dynamic (EURODYN 2014). Faculty of Engineering of University of Porto, pp. 3467-3474.
Huang M, Huang H, Hao R, et al. (2021) Studies on secondary progressive collapse - resistance mechanisms of reinforced concrete subassemblages. Structural Concrete:1-17.
Izzuddin B, Vlassis A, Elghazouli A, et al. (2008) Progressive collapse of multi-storey buildings due to sudden column loss—Part I: Simplified assessment framework. Engineering Structures 30:1308-1318.

Izzuddin BA, Nethercot DA (2009) Design-oriented approaches for progressive collapse assessment: Load-factor vs. Ductility-centred methods Structures Congress 2009: Don't Mess with Structural Engineers: Expanding Our Role. pp. 1-10.

JCSS (2001) Probabilistic model code. Joint Committee on Structural Safety.

Kim S, Lee C-H, Lee K (2015) Effects of floor slab on progressive collapse resistance of steel moment frames. Journal of Constructional Steel Research 110:182-190.

Kolay C, Ricles JM (2014) Development of a family of unconditionally stable explicit direct integration algorithms with controllable numerical energy dissipation. Earthquake engineering & structural dynamics 43:1361-1380.

Kolay C, Ricles JM (2016) Assessment of explicit and semi‐explicit classes of model‐based algorithms for direct integration in structural dynamics. International Journal for Numerical Methods in Engineering 107:49-73.

Lee M, Yoo M, Jung HS, et al. (2020) Study on dynamic behavior of bridge pier by impact load test considering scour. Applied Sciences-Basel 10:6741.

Liu M (2013) Pulldown analysis for progressive collapse assessment. Journal of Performance of Constructed Facilities 29:04014027.

Liu M, Pirmoz A (2016) Energy-based pulldown analysis for assessing the progressive collapse potential of steel frame buildings. Engineering Structures 123:372-378.

Lowes LN, Altoontash A (2003) Modeling reinforced-concrete beam-column joints subjected to cyclic loading. Journal of Structural Engineering 129:1686-1697.

Lu X, Lu XZ, Guan H, et al. (2013) Collapse simulation of reinforced concrete high-rise building induced by extreme earthquakes. Earthquake engineering & structural dynamics 42:705-723.

Main JA (2014) Composite floor systems under column loss: collapse resistance and tie force requirements. Journal of Structural Engineering 140:A4014003.

Mander JB, Priestley MJN, Park R (1988) Theoretical stress-strain model for confined concrete. Journal of Structural Engineering 114:1804-1826.

Mazzoni S, McKenna F, Scott MH, et al. (2006) OpenSees command language manual. Berkeley, California, United States.

Naji A (2019) Progressive collapse analysis of steel moment frames: An energy-based method and explicit expressions for capacity curves. Journal of Performance of Constructed Facilities 33:04019008.

Newmark NM (1953) An engineering approach to blast resistant design. Transactions of the American Society of Civil Engineers 121:1.

OpenSees (2006) Open system for earthquake engineering simulation. University of California, Berkeley.

Parisi F, Scalvenzi M (2020) Progressive collapse assessment of gravity-load designed European RC buildings under multi-column loss scenarios. Engineering Structures 209:110001.
Parisi F, Scalvenzi M, Brunesi E (2019) Performance limit states for progressive collapse analysis of reinforced concrete framed buildings. Structural Concrete 20:68-84.
Peng YB, Ding LC, Chen JB (2019) Performance evaluation of base-isolated structures with sliding hydromagnetic bearings. Structural Control & Health Monitoring 26:e2278.
Peng YB, Ding LC, Chen JB, et al. (2020) Shaking table test of seismic isolated structures with sliding hydromagnetic bearings. Journal of Structural Engineering 146:04020174.
Pham AT, Tan KH, Yu J (2017) Numerical investigations on static and dynamic responses of reinforced concrete sub-assemblages under progressive collapse. Engineering Structures 149:2-20.
Powell G (2005) Progressive collapse: Case studies using nonlinear analysis Structures Congress 2005: Metropolis and Beyond. pp. 1-14.
Qian K, Li B (2012) Dynamic performance of RC beam-column substructures under the scenario of the loss of a corner column—Experimental results. Engineering Structures 42:154-167.
Qian K, Li B, Ma JX (2014) Load-carrying mechanism to resist progressive collapse of rc buildings. Journal of Structural Engineering 141:04014107.
Russell J, Owen J, Hajirasouliha I (2015) Experimental investigation on the dynamic response of RC flat slabs after a sudden column loss. Engineering Structures 99:28-41.
Russell J, Owen J, Hajirasouliha I (2019a) Dynamic column loss analysis of reinforced concrete flat slabs. Engineering Structures 198:109453.
Russell JM, Owen JS, Hajirasouliha I (2019b) Dynamic column loss analysis of reinforced concrete flat slabs. Engineering Structures 198:109453.
Stevens NJ, Uzumeri SM, Will GT (1991) Constitutive model for reinforced concrete finite element analysis. Structural Journal 88:49-59.
Subki NEA, Mansor H, Hamid YS, et al. (2019) Progressive collapse assessment: A review of the current energy-based alternate load path (alp) method MATEC Web of Conferences. EDP Sciences, pp. 02012.
Szyniszewski S, Krauthammer T (2012) Energy flow in progressive collapse of steel framed buildings. Engineering Structures 42:142-153.
Tsai M-H (2011) Analytical load and dynamic increase factors for progressive collapse analysis of building frames AEI 2011: Building Integration Solutions. pp. 172-179.
Tsai MH (2010) An analytical methodology for the dynamic amplification factor in progressive collapse evaluation of building structures. Mechanics Research Communications 37:61-66.

Tsai MH, Lin BH (2008) Investigation of progressive collapse resistance and inelastic response for an earthquake-resistant RC building subjected to column failure. Engineering Structures 30:3619-3628.

Vecchio FJ, Collins MP (1986) The modified compression-field theory for reinforced-concrete elements subjected to shear. Journal of the American Concrete Institute 83:219-231.

Wang CH, Xiao JZ, Liang CF (2021) Study on nonlinear damping behavior of damaged recycled aggregate concrete beams. Structural Concrete:1429-1444.

Wu JY, Li J, Faria R (2006) An energy release rate-based plastic-damage model for concrete. International Journal of Solids and Structures 43:583-612.

Xu GQ, Ellingwood BR (2011) An energy-based partial pushdown analysis procedure for assessment of disproportionate collapse potential. Journal of Constructional Steel Research 67:547-555.

Yi WJ, He QF, Xiao Y, et al. (2008) Experimental study on progressive collapse-resistant behavior of reinforced concrete frame structures. ACI Structural Journal 105:433-439.

Yılmaz İ, Arslan E, Kızıltaş EÇ, et al. (2020) Development of a prediction method of Rayleigh damping coefficients for free layer damping coatings through machine learning algorithms. International Journal of Mechanical Sciences 166:105237.

Yu XH, Qian K, Lu DG, et al. (2017) Progressive collapse behavior of aging reinforced concrete structures considering corrosion effects. Journal of Performance of Constructed Facilities 31:04017009.

Zheng Z, Tian Y, Yang ZB, et al. (2020) Hybrid framework for simulating building collapse and ruin scenarios using finite element method and physics engine. Applied Sciences-Basel 10:4408.

CHAPTER V

Quantification of model uncertainties of the energy-based method for dynamic column removal scenarios

Partly redrafted after:

Ding L, Van Coile R, Botte W & Caspeele R, *"Quantification of model uncertainties of the energy-based method for dynamic column removal scenarios"*, Engineering Structures, 237 (2021):112057

Ding L, Van Coile R, Botte W & Caspeele R, *"Performance assessment of an energy–based approximation method for the dynamic capacity of RC frames subjected to sudden column removal scenarios"*, Applied Sciences, 11 (2021): 7492.

V.1 Introduction

When designing a structure with respect to robustness, it must also be taken into consideration that progressive collapses caused by extreme events are low-probability high-consequence phenomena (Adam *et al.*, 2018; Parisi *et al.*, 2019; Parisi and Scalvenzi, 2020). In order to be able to accurately predict the structural response, it is important to study the progressive collapse behaviour using a probabilistic approach (Faber, 2004; Ellingwood, 2006; Gulvanessian and Vrouwenvelder, 2006; Le and Xue, 2014; Li *et al.*, 2016; Song, 2020) since it has been found that there is a significant influence of many uncertainties, e.g. randomness from material properties, on the structural behaviour. Such probabilistic considerations are made e.g. in (Kwon and Elnashai, 2006; Biondini and Frangopol, 2016; Monteiro *et al.*, 2016; Biondini and Frangopol, 2017; Chen *et al.*, 2018; Astroza and Alessandri, 2019; Arteta *et al.*, 2020; He *et al.*, 2020; Jovanović *et al.*, 2020; Nagavedu Jayakumar and Kanchi, 2020; Vereecken *et al.*, 2020; Botte *et al.*, 2021; Gino *et al.*, 2021; Thienpont *et al.*, 2021). Moreover, when quantifying robustness indices (Sørensen *et al.*, 2012; Li *et al.*, 2016; Feng *et al.*, 2020), both the probabilistic-based method and the risk-based method require to perform a reliability analysis. Considering that the EBM is an approximate approach, the quantitative assessment of the model uncertainty associated to the EBM becomes important when the EBM is applied to quantify the reliability or robustness of a RC building structure following a sudden column removal scenario. Such information is currently lacking in literature. The model uncertainty information of the EBM is crucial to adequately quantify the failure probability of a system when the EBM is adopted.

In terms of experimental investigations, to date only two series of experimental investigations have been reported in literature (see Herraiz *et al.* (2015)) that enable to verify the effectiveness of the EBM, where a 2x1 bay flat slab structure subjected to a corner column removal or a penultimate column removal was investigated in a dynamic manner. To date there are insufficient experimental results to allow for a direct quantification of the EBM accuracy from experimental data. Therefore, the EBM accuracy can reasonably only be determined through comparison against nonlinear dynamic analyses.

In the previous Chapter IV the EBM for predicting the dynamic load-bearing capacity curve or the dynamic resistance was investigated in a deterministic way for a RC slab and a RC frame. The two numerical examples are consecutively adopted in this chapter to quantify the model uncertainty of the use of the EBM.

Considering the above, this chapter hence focuses on quantifying the model uncertainty of the EBM approach both for the RC slab (section V.3) and the RC frame (section V.4) subjected to notional sudden support removal scenarios. In section V.5 the main conclusions of this chapter are drawn.

V.2 Methodology: quantification of the model uncertainty associated to the application of EBM

As discussed before, an approximate result is obtained when using the EBM. The EBM curve completely depends on the static pushdown curve (see Figure IV.1c). Considering it is an approximate approach, it is therefore important to quantitatively assess the performance of the EBM, i.e. quantifying its model uncertainty through comparison to the more accurate dynamic analysis results. To evaluate this model uncertainty, the following three major steps are applied (see also the flowchart for the model uncertainty quantification of the EBM shown in Figure V.1):

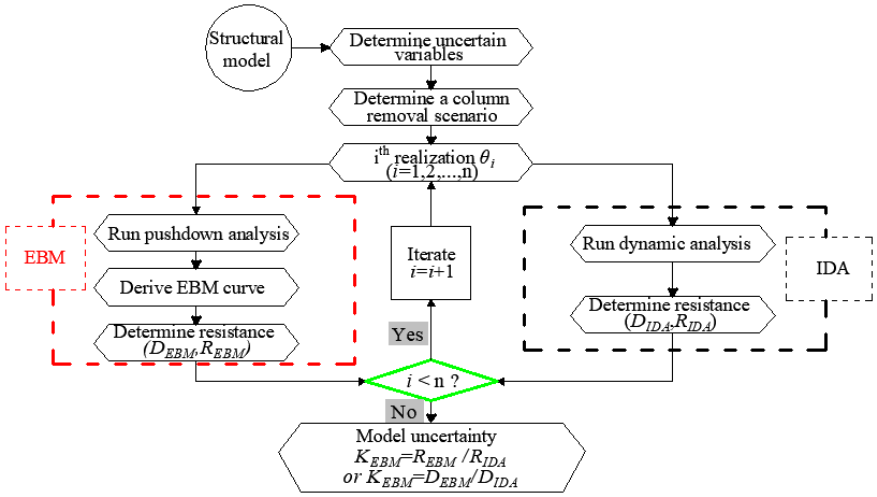

Figure V.1. Flowchart for the model uncertainty quantification.

a) Initially, the appropriate random variables and a column removal scenario are selected.
b) Subsequently, both the nonlinear static and dynamic analyses are carried out. In case of the former, the pushdown curve is subsequently used to derive the EBM curve and the corresponding dynamic resistance for every realization (the left branch in Figure V.1). In case of the latter, incremental dynamic analyses (IDA) are executed to accurately determine the dynamic resistance for every realization (the right branch in Figure V.1).
c) Finally, the model deviation for the EBM comparing to the IDA are calculated for both the resistances and the corresponding displacements:

$$K_{EBM} = \frac{R_{EBM}}{R_{IDA}} \text{ or } \frac{D_{EBM}}{D_{IDA}} \tag{V.1}$$

where K_{EBM} is the ratio of EBM/IDA. R_{EBM} is the ultimate load-bearing capacity according to the EBM, while R_{IDA} is the ultimate capacity according to the IDA. D_{EBM} is the maximum displacement calculated according to the EBM, while D_{IDA} is the maximum displacement calculated from the IDA.

V.3 Numerical example A: the RC slab

V.3.1 Probabilistic modelling of input variables

The FE model with regard to the real-scale one-way RC slab (Gouverneur *et al.*, 2013b) investigated in section IV.3 is further adopted for static and dynamic stochastic analyses in this section. First, eight parameters are selected as stochastic input variables based on other investigations (Gouverneur *et al.*, 2013b; Gouverneur *et al.*, 2013a; Botte, 2017; Yu *et al.*, 2017; Droogné *et al.*, 2018; Feng *et al.*, 2020). The developed FE model and the random parameters are combined to quantify the uncertainty propagation when applying the EBM. The probabilistic models are presented in Table V.1. These parameters are the density of the concrete, the compressive strength of the concrete, the yield stress of the reinforcement, the tensile strength of the reinforcement, the reinforcement strain at maximum stress, the Young's modulus of the reinforcement, the cross-section of the reinforcement and the stiffness of the horizontal springs (see Figure IV.2b). The other input parameters are considered deterministic.

Table V.1. Probabilistic models for the random variables.

Name	Units	Distribution	Mean	COV
Density of concrete ρ_c	kg/m^3	N	2400	0.04
Concrete compressive strength f_{cm}	MPa	LN	36.2	0.10
Reinforcement yield stress f_{ym}	MPa	N	555	0.03
Reinforcement tensile strength f_{um}	MPa	LN	605	0.03
Reinforcement strain at maximum stress ε_u	%	LN	8.3	0.15
Reinforcement Young's modulus E_s	GPa	N	207.9	0.08
Reinforcement cross-section A_s	mm^2	N	1256	0.02
Stiffness of horizontal spring k	kN/mm	LN	151.5	0.25

Several sampling techniques can be adopted, such as the Generalized F-discrepancy (GF-discrepancy) technique (Chen *et al.*, 2016), the Sobol point set (Li and Chen, 2009), and the correlation reducing Latin Hypercube Sampling (Olsson et al., 2003). In this section, Latin Hypercube Sampling (LHS) is used in combination with the developed FE model to perform static and dynamic stochastic

analyses. The advantage of LHS is that it allows to limit the number of calculations to an acceptable amount. As the standard LHS may bring undesired spurious correlation into the sample scheme, correlation reducing Latin Hypercube Sampling is used to avoid this unwanted effect (Olsson *et al.*, 2003). 60 Latin-Hypercube samples (in order to limit the computational demand) are generated based on the probabilistic models. Eventually, each sample is used as an input for the FE model of the RC slab to determine the responses obtained both by the EBM and by IDA.

V.3.2 Stochastic analysis

Based on the FE model and the values of the material properties, all Latin-Hypercube samples are evaluated considering both static pushdown analyses and direct dynamic analyses. For the former, only one pushdown analysis is executed for every realisation. For the latter, the incremental dynamic analyses (IDA) technique is used for every slab realization. Firstly, a load interval of 10.0 kN is employed from 40.0 kN to 160.0 kN, i.e. 13 dynamic simulations. Next, to obtain a 2.0 kN resolution for the maximum dynamic load, another 4 simulations are executed for every 2.0 kN in the interval between the last non-failed simulation and the first failed simulation. Subsequently, the curves from the pushdown analyses are converted into predicted dynamic capacity curves according to the EBM and compared with the results of IDA. Note that strain rate effects and damping are not taken into account (considering the analysis and observations from section IV.3.3). Model uncertainy incorporating damping in relation to the EBM still needs further investigation when applying continuum models. A support removal duration of 10^{-2} ms is adopted here for the IDA. Furthermore, it needs to be mentioned that the numerical results deviate from the observed experimental data after the first load peak is reached (section IV.3.2), but this does not prevent to quantify the model uncertainty of the EBM compared to direct dynamic analyses as performed here. Nevertheless, this indicates the importance to quantify also a model uncertainty with respect to the prediction of the highly nonlinear post-peak behaviour in case of large deformations and membrane actions, for which however at this stage only very limited data is available.

Figure V.2 shows the results of static pushdown analyses (designated as the curve 'pushdown'), the results of EBM (designated as 'EBM') and the results of the direct dynamic analyses (designated as 'IDA') as well as its maximum load value (designated as 'Max-IDA'), and this for every realization of the Latin Hypercube sampling. It is observed that the responses are highly sensitive to the realisations of the variables. However, good agreement is observed between EBM and IDA in almost all cases.

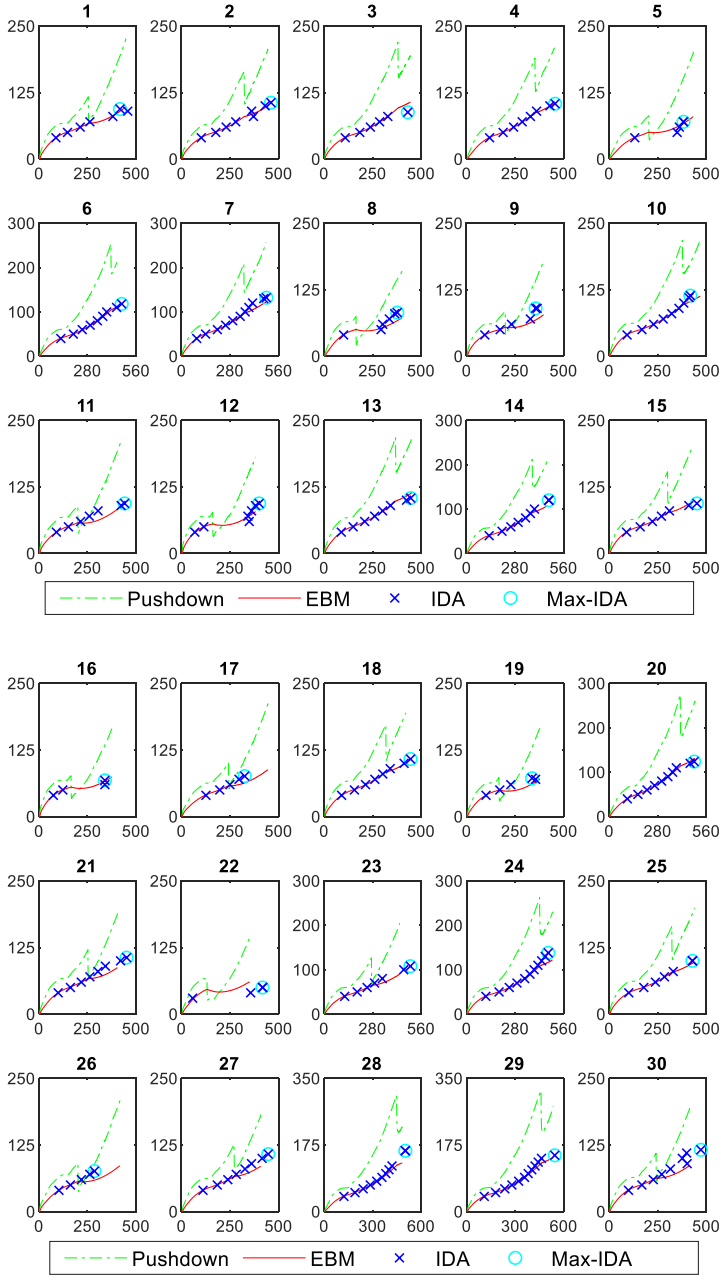

Figure V.2. Comparison for the results of stochastic analyses for every realization.

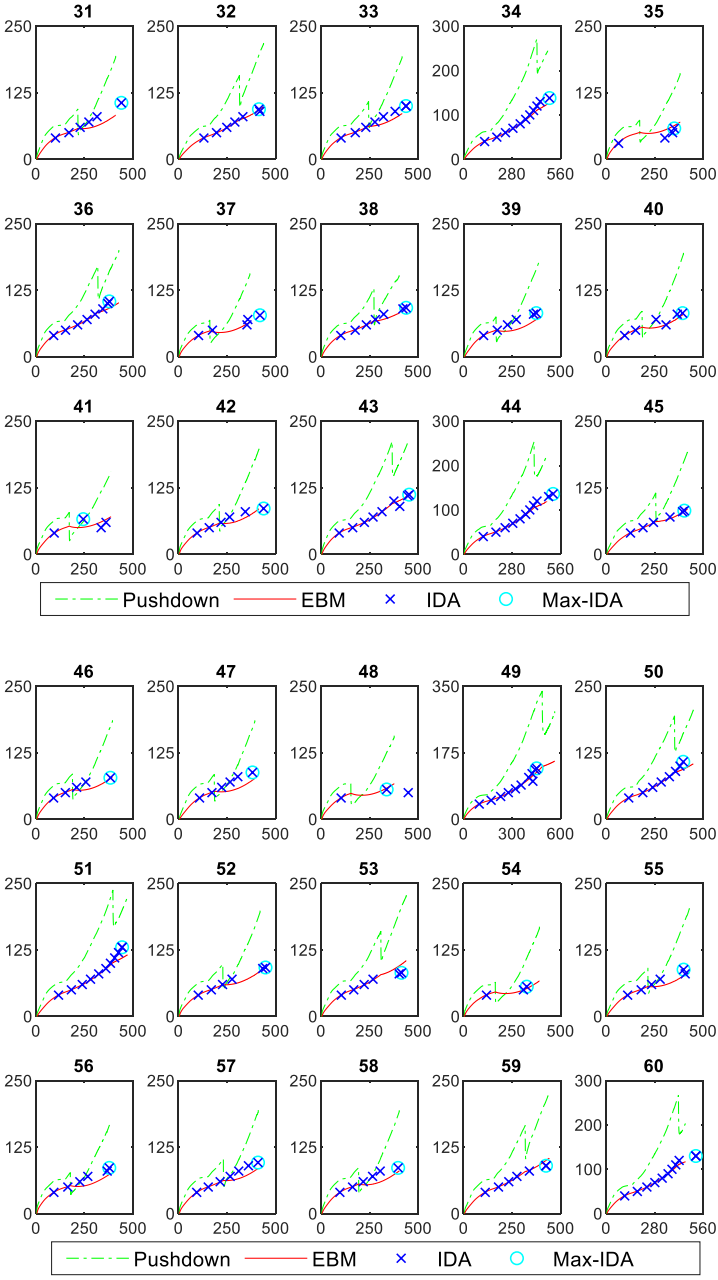

Figure V.2. Comparison for the results of stochastic analyses for every realization (cont'd).

The EBM curves are derived from the pushdown curves, i.e. the EBM curves depend on the pushdown curves and are calculated on the basis of conservation of energy. The results of the EBM evaluation corresponding to the stage before the first load peak (the rupture of top reinforcement) in the pushdown curve are almost identical to the results of IDA for all the realizations (Figure V.2). Note that the first load-peaks for IDA in cases No. 22 and No. 35 have been calculated separately and both values are 30.0 kN (the first load-peak for IDA is lower than 40.0 kN). However, notable deviations are found between EBM and IDA in the stage after the aforementioned first load peak. This can be explained by the fact that rupture of the top reinforcement causes a sudden decrease of load-bearing capacity in the pushdown curve (i.e. the first load peak). The EBM curve is affected by this sudden decrease of the pushdown curve. For instance, the rupture of top reinforcement may occur at different stages in the pushdown curves, see e.g. No. 6, No. 7, and No. 8. The rupture of the top reinforcement occurs much earlier in case No. 8 compared to cases No. 6 and No. 7. Moreover, the early rupture of top reinforcement in case No. 8 even causes the EBM curve to decrease. The deviation between the EBM and the IDA in case of No. 8 is therefore more significant than in the other two cases.

Those cases that show a clear difference between the two approaches relate to differences in predictions occurring after the first load peak of the static pushdown analysis, e.g. leading to an immediate follow-up failure of the second reinforcement layer in the IDA (e.g. No. 17 and No. 26), whereas this is not predicted as such by the EBM. Two situations are observed for the pushdown curves. The first situation indicates two load peaks, where the second load peak is the ultimate load-bearing capacity, and the smaller first load peak is due to the rupture of the top layer reinforcement over the inner support (e.g. No. 2 and No. 45). The other situation is where the first load peak has a larger value than the second load peak (e.g. No. 3 and No. 51). As the dynamic load-bearing curves of EBM completely depend on the pushdown curves, the two situations result in different ultimate capacities for EBM if different limit (or failure) criteria for the pushdown curve are taken into account.

As a conservative approach, a limit criterion can be defined as the rupture of one reinforcement layer (i.e. the top reinforcement layer in the case under investigation) although the slab can in some cases still take a higher load. This failure criterion is hence associated with the appearance of the first load peak in the pushdown curve and the rupture of the top layer of the reinforcement in the IDA curve. Note that even if the second load peak is lower in some cases, it results in an additional capacity in the EBM curve, i.e. the EBM curve keeps increasing after the first load peak.

In case the limit criterion relates to the first load peak (associated with rupture of the top reinforcement layer), the results of the load-bearing capacities are illustrated in Figure V.3a for all Latin Hypercube simulations. Again, it is observed that the EBM results correspond well to the results obtained through the IDA, both with respect to the loads corresponding to the first load peaks as well as for the associated displacements (see Figure V.3b and Figure V.3c, respectively).

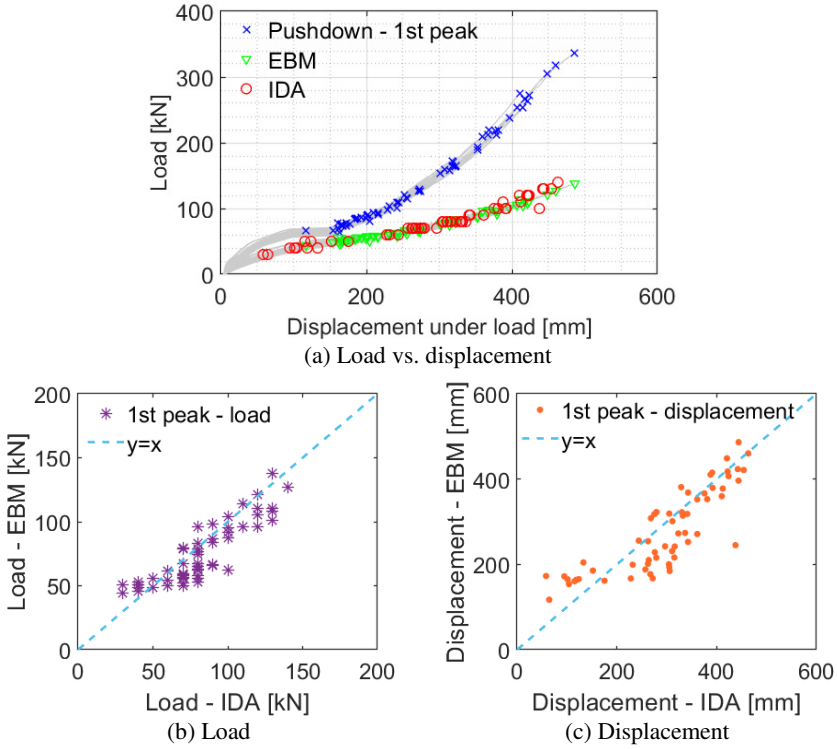

(a) Load vs. displacement

(b) Load

(c) Displacement

Figure V.3. Comparison of the first load peak: (a) load-displacement relationship; (b) comparison of load corresponding to the rupture of one reinforcement layer; and (c) comparison of the associated displacement.

In case a quantification of the ultimate load-bearing capacity is envisaged (regardless of whether this is occurring as a result of a post-peak behaviour associated with larger displacements and a complex stress redistribution), Figure V.4a represents the results of this ultimate load-bearing capacity. Figure V.4b,c present the comparison between the EBM and IDA for ultimate load-bearing capacities as well as the displacements corresponding to them, respectively. Again, a good agreement is found for the prediction of the ultimate load-bearing capacity

by the EBM, although the performance is less accurate when assessing the associated displacements.

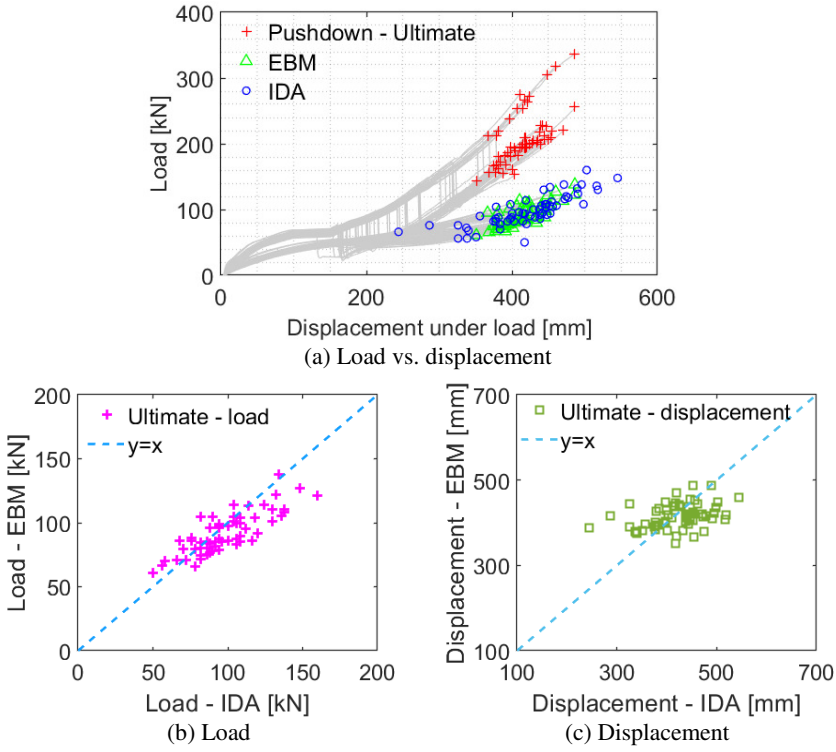

(a) Load vs. displacement

(b) Load

(c) Displacement

Figure V.4. Comparison of the ultimate load-bearing capacity: (a) load-displacement relationship; (b) comparison of load; and (c) comparison of displacement.

Finally, for completeness, also the prediction of the load-bearing capacity and associated displacements by the EBM in relation to the second load peak in the pushdown analysis is analysed (i.e. relating to the rupture of both reinforcement layers), see Figure V.5a. Although in the pushdown analysis the second load peaks may be lower than the highest load peaks, the dynamic ultimate capacities of EBM based on the pushdown curves will be larger in these cases (Figure V.5a). The comparison of the loads associated to this limit criterion and the corresponding ultimate displacements are presented in Figure V.5b,c, respectively. Again, reasonably good agreements are observed for the EBM, when comparing to the IDA results.

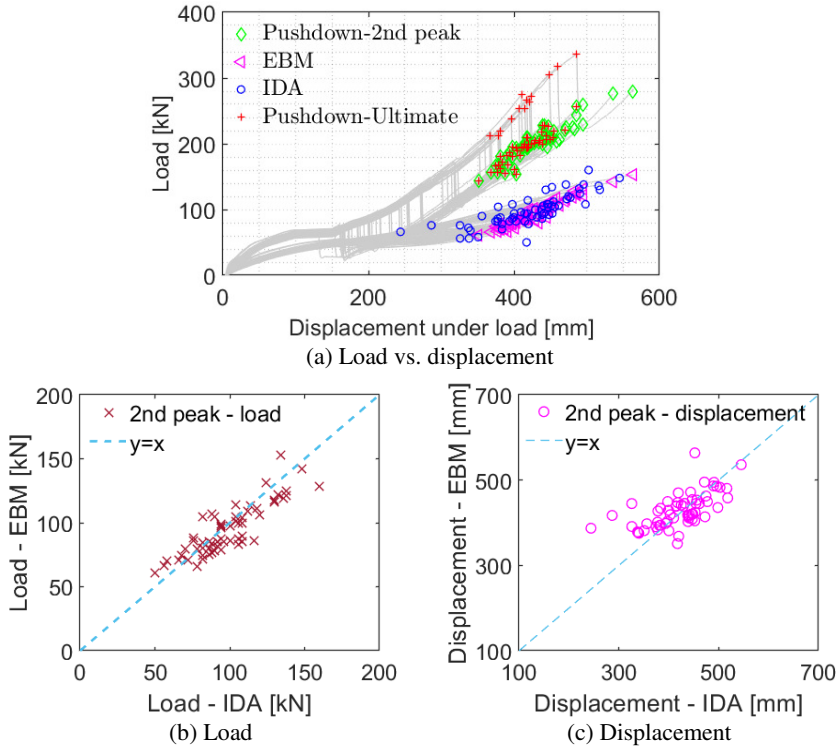

(a) Load vs. displacement

(b) Load

(c) Displacement

Figure V.5. Comparison of the second load peak (ultimate displacement): (a) load-displacement relationship; (b) comparison of load; and (c) comparison of displacement.

V.3.3 Model uncertainty quantification of EBM versus IDA analyses

To evaluate the performance of the EBM quantitatively, ratios of the loads of the EBM to those from the direct dynamic analysis (IDA) (i.e. corresponding to Figure V.3b, Figure V.4b and Figure V.5b) are calculated using Eq. (V.1). Furthermore, ratios of the displacements (corresponding to Figure V.3c, Figure V.4c and Figure V.5c) are calculated as well. As mentioned before, these values can be related to load-bearing capacity associated to the rupture of one reinforcement layer (Figure V.3), the ultimate load-bearing capacity (as the maximal load-bearing capacity observed, regardless of whether or not this relates to a post-peak behaviour after rupture of the first reinforcement layer) (Figure V.4) or the load-bearing capacity associated to the rupture of both reinforcement layers (Figure V.5). The mean values and standard deviations (St.D.) of the ratios K_{EBM} are shown in Table V.2. Lognormal distributions are found to represent the distributions of the ratios well. These models can be considered as a model uncertainty for the application of the EBM in structural reliability calculations.

Table V.2. Ratios of EBM/IDA.

Case		K_{EBM} [-]	
		Mean (μ)	**St.D. (σ)**
$K_{EBM} = \frac{R_{EBM}}{R_{IDA}}$	First peak	0.95	0.20
	Ultimate load-bearing capacity	0.96	0.13
	Second peak	0.98	0.13
$K_{EBM} = \frac{D_{EBM}}{D_{IDA}}$	First peak	1.02	0.38
	Ultimate load-bearing capacity	1.00	0.15
	Second peak	1.03	0.13

Further, histograms of the ratios in relation to the three situations are presented in Figure V.6. Figure V.6a shows ratios of the loads of the first load peaks, where a lognormal distribution LN(0.95, 0.20) is found to represent the histogram, while a LN(1.02,0.38) is fitted for the displacements of the first peaks as presented in Figure V.6b. Figure V.6c presents the ratios of the loads of the ultimate load-bearing capacity, where a lognormal distribution LN(0.96, 0.13) is used to fit the probability density function (PDF), while a LN(1.00,0.15) is considered for the displacements of the ultimate load-bearing peaks as shown in Figure V.6d. Figure V.6e,f show the ratios for the loads and the displacements of the second load peaks respectively, where a lognormal distribution LN(0.98, 0.13) for the loads and a lognormal distribution LN(1.03,0.13) for displacements are found to fit the histograms, respectively.

V.3.4 Conclusions in relation to the RC slab

In relation to the previous analyses for the RC slab, both stochastic static analyses and stochastic dynamic analyses were executed considering eight stochastic input variables using Latin Hypercube sampling. The recorded load-displacement curves of the stochastic static analyses were further used to approximate the maximum dynamic responses through the application of the EBM. The results of EBM were compared with the results of direct dynamic analyses (i.e. IDA) to assess the performance of EBM in a probabilistic way. On the basis of these simulations, probabilistic models were proposed for the model uncertainty of EBM compared to direct dynamic analyses, in particular in relation to the prediction of the loads and displacements associated to the first rupture of reinforcement, the ultimate load-bearing capacity (regardless whether or not this is the result of a post-peak behaviour after the rupture of the first reinforcement layer) and the rupture of the second reinforcement layer. Comparing to the IDA results, a good performance for the EBM was observed before the first load peak in the pushdown curve (EBM curve vs. IDA curve), while a larger deviation could be found beyond the first load

peak. In generally, the EBM could give a conservative result with regard to the load-bearing capacity. Overall, a good agreement was found between EBM and IDA.

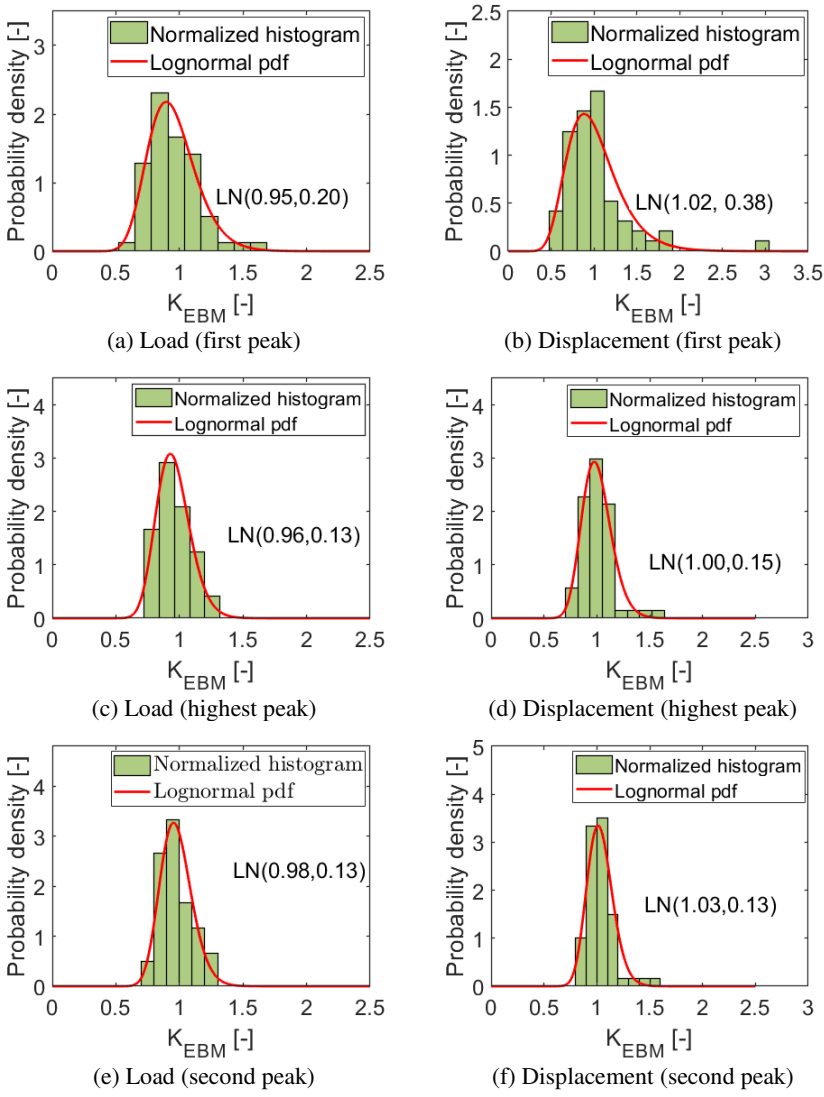

Figure V.6. Histograms and PDFs of the ratios of EBM/IDA: (a) load corresponding to first peak; (b) displacement of first peak; (c) load corresponding to ultimate peak; (d) displacement of ultimate peak; (e) load corresponding to second peak; and (f) displacement of second peak.

The model uncertainty of the loads at the first load peaks obtained through the EBM compared to IDA was found to be represented well by a lognormal distribution with mean of 0.95 and a standard deviation of 0.20, i.e. LN(0.95,0.20). With regard to the ultimate load-bearing capacities, a lognormal distribution LN(0.96,0.13) was obtained. In terms of the model uncertainty for the loads of the second load peaks, a lognormal distribution LN(0.98,0.13) was found to fit the histogram.

When comparing the associated displacements, the model uncertainty for displacements at the first load peaks was found to be represented well by a lognormal distribution with mean of 1.02 and a standard deviation of 0.38, while for the displacements at the ultimate load-bearing capacities, a lognormal distribution LN(1.00,0.15) was found to be appropriate. With regard to the model uncertainty for the displacements of the second load peaks, a lognormal distribution LN(1.03,0.13) was found to fit the histogram for the displacements.

V.4 Numerical example B: the RC frame

V.4.1 Probabilistic models of random variables

The FE model of the RC frame in section IV.4 is consecutively used to investigate the influence of uncertainties and to quantify the model uncertainty related to the use of the EBM. In order to calculate the stochastic responses for the three cases (i.e. Cases A, B and C), eight input parameters are selected as random variables, which are presented in Table V.3. c is the concrete cover, which is modelled as a bounded Beta distribution (Holický and Sýkora, 2010), with a mean value equal to a specified value of 30 mm, a standard deviation of 5 mm, a lower bound of 0 mm and an upper bound of three times of the mean value, i.e. 90 mm. f_{cm} is the mean concrete compressive strength, while ε_{c1} is the peak compressive strain (JCSS, 2001; Holický and Sýkora, 2010; fib, 2013; Feng *et al.*, 2020). For modelling the concrete tensile strength, $Y_{2,j}$ is employed to reflect variations due to factors not well accounted for by concrete compressive strength, i.e. $f_{ctm} = 0.3(f_{ck})^{2/3}Y_{2,j}$ (JCSS, 2001). E_s, f_{ym}, f_{um} and ε_u are the modulus of elasticity, the yield stress, the tensile strength and the ultimate strain of the reinforcing steel, respectively (JCSS, 2001; Holický and Sýkora, 2010; fib, 2013; Feng *et al.*, 2020).

V.4.2 Stochastic analysis

Based on the probabilistic models presented in Table V.3, 10 000 Latin Hypercube samples (LHS) are generated. The large amount of samples are used to fully represent the sampling space. Considering the standard LHS may bring undesired spurious correlation into the sample scheme, correlation reduced Latin Hypercube Sampling (CLHS) is used to avoid this unwanted effect (Olsson *et al.*, 2003). It is worth noting that all the parameters are assumed to be independent except the yield

stress f_{ym} and the tensile strength f_{um} of reinforcement for which a correlation coefficient of 0.86 is considered (JCSS, 2001). Note that these two parameters, i.e. yield stress and tensile strength, are correlated on the basis of the requirement of the ductility class C for the reinforcing steel (CEN, 2004).

Table V.3. Probabilistic models for random variables.

Variable (related to)	Units	Distribution	Mean	COV
Concrete cover c	mm	Beta	30	0.17
Concrete compressive strength f_{cm}	MPa	Lognormal	28	0.18
Concrete compressive strain at peak stress ε_{c1}	%	Lognormal	0.21	0.15
Model uncertainty for tensile strength $Y_{2,j}$	-	Lognormal	1	0.30
Rebar elastic modulus E_s	GPa	Normal	205	0.08
Rebar yield stress f_{ym}	MPa	Lognormal	560	0.05
Rebar ultimate strength f_{um}	MPa	Lognormal	655	0.06
Rebar fracture strain ε_u	%	Lognormal	12	0.15

Subsequently, both a pushdown analysis and an IDA are carried out for every sample for every column removal case, i.e. Case A, Case B and Case C. The loading schemes are identical to the corresponding deterministic analyses in section IV.4. In order to reduce the computational demand in the stochastic dynamic analyses, a resolution level of 0.5 kN/m (compared to 0.05 kN/m used for the deterministic dynamic analysis in section IV.4) is used for the IDA when determining the ultimate load-bearing capacity. The damping ratio DR = 5% (Rayleigh damping proportional to the mass matrix and the tangent stiffness matrix) is considered in the stochastic dynamic analyses.

The histograms of the ultimate load-bearing capacity from both static and dynamic analyses are shown in Figure V.7 and a summary of the results is presented in Table V.4. Note that the resistances obtained through the static pushdown analyses are considered to correspond to first failures as discussed before. The results for Cases A, B, and C are presented in Figure V.7a,b,c, respectively, where both the results from the static pushdown analyses and IDA are shown in order to compare with each other. Lognormal distributions are found to fit the histograms well for the three cases. The resistance from the pushdown analysis is found to be larger than that of the IDA, as also already evidenced in the previous section IV.4. Mean values and standard deviations (St.D.) for the stochastic pushdown and IDA analyses are summarized in Table V.4. Furthermore, it was found that the resistance in case of the exterior column loss scenario (Case A) is significantly lower than those for the interior column loss scenarios (Case B and Case C), since it is more difficult to

redistribute the unbalanced load in the former case (or less alternate load paths are available).

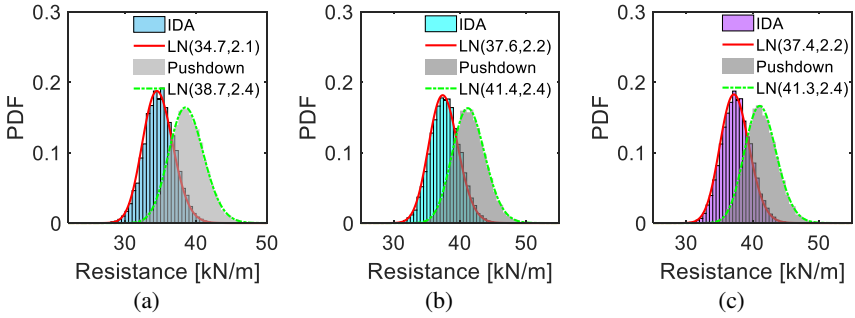

Figure V.7. Histograms and PDFs of resistances for stochastic pushdown and IDA analyses: (a) Case A; (b) Case B; and (c) Case C.

Table V.4. Mean, standard deviation and deviation of the ultimate load-bearing capacity.

	Case A		**Case B**		**Case C**	
	Mean	**St.D.**	**Mean**	**St.D.**	**Mean**	**St.D.**
$R_{Pushdown}$ [kN/m]	38.7	2.4	41.4	2.4	41.3	2.4
R_{IDA} [kN/m]	34.7	2.1	37.6	2.2	37.4	2.2
R_{EBM} [kN/m]	33.6	2.1	37.2	2.1	36.9	2.1
$(R_{EBM} - R_{IDA})/R_{IDA}$	-3.17%	-	-1.06%	-	-1.34%	-

Next, the EBM is adopted to calculate the dynamic capacity curves from the pushdown curves. It is important to indicate that, also here, the EBM curve is calculated based on the pushdown curve up to the first failure (i.e. the first load peak as it is the ultimate load-bearing capacity) in the frame. The predicted dynamic load-bearing capacity curves are similar to those of the deterministic analyses (see section IV.4). The histograms and PDFs of the ultimate load-bearing capacities from EBM are presented in Figure V.8 for the three cases, where lognormal distributions are found to be appropriate to fit the histograms. Only a small deviation between the EBM result and the IDA result is observed for Case A (Figure V.8a), while little difference is observed between the EBM results and the IDA results for both Case B and Case C (Figure V.8b,c). The mean resistances from EBM and their deviations comparing to the IDA results are summarized in Table V.4. The maximum deviation is -3.17% in Case A and much smaller deviations are found for the other two cases, which demonstrates that the EBM has a good performance to predict the dynamic resistance, also when uncertainties on variables are taken into account.

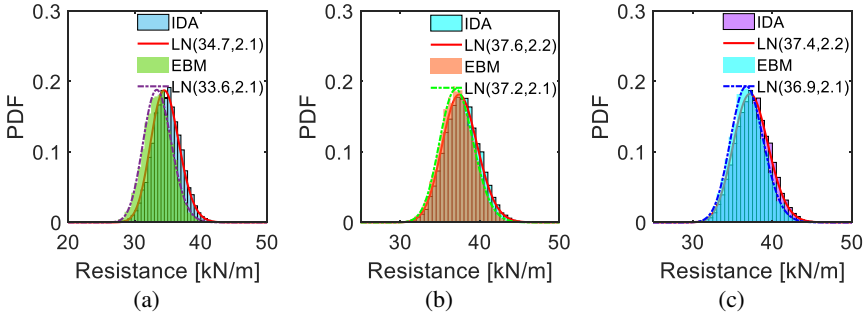

Figure V.8. Resistances of IDA and EBM: (a) histograms and PDFs for Case A; (b) histograms and PDFs for Case B; and (c) histograms and PDFs for Case C.

In order to better compare the EBM and IDA results, the resistances and the corresponding displacements are compared in Figure V.9 and Figure V.10, respectively. Figure V.9a,b,c shows the comparisons of the resistances between EBM and IDA for Cases A, B and C, respectively. It can be seen that the data points are located along the line y=x, which means similar results are obtained between EBM and IDA. Moreover, coefficients of determination (R^2) are calculated to be 0.67, 0.93 and 0.92 for the three cases, respectively. Apparently, the deviation in Case A is larger (R^2 = 0.67), since the dynamic response is not a SDOF oscillation, as discussed before. In general, the IDA results are found to be slightly larger, since the assumptions (e.g. damping effect) discussed in section V.2 will result in a higher resistance compared to when using EBM. This means the EBM provides a conservative result for resistance assessment.

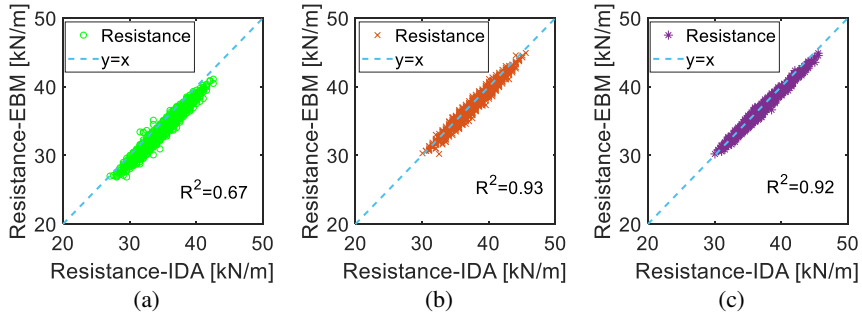

Figure V.9. Comparison of resistances between EBM and IDA: (a) Case A; (b) Case B; and (c) Case C.

Figure V.10a,b,c shows the comparisons of the corresponding displacements between EBM and IDA for Cases A, B and C, respectively. Also in this case, the data points are situated along the line y=x. However, a larger variation is observed for the displacement responses, since the response varies fast in the highly nonlinear stage (see the load-displacement curves in Figure IV.23). This can also be verified from coefficients of determination (R^2) which are calculated to be 0.77, 0.74 and 0.80 for the three cases, respectively.

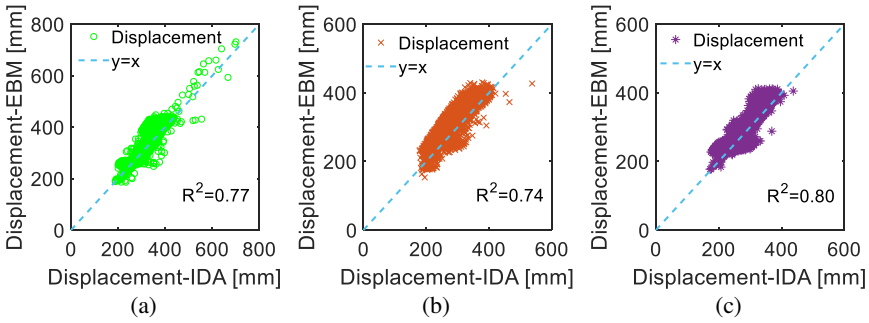

Figure V.10. Comparison of corresponding displacements between EBM and IDA: (a) Case A; (b) Case B; and (c) Case C.

V.4.3 Model uncertainty quantification

To quantitatively evaluate the performance of the EBM, the ratios K_{EBM} of the resistances of the EBM to those from the incremental dynamic analyses (IDA) are calculated according to Eq. (V.1), as well as for the ratios of the displacements. The mean and standard deviation of the ratios K_{EBM}, for Cases A, B and C separately and a total for the three cases A, B and C considered, are shown in Table V.5.

Histograms and PDFs of the ratios with regard to the resistances are presented in Figure V.11. Figure V.11a,b,c show ratios in terms of the resistances for Cases A, B, and C respectively, where lognormal distributions LN(0.97,0.01), LN(0.99,0.01), and LN(0.99,0.01) are found to represent the histograms. Figure V.11d presents the ratios of the ultimate capacities of all three cases as a total (case 'all' in Table V.5) for which a lognormal distribution LN(0.98,0.02) is fitted.

Histograms and PDFs of the ratios in terms of the corresponding displacements for the three cases are presented in Figure V.12. Figure V.12a,b,c,d show the ratios of the displacements respectively for Cases A, B, C and 'all', where lognormal distributions LN(1.05,0.08), LN(1.08,0.08), LN(1.06,0.08), and LN(1.07,0.08) are fitted for the cases, respectively.

The values of the model uncertainties associated with the resistances are close to unity and the standard deviations are very small. This indicates that the EBM has a good accuracy in calculating the dynamic resistances. On the other hand, a slightly less performance is found in relation to the computation of the corresponding displacements, as the mean values are deviating more from 1 and the standard deviations are considerably larger compared to the model uncertainties on the loads.

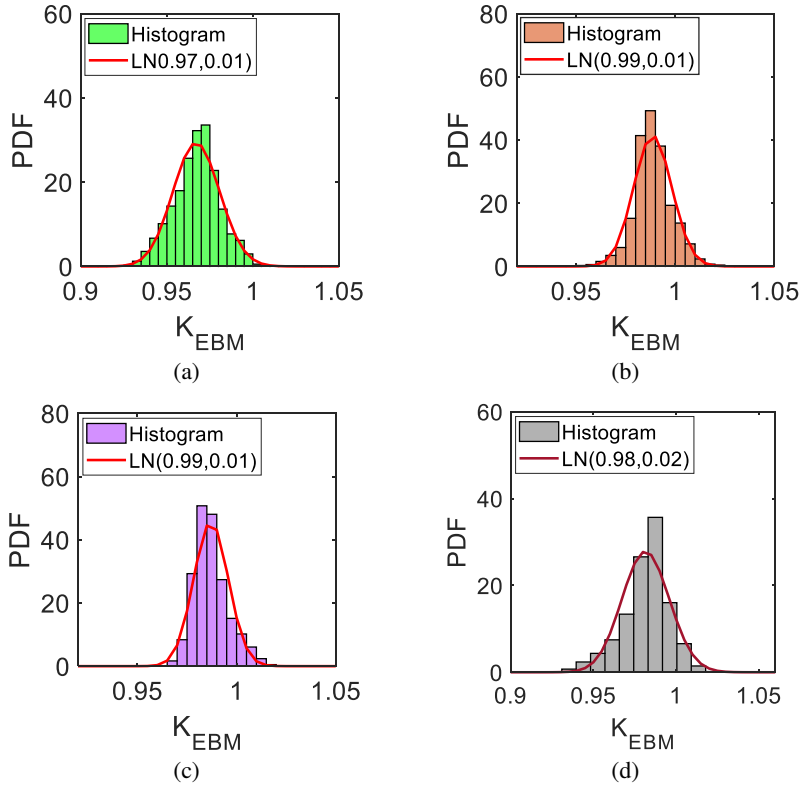

Figure V.11. Histograms and PDFs for the ratios of EBM/IDA regarding resistances: (a) Case A; (b) Case B; (c) Case C; and (d) all three cases.

According to these results, a good performance has been found for the model uncertainties involved in the application of the EBM instead of the more complex IDA, especially for the prediction of the resistance, i.e. resulting in a small bias and small standard deviation. The model uncertainty models can be adopted in a probabilistic design situation, for instance, as follows:

1) Perform stochastic nonlinear static analyses with specified random variables and column removal scenarios;
2) Apply the EBM, i.e. Eq. (IV.1), to calculate dynamic ultimate load-bearing capacities R, according to the static capacity curves from step 1; and
3) Evaluate the failure probability P_f through the following limit state function Z:

$$Z = K_R \cdot \left(R / K_{EBM} \right) - K_L \cdot L \tag{V.2}$$

where K_R and K_L are the resistance and load model uncertainties (JCSS, 2001); L is the load effect; and K_{EBM} is the additional model uncertainty relating to the application of the EBM instead of IDA (Table V.5). When the model uncertainty is not considered in Eq. (V.2), it gives a conservative result, since the EBM cannot take dynamic effects into account.

V.4.4 Conclusions and discussions in relation to the RC frame

Based on the FE model of the RC frame, both static and dynamic stochastic analyses were executed considering eight stochastic input variables using Latin Hypercube sampling. The EBM was adopted to calculate the dynamic responses on the resulted load-displacement curves from the static stochastic analyses. The results obtained by the EBM were compared with the results of direct dynamic analyses (IDA) to assess the performance of EBM in a probabilistic way. On the basis of these simulations, probabilistic models were proposed for the model uncertainty of EBM compared to direct dynamic analyses, in particular in relation to the prediction of the load bearing capacity and the corresponding maximum displacements with regard to different column removal scenarios. Good agreement was found between EBM and direct dynamic analyses (IDA).

Table V.5. Ratios of EBM/IDA.

Case		K_{EBM} **[-]**	
		Mean (μ)	**St.D. (σ)**
$K_{EBM} = \frac{R_{EBM}}{R_{IDA}}$	Case A	0.97	0.01
	Case B	0.99	0.01
	Case C	0.99	0.01
	All	0.98	0.02
$K_{EBM} = \frac{D_{EBM}}{D_{IDA}}$	Case A	1.05	0.08
	Case B	1.08	0.08
	Case C	1.06	0.08
	All	1.07	0.08

Probabilistic models were proposed for the model uncertainty of EBM compared to IDA. For the different removal scenarios considered as a total, a lognormal distribution with mean of 0.98 and a standard deviation of 0.02, i.e. LN(0.98,0.02),

was fitted for the resistances, while a lognormal distribution LN(1.07,0.08) was obtained for the displacements. These values are of particular interest to be included as additional model uncertainty in probabilistic analyses in case EBM is applied for the quantification of alternate load path resistances considering dynamic behaviour.

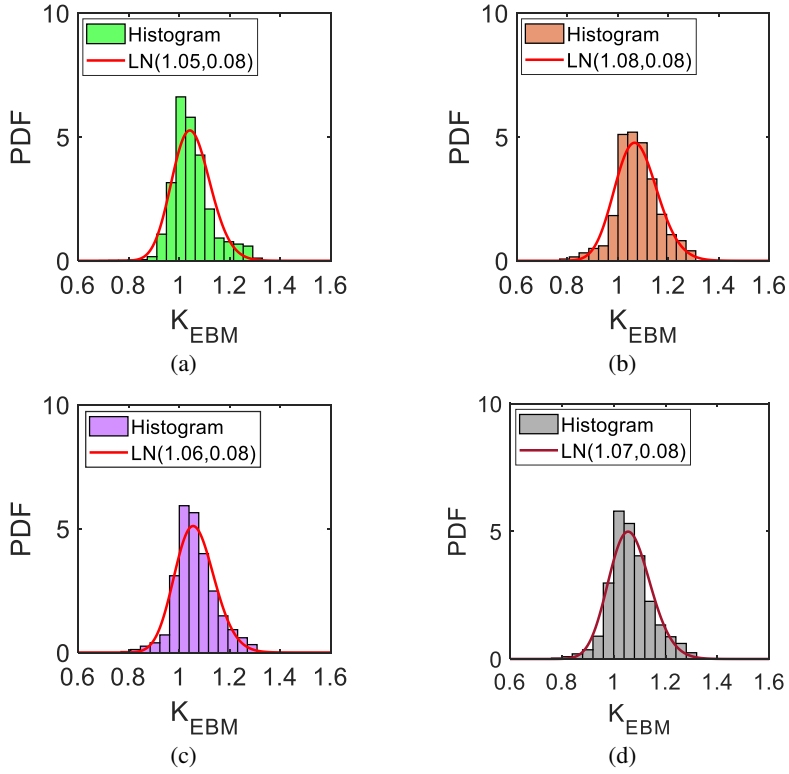

Figure V.12. Histograms and PDFs of the ratios of EBM/IDA for displacements: (a) Case A; (b) Case B; (c) Case C; and (d) all three cases.

V.5 Summary and conclusions

In this chapter, stochastic analyses have been carried out both for the RC slab and the RC frame (deterministic analyses were performed in Chapter IV), in order to quantify the model uncertainty of the EBM instead of the use of the direct dynamic analysis. The Latin Hypercube sampling technique was used in both numerical examples. The results of stochastic static pushdown analyses were adopted in the EBM to derive the approximate maximum dynamic responses. The results of EBM were compared with the results of direct dynamic analyses to assess the

performance of the EBM in a probabilistic way. Good agreement was found between EBM and the direct dynamic analysis. On the basis of these simulations, probabilistic models were proposed for the model uncertainty of EBM compared to the direct dynamic analysis, i.e. the ratio of EBM to the direct dynamic analysis.

The values of the model uncertainties associated with the resistances for both cases were close to unity and the standard deviations were very small. This indicated that the EBM had a good accuracy in calculating the dynamic resistances. On the other hand, slightly less performance was found in relation to computation of the corresponding displacements, as the mean values were deviating more from 1 and larger standard deviations were observed.

Although the performance of the EBM has been verified and its model uncertainty has been calculated, it must be emphasized that the results are based on a particular RC slab and a RC frame and that further investigations in relation to the assessment of dynamic column removal scenarios might be considered in a similar manner as illustrated in this chapter, before coming to a more generally applicable proposal for the model uncertainty involved.

V.6 References

Adam JM, Parisi F, Sagaseta J, et al. (2018) Research and practice on progressive collapse and robustness of building structures in the 21st century. Engineering Structures 173:122-149.

Arteta CA, Piedrahita J, Ortiz A, et al. (2020) Quantifying the uncertainty in modeling of RC walls. 17th World Conference on Earthquake Engineering. Sendai, Japan, pp. 1-12.

Astroza R, Alessandri A (2019) Effects of model uncertainty in nonlinear structural finite element model updating by numerical simulation of building structures. Structural Control and Health Monitoring 26:e2297.

Biondini F, Frangopol DM (2016) Life-cycle performance of deteriorating structural systems under uncertainty: Review. Journal of Structural Engineering 142:F4016001.

Biondini F, Frangopol DM (2017) Time-variant redundancy and failure times of deteriorating concrete structures considering multiple limit states. Structure and Infrastructure Engineering 13:94-106.

Botte W (2017) Quantification of structural reliability and robustness of new and existing concrete structures considering membrane action. PhD diss. Ghent University.

Botte W, Vereecken E, Taerwe L, et al. (2021) Assessment of posttensioned concrete beams from the 1940s: Large-scale load testing, numerical analysis and Bayesian assessment of prestressing losses. Structural Concrete 22:1500-1522.

CEN (2004) Eurocode 2: Design of concrete structures—Part 1-1: General rules and rules for buildings. EN 1992-1-1.
Chen J, Yang J, Li J (2016) A GF-discrepancy for point selection in stochastic seismic response analysis of structures with uncertain parameters. Structural safety 59:20-31.
Chen JB, He JR, Ren XD, et al. (2018) Stochastic harmonic function representation of random fields for material properties of structures. Journal of Engineering Mechanics 144:04018049.
Droogné D, Botte W, Caspeele R (2018) A multilevel calculation scheme for risk-based robustness quantification of reinforced concrete frames. Engineering Structures 160:56-70.
Ellingwood BR (2006) Mitigating risk from abnormal loads and progressive collapse. Journal of Performance of Constructed Facilities 20:315-323.
Faber MH (2004) Failure consequences and reliability acceptance criteria for exceptional building structures: A study taking basis in the failure of the World Trade Center Twin Towers. vdf Hochschulverlag AG.
Feng D, Xie S, Xu J, et al. (2020) Robustness quantification of reinforced concrete structures subjected to progressive collapse via the probability density evolution method. Engineering Structures 202:109877.
fib (2013) Model code for concrete structures 2010.
Gino D, Castaldo P, Giordano L, et al. (2021) Model uncertainty in non‐linear numerical analyses of slender reinforced concrete members. Structural Concrete 22:845-870.
Gouverneur D, Caspeele R, Taerwe L (2013a) Effect of reinforcement curtailment on deflections, strain and crack development in RC slabs under catenary action. Magazine of Concrete Research 65:1336-1347.
Gouverneur D, Caspeele R, Taerwe L (2013b) Experimental investigation of the load-displacement behaviour under catenary action in a restrained reinforced concrete slab strip. Engineering Structures 49:1007-1016.
Gulvanessian H, Vrouwenvelder T (2006) Robustness and the Eurocodes. Structural Engineering International 16:167-171.
He JR, Chen JB, Ren XD, et al. (2020) A shake table test study of reinforced concrete shear wall model structures exhibiting strong non-linear behaviors. Engineering Structures 212:110481.
Herraiz B, Vogel T, Russell J (2015) Energy-based method for sudden column failure scenarios: theoretical, numerical and experimental analysis IABSE Workshop Helsinki 2015: Safety, Robustness and Condition Assessment of Structures. International Association for Bridge and Structural Engineering IABSE, pp. 70-77.
Holický M, Sýkora M (2010) Stochastic models in analysis of structural reliability. The international symposium on stochastic models in reliability engineering, life sciences and operation management.

JCSS (2001) Probabilistic model code. Joint Committee on Structural Safety.
Jovanović B, Van Coile R, Hopkin D, et al. (2020) Review of current practice in probabilistic structural fire engineering: permanent and live load modelling. Fire Technology 57:1-30.
Kwon O-S, Elnashai A (2006) The effect of material and ground motion uncertainty on the seismic vulnerability curves of RC structure. Engineering Structures 28:289-303.
Le JL, Xue B (2014) Probabilistic analysis of reinforced concrete frame structures against progressive collapse. Engineering Structures 76:313-323.
Li J, Chen J (2009) Stochastic dynamics of structures. John Wiley & Sons.
Li Y, Lu X, Guan H, et al. (2016) Probability-based progressive collapse-resistant assessment for reinforced concrete frame structures. Advances in Structural Engineering 19:1723-1735.
Monteiro R, Delgado R, Pinho R (2016) Probabilistic seismic assessment of RC bridges: Part I — uncertainty models. Structures 5:258-273.
Nagavedu Jayakumar Y, Kanchi BR (2020) Probabilistic studies on mechanics - based shear capacity models for reinforced concrete beams with stirrups. Structural Concrete 21:376-392.
Olsson A, Sandberg G, Dahlblom O (2003) On Latin hypercube sampling for structural reliability analysis. Structural safety 25:47-68.
Parisi F, Scalvenzi M (2020) Progressive collapse assessment of gravity-load designed European RC buildings under multi-column loss scenarios. Engineering Structures 209:110001.
Parisi F, Scalvenzi M, Brunesi E (2019) Performance limit states for progressive collapse analysis of reinforced concrete framed buildings. Structural Concrete 20:68-84.
Song X (2020) Reliability analysis of code-conforming steel-frame structures against column-loss scenarios. Journal of Structural Engineering 146:04020025.
Sørensen JD, Rizzuto E, Narasimhan H, et al. (2012) Robustness: theoretical framework. Structural Engineering International 22:66-72.
Thienpont T, Van Coile R, Caspeele R, et al. (2021) Burnout resistance of concrete slabs: Probabilistic assessment and global resistance factor calibration. Fire Safety Journal 119:103242.
Vereecken E, Botte W, Lombaert G, et al. (2020) A Bayesian inference approach for the updating of spatially distributed corrosion model parameters based on heterogeneous measurement data. Structure and Infrastructure Engineering:1-17.
Yu XH, Lu DG, Qian K, et al. (2017) Uncertainty and sensitivity analysis of reinforced concrete frame structures subjected to column loss. Journal of Performance of Constructed Facilities 31:04016069.

PART C

QUANTIFICATION OF STRUCTURAL ROBUSTNESS CONSIDERING STRUCTURAL DYNAMIC BEHAVIOUR

CHAPTER VI

Reliability-based robustness quantification of RC structures subjected to sudden column removal scenarios

VI.1 Introduction

In the previous two chapters (i.e. Chapter IV and Chapter V) the energy-based method (EBM) for the prediction of the dynamic load-bearing capacity curve or the dynamic ultimate resistance has been investigated in a deterministic way (section IV.4) and in a probabilistic way (section V.4) for the RC frame. As the computational demand for the EBM is almost identical to that of the associated static nonlinear analysis, the calculation demand can be significantly reduced if the EBM rather than the direct dynamic analysis is adopted. Furthermore, probabilistic models for the model uncertainty of the use of the EBM comparing to the more accurate dynamic analyses have been proposed in section V.4 (Chapter V) with regard to the RC frame. The EBM and associated model uncertainty models can be further employed to evaluate the failure probability (or reliability) or structural robustness of the RC frame.

This chapter focuses on investigating the performance of the EBM in the context of the probabilistic or reliability-based structural robustness quantification, taking into account dynamic effects and incorporating the model uncertainty models in relation to the use of the EBM comparing to the more accurate dynamic analyses. Details of the proposed EBM-based structural robustness assessment approach will be presented in section VI.2. The stochastic analyses for the intact structural system with regard to the RC frame (see section V.4) are carried out in section VI.3. Failure probabilities and reliability indices for both intact and damaged structural systems (three cases with one column loss each) are calculated in section VI.4. Further, reliability indices are calculated in order to quantify the reliability-based robustness indices in section VI.5. Eventually, conclusions are drawn in VI.6.

VI.2 Reliability-based robustness quantification using the EBM

To quantify the structural robustness of a structural system, the deterministic-based method neglects the inherent randomness involved in the structural properties and external loads, which may significantly affect the robustness of the structures. The risk-based method is comprehensive but complex and subjective, which reduces the calculability and application potential of the risk-based approach. On the other hand, the reliability-based method is simple and objective (Feng *et al.*, 2020; Feng *et al.*, 2021), and enables to take the uncertainty of variables into account. Therefore, this approach is adopted in this section.

The reliability-based robustness index proposed by (Frangopol and Curley, 1987; Fu and Frangopol, 1990) has been widely used. The reliability-based redundancy index, which has already been introduced in Chapter II and is rewritten here, can be calculated as follows:

$$\beta_{R,1} = \frac{\beta_{intact}}{\beta_{intact} - \beta_{damaged}} \quad \text{(VI.1)}$$

where $\beta_{R,1}$ is the redundancy or robustness index; β_{intact} and $\beta_{damaged}$ are the reliability indices of the intact and damaged structures, respectively.

The redundancy index varies between (0, +∞), where a high value correspond to high redundancy and vice versa. To quantify the reliability-based robustness, reliability indices of both intact and damaged situations are required to be determined.

In general, the probability of progressive collapse P[C] for a structural system due to an accidental event is a product of three probabilities when subjected to column removal scenarios, see Eq. (VI.2) (Ellingwood and Dusenberry, 2005; Li *et al.*, 2016; Feng *et al.*, 2020), i.e. (i) the probability of the accidental event P[E], (ii) the conditional probability of the local damage given that the accidental event occurs P[D|E], and (iii) probability of structural collapse given the local damage occurs P[C|D]:

$$\mathrm{P}[C] = \mathrm{P}[C \mid D]\,\mathrm{P}[D \mid E]\,\mathrm{P}[E] \quad \text{(VI.2)}$$

However, the probability P[E] is difficult to be accurately identified and modelled due to the lack of data. Therefore, the alternate load path approach is often assumed to be threat-independent to focus more on the inherent progressive collapse resistance of the structure itself (Adam *et al.*, 2018; Feng *et al.*, 2020). Therefore, only the collapse probability given the initial local failure is used to quantify the robustness.

An incremental dynamic analysis (IDA) can be adopted to determine the dynamic ultimate load-bearing capacity of a structure by successively increasing the intensity of the imposed load on the structure, i.e. a series of NTHA until failure occurs (i.e the ultimate capacity is determined), see e.g. (Parisi and Scalvenzi, 2020). However, the computational demand for such stochastic analyses is very cumbersome as a large number of NTHA may be required to determine the dynamic resistances. A possible way to reduce the calculation demand is to adopt the EBM. Only one pushdown analysis is required for each sample in the stochastic analysis, which means it has a significant advantage with respect to the computational demand (only with a little more calculation demand than that of the static pushdown analysis).

Hence, a novel approach for the reliability-based robustness or redundancy quantification using the EBM is therefore proposed. In this framework as shown in

Figure VI.1, the EBM is used to replace the IDA analysis in the context of structural robustness calculation.

For the intact situation, the resistances can be obtained by static analyses as no dynamic effects are involved, i.e. no column loss, see the left branch in Figure VI.1. After the load-bearing capacities for all the realisations have been determined, the failure probability and reliability index for the intact structural system can be calculated. For the damaged structural system, the EBM is used to replace the IDA method to determine dynamic resistances in case of a sudden column removal scenario. For every realisation, a static pushdown analysis is first carried out and then the obtained load-displacement curve (or pushdown curve) is used to derive the dynamic capacity curve (or EBM curve) (i.e. the right branch in Figure VI.1). The reliability index for the damaged system can be computed after the dynamic capacities for all the realisations have been obtained.

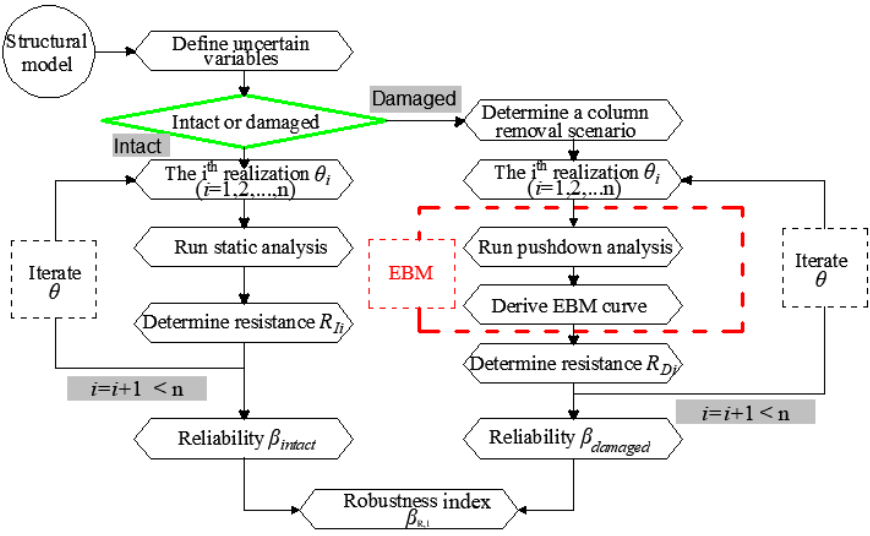

Figure VI.1. Flowchart of the reliability-based robustness quantification framework using the EBM.

As illustrated in Figure VI.1, the following three major procedures are required in the EBM-based structural robustness or redundancy quantification:

1) Determine uncertain variables for a structural model;
2) Calculate reliability indices in relation to both intact and damaged (single column removal scenario) situations, as required in Eq. (VI.1). For the damaged structural system, static pushdown analyses are first performed. Subsequently, the EBM is adopted to approximately calculate the

maximum dynamic capacities on the basis of the load-displacement curves of the static pushdown analyses; and

3) Compute the reliability-based robustness or redundancy index according to (Eq. (VI.1)).

According to the results obtained in the previous chapter, the model uncertainties involved in the application of the EBM instead of the more complex IDA, are adopted in the limit state function in relation to the calculation of the failure probability or reliability of the damage situation (the right branch in Figure VI.1). The limit state function Z is defined as follows:

$$Z = K_R \cdot \left(R / K_{EBM} \right) - K_L \cdot L \tag{VI.3}$$

where K_R and K_L are the resistance and load model uncertainties (JCSS, 2001); R is the dynamic resistance; L is the load effect; and K_{EBM} is the additional model uncertainty relating to the application of the EBM instead of IDA (Table V.5). Note that K_{EBM} is not implemented in the limit state function in relation to the intact situation and that limit state function can be defined as follows:

$$Z = K_R \cdot R - K_L \cdot L \tag{VI.4}$$

Several methods, such as the first-order reliability method (FORM), the second-order reliability method (SORM), Monte Carlo simulations, etc. can be adopted to calculate the failure probability on the basis of the limit state function (Gollwitzer and Rackwitz, 1983; Fujita and Rackwitz, 1988; Engelund and Rackwitz, 1993; JCSS, 2001; Li and Chen, 2009; Van Coile *et al.*, 2017; Li, 2020). In this chapter, reliability indices (failure probabilities) of the intact and damaged situations are calculated using Eq. (VI.5) according to the corresponding limit state functions by performing SORM analyses:

$$\beta = -\Phi^{-1}\left(\mathrm{P}[Z < 0] \right) \tag{VI.5}$$

where Φ^{-1} is the inverse of the standard normal distribution function. Note that the resistances are fitted by distributions before they are employed to calculate the failure probability and reliability.

As a numerical example for the application of the EBM-based structural robustness assessment, the RC frame (Figure IV.16) investigated in the previous two chapters is adopted in this chapter as well. The same FE model and structural parameters are used here.

For the RC frame subjected to one single column removal scenario (damaged situation), both static and dynamic resistances in terms of the three cases (i.e. Case A, Case B and Case C) have already been calculated in Chapter V on the basis of

the probabilistic models as shown in Table V.3. The relevant results for the three cases will be directly used in this chapter.

VI.3 Intact structural system

The resistance in relation to the intact situation (without column loss) for the RC frame (Figure IV.16) has not yet been calculated. Therefore, it is calculated in this section. For the intact structural system, only static analyses are performed. Uniform line loads are imposed on all the beams and increased until a failure occurs, i.e. load-controlled loading. Both a deterministic analysis and stochastic analyses are carried out for the intact situation. Note that the same parameters are used here for the intact situation as those adopted in section IV.4 (deterministic analyses) and section V.4 (stochastic analyses) with regard to the damaged situations of the RC frame.

The deterministic analysis is first carried out. The vertical imposed load on the beams vs. vertical displacement at the mid-span of the middle beam in the first floor (for an illustration purpose) is presented in Figure VI.2a. The ultimate load-bearing capacity is 123.0 kN/m, which is obtained at the first failure (three plastic hinges occur in the outer beam in the fifth floor).

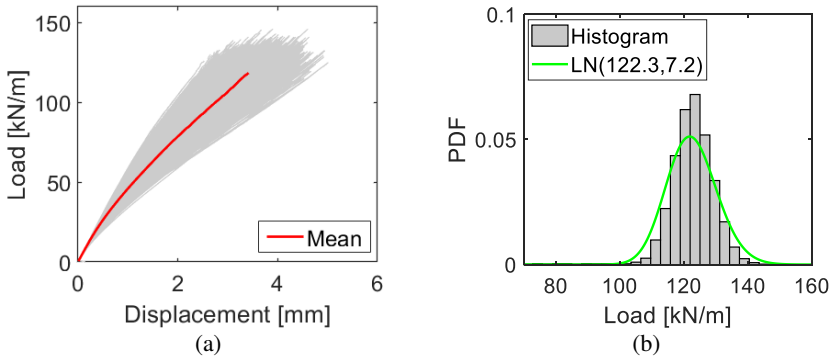

Figure VI.2. Results for the intact structural system: (a) load-displacement (at the mid-span of the internal beam in the first floor, between columns B and C) relationship of the deterministic analysis; and (b) histograms and PDF of the resistances from the stochastic analyses.

Subsequently, the stochastic analyses are conducted. The eight random variables as shown in Table V.3 (i.e. 10 000 samples similar to stochastic analyses for damaged situations) are adopted for the intact situation. In terms of the results of the stochastic analyses, the histogram and PDF of the resistances are presented in

Figure VI.2b. A lognormal distribution LN(122.3,7.2) is fitted to the distribution of the resistances in relation to the intact system.

VI.4 Reliability evaluation

To evaluate the failure probability or reliability of the RC frame in both the damaged situations and in the intact situation, the limit state function Z as defined in Eq. (VI.3) or Eq. (VI.4) is adopted. The load effect L is calculated as follows:

$$L=\left(DL+LL\right)\cdot W=\left(DL+LL\right)\cdot 6 \tag{VI.6}$$

where W with a value of 6.0 m is the distance between two adjacent frames; and DL and LL are the dead load action and live load action on the beams, respectively. The DL is modelled as a normal distribution, while the LL model considers an arbitrary-point-in-time live load (Jovanović *et al.*, 2020), see Table VI.1. Moreover, the probabilistic models for the load model uncertainty K_L and the resistance model uncertainty K_R are presented in Table VI.1 according to (JCSS, 2001; Holický and Sýkora, 2010).

Table VI.1. Additional probabilistic models for random variables.

Variable	Units	Distribution	Mean	COV
DL	kN/m^2	Normal	5	0.1
LL	kN/m^2	Gamma	0.6	0.6
K_L	-	Lognormal	1	0.1
K_R	-	Lognormal	1	0.15

VI.4.1 Reliability evaluation of the intact situation

The reliability index of the intact structural system is calculated on the basis of the stochastic analyses results in section VI.3 and the probabilistic models in Table VI.1. The failure probability ($P_{f,\text{intact}}$) and reliability index ($\beta_{f,\text{intact}}$) are evaluated according to the limit state function as follows:

$$Z=K_R\cdot R-K_L\cdot\left(DL+LL\right)\cdot 6 \tag{VI.7}$$

where R is the resistance of the intact system obtained in section VI.3, i.e. LN(122.3,7.2).

However, it is worth noting that the resistance for the intact system is quite high, i.e. a low failure probability is obtained as the structure has considerable reserve capacity. To determine such a small failure probability, the software COMREL 8.1 (Consult, 2018) is employed to calculate the failure probability through the use of the SORM (Fujita and Rackwitz, 1988; Engelund and Rackwitz, 1993). Finally, a

reliability index of 5.9 is obtained for the intact system (reference period of one year).

VI.4.2 Reliability evaluation of the damaged situation

When the EBM is adopted in case of the damaged situations, i.e. Cases A, B, and C for the different single-column removal scenarios, the failure probabilities ($P_{f,\text{damaged}}$) and reliability indices ($\beta_{f,\text{damaged}}$) are evaluated through a limit state function as follows:

$$Z = K_R \cdot \left(R / K_{EBM} \right) - K_L \cdot \left(DL + LL \right) \cdot 6 \qquad \text{(VI.8)}$$

where R is the resistance of the damaged system with respect to the EBM obtained in section V.4 (Table V.4); and K_{EBM} is the additional model uncertainty relating to the application of the EBM instead of IDA (Table V.5). Note that the failure probabilities for the static results and accurate IDA results are calculated as well in which the limit static function Eq. (VI.7) is adopted.

For the three column removal cases, the failure probabilities and reliability indices are calculated. The results for the three cases are presented in Table VI.2. For Case A, the obtained failure probabilities (and reliability indices) for pushdown and IDA analyses according to Eq. (VI.7) are 0.26 (0.64) and 0.45 (0.13), respectively. For the results from EBM, the failure probability (and reliability index) is calculated according to Eq. (VI.8), where the additional model uncertainty K_{EBM} in relation to the EBM is taken into account. Three situations are considered:

1) K_{EBM} in relation to 'all' cases in Table V.5 (designated as 'EBM_1'), in which an overall model uncertainty for the EBM is considered.
2) K_{EBM} in terms of the corresponding individual case in Table V.5 (designated as 'EBM_2').
3) Without the consideration of K_{EBM}, i.e. Z defined in Eq. (VI.7), (designated as 'EBM_3').

The associated probabilities (and reliability indices) for the three situations EBM_1, EBM_2 and EBM_3 are 0.47 (0.08), 0.45 (0.13), and 0.51 (-0.03) in Case A, respectively. The results for the other cases are presented in Table VI.2. In general the obtained failure probabilities for IDA and EBM are quite close (see Table VI.2), although a larger deviation of 13.3% is found for Case A in relation to EBM_3 (without the consideration of K_{EBM}). In the situation EBM_1 in which the general model uncertainty K_{EBM} is considered, the results for EBM_1 are close to the IDA results. In the situation EBM_2 in which with the corresponding individual model uncertainty K_{EBM} is accounted for, it is as expected that the results EBM_2 are almost identical to the IDA results. However, when no model uncertainty K_{EBM} is involved in, i.e. the situation EBM_3, a generally relative large deviation is observed. Hence, this stresses the importance of taking the model uncertainty K_{EBM} into account.

As expected, the reliability index (β) of dynamic resistance (IDA) is significantly lower, i.e. 0.2 times, than that of the static resistance (pushdown). The failure probabilities ($P_{f,\text{damaged}}$) of dynamic resistance (IDA) is 1.7 times as high as that of static resistance (pushdown). Likewise, the failure probabilities and reliability indices in terms of Case B and Case C are calculated and presented in Table VI.2. The failure probabilities ($P_{f,\text{damaged}}$) of dynamic resistances (IDA) are 1.8 times as high as those of static resistances (pushdown) for both Case B and Case C. These results show that it is of paramount importance to include dynamic effects when assessing the structural reliability in relation to sudden column removal scenarios.

Table VI.2. Failure probability $P_{f,\text{damaged}}$ (and reliability index β_{damaged}) and deviation.

	Case A		**Case B**		**Case C**	
	$P_{f,\text{damaged}}$	β_{damaged}	$P_{f,\text{damaged}}$	β_{damaged}	$P_{f,\text{damaged}}$	β_{damaged}
Pushdown	0.26	0.64	0.17	0.95	0.18	0.92
IDA	0.45	0.13	0.31	0.50	0.32	0.47
EBM_1	0.47	0.08	0.29	0.55	0.31	0.50
(EBM_1-IDA)/IDA	**4.4%**	-	**-6.5%**	-	**-3.1%**	-
EBM_2	0.45	0.13	0.31	0.50	0.32	0.47
(EBM_2-IDA)/IDA	0.0%	-	0.0%	-	0.0%	-
EBM_3	0.51	-0.03	0.32	0.47	0.34	0.41
(EBM_3-IDA)/IDA	**13.3%**	-	**3.2%**	-	**6.3%**	-

According to the analysis results, it is also found that the failure probability of Case A is higher than Case B and Case C in terms of both static pushdown and IDA analyses. This can be attributed to the fact that Case A is more critical than the other two cases for the RC frame subjected to one column removal, as there is less opportunity for the development of alternate load paths to redistribute the unbalance loads in an exterior column removal scenario (i.e. Case A). A good performance for the EBM-based structural robustness quantification approach is also observed with respect to the reliability calculations.

VI.5 Robustness quantification

Based on the reliability indices of both the intact and the damaged situations, the reliability-based redundancy or robustness index as defined in Eq. (VI.1) can be calculated. The reliability-based robustness indices are summarized in Table VI.3. The robustness index obtained through the static pushdown analysis is larger (i.e. suggesting more robustness) than that from the dynamic analysis (IDA). It thus shows that the pushdown analysis may overestimate the robustness. However, it is up to date not clear what can be considered as a 'large' difference between robustness indices. Moreover, almost identical redundancy indices are obtained between IDA and EBM (with consideration of the model uncertainty), where the

deviations are -1.0%, 0.9% and 0.0% for Case A, Case B and Case C, respectively. This result confirms the proposed EBM-based robustness or redundancy robustness quantification method has also a good performance in the context of redundancy and robustness quantification for RC frames subjected to sudden column loss scenarios. Moreover, the exterior column loss for the RC frame (i.e. Case A) is less robust than the other two case, as less alternate load paths are available.

Table VI.3. Reliability-based robustness index.

	Case A	**Case B**	**Case C**
Pushdown	1.12	1.19	1.19
IDA	1.02	1.09	1.09
EBM_1	1.01	1.10	1.09
(EBM_1-IDA)/IDA	-1.0%	0.9%	0.0%
EBM_2	1.02	1.09	1.09
(EBM_2-IDA)/IDA	0.0%	0.0%	0.0%
EBM_3	1.00	1.09	1.08
(EBM_3-IDA)/IDA	-2.0%	0.0%	-0.9%

VI.6 Conclusions

An approach for structural robustness or redundancy quantification incorporating the energy-based method (EBM) was proposed in this chapter. A RC frame under different column removal scenarios at the ground floor was adopted as a case study to illustrate the application the proposed EBM-based structural robustness or redundancy quantification. Reliability indices of both intact and damaged structural system were calculated by using the SORM method.

The failure probabilities of the static analyses, EBM analyse and the IDA analyses were calculated and compared. The failure probabilities of static analyses were observed to be significantly lower than those of the EBM and IDA analyses. This indicated that the influence of dynamic effects was significant. The failure probability of the EBM analyses were close to the IDA analyses. A slightly larger deviation with respect to EBM was found for the exterior column removal case (i.e. Case A), which can again be attributed to the fact that the single deformation mode assumption was not satisfied. A better performance of the EBM was observed for the two interior column removal cases (i.e. Case B and Case C). Moreover, the failure probability of Case A was higher than Case B and Case C in terms of both static pushdown and IDA analyses, since there was less opportunity for the development of alternate load paths to redistribute the unbalance loads in the exterior column removal scenario.

The influence of the model uncertainty K_{EBM} in relation to the use of the EBM instead of the IDA was investigated. Three situations were considered: K_{EBM} in relation to the 'all' case (designated as 'EBM_1'); K_{EBM} in relation to the corresponding individual case in Table V.5 (designated as 'EBM_2'); and without the consideration of K_{EBM} (designated as 'EBM_3'). In the case EBM_1 the results EBM_1 were close to the IDA results of the reliability analyses. In the case EBM_2 the results EBM_2 were almost identical to the IDA results. However, in the case EBM_3, a relative large deviation was observed for the critical exterior column removal case, since no model uncertainty was taken into account. Hence, it can be concluded that the obtained failure probability was more accurate when the model uncertainty K_{EBM} was included, in particular for the critical Case A, i.e. an exterior column loss.

Eventually, reliability-based robustness or redundancy indices were calculated. As anticipated, the redundancy indexes for the static resistances were significantly larger than the resistances from EBM or IDA, stressing the importance to take dynamic effects into account. The pushdown analysis may overestimate the robustness. Little deviation was observed for the redundancy indices between EBM and IDA, which indicated again the good performance of the proposed EBM-based approach.

VI.7 References

Adam JM, Parisi F, Sagaseta J, et al. (2018) Research and practice on progressive collapse and robustness of building structures in the 21st century. Engineering Structures 173:122-149.

Consult RCP (2018) COMREL User's Manual.

Ellingwood BR, Dusenberry DO (2005) Building design for abnormal loads and progressive collapse. Computer-Aided Civil and Infrastructure Engineering 20:194-205.

Engelund S, Rackwitz R (1993) A benchmark study on importance sampling techniques in structural reliability. Structural safety 12:255-276.

Feng D, Xie S, Xu J, et al. (2020) Robustness quantification of reinforced concrete structures subjected to progressive collapse via the probability density evolution method. Engineering Structures 202:109877.

Feng DC, Xie SC, Li Y, et al. (2021) Time-dependent reliability-based redundancy assessment of deteriorated RC structures against progressive collapse considering corrosion effect. Structural safety 89:102061.

Frangopol DM, Curley JP (1987) Effects of damage and redundancy on structural reliability. Journal of Structural Engineering 113:1533-1549.

Fu G, Frangopol DM (1990) Balancing weight, system reliability and redundancy in a multiobjective optimization framework. Structural safety 7:165-175.

Fujita M, Rackwitz R (1988) Updating first-and second-order reliability estimates by importance sampling. Doboku Gakkai Ronbunshu 1988:53-59.
Gollwitzer S, Rackwitz R (1983) Equivalent components in first-order system reliability. Reliability Engineering 5:99-115.
Holický M, Sýkora M (2010) Stochastic models in analysis of structural reliability. The international symposium on stochastic models in reliability engineering, life sciences and operation management.
JCSS (2001) Probabilistic model code. Joint Committee on Structural Safety.
Jovanović B, Van Coile R, Hopkin D, et al. (2020) Review of current practice in probabilistic structural fire engineering: permanent and live load modelling. Fire Technology 57:1-30.
Li J (2020) A PDEM-based perspective to engineering reliability: From structures to lifeline networks. Frontiers of Structural and Civil Engineering:1-10.
Li J, Chen J (2009) Stochastic dynamics of structures. John Wiley & Sons.
Li Y, Lu X, Guan H, et al. (2016) Probability-based progressive collapse-resistant assessment for reinforced concrete frame structures. Advances in Structural Engineering 19:1723-1735.
Parisi F, Scalvenzi M (2020) Progressive collapse assessment of gravity-load designed European RC buildings under multi-column loss scenarios. Engineering Structures 209:110001.
Van Coile R, Balomenos GP, Pandey MD, et al. (2017) An unbiased method for probabilistic fire safety engineering, requiring a limited number of model evaluations. Fire Technology 53:1705-1744.

CHAPTER VII

Reliability and risk-based robustness quantification using a multilevel calculation scheme for RC frames subjected to column removal scenarios taking into account dynamic effects

VII.1 Introduction

With respect to robustness assessment, it is more comprehensive to account for the relationship between the occurrence probability of the accidental events (and the probability of structural collapse) and the associated consequences. This indicates that a risk-based robustness index is more powerful and comprehensive. A risk-based robustness index based on a complete risk analysis was proposed in (Baker *et al.*, 2008), in which the consequences were divided into direct and indirect effects. The risk-based robustness index has been applied to investigate the structural robustness of a composite frame (Izzuddin *et al.*, 2012). Droogné *et al.* (2018) developed a multilevel calculation scheme for conditional risk-bask robustness quantification of RC frames, where a structural system was divided into a directly affected part (DAP) and an indirectly affected part (IAP). The calculations on different parts were performed independently, hence establishing a hybrid model, i.e. a detailed FE model for the DAP and an analytical model for the IAP. In this approach, the robustness quantification was carried out at different levels of structural idealization in order to further reduce the computational effort.

In this chapter, the multilevel calculation scheme proposed by Droogné *et al.* (2018) is further expanded and evaluated in relation to the structural robustness quantification of RC building structures taking into account dynamic effects. The influence of dynamic effects on both the DAP and IAP are investigated. In order to reduce the computational effort, the macro-based FE modelling technique is adopted to develop the numerical models. The performance of the multilevel calculation scheme for reliability analysis is evaluated against results from probabilistic analyses of the entire systems considering both static and dynamic situations with regard to two RC frames. Further, an effective way to determine the equivalent boundary conditions for the DAP from multi-storey frames is proposed and evaluated.

The sections in this chapter are arranged as follows: section VII.2 presents the methodology with regard to the multilevel calculation scheme. The descriptions and numerical modelling assumptions for two RC frames are presented in section VII.3. Subsequently, deterministic analyses and stochastic analyses are carried out in section VII.4 and section VII.5, respectively. Further, the failure probabilities and conditional risk-based robustness indices are calculated, compared and discussed in section VII.6. Concluding remarks are addressed in section VII.7.

VII.2 Methodology

VII.2.1 Multilevel calculation scheme for structural reliability analysis

In a reliability evaluation, the aforementioned static and dynamic analyses may demand huge computational efforts as repeated sampling is needed to take into account the uncertainties with respect to e.g. the mechanical material properties. In order to reduce the computational demand, a multilevel calculation scheme for reliability or robustness analysis was proposed by Droogné *et al.* (2018), where a structural system is divided into three parts: a DAP, an IAP, and an unaffected part.

The reliability assessment is carried out at different levels of structural idealization. A detailed nonlinear FE model is adopted only for low levels of structural idealization (i.e. DAP) in order to accurately account for the nonlinear behaviour of the structural component. In the IAP, higher levels of structural idealization are considered, allowing for more simplified modelling. For instance, Figure VII.1a shows a RC building (Droogné *et al.*, 2018) subjected to the notional removal of a central edge column. The bays immediately above the removed column are considered as the DAP (Figure VII.1b,c). The IAP is the remaining part of the frame in which the column is lost (Figure VII.1b). The remainder of the building is the unaffected part and is assumed to be unaffected by the notional column removal. Since the failure probability of the unaffected part will be small compared to the failure probabilities of DAP and IAP (Droogné *et al.*, 2018), this part can be omitted in the multilevel calculation scheme. Note that the building was designed with the assumption that horizontal stiffness in the plane of the frame was provided by the frames, while horizontal stiffness in the other direction was provided by bracings and therefore as a simplification the analysis can be performed by only considering 2D frames (Droogné *et al.*, 2018).

VII.2.1.1 Directly affected part

Figure VII.1c shows the DAP from the RC frame subjected to a notional central column removal (Figure VII.1b). The interconnections between the DAP and the IAP can be simulated using springs, i.e. boundary conditions with horizontal and rotational springs. The DAP consists of beams at different floors, connected by columns. Neglecting small differences in axial deformation of the column, all continuous beams are considered to have the same deflection at the position of the column. In addition, all beams of DAP have the same dimensions and imposed loads. When, furthermore, it is assumed that the boundary conditions at each floor are the same, and thus can be modelled with springs with the same spring constants (Droogné *et al.*, 2018), the calculation scheme of Figure VII.1c simplifies to Figure

VII.1d. Note that because of the assumption of equal deformations at each floor, possible Vierendeel actions in the frame over the removed column are neglected. Although the assumption results in approximate responses, it is a frequently used simplification and has been used in several studies (Izzuddin *et al.*, 2008; Li *et al.*, 2014; Droogné *et al.*, 2018). Therefore, the study of one (symmetrical situation) or two beams, immediately above the removed column, with a detailed FE model as can be seen in Figure VII.1d, is considered sufficient. The detailed equivalent DAP model can accurately account for the nonlinear responses of the structural elements such as large deformations, compressive arch action, and tensile catenary action. Both geometrical and material nonlinearities can be taken into account. This is important since large deformations are expected. The detailed equivalent FE model for the DAP can be built using FE software, such as Abaqus (Abaqus, 2014) and OpenSees (OpenSees, 2006).

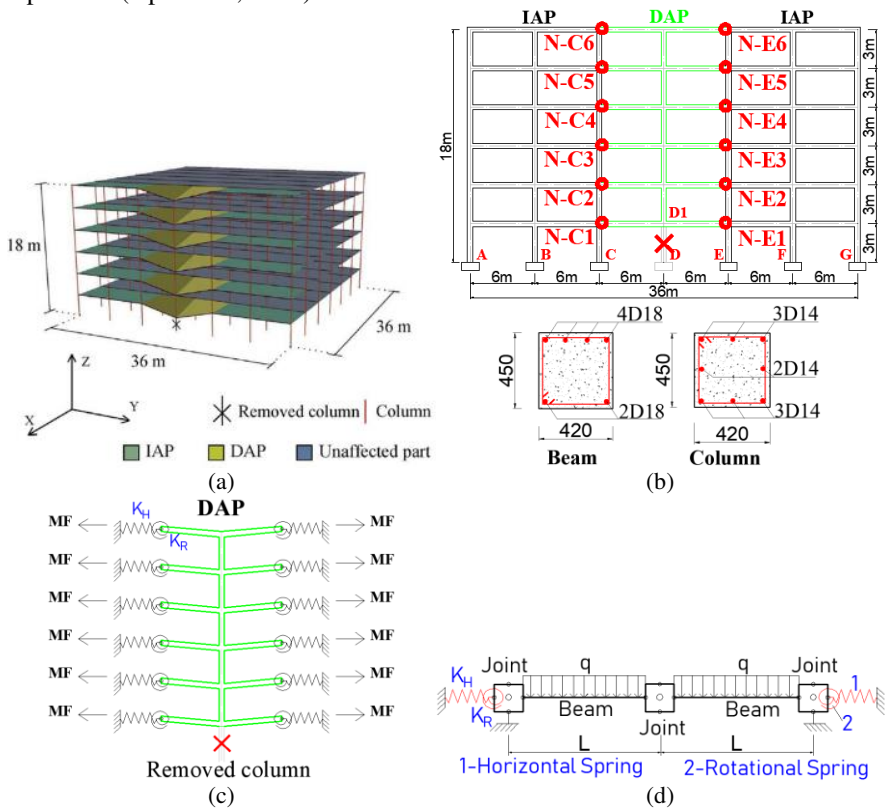

Figure VII.1. (a) A RC building subjected to an edge column removal scenario (Droogné et al., 2018); (b) layout of the edge frame (designated as 'F6B6' and dimensions in m) and cross-sections of beams and columns (dimensions in mm); (c) directly affected part (DAP) with equivalent boundary conditions; and (d) equivalent DAP model.

VII.2.1.2 Indirectly affected part

Membrane forces (*MFs*) can develop in the elements of the DAP (Figure VII.1c), but will be limited to the resisting capacity of the IAP, i.e. R_{IAP}. Although a detailed analysis or advanced software packages can be adopted to determine the R_{IAP}, a practical plastic analysis is employed here as smaller deformations are expected for the IAP. The failure mode is assumed as plastic hinges in ground storey columns (Figure VII.2a), since this requires less energy when the plastic hinges develop in the columns than when a plastic hinge develops in the beams (Droogné *et al.*, 2018). Based on the principle of conservation of energy and the assumed failure mode, a relationship of the horizontal membrane force against the plastic moment of the columns can be obtained (Droogné *et al.*, 2018):

$$\theta \cdot \sum_{i=1}^{n} M_{pl,Ci} = N \cdot \left(H \cdot \theta \cdot MF \right) \tag{VII.1}$$

where θ [radian] is the rotation angle of the deformed frame. $M_{pl,Ci}$ is the plastic moment of the respective columns at the ground storey of the IAP. N is the number of the floors of the building. H is the height of the first storey. MF is the membrane force at the beam ends of each floor level. Note that the same MF acting at each floor is assumed due to the assumed deformed state of the DAP and IAP.

In the simple plastic analysis for determining the resistance R_{IAP} (maximum capacity for MF), the resistance mechanism of the IAP is assumed to be a bilinear model, as shown in Figure VII.2b. The plastic analysis for the IAP is simple and has proven to be effective (Droogné *et al.*, 2018). More details will be introduced in section VII.4.

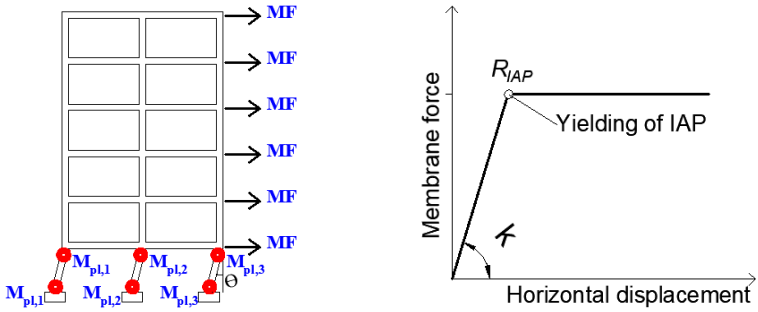

Figure VII.2. Indirectly affected part (IAP): (a) assumed failure mode; and (b) bilinear model.

VII.2.2 Risk-based robustness assessment

A risk-based robustness index provides a comprehensive measure that takes into account both the probability of structural collapse and the potential associated consequences. The risk-based robustness index proposed by Baker *et al.* (2008) is applied as follows:

$$I_{\mathrm{Rob}} = \frac{R_{\mathrm{direct}}}{R_{\mathrm{direct}} + R_{\mathrm{indirect}}} \tag{VII.2}$$

$$R_{\mathrm{direct}} = \sum_{k=1}^{n_{\mathrm{exp}}} \sum_{l=1}^{n_{\mathrm{D}}} C_{\mathrm{Dir}} \cdot P\left[D_l \mid E_k\right] \cdot P\left[E_k\right] \tag{VII.3}$$

$$R_{\mathrm{indirect}} = \sum_{k=1}^{n_{\mathrm{exp}}} \sum_{l=1}^{n_{\mathrm{D}}} C_{\mathrm{Ind}} \cdot P\left[F \mid D_l, E_k\right] \cdot P\left[D_l \mid E_k\right] \cdot P\left[E_k\right] \tag{VII.4}$$

where I_{Rob} is the robustness index. R_{direct} and R_{indirect} are the direct risks and indirect risks, respectively. C_{Dir} is the direct consequence, which is related to an initial damage. C_{Ind} is the indirect consequence, which is related to the subsequent damage of the system after the initial damage. $P[E_k]$ is the probability of an exposure event E_k. $P[D_l|E_k]$ is the probability of having a damage D_l given the exposure event E_k. $P[F|D_l,E_k]$ is the failure probability given a certain damage D_l and exposure event E_k.

The robustness index I_{Rob} varies between zero and unity. A robust system is considered to have $I_{\mathrm{Rob}} = 1$ where indirect risks do not contribute significantly to the total system risk. If the probability of a certain exposure and damage is difficult to assess, the robustness index I_{Rob} can be expressed conditionally on the exposure E_k and the damage D_l. For instance, for a certain damage state D_l which is caused by a certain exposure event E_k, a conditional robustness index is expressed as follows (Baker *et al.*, 2008):

$$I_{\mathrm{Rob}} | D_l, E_k = \frac{R_{\mathrm{direct}}}{R_{\mathrm{direct}} + R_{\mathrm{indirect}}} = \frac{C_{\mathrm{Dir}}}{C_{\mathrm{Dir}} + P\left[F \mid D_l, E_k\right] C_{\mathrm{Ind}}} \tag{VII.5}$$

In the aforementioned multilevel calculation scheme the failure probabilities of the DAP and IAP of a structural system are assessed separately, thus the conditional robustness index in Eq. (VII.5) for the threat-independent alternate load path method, can be calculated as follows (Droogné *et al.*, 2018):

$$I_{\mathrm{Rob}} | D, E = \frac{R_{\mathrm{direct}}}{R_{\mathrm{direct}} + R_{\mathrm{indirect}}} = \frac{C_{\mathrm{Dir}}}{C_{\mathrm{Dir}} + P\left[F_{\mathrm{DAP}} \cap \overline{F_{\mathrm{IAP}}}\right] C_{\mathrm{DAP}} + P\left[F_{\mathrm{IAP}}\right] C_{\mathrm{IAP}}} \tag{VII.6}$$

where C_{DAP} and C_{IAP} are the consequences corresponding to the failure of DAP and IAP, respectively. Here, the subscripts for D_l and E_k are not written any more in the text for brevity. $P[F_{\mathrm{DAP}} \cap \overline{F_{\mathrm{IAP}}}]$ is the failure probability of the event corresponding to failure of the DAP but survival of the IAP. $P[F_{\mathrm{IAP}}]$ is the failure probability of the IAP. Note that a distinction is made between consequences associated to failure of the DAP only and consequences for failure of the IAP (regardless of whether the DAP fails or not). The DAP will also fail in case the IAP fails, resulting from the removal of the boundary conditions of the DAP.

VII.3 Numerical case study: description and modelling of RC frames

VII.3.1 Description of the RC frames

Two RC frames from two office buildings designed according to the Eurocodes (CEN, 2002; CEN, 2004) by Droogné *et al.* (2018) are employed. The two RC frames are the edge frames of the two buildings. The two buildings have the same useful office space but different structural layouts. The floor consists of precast hollow core concrete slabs and the slabs are resting on the transverse beams, which transfer the loads in one direction to the frames. Therefore, 2D frames are analysed as a simplification, i.e. no 3D effects are considered. The permanent load imposed on the floors (including the self-weight of the floors) is 6.25 kN/m^2 and the live load for an office building is 3.0 kN/m^2 (CEN, 2002). Concrete type C30/37 and steel BE500S (ductility class C) are adopted. The concrete cover is 30 mm in all elements. More details can be found in (Droogné *et al.*, 2018).

The layout of building 1 is shown in Figure VII.1a. The edge frame (designated as 'F6B6') of building 1 is presented in Figure VII.1b, which is a 6-storey and 6-bay RC frame. The height of each storey is 3.0 m, and the span for each bay is 6.0 m. The cross-sections and reinforcement layouts of beams and columns are presented in Figure VII.1b and a summary is presented in Table VII.1.

Also the description of building 2 can be found in (Droogné *et al.*, 2018). The edge frame (designated as 'F3B12') of the building 2 is presented in Figure VII.3a, which is a 3-storey and 12-bay RC frame. The height of each storey is 3.0 m, and the span for each bay is 6.0 m. The cross-sections and reinforcement layouts of beams and columns are presented in Figure VII.3b and a summary is drawn in Table VII.1.

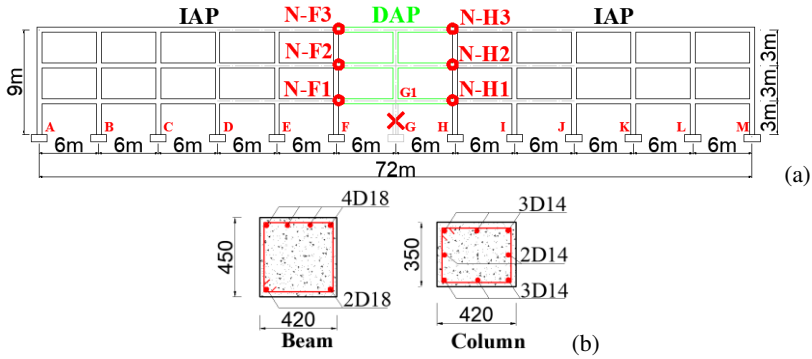

Figure VII.3. Frame F3B12: (a) layout of the frame (dimensions in m); and (b) cross-sections of beam and column (dimensions in mm).

Table VII.1. Geometrical properties (Units: mm) of the edge frames of the two buildings (Droogné et al., 2018).

Case		Frame F6B6	Frame F3B12
Column	Dimensions b x h	420 x 450	420 x 350
	Reinforcement	8 ϕ 14	8 ϕ 14
Beam	Dimensions b x h	420 x 450	420 x 450
	Top reinforcement	4 ϕ 18	4 ϕ 18
	Bottom reinforcement	2 ϕ 18	2 ϕ 18
	Shear reinforcement	ϕ 10 @ 150	ϕ 10 @ 150

VII.3.2 Finite element modelling approach

Two-dimensional numerical FE models of the two RC frames are built using OpenSees (2006), where the macro-based FE modelling technique is adopted (Bao *et al.*, 2008; Brunesi and Nascimbene, 2014). For each frame (both F6B6 and F3B12), two FE models are developed in OpenSees: an equivalent DAP model (Figure VII.1d) and a model of the entire system (Figure VII.1b or Figure VII.3a). Regarding the equivalent DAP model (Figure VII.1d), two beams and three connected beam-column joints are modelled (only one floor). Moreover, horizontal and rotational linear springs are used as boundary conditions. The determination of the spring constants will be investigated in section VII.4.2. Results obtained from the model of the entire system (as a reference) are regarded as the accurate ones to evaluate the performance of the multilevel calculation scheme method. The evaluation is done considering removal of the central column of the frame.

For modelling the beams and columns, the force-based fibre beam-column element in OpenSees is adopted (Mazzoni *et al.*, 2006), which is same to that in section IV.4.1.1. In addition, the co-rotational transformation in OpenSees is adopted to consider geometrical nonlinearity. For beam-to-column connections, the Joint2D element in OpenSees is applied, which is idealized as a parallelogram-shaped shear panel with adjacent elements connected to its midpoints (Mazzoni *et al.*, 2006). More details with regard to the modelling techniques can be found in section IV.4.1.1.

VII.3.3 Materials

Concrete of type C30/37 (CEN, 2004; fib, 2013) is used for both RC frames, i.e. the characteristic cylinder compressive strength is f_{ck} = 30 MPa (Droogné *et al.*, 2018). The mean compressive strength of concrete is assumed to be $f_{cm} = f_{ck} + 8$ = 38 MPa according to *fib* Model Code 2010 (fib, 2013), while the mean value of tensile strength is $f_{ctm} = 0.3(f_{ck})^{2/3} = 2.9$ MPa. The mechanical properties of concrete are summarized in Table VII.2. The uniaxial plastic-damage model in OpenSees is adopted for concrete fibres, i.e. ConcreteD material (Wu *et al.*, 2006; Feng *et al.*, 2019a). Stirrup-confinement effects on the compressive behaviour and the effect of tension stiffening on the tensile behaviour are taken into account, respectively (Mander *et al.*, 1988; Stevens *et al.*, 1991).

Table VII.2. Mechanical properties for materials (Droogné et al., 2018).

Material	Parameter	Units	Mean value
Concrete	Compressive strength f_{cm}	MPa	38
	Compressive peak strain ε_{c1}	%	0.23
	Tensile strength f_{ctm}	MPa	2.9
	Young's modulus E_{ci}	GPa	33.6
Steel	Yield strength f_{ym}	MPa	555
	Tensile strength f_{um}	MPa	605
	Ultimate strain ε_u	%	7.5
	Young's modulus E_s	GPa	200

The mean yield stress and tensile strength of reinforcing steel are f_{ym} = 555 MPa and f_{um} = 605 MPa, respectively (Droogné *et al.*, 2018). The ultimate strain of the reinforcement is assumed to be ε_u = 7.5% (Droogné *et al.*, 2018). The Young's modulus E_s = 200 GPa is adopted. The mechanical properties of reinforcement are summarized in Table VII.2. The uniaxial Giuffre-Menegotto-Pinto steel material model, i.e. the Steel02 material in OpenSees (Mazzoni *et al.*, 2006), is adopted for reinforcing steel.

The min-max material model in OpenSees can be adopted to model the material failure (OpenSees, 2006; Feng *et al.*, 2019b). If the strain of the material exceeds the predefined minimum or maximum strain values, the material is assumed to have failed and zero stress and stiffness are returned.

VII.4 Deterministic analysis

For the two RC frames, FE models (the model of the entire system and the equivalent DAP model) are developed in OpenSees and analysed both in static and dynamic approaches to determine the ultimate load-bearing capacities. Regarding the IAP, a simple analytical analysis is adopted.

VII.4.1 Model of the entire system: pushdown and IDA analyses

A nonlinear static pushdown analysis is first performed for the model of the entire structural system subjected to a central column removal scenario (F6B6 or F3B12). Self-weight is first calculated. Subsequently, uniform loads are gradually increased on all beams of the damaged RC frame (i.e. the system with the central column removed), following a displacement-controlled approach, with a displacement control point at the top of the removed column. The imposed load is recorded in function of the displacement at the control point, resulting in the pushdown curve (curve 'Pushdown-Entire') in Figure VII.4a in case F6B6 or the pushdown curve (curve 'Pushdown-Entire') in Figure VII.4c for F3B12. The static ultimate load-bearing capacities (and corresponding displacements) are 26.9 kN/m (105.8 mm) and 27.8 kN/m (116.4 mm) for F6B6 and F3B12, respectively (Table VII.3). Note that compressive arch action is observed, catenary action is not observed.

Table VII.3. Ultimate load-bearing capacity (R) and membrane force (MF).

Case		**F6B6**	**F3B12**
R	Pushdown	26.9	27.8
[kN/m]	IDA	25.6	26.2

To determine the dynamic ultimate load-bearing capacity, an IDA is carried out by progressively increasing the intensity of downward line loads on all beams for each frame, i.e. a series of NTHA. For every load level, one NTHA is executed, where the loads on the beams are first applied (including self-weight) followed by the quasi-instantaneous removal of the central column (considering a removal time duration of 0.001 s). The explicit Kolay-Ricles-alpha algorithm (Kolay and Ricles, 2014; Kolay and Ricles, 2016; Feng *et al.*, 2019a) in OpenSees is employed to execute the dynamic column removal analysis, where the time step is set as 0.001 s (Feng *et al.*, 2019a). The dynamic response of the first 6.0 s for each NTHA is recorded at the top of the removed column (control point). The damping ratio is set as 5% in all dynamic analyses (Tsai and Lin, 2008; Brunesi *et al.*, 2015). Rayleigh

damping is adopted in which the damping is proportional to the mass matrix and tangent stiffness matrix. To accurately determine the ultimate load-bearing capacity, the load increment of the IDA is progressively reduced near the ultimate capacity. A final load increment resolution of 0.05 kN/m is applied near the load for which failure (rupture of reinforcement) occurs.

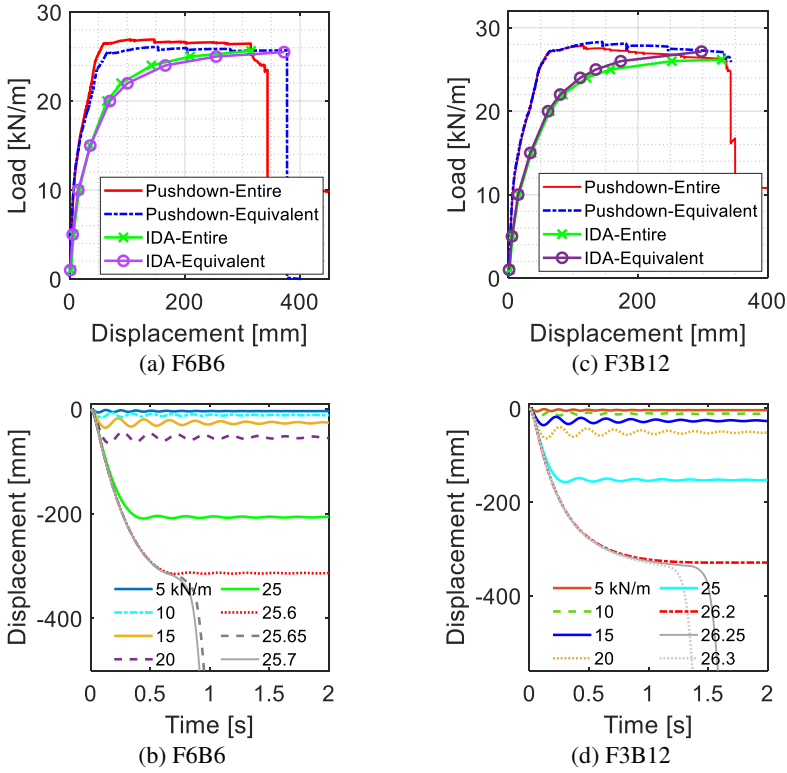

Figure VII.4. Results for F6B6 and F3B12: (a) F6B6 - load-displacement relationship; (b) F6B6 - time-history displacement response for IDA; (c) F3B12 - load-displacement relationship; and (d) F3B12 - time-history displacement response for IDA.

The time-history displacement responses at the control points from the IDA are presented in Figure VII.4b,d for F6B6 and F3B12, respectively. The system oscillates around the equilibrium position and the oscillation decays due to the damping effect after the sudden column removal. An ultimate dynamic load-bearing capacity (and corresponding displacement) of 25.6 kN/m (315.0 mm) is obtained for F6B6 (Figure VII.4b). An ultimate dynamic load-bearing capacity

(and corresponding displacement) of 26.2 kN/m (329.1 mm) is obtained for F3B12 (Figure VII.4d). The peak displacements obtained from the NTHA analyses against the corresponding imposed loads are shown in Figure VII.4a,c (curve 'IDA-Entire') for F6B6 and F3B12 respectively, i.e. the IDA curves. Compared to the ultimate load-bearing capacities obtained from pushdown analyses (Table VII.3), the dynamic resistances are lower (95.2% and 94.2% of the static resistances respectively), i.e. the static analysis slightly overestimates the ultimate load-bearing capacity in the sudden column removal scenario. However, the overestimation of stiffness (underestimation of maximum displacement) is much more significant at a small load level, see Figure VII.4a,c. Similar phenomena were observed in other studies (Tsai and Lin, 2008; Tsai, 2012; Brunesi and Nascimbene, 2014; Brunesi *et al.*, 2015). For example, the calculated force-based DAF decreased from almost 2.70 to 1.11 with increasing the imposed load (Brunesi and Nascimbene, 2014). The large DAF for small imposed load levels means the consideration of dynamic effects is more important in those cases.

The axial forces in the ground-floor columns are also analysed. According to the analysis results and other studies (Adam *et al.*, 2020; Alshaikh *et al.*, 2020), only the axial forces in the neighbouring columns of the removed central column are significantly influenced by the column removal event (Adam *et al.*, 2020). The axial force of the removed column mainly redistributes to the neighbouring columns. The residual axial force (after the oscillation completely decayed) from a nonlinear dynamic analysis (NTHA) is almost identical to the axial force from a nonlinear static analysis. A DAF for the axial force can be calculated from the ratio of peak axial force (N_{peak}) to the residual axial force ($N_{residual}$) in a time-history axial force response, i.e. DAF=$N_{peak}/N_{residual}$. Regarding F6B6, the DAF decreases from 1.25 to 1.03 with increasing imposed loads, see Figure VII.5a. With regard to F3B12, the DAF decreases from 1.27 to 1.03 with increasing imposed loads, see Figure VII.5c. Hence, the DAFs are observed to significantly decrease with increasing imposed loads. The dynamic effects have a more significant influence on the axial forces in the neighbouring columns in case of relative small imposed loads or normal design loads. However, only a slight influence is observed in relation to the ultimate load-bearing capacity.

The shear forces in the neighbouring columns of the removed central column are significantly enlarged by the column removal event. Moreover, shear forces in the neighbouring columns are found to be significantly larger than those in the other columns. Time-history responses of shear force in column C in case of F6B6 are presented in Figure VII.5b, while shear forces in column F in case of F3B12 are shown in Figure VII.5d. The residual shear force in a time-history response is larger than from the pushdown analysis at a same load level (i.e. proportional to the corresponding horizontal deformation), which is different to that with regard to the

axial forces. However, no shear failures occur in both columns and beams, for the example under consideration.

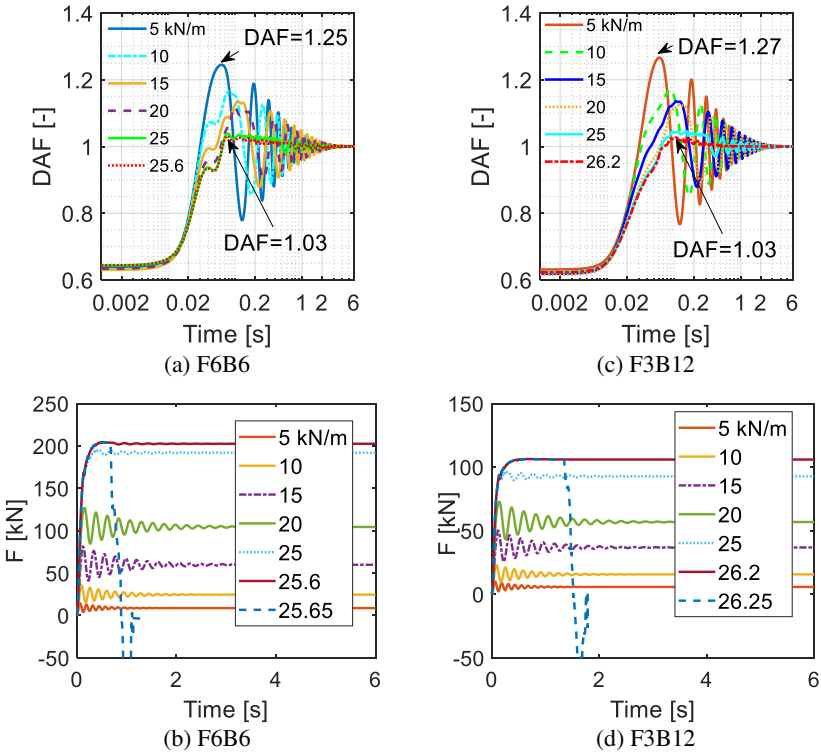

Figure VII.5. Results for F6B6 and F3B12: (a) F6B6 – DAF for axial force in column C; (b) F6B6 - time-history shear force response in column C for IDA; (c) F3B12 - DAF for axial force in column F; and (d) F3B12 – time-history shear force response in column F for IDA.

VII.4.2 Boundary conditions for the DAP

An effective way to determine the boundary conditions (i.e. the horizontal and rotational spring constants) of the equivalent DAP model (Figure VII.1d) is proposed as follows:

1) perform a static pushdown analysis for the model of the entire system;
2) calculate the boundary conditions (the horizontal and rotational spring constants) at different floors for the DAP (Figure VII.1b,c and Figure VII.3a), according to the responses of the axial force vs. horizontal displacement relationship and the moment vs. rotational displacement relationship at the beam ends from step 1; and

3) calculate the mean values of all the spring constants, i.e. the horizontal and rotational spring constants from all the floors in step 2. The mean spring constants are adopted for the equivalent DAP model.

It should be noted that these steps are valid in case of a 'regular' frame where all floors/beams/columns are the same, otherwise a more elaborate model is required. Regarding the frame F6B6, the axial force vs. horizontal displacement relationships and moment vs. rotational displacement relationships at the beam ends of the DAP from the first floor to the sixth floor (nodes N-C1 to N-C6 in Figure VII.1b) are presented in Figure VII.6a and Figure VII.6b. Note that these curves are obtained from static pushdown analyses of the entire system model. Based on the axial force vs. horizontal displacement relationships and the moment vs. rotation relationships, the approximate linear horizontal spring constants and linear rotational spring constants for every floor are calculated. The maximum axial forces (or membrane force *MF*) in beams, horizontal spring constants K_H, moments M, rotational spring constants K_R for all the six floors and their mean values are summarized in Table VII.4. Significantly different horizontal spring constants K_H are obtained for the different floors (Table VII.4). The horizontal spring constant at the first floor (sixth floor), with a value of 45.4 kN/mm (7.8 kN/mm), is the largest (second largest), see Figure VII.6a. The rotational spring constant from the first (sixth) floor 2.9 x 10^5 kNm/rad (1.2 x 10^5 kNm/rad) is the largest (smallest), see Figure VII.6b.

Table VII.4. Membrane forces, moments, and equivalent spring constants from different floors.

Case		***MF* [kN]**	**K_H [kN/mm]**	***M* [kNm]**	**K_R [kNm/rad]**
F6B6	Floor 1	431.5	45.4	348.6	2.9 x 10^5
	Floor 2	23.34	2.0	273.2	2.4 x 10^5
	Floor 3	-31.07	-2.8	274.4	2.4 x 10^5
	Floor 4	-10.6	-1.0	275.3	2.3 x 10^5
	Floor 5	0.9	0.1	274.7	2.5 x 10^5
	Floor 6	85.9	7.8	299.6	1.2 x 10^5
	Mean	83.3	8.6	291.0	2.3 x 10^5
F3B12	Floor 1	387.0	47.8	344.3	1.8 x 10^5
	Floor 2	90.2	8.2	303.2	1.8 x 10^5
	Floor 3	48.4	4.5	284.7	0.9 x 10^5
	Mean	175.2	20.2	310.7	1.5 x 10^5

In order to prove the effectiveness of the mean spring constants adopted as the boundary conditions for the equivalent DAP model (Figure VII.1d), seven cases with different boundary conditions from Table VII.4 for the equivalent DAP model (F6B6) are investigated: six cases (case 'F1', case 'F2', case 'F3', case' F4', case 'F5' and case 'F6') where for each case the horizontal spring constant and

rotational spring constant from the corresponding floor in Table VII.4 are adopted for the equivalent DAP model; and one more case 'Mean' (Table VII.4) where the mean value of the horizontal and rotational spring constants listed in Table VII.4 is implemented. The load-displacement responses of the pushdown analyses for the seven cases are presented in Figure VII.6c,d. It is found that case 'F1' overestimates the response when compared to the load-displacement response of the entire system model ('Entire' 'in Figure VII.6c,d), while the other cases underestimate the responses.

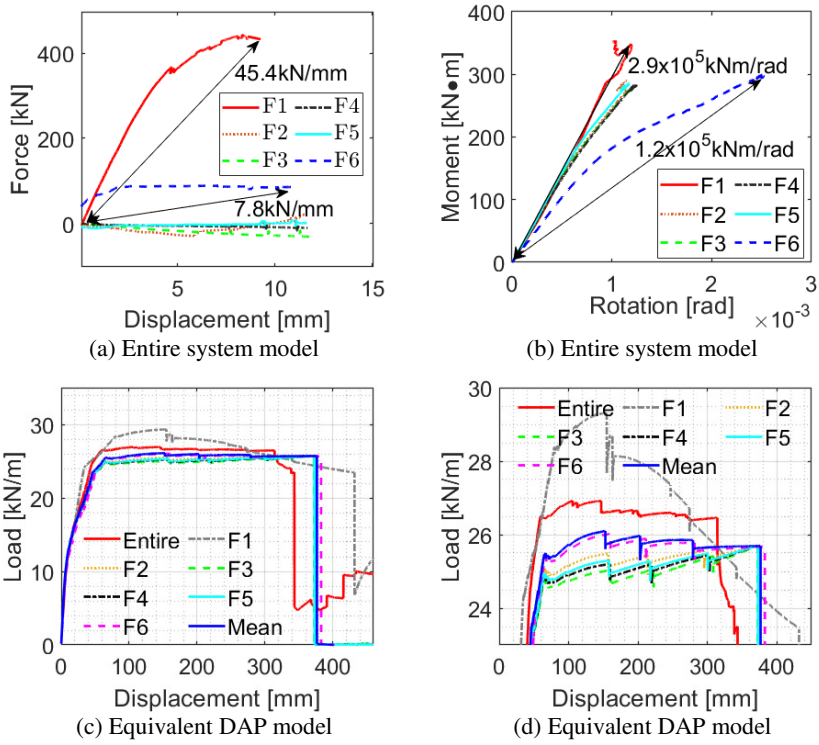

(a) Entire system model

(b) Entire system model

(c) Equivalent DAP model

(d) Equivalent DAP model

Figure VII.6. Frame F6B6: (a) axial force vs. horizontal displacement relationship; (b) moment vs. rotational displacement relationship; (c) load-displacement relationship; and (d) zoom in on the load-displacement relationship in (c).

For the seven considered cases for F6B6, the static resistances R_{Eq}, membrane forces MF_{Eq} in the horizontal springs, and moments M_{Eq} in the rotational springs are summarized in Table VII.5. Note that the equivalent DAP model in Figure VII.1d is investigated. Comparing with the resistance of the entire system R_{Ent} =

26.9 kN/m (Table VII.3), the deviations in percentage of the static resistances for the seven cases (Table VII.5) are 8.9%, -4.5%, -4.5%, -4.5%, -4.5%, -3.3%, and -3.1%, respectively. Comparing with the mean membrane force of the entire system MF_{Ent} = 83.3 kN (Table VII.4), the deviations in percentage of the membrane forces for the seven cases (Table VII.5) are 405.6%, -72.7%, -136.4%, -112.5%, -98.9%, 0.2%, and 12.1%, respectively. On the other hand, it is found that the membrane forces in Table VII.5 for the individual cases are close to the individual cases in Table VII.4, e.g. Case F1 vs. Floor 1. Comparing with the mean moment of the entire system M_{Ent} = 291.0 kNm (Table VII.4), the deviations in percentage of the moments for the seven cases are also presented in Table VII.5. Among these cases, the case 'Mean' can well reproduce the mean responses (the values presented in Table VII.4), although the membrane force is slightly overestimated.

Table VII.5. Static resistances R_{Eq}, membrane forces MF_{Eq}, moments M_{Eq}, and deviation in percentage.

Case		**F1**	**F2**	**F3**	**F4**	**F5**	**F6**	**Mean**
F6B6	R_{Eq} [kN/m]	29.3	25.7	25.7	25.7	25.7	26.0	26.1
	$(R_{Eq}-R_{Ent})/R_{Ent}^{*}$ [%]	8.9	-4.5	-4.5	-4.5	-4.5	-3.3	-3.1
	MF_{Eq} [kN]	421.2	22.7	-30.3	-10.4	0.9	83.5	93.4
	$(MF_{Eq}-MF_{Ent})/MF_{Ent}^{*}$ [%]	405.6	-72.7	-136.4	-112.5	-98.9	0.2	12.1
	M_{Eq} [kNm]	343.2	292.0	282.5	286.1	288.1	302.8	304.6
	$(M_{Eq}-M_{Ent})/M_{Ent}^{*}$ [%]	17.9	0.3	-2.9	-1.7	-1.0	4.1	4.7
F3B12	R_{Eq} [kN/m]	31.1	27.7	27.3	-	-	-	28.8
	$(R_{Eq}-R_{Ent})/R_{Ent}^{**}$ [%]	11.9	-0.4	-1.8	-	-	-	3.6
	MF_{Eq} [kN]	401.6	91.6	49.4	-	-	-	203.1
	$(MF_{Eq}-MF_{Ent})/MF_{Ent}^{**}$ [%]	129.2	-47.7	-71.8	-	-	-	15.9
	M_{Eq} [kNm]	342.6	304.3	296.3	-	-	-	318.1
	$(M_{Eq}-M_{Ent})/M_{Ent}^{**}$ [%]	10.3	-2.1	-4.6	-	-	-	2.4

*R_{Ent} = 26.9 kN/m is the static resistance of the entire system of frame F6B6; MF_{Ent} = 83.3 kN is the mean membrane force in Table VII.4; M_{Ent} = 291.0 kNm is the mean moment in Table VII.4.

**R_{Ent} = 27.8 kN/m is the static resistance of the entire system of frame F3B12. MF_{Ent} = 175.2 kN is the mean membrane force in Table VII.4; M_{Ent} = 310.7 kNm is the mean moment in Table VII.4.

For the frame F3B12, the axial force vs. horizontal displacement relationships (or moment vs. rotational displacement relationships) at the beam ends of the DAP from the first floor to the third floor (nodes N-F1 to N-F3 in Figure VII.3a) are shown in Figure VII.7a (Figure VII.7b). Similarly, the maximum axial forces (or *MF*) in beams, calculated horizontal spring constants K_H, moments M, calculated rotational spring constants K_R of all the three floors and their mean values have been summarized in Table VII.4 as well.

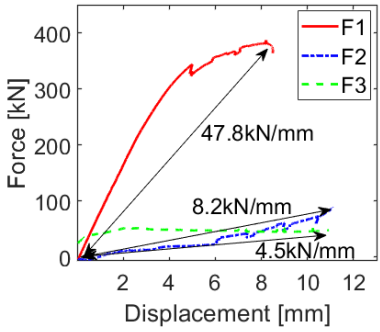

(a) Entire system model

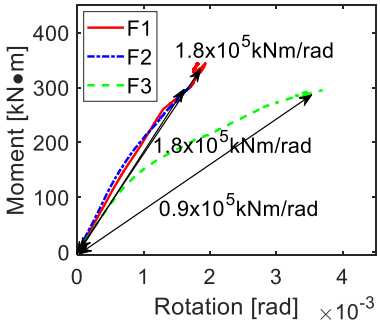

(b) Entire system model

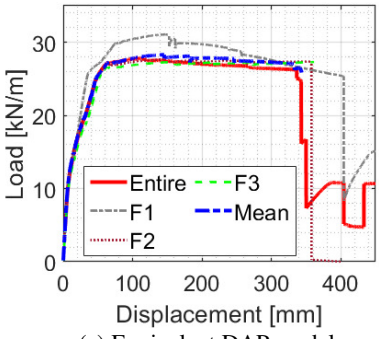

(c) Equivalent DAP model

Figure VII.7. Frame F3B12: (a) axial force vs. horizontal displacement relationship; (b) moment vs. rotational displacement relationship; and (c) load-displacement relationship.

In the same manner, four cases with different boundary conditions derived from observed equivalent stiffnesses for the three floors and their mean values (case 'F1', case 'F2', case 'F3', case 'Mean', see Table VII.4) are adopted for the equivalent DAP model of F3B12 (Figure VII.1d). The load-displacement responses of the pushdown analyses for the four cases are presented in Figure VII.7c. The

case ‘F1’ significantly overestimates the response when comparing to the load-displacement response of the entire system (‘Entire’ in Figure VII.7c), while the other cases result in closer approximations. The static resistances R_{Eq}, membrane forces MF_{Eq} in the horizontal springs, and moments M_{Eq} in the rotational springs for the four cases are summarized in Table VII.5. Although the membrane force is slightly overestimated, the case ‘Mean’ can well reproduce the mean responses in Table VII.4.

In the previous investigation for determining approximate boundary conditions, the case ‘Mean’ shows overall a good performance for both F6B6 and F3B12. Although the assumption of the mean values as the boundary conditions is a simple approximation and can still be improved using other advanced methods (e.g. create a FE model for the IAP part and perform an elastic-plastic analysis to determine the boundary conditions), the results with regard to resistance, membrane force in the horizontal spring, and moment in the rotational spring approximate the mean responses of the entire system (Table VII.5). This confirms the feasibility of adopting the assumption in section VII.2, where the same boundary conditions are assumed for all the floors. Although a nonlinear static analysis for analysing the entire system model is needed to determine the spring constants, the developed equivalent DAP model can be further adopted to the nonlinear dynamic analyses. Since the equivalent DAP model is adopted for the dynamic analyses (i.e. no dynamic analysis for the entire system model), the calculation demand can be significantly reduced.

VII.4.3 Multilevel calculation scheme with DAP and IAP

VII.4.3.1 Directly affected part: pushdown and IDA analyses

According to the previous study, the boundary conditions with the mean spring constants (i.e. case ‘Mean’ in Table VII.4) are adopted for the equivalent DAP models for both frames F6B6 and F3B12. Pushdown and IDA analyses, similar to those performed for the entire system model (in section VII.4.1), are carried out for the equivalent DAP models. The load-displacement curves are presented in Figure VII.4a,c for F6B6 and F3B12, respectively. Comparison with the responses of the entire system model confirms that the equivalent model gives a good approximation of the entire frame response, both for the pushdown curves (curve ‘Pushdown-Equivalent’ in Figure VII.4a,c) and the IDA curves (curve ‘IDA-Equivalent’ in Figure VII.4a,c). The ultimate load-bearing capacities for the equivalent DAP models in cases F6B6 and F3B12 are summarized in Table VII.6 as well. Comparing to the static (or dynamic) resistance of the entire system model, the deviations in percentage for the resistances from the equivalent DAP models are -3.0% and 3.6% (-0.4% and 3.8%, see Table VII.6) in cases F6B6 and F3B12, respectively. The maximum deviation in percentage is 3.8% (F3B12 - IDA). It is

concluded that the equivalent DAP model has a good performance. In addition, the resistances from IDA are found to be lower than the values from pushdown analyses (the equivalent DAP models), i.e. 97.7% and 94.4% for F6B6 and F3B12 respectively.

Table VII.6. Ultimate load-bearing capacity (R) and membrane force (MF).

Case			***R*** [kN/m]	**Error [%]**	***MF*** [kN]	**Error [%]**
F6B6	Entire system model	Pushdown	26.9	-	83.3*	-
		IDA	25.6	-	81.5*	-
	Equivalent DAP model - ultimate	Pushdown	26.1	-3.0	93.4	12.1
		IDA	25.5	-0.4	93.4	14.6
	Equivalent DAP model - yield	Pushdown	23.5	-	19.9	-
		IDA	17.0	-	19.8	-
F3B12	Entire system model	Pushdown	27.8	-	175.2*	-
		IDA	26.2	-	167.1*	-
	Equivalent DAP model - ultimate	Pushdown	28.8	3.6	203.1	15.9
		IDA	27.2	3.8	199.3	19.3
	Equivalent DAP model - yield	Pushdown	25.2	-	46.3	-
		IDA	18.0	-	46.2	-

* The MF in case of entire system model is the mean value of MF in all floors.

The time-history displacement responses from the equivalent DAP models are presented in Figure VII.8a,d for F6B6 and F3B12, respectively. Moreover, a force-based DAF is calculated as DAF = $R_{pushdown}/R_{IDA\text{-}peak}$, where $R_{pushdown}$ and $R_{IDA\text{-}peak}$ are the loads on the pushdown and IDA curves at a same displacement (Figure VII.4a,c and Figure VII.8b,e), respectively. The DAFs are shown in Figure VII.8b,e for F6B6 and F3B12, respectively. The DAF in case F6B6 (or F3B12) decreases from 1.78 to 1.01 (or from 1.85 to 1.01). The DAF significantly decreases when the imposed load increases. Although the DAFs at the ultimate displacements are almost equal to unity, dynamic effects have a great influence (i.e. amplification) in the smaller displacement levels.

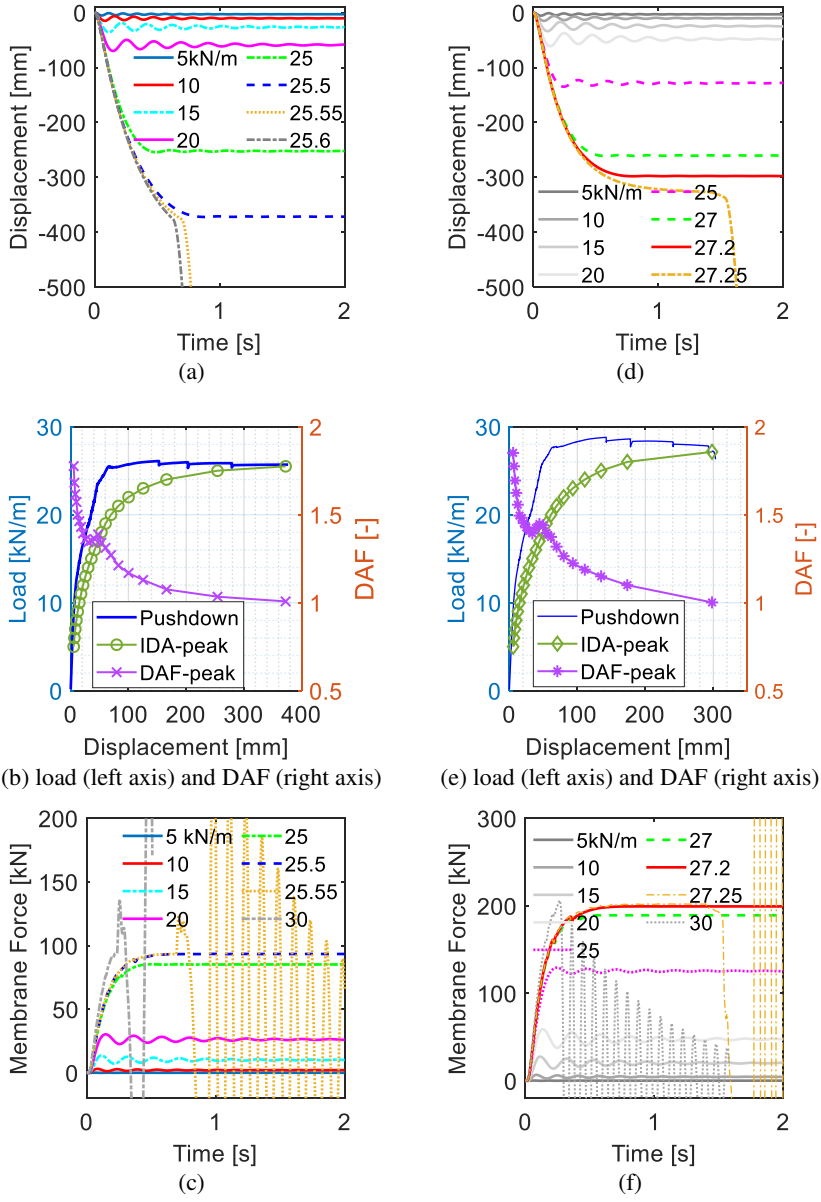

Figure VII.8. Time-history displacement and membrane force (MF) responses from DAP: (a) F6B6 - time-history displacement response; (b) F6B6 – force-based DAF; (c) F6B6 – time-history MF response; (d) F3B12 - time-history displacement response; (e) F3B12 – force-based DAF; and (f) F3B12 - time-history MF response.

The time-history responses for membrane forces in the horizontal springs are presented in Figure VII.8c,f for F6B6 and F3B12, respectively. Note that the membrane forces are very small when the imposed load is 5.0 kN/m, where the peak values are 0.15 kN and 0.32 kN for F6B6 and F3B12, respectively. Membrane force or compressive arch action is easy to be observed from 10.0 kN/m for both F6B6 and F3B12 (larger membrane forces in Figure VII.8c,f). Further, the peak values of the time-history membrane force responses (Figure VII.8c,f) against the peak displacements (Figure VII.8a,d) are plotted in Figure VII.9a,c for F6B6 and F3B12, respectively. Compared to the membrane force - vertical displacement relationships from pushdown analyses (curve 'pushdown'), the peak membrane forces - peak displacement relationships from the IDA (curve 'IDA-peak') are almost identical to those 'pushdown' curves. Moreover, the same holds for the residual membrane forces vs. residual displacement relationships from the IDA analyses (curve 'IDA-residual'), which are almost identical to the curves from the pushdown analyses. This is logical as the same boundary conditions (springs) are adopted in both pushdown and IDA analyses. Thus, the maximum membrane force for a dynamic analysis can also be obtained from the static membrane force vs. displacement curve. Note that in Figure VII.9a a sudden jump in membrane force towards higher values is observed. This is because the sudden failure at the beam ends results in a sudden increase of vertical displacement. The force in the spring is proportional to the displacement and therefore a sudden large force is observed. It does not mean the structure can carry additional loads.

However, the same imposed loads will result in different vertical displacement responses (Figure VII.8b,e) and hence different membrane forces (Figure VII.9b,d) for the static and dynamic analyses. A DAF is calculated as DAF = MF_{IDA}/ $MF_{pushdown}$, where $MF_{pushdown}$ and MF_{IDA} are the membrane forces on the membrane force vs. load curves from pushdown and IDA (peak or residual value) analyses at a same imposed load (Figure VII.9b,d), respectively. The curves of the DAF vs. the corresponding imposed load are presented in Figure VII.9b,d for the two cases, which both are observed to first increase, then decrease, and increase again. Moreover, the DAFs for both cases vary between 2 to 4 when the imposed loads are larger than 15.0 kN/m, which means the influence of dynamic effects are very significant.

VII.4.3.2 Indirectly affected part: analytical analyses

As smaller deformations are expected for the IAP (section VII.2.1), a simple plastic analysis is employed to determine the resistance of the IAP, i.e. R_{IAP}. In order to determine R_{IAP} using Eq. (VII.1), the plastic moment capacities $M_{pl,Ci}$ of the respective columns at the ground storey of the IAP can be calculated based on the

work by Monti and Petrone (2015). Closed-form equations for moment-curvature laws of RC sections subjected to bending moment and axial load were developed and validated (Monti and Petrone, 2015; Droogné *et al.*, 2018). The closed-form equations provide the yield and ultimate moments and curvatures as a function of the following parameters: the cross-sections effective depth; the steel yielding strain and concrete ultimate strain; the longitudinal reinforcement ratio and transverse shear reinforcement ratio; and the axial force on the sections. As a limited compressive normal force has a beneficial influence on the capacity of the cross-section, a conservative approximation for the column moment capacity is to consider only the dead loads on the IAP, i.e. no service live load is taken into account (Droogné *et al.*, 2018). In addition, the load originally carried by the notionally removed column is redistributed to the closest neighbouring columns of the same frame in the damaged situation. The corresponding capacity for membrane force *MF* (i.e. R_{IAP}) can be calculated on the basis of these assumptions and the closed-form equations from (Monti and Petrone, 2015).

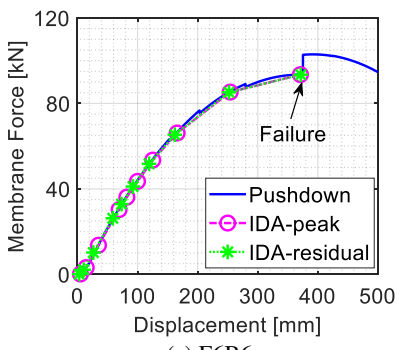

(a) F6B6

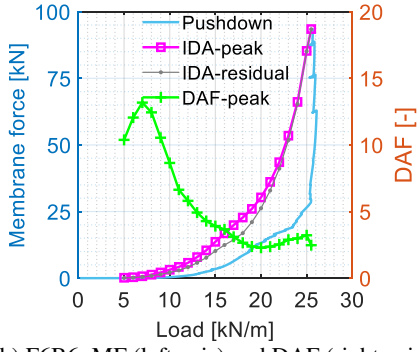

(b) F6B6: MF (left axis) and DAF (right axis)

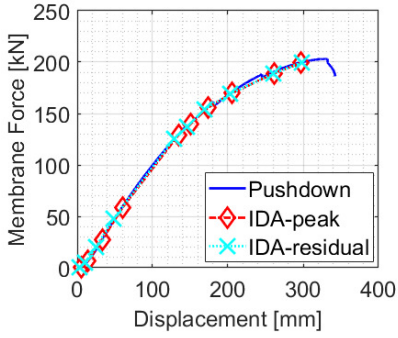

(c) F3B12

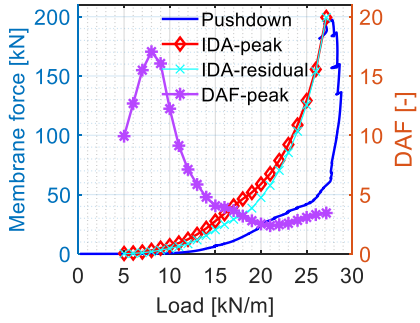

(d) F3B12: MF (left axis) and DAF (right axis)

Figure VII.9. Membrane force (MF): (a) F6B6 - MF vs. vertical displacement; (b) F6B6 - MF vs. load and DAF; (a) F3B12 - MF vs. vertical displacement; and (b) F3B12 - MF vs. load and DAF.

When determining R_{IAP} using Eq. (VII.1), either the yield or the ultimate moment can be adopted as plastic moment capacity of the columns. The closed-form equations result in the moment vs. curvature curves (moment of all the columns on one side) as shown in Figure VII.10a for the cases F6B6 and F3B12. Note that the moment vs. curvature curves are determined from the yield moment and the ultimate moment and the corresponding curvatures (i.e. two points), which are calculated according to the closed-form equations proposed by Monti and Petrone (2015). The calculated R_{IAP} from the different moment capacities are summarized in Table VII.7. The resistances are 89.4 kN and 99.0 kN respectively resulting from the yield moment 804.9 kNm and ultimate moment 890.9 kNm for F6B6, while the resistances are 216.5 kN and 239.4 kN respectively resulting from the yield moment 974.2 kNm and ultimate moment 1077.1 kNm in relation to F3B12. The resistance from the ultimate moment is remarkably larger than that from the yield moment. The resistance for F3B12 is significantly larger than that of F6B6 because the frame F3B12 has more bays and thus more columns contributing to the total moment capacity.

The yield and ultimate moments in RC components are usually corresponding to the yield and ultimate strains of the reinforcing steel. As there is a significant difference for the deformation implied by the two situations, the membrane force developed in the springs (considered proportional to the deformation) of the DAP should also be distinguished. The maximum *MF* (with ultimate strain for rebar) from the pushdown analyses for the equivalent DAP models are 93.4 kN and 203.1 kN (Table VII.6) respectively for F6B6 and F3B12, which are smaller than the corresponding R_{IAP} calculated from the ultimate moment, i.e. 99.0 kN and 239.4 kN respectively for F6B6 and F3B12.

For comparison purposes, Table VII.6 also provides the resistances (R) from the pushdown and IDA analyses for the equivalent DAP model where the stress in the rebars is limited to the yield value (case 'Equivalent DAP model-yield'). The load-bearing capacities (R) are significantly lower, especially for IDA results. Regarding the membrane forces in the horizontal springs from the pushdown analyses (similar for the IDA results), the maximum *MF* (with yield strain for rebar) for the DAP models are 19.9 kN and 46.3 kN respectively for F6B6 and F3B12 (Table VII.6), which are significantly smaller than the corresponding R_{IAP} calculated from the yield moment, i.e. 89.4 kN and 216.5 kN for F6B6 and F3B12 (Table VII.7) respectively. Consequently, these results indicate that the IAP will not fail because of excessive membrane force capacity of the IAP, for this deterministic case study. The yield strain for the rebar is a conservative assumption.

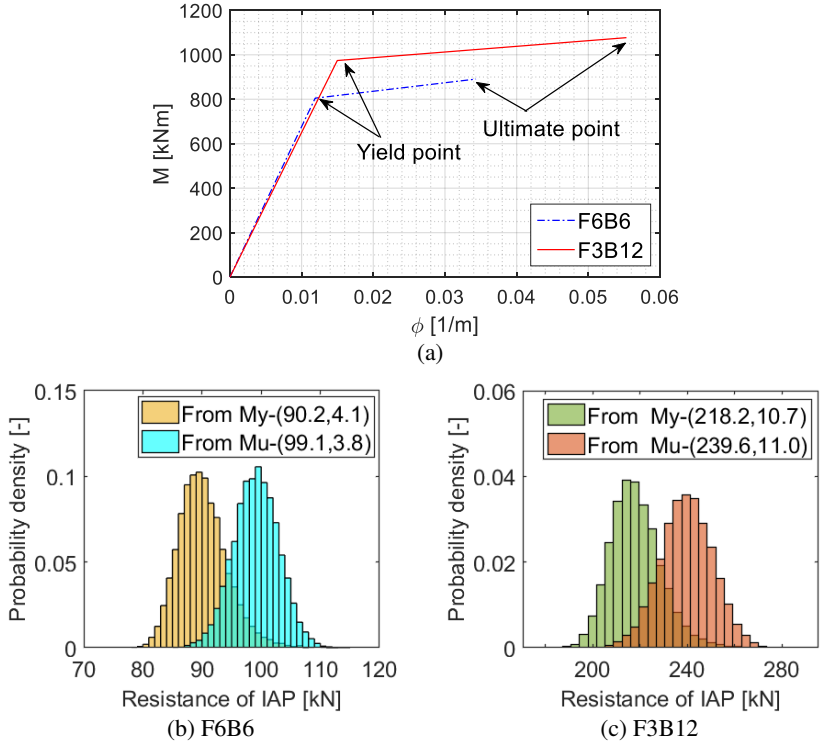

Figure VII.10. Results for IAP: (a) moment-curvature relationship of the columns; (b) F6B6 - histogram of resistance; and (c) F3B12 - histogram of resistance.

Table VII.7. Plastic moment and resistance of the IAP (deterministic and stochastic analyses).

Case		**Deterministic analysis**		**Stochastic analysis (R_{IAP})**	
		M [kNm]	***R*$_{IAP}$** [kN]	**Mean** [kN]	**St.D.** [kN]
F6B6	From yield moment M_y	804.9	89.4	90.2	4.1
	From ultimate moment M_u	890.9	99.0	99.1	3.8
F3B12	From yield moment M_y	974.2	216.5	218.2	10.7
	From ultimate moment M_u	1077.1	239.4	239.6	11.0

The dynamic effects mainly influence the capacity of IAP by amplifying the axial forces in the columns. However the DAF for the axial force becomes quite close to unity at the ultimate load-bearing capacity for the two frames (DAF = 1.03 for

F6B6 in Figure VII.4c, and DAF = 1.03 for F3B12 in Figure VII.4f). Therefore, the dynamic effects have limited influence on the resistance of IAP for the two frames and can be neglected.

Moreover, the shear capacity of the IAP (for all the columns on one side of the removed column) are calculated for both frames. The following equations recommended in Eurocode (CEN, 2004) are adopted to calculate the shear capacity of a RC column:

$$V = V_c + V_s \tag{VII.7}$$

$$V_c = \max\left[\left(C_c k(100\rho_l f_c)^{1/3} + k_1\sigma_{cp}\right)b_w d, \left(v_{\min} + k_1\sigma_{cp}\right)b_w d\right] \tag{VII.8}$$

$$V_s = \min\left[\frac{A_{sw}}{s} z f_{yw}\cot\theta, \alpha_{cw} b_w z \nu_1 f_c / \left(\cot\theta + \tan\theta\right)\right] \tag{VII.9}$$

where V is the shear capacity of a RC column; V_c is the concrete contribution to the shear strength of the column; V_s is stirrup contribution to the shear strength of the column; C_c is a factor with a recommended value is 0.18; $k = 1 + \sqrt{200/d} \leq 2$; d is the effective depth; $\rho_l = A_{sl}/(b_w d) \leq 0.02$; A_{sl} is the area of the tensile reinforcement; b_w is the smallest width of the cross-section in the tensile area; f_c is concrete compressive strength; k_1 is a factor with a recommended value of 0.15; $\nu_{\min} = 0.035k^{3/2}f_c^{1/2}$; $\sigma_{cp} = N_E/A_c < 0.2f_c$; N_E is the axial force in the cross-section and a positive value for compression; A_c is the cross sectionional area of concrete; A_{sw} is the cross-sectional area of the shear reinforcement; s is the spacing of the stirrups; f_{yw} is the yield stress of the shear reinforcement; $\nu_1 = 0.6(1 - f_c/250)$ is a strength reduction factor for concrete cracking in shear; α_{cw} is a coefficient taking account of the state of the stress in the compression chord; $z = 0.9d$ is the inner lever arm; θ is the angle between the concrete compression strut and the column axis perpendicular to the shear force, where $\cot\theta = 1$ is adopted (the recommended limits are $1 \leq \cot\theta \leq 2.5$). Considering a compressive axial load in column benefits its shear capacity, only axial forces from dead loads are therefore adopted, as this gives a conservative result. Finally, shear capacities in all the ground floor columns on one side are summed and the total shear resistances are 1118.0 kN and 1720.8 kN for F6B6 and F3B12, respectively. The shear resistances are significantly larger than the ultimate resistance of the IAP as shown in Table VII.7, which are 594.0 kN (six floors in F6B6, i.e. 6 x R_{IAP} in Table VII.7) and 718.2 kN (three floors in F3B13, i.e. 3 x R_{IAP} in Table VII.7). Hence, no shear failure will occur, as the bending failue will occur first.

VII.5 Stochastic analysis

VII.5.1 Probabilistic modelling of input variables

In order to calculate the failure probabilities for the two RC frames, 12 variables are selected as random variables, which are presented in Table VII.8. c is the concrete cover, which is modelled as a bounded Beta distribution (Holický and Sýkora, 2010), with a mean value equal to the specified value of 30 mm, a standard deviation of 5 mm, a lower bound of 0 mm and an upper bound of three times the mean value, i.e. 90 mm. f_{cm} is the concrete compressive strength, while ε_{c1} is the peak compressive strain (JCSS, 2001; Holický and Sýkora, 2010; fib, 2013; Droogné *et al.*, 2018; Feng *et al.*, 2020). For modelling the concrete tensile strength, $Y_{2,j}$ is employed to reflect variations due to factors not well accounted for by concrete compressive strength, i.e. $f_{ctm} = 0.3\ (f_{ck})^{2/3}\ Y_{2,\mathrm{j}}$ (JCSS, 2001). E_s, f_{ym}, f_{um} and ε_u are the modulus of elasticity, the yield stress, the tensile strength and ultimate strain of the reinforcement, respectively (JCSS, 2001; Holický and Sýkora, 2010; fib, 2013; Droogné *et al.*, 2018; Feng *et al.*, 2020). *DL* and *LL* are the dead load and the live load, respectively. The *LL* model considers an arbitrary-point-in-time live load (Jovanović *et al.*, 2020). K_L and K_R are the load model uncertainty and resistance model uncertainty, respectively (JCSS, 2001; Holický and Sýkora, 2010). The other parameters are considered to be deterministic.

Table VII.8. Probabilistic models of stochastic variables.

Variable (related to)	Units	Distribution	Mean	CoV
Concrete cover c	mm	Beta	30	0.17
Concrete compressive strength f_{cm}	MPa	Lognormal	38	0.1
Concrete compressive strain at peak stress ε_{c1}	%	Lognormal	0.23	0.15
Model uncertainty for tensile strength $Y_{2,j}$	-	Lognormal	1	0.30
Rebar elastic modulus E_s	GPa	Normal	200	0.08
Rebar yield stress f_{ym}	MPa	Lognormal	555	0.03
Rebar ultimate strength f_{um}	MPa	Lognormal	605	0.03
Rebar fracture strain ε_u	%	Lognormal	7.5	0.15
Dead load of the floor *DL*	kN/m^2	Normal	6	0.04
Live load on the floor *LL*	kN/m^2	Gamma	0.6	0.6
Load model uncertainty K_L	-	Lognormal	1	0.1
Resistance model uncertainty K_R	-	Lognormal	1	0.15

Based on the probabilistic models presented in Table VII.8, 10 000 random samples are generated using the Latin Hypercube sampling (LHS) technique. It is worth noting that all the parameters are assumed to be independent except for the

yield stress f_{ym} and the tensile strength f_{um} of reinforcing steel (the correlation coefficient is 0.95) (JCSS, 2001).

VII.5.2 Entire system model: pushdown and IDA analyses

Both a pushdown analysis and an IDA are carried out for every sample for the entire system model of F6B6, as well as for F3B12, considering the central column removal scenario. The loading scheme is identical to the deterministic analysis in section VII.4. In order to reduce the computational demand when determining the ultimate load-bearing capacity, the load increment resolution at the ultimate capacity is taken as 0.5 kN/m for the IDA analyses. The pushdown and IDA curves obtained for every sample are similar to the results of the deterministic analyses.

The histograms of ultimate load-bearing capacities (from both the pushdown and IDA analyses) for the entire system model for F6B6 (F3B12) are presented in Figure VII.11a (Figure VII.11d). Mean values and standard deviations (St.D.) for the pushdown and IDA analysis results are listed in Table VII.9. Both for F6B6 and F3B12, the mean resistances from IDA are found to be lower than those from the pushdown analyses (Figure VII.11a,d), i.e. 93.4% and 92.8% ($R_{IDA}/R_{pushdown}$) respectively for F6B6 and F3B12.

VII.5.3 Multilevel calculation scheme with DAP and IAP

VII.5.3.1 Directly affected part

Regarding the equivalent DAP model for F6B6 or F3B12, both a pushdown analysis and an IDA are carried out for every sample. The loading schemes are identical to the deterministic analyses in section VII.4.3. Note that different boundary conditions of different spring constants (calculated similar to that in section VII.4.2) for every realization are adopted. Again, the load increment resolution of 0.5 kN/m is used to reduce the computational demand in the stochastic IDA analyses. The pushdown and IDA curves obtained for every sample are similar to the results of the deterministic analyses. The histograms of the resistances are shown in Figure VII.11b,e and a summary of the results (resistance R and maximum membrane force MF) is presented in Table VII.9.

Figure VII.11b shows the histograms of resistances (from both the pushdown and IDA analyses, i.e. 'IDA-ultimate' and 'Pushdown-ultimate') for the equivalent DAP model in terms of F6B6, and Figure VII.11e for the equivalent DAP model with regard to F3B12. Note that the resistances are calculated when the failure criterion for the rebar is its ultimate strain. The mean resistances from IDA are

found to be lower than those from pushdown analyses, i.e. 96.2% and 94.4% ($R_{IDA}/R_{pushdown}$) respectively for F6B6 and F3B12.

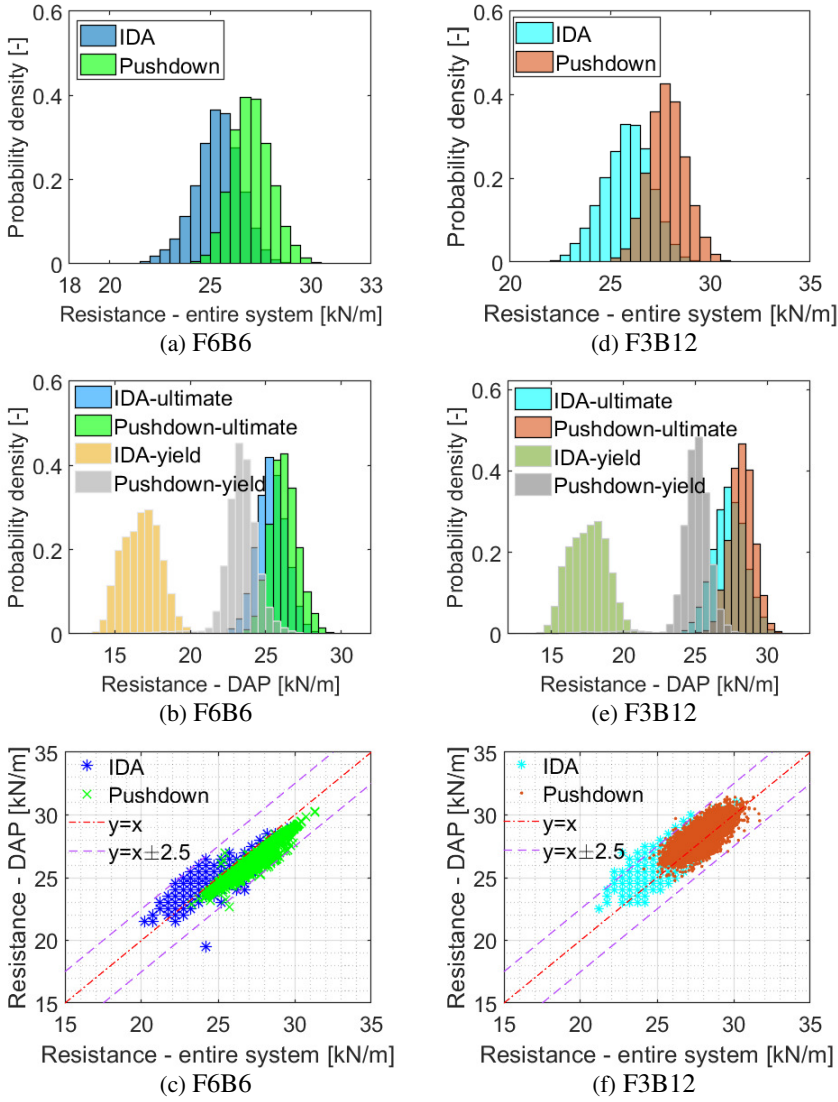

Figure VII.11. Histogram of resistance (R) and comparison of results: (a) F6B6 - R for the entire system model; (b) F6B6 - R from the equivalent DAP model; (c) F6B6 - comparison between the entire system model and the equivalent DAP model; (d) F3B12 - R for the entire system model; (e) F3B12 - R from the equivalent DAP model; and (f) F3B12 - comparison between the entire system model and the equivalent DAP model.

Comparing with the results obtained from the analyses for the entire system models, the results of the equivalent DAP models for F6B6 and F3B12 are found to be very close to those of the entire system when the ultimate strain is adopted for the reinforcing steel. For example, the pushdown results for the entire system model and the equivalent DAP model in case of F6B6 are 27.1 kN and 26.2 kN (deviation in percentage is -3.3%), while the IDA results for the entire system model and the equivalent DAP model are 25.3 kN and 25.2 kN (deviation in percentage is -0.4%). Meanwhile, the values of standard deviations (St.D.) are almost identical. A good agreement can be observed for F3B12 as well.

Table VII.9. Ultimate load-bearing capacities (*R*) and membrane force (*MF*) according to stochastic analyses.

Case			***R*** [kN/m]		***MF*** [kN]	
			Mean	**St.D.**	**Mean**	**St.D.**
F6B6	Entire system model	Pushdown	27.1	1.0	-	-
		IDA	25.3	1.1	-	-
	Equivalent DAP model-ultimate	Pushdown	26.2	0.9	92.9	10.2
		IDA	25.2	1.0	89.2	10.2
	Equivalent DAP model-yield	Pushdown	23.4	1.3	19.0	3.5
		IDA	16.5	1.2	20.1	3.7
F3B12	Entire system model	Pushdown	27.8	0.9	-	-
		IDA	25.8	1.2	-	-
	Equivalent DAP model-ultimate	Pushdown	28.3	0.9	191.8	34.2
		IDA	26.7	1.1	182.8	30.7
	Equivalent DAP model-yield	Pushdown	24.9	1.4	43.5	7.1
		IDA	17.3	1.3	45.9	7.3

The aforementioned pushdown and IDA analyses for the equivalent DAP model are performed a second time considering the yield strain as the failure criterion for the rebar. The histograms for resistances are shown in Figure VII.11b,e ('IDA-yield' and 'Pushdown-yield') and a summary of the results is presented in Table VII.9 as well. Compared to the resistances calculated from the ultimate strain, the resistances calculated considering the limiting yield strain are significantly lower. The mean resistances $R_{steel,yield}$ from pushdown (and IDA) analyses when considering the yield strain limit are 89.3% and 88.0% (65.5% and 64.8%) of the values $R_{steel,ultimate}$ calculated with the ultimate strain limit in cases of F6B6 and F3B12 respectively, i.e. $R_{steel,yield}/R_{steel,ultimate}$. Moreover, the mean resistances from IDA (with yield strain limit) are found to be significantly lower than those from pushdown analyses (with yield strain limit), i.e. 70.5% and 69.5% ($R_{IDA}/R_{pushdown}$) for F6B6 and F3B12 respectively. Compared to 96.2% and 94.4% ($R_{IDA}/R_{pushdown}$)

respectively for F6B6 and F3B12 (the equivalent system models) found when considering the ultimate strain limit, the ratios are significantly lower. This indicates and confirms again that the nonlinear static analysis is highly non-conservative (i.e. a significant influence by the dynamic effects exists) at the small deformation level, i.e. at the yield strain. Hence, accounting for dynamic effects is of great importance. This is also found in some other studies (Tsai and Lin, 2008; Brunesi and Nascimbene, 2014; Brunesi *et al.*, 2015), where the nonlinear static approach is found to be highly non-conservative for progressive collapse evaluation at low-medium displacement levels where immediate occupancy and serviceability limit states govern structural performance.

VII.5.3.2 Indirectly affected part

For the IAP of F6B6 and F3B12, the analytical solution, as presented in section VII.4.3, is adopted to perform the stochastic analysis. Since the resistance of the IAP, i.e. R_{IAP}, can be determined based on either the yield or the ultimate moments of the columns, different resistances R_{IAP} are obtained and presented in Figure VII.10 and Table VII.7. Figure VII.10b (or Figure VII.10c) shows the histograms of the resistances for F6B6 (or F3B12). For both frames, the mean resistance results from the yield moment of the columns is lower than that from the ultimate moment (Table VII.7).

According to the results of previous analyses when considering the yield strain limit, the maximum membrane forces (*MFs*) in the horizontal spring of equivalent DAP model (Table VII.9) are much lower than the resistance R_{IAP} of the IAP (Table VII.7), for both frames. This indicates that no failure is deemed to occur in the IAP. Moreover, from dynamic analysis the load-bearing capacity (R) of the DAP is observed to be significantly lower (i.e. leading to very large failure probabilities). The results considering the yield strain limit are very conservative. Nevertheless, the option to consider the yield strain can depend on the desired accuracy of the predictions and the user's choice. One can use the ultimate values and a higher capacity and lower failure probability are to be expected instead of when using the very conservative assumption of only allowing for the yield values. Only the results with regard to the ultimate strain limit are further investigated in the following.

VII.6 Risk-based robustness quantification

VII.6.1.1 Reliability evaluation

VII.6.1.1.1 Entire system model

In order to calculate the failure probabilities for the entire system models of the two RC frames subjected to a central column removal scenario, a limit state function (LSF) Z_1 is defined as follows:

$$Z_1 = K_R R - K_L \left(L_{DL} + L_{LV} \right) \tag{VII.10}$$

where Z_1 is the LSF; K_L and K_R are the load model and resistance model uncertainties (Table VII.8), respectively; R is the resistance obtained from the stochastic pushdown or IDA analysis; L_{DL} and L_{LL} are the load actions of *DL* and *LL* on the beams (Table VII.8). Considering the previously obtained resistances, the failure probabilities (P_f) and reliability indices (β) can be evaluated using the Monte Carlo simulation (MCS) with the aforementioned Latin Hypercube samples. The result of the reliability analysis is summarized in Table VII.10. When applying the IDA, the failure probability for the entire system model is evaluated to be significantly higher than when considering a static pushdown analysis.

Table VII.10. Failure probability and reliability index.

Entire system model

Case		P_f	β
F6B6	Pushdown	0.051	1.635
	IDA	0.105	1.254
F3B12	Pushdown	0.040	1.751
	IDA	0.089	1.347

Multilevel calculation scheme

Case		**System**		**DAP**		**IAP**	
		$P\,[F_{DAP} \cup F_{IAP}]$	β	$P\,[F_{DAP}]$	β	$P\,[F_{IAP}]$	β
F6B6	Pushdown	0.072	1.461	0.072	1.461	0.0002	3.540
	IDA	0.109	1.232	0.109	1.232	0.0004	3.353
F3B12	Pushdown	0.033	1.838	0.033	1.838	-	-
	IDA	0.063	1.530	0.063	1.530	0.0001	3.719

VII.6.1.1.2 Multilevel calculation scheme: DAP

The failure probability P_f (and reliability index β) for the DAP is calculated considering the equivalent DAP model (Figure VII.1d) and using LSF Z_1 as defined in Eq. (VII.10). The capacity of the model is calculated considering the ultimate strain for the rebar, as listed in Table VII.9. In terms of F6B6, the failure probabilities P_f (or β) are 0.072 (1.461) and 0.109 (1.232) for the pushdown and IDA resistances (Table VII.10), respectively. With regard to F3B12, the failure probabilities P_f (or β) are 0.033 (1.838) and 0.063 (1.530) for the pushdown and

IDA resistances, respectively. The failure probability with regard to the IDA is remarkable higher than that from the pushdown analysis for both cases.

VII.6.1.1.3 Multilevel calculation scheme: IAP

To calculate the failure probabilities for the IAP of the two RC frames, a limit state function (LSF) Z_2 is defined as follows:

$$Z_2 = R_{IAP} - MF_{DAP} \tag{VII.11}$$

where Z_2 is the LSF for IAP; R_{IAP} is the resistance obtained from the stochastic analysis for the IAP in section VII.5.3; and MF_{DAP} is the membrane force from the horizontal spring of the equivalent DAP model. Considering the previously obtained resistances, the failure probability (P_f) and reliability index (β) are evaluated using Monte Carlo simulations. Note that no model uncertainty is incorporated due to the lack of sufficient data for membrane forces (Droogné *et al.*, 2018). The membrane force MF_{DAP} is a result obtained from the DAP analysis, i.e. the force in the horizontal spring. Note that two situations can be distinguished (Droogné *et al.*, 2018):

(i) No failure of the DAP, i.e. $Z_1 \geq 0$. The failure probability of the IAP conditional on the survival of the DAP $P[F_{\mathrm{IAP}}|\overline{F_{\mathrm{DAP}}}]$ can be calculated using LSF Z_2. In this case, the membrane force MF_{DAP}, corresponding to the total load $DL + LL$, is obtained from the DAP analysis for a certain sample. If the IAP is unable to balance this membrane force, then the failure of the IAP also results in consequences for the DAP, since the DAP will lose stability resulting from the failure of its boundary conditions.

(ii) Failure of the DAP: i.e. $Z_1 < 0$. The failure probability of the IAP conditional on the failure of the DAP $P[F_{\mathrm{IAP}}|F_{\mathrm{DAP}}]$ can be calculated using LSF Z_2. The membrane force MF_{DAP} corresponding to the ultimate load-bearing capacity of the DAP is considered in the evaluation.

Accordingly, the failure probability (P_f) of the IAP can be calculated as follows:

$$P\left[F_{\mathrm{IAP}}\right]=P\left[F_{\mathrm{IAP}}|\overline{F_{\mathrm{DAP}}}\right]\cdot(1-P\left[F_{\mathrm{DAP}}\right])+P\left[F_{\mathrm{IAP}}|F_{\mathrm{DAP}}\right]\cdot P\left[F_{\mathrm{DAP}}\right] \tag{VII.12}$$

where $P[F_{\mathrm{IAP}}]$ is the failure probability of the IAP. $P[F_{\mathrm{DAP}}|\overline{F_{\mathrm{DAP}}}]$ is the failure probability of the IAP conditional on the survival of the DAP, i.e. situation (i). $P[F_{\mathrm{DAP}}]$ is the failure probability of the DAP. And $P[F_{\mathrm{IAP}}|F_{\mathrm{DAP}}]$ is the failure probability of the IAP conditional on the failure of the DAP, i.e. situation (ii).

For the resistance of the IAP, the R_{IAP} value is calculated from the ultimate moment of the columns (section VII.5.3). The membrane force MF_{DAP} considers the corresponding horizontal forces in the horizontal springs. The results for the two frames are summarized in Table VII.10. Regarding the static pushdown cases, P_f

(or β) is 0.0002 (3.54) for F6B6 while no failure is observed in the Monte Carlo evaluation (10 000 simulations) for F3B12. For the IDA analyses, P_f (or β) are 0.0004 (3.353) and 0.0001 (3.719) for F6B6 and F3B12, respectively. Regarding F6B6, the failure probability from the IDA is two times that from the pushdown analysis.

VII.6.1.1.4 Multilevel calculation scheme: combining DAP and IAP

The total system failure probabilities of the two frame systems can be calculated by combining the previous failure probabilities for DAP and IAP as follows:

$$\begin{aligned} P\left[F_{\mathrm{DAP}} \cup F_{\mathrm{IAP}}\right] &= P\left[F_{\mathrm{DAP}}\right] + P\left[F_{\mathrm{IAP}}\right] - P\left[F_{\mathrm{DAP}} \cap F_{\mathrm{IAP}}\right] \\ &= P\left[F_{\mathrm{DAP}}\right] + P\left[F_{\mathrm{IAP}}\right] - P\left[F_{\mathrm{IAP}} | F_{\mathrm{DAP}}\right] \cdot P\left[F_{\mathrm{DAP}}\right] \end{aligned} \tag{VII.13}$$

where $P[F_{\mathrm{DAP}} \cup F_{\mathrm{IAP}}]$ is the failure probability of the structural system subjected to the accidental situation (central column removal) in case F6B6 or F3B12. And $P[F_{\mathrm{DAP}} \cap F_{\mathrm{IAP}}]$ is the failure probability if both DAP and IAP fail.

The failure probabilities P_f (or β) for the two frame systems using the multilevel calculation scheme method are calculated using Eq. (VII.13). The results are presented in Table VII.10 (ultimate strain for rebar). The failure probabilities P_f (or β) are 0.072 (1.461) and 0.109 (1.232) respectively for the pushdown and IDA results for F6B6, while P_f (or β) are 0.033 (1.838) and 0.063 (1.530) respectively for the pushdown and IDA results of F3B12. The failure probabilities with regard to the IDA are higher than those from the pushdown analyses, i.e. 151.4% and 190.9% ($P_{f,IDA}$/ $P_{f,Pushdown}$) for F6B6 and F3B12, respectively.

Based on these results, the following conclusions can be drawn. Compared to the accurate results from the entire system model, the multilevel calculation scheme performs well (both in static and dynamic cases) although a slight deviation for the failure probability is observed. Within the multilevel calculation scheme, the failure probability of the structural system is governed by $P[F_{\mathrm{DAP}}]$, which extends the conclusion by Droogné *et al.* (2018) from static analyses to situations with consideration of dynamic effects. Compared with the failure probabilities from the static pushdown analyses, the probabilities from the dynamic analyses (IDA) are significantly higher both for DAP and IAP. This indicates that it is of great importance to take into account the dynamic effects. Note that no tensile catenary action is observed for the two frames. Failure of the IAP may become more important if tensile catenary action can be developed, resulting in large membrane forces in the IAP.

Taking into account that the influence of the IAP on the occurrence of failure is limited, the static and dynamic resistances from the entire system model and equivalent model are compared with each other in Figure VII.11c,f. Although the scatter of realisations (the results of the equivalent DAP model vs. the results of the entire system evaluation) is situated along the line y=x, a significant deviation can be observed from the line y=x but concentrated in the range y=x±2.5 kN/m.

Since F3B12 has more bays in the IAP and hence can provide a stronger restriction (a larger spring constant) on the DAP, the failure probability for F3B12 is smaller than that of F6B6 in both static and dynamic situations.

VII.6.2 Robustness assessment

The obtained failure probabilities (considering ultimate strain for rebar) can be used to quantify the robustness using the conditional risk-based robustness index as defined by Eq. (VII.6). The consequences are expressed as the relative costs to the total building costs C_{tot} as follows:

$$I_{\text{Rob}} \mid \text{D,E} = \frac{C_{\text{Dir}} / C_{\text{tot}}}{C_{\text{Dir}} / C_{\text{tot}} + P\left[F_{\text{DAP}} \cap \overline{F_{\text{IAP}}}\right] C_{\text{DAP}} / C_{\text{tot}} + P\left[F_{\text{IAP}}\right] C_{\text{IAP}} / C_{\text{tot}}} \qquad \text{(VII.14)}$$

For the ratio of the direct costs to the total building costs: $C_{\text{Dir}}/C_{\text{tot}}$ =0.1% is adopted from the investigation by Droogné *et al.* (2018). The relative indirect costs associated with the failure of the DAP and IAP are on the basis of the study by Droogné *et al.* (2018) as well. The relative indirect costs are estimated based on two other studies: the work by (Faber *et al.*, 2004) on the failure of the World Trade Centre in 2001; and on the failure cost evaluation for office buildings studied by (Kanda, 1996). The values of relative failure costs, compared to the total construction cost, are summarized in Table VII.11 in the context of total collapse of the building. A 'low' scenario and a 'high' scenario are given in the referenced studies due to several uncertainties. In the following, only the 'low' scenarios are employed to calculate the robustness index. Note that the considered values are strongly case-dependent. In the 'low' scenario of Faber *et al.* (2004), the costs associated with the rescue and clean-up, structure, inventory of building, fatalities, environmental and cultural aspects, and impact to economy are considered (Table VII.11). In the 'low' scenario of Kanda (1996), only the costs regarding to structure and inventory are taken into account.

To determine the failure costs for the DAP and IAP, the relative costs in case of collapse of each part are assumed to be proportional to the total building volume according to the assumption adopted in (Droogné *et al.*, 2018). Only the cost 'impact to economy' do not need to be adjusted, assuming that all business affairs are stopped due to the large extent of the damage from the DAP or IAP. Therefore, the relative failure cost of DAP or IAP can be calculated as follows:

$$\frac{C_{\text{DAP or IAP}}}{C_{\text{tot}}} = \left(\frac{C_{\text{res\&cle}}}{C_{\text{tot}}} + \frac{C_{\text{stru}}}{C_{\text{tot}}} + \frac{C_{\text{inv}}}{C_{\text{tot}}} + \frac{C_{\text{fat}}}{C_{\text{tot}}} + \frac{C_{\text{env}}}{C_{\text{tot}}} \right) \cdot \frac{V}{V_{\text{tot}}} + \frac{C_{\text{eco}}}{C_{\text{tot}}} \qquad \text{(VII.15)}$$

where V/V_{tot} is the ratio of the collapsed building volume in case of failure of the DAP or IAP to the total building volume. Note that the volume is associated to the entire frame if the IAP fails.

Table VII.11. Relative failure costs comparing to the total building cost (Units: %) (Droogné et al., 2018).

Scenario	**Faber *et al.* (2004)**		**Kanda (1996)**	
	Low	High	Low	High
Rescue & Clean-up* $C_{\text{res\&cle}}/C_{\text{tot}}$	36.2	36.2	-	-
Structure $C_{\text{stru}}/C_{\text{tot}}$	100.0	100.0	60.0	130.0
Inventory of building $C_{\text{inv}}/C_{\text{tot}}$	55.3	55.3	10.0	200.0
Fatalities** $C_{\text{fat}}/C_{\text{tot}}$	117.0	117.0	0.0	200.0
Environmental and cultural aspects* $C_{\text{env}}/C_{\text{tot}}$	2.1	2.1	-	-
Impact to economy $C_{\text{eco}}/C_{\text{tot}}$	193.6	1408.5	0.0	50.0
Total relative failure cost	504.2	1719.1	70.0	580.0

* Not considered by Kanda (1996).

** As listed in the references. Different approaches can be followed for quantifying the cost associated with risk to human life.

Table VII.12. Risk-based robustness indices.

Case	**F6B6**		**F3B12**	
	Case 1 (Faber)	**Case 2** (Kanda)	**Case 3** (Faber)	**Case 4** (Kanda)
Pushdown	0.007	0.262	0.015	0.609
IDA	0.004	0.189	0.008	0.447
IDA/Pushdown	66.1%	72.3%	52.7%	73.4%

Considering the above, conditional risk-based robustness indices are calculated using Eqs. (VII.14) and (VII.15). A summary is presented in Table VII.12 for both frames. Compared to the results from the 'low' scenario of Faber *et al.* (Table VII.11), the robustness indices from the 'low' scenario of Kanda are much larger (Table VII.12 and Figure VII.12). Note that logarithmic axis scale is used for the vertical axis in Figure VII.12. Although only the case $C_{\text{Dir}}/C_{\text{tot}} = 0.1\%$ is studied here, a similar conclusion can be obtained for a higher assumed direct cost ratio.

However, the conditional risk-based robustness indices should be regarded relative to each other for comparing different designs, i.e. the exact value of the failure costs are considered less important under the same assumptions (Droogné *et al.*, 2018).

Figure VII.12. Conditional risk-based robustness indices for F6B6 and F3B12.

Comparing to the robustness indices calculated from pushdown results, the robustness indices from IDA are significantly smaller (Table VII.12). Moreover, the dynamic effects have an influence on both the DAP and IAP and therefore the associated failure costs. This indicates that it is of paramount importance to include dynamic effects when assessing the structural performance in the context of progressive collapse scenarios.

VII.7 Conclusions

The computationally efficient multilevel calculation scheme proposed by Droogné *et al.* (2018) was further investigated, taking into account dynamic effects. In order to investigate the performance of the multilevel calculation scheme when considering the dynamic effects, both static nonlinear pushdown analyses and dynamic analyses (IDA) were carried out for two RC frames using OpenSees. Comparing to the results from the entire system model, a good performance was found for the equivalent DAP model both for static and dynamic analyses. The equivalent DAP model was further adopted to investigate the behaviour of the DAP, while an analytical method was used to determine the resistance of the IAP. Eventually, the resistances of the DAP, membrane forces from the DAP, resistances of the IAP, failure probabilities (or reliabilities) and robustness indices from the dynamic analyses were calculated and compared with those from the static pushdown analyses. The results showed that the dynamic effects are of paramount importance when assessing the reliability or robustness of a structure subjected to

column removal scenarios. Moreover, the multilevel calculation scheme approach proved to have a good performance although the dynamic effects had great influences on both the DAP and IAP.

For the multi-storey RC frames, the average values of the stiffness from all the floors can be adopted as the boundary conditions of the equivalent DAP model and this showed an overall good performance. For instance, the maximum deviation for the resistance was only 3.8% (F3B12 - IDA) for the deterministic analyses of the two RC frames. Since the equivalent DAP model showed a good performance for both static and dynamic analyses, it can be applied to replace the entire system model in dynamic analyses. Hence, the calculation effort was significantly reduced.

A significant influence resulting from dynamic effects on the DAP was found. The force-based DAF calculated from the pushdown and IDA curves decreased from 1.78 to 1.01 (or from 1.85 to 1.01) in the case F6B6 (or F3B12). The influence at low-medium displacement levels was found to be significant. However, the DAFs for the membrane forces were observed to be always larger than 2.0 for the two cases. The nonlinear static approach was found to be highly non-conservative for progressive collapse evaluation.

It was found that the influence of dynamic effects on the resistance of the IAP was limited, since the DAF for the axial force was close to unity at the ultimate load-bearing capacity. Regarding F6B6 (or F3B12), the DAF for the axial force decreased from 1.25 to 1.03 (or from 1.27 to 1.03) when increasing the imposed loads.

An approximate failure probability was obtained using the multilevel calculation scheme method for both static and dynamic situations, and compared to more accurate results from the entire system model. This indicated that the multilevel calculation scheme still has a good performance in a dynamic situation although dynamic effects had a great influence on the behaviour of both the DAP and IAP.

The system failure probabilities in terms of the dynamic analyses (IDA) were 151.4% and 190.9% higher as those from the static analyses for F6B6 and F3B12, respectively. Moreover, compared to the results from static analyses, the conditional risk-based robustness indices from IDA were significantly smaller. Therefore, it is of great importance to include dynamic effects when assessing the performance of a structure subjected to progressive collapse.

VII.8 References

Abaqus (2014) ABAQUS user's manual. Version 6.14. ABAQUS Providence, RI.

Adam JM, Buitrago M, Bertolesi E, et al. (2020) Dynamic performance of a real-scale reinforced concrete building test under a corner-column failure scenario. Engineering Structures 210:110414.
Alshaikh IMH, Abu Bakar BH, Alwesabi EAH, et al. (2020) Experimental investigation of the progressive collapse of reinforced concrete structures: An overview. Structures 25:881-900.
Baker JW, Schubert M, Faber MH (2008) On the assessment of robustness. Structural safety 30:253-267.
Bao Y, Kunnath SK, El-Tawil S, et al. (2008) Macromodel-based simulation of progressive collapse: RC frame structures. Journal of Structural Engineering 134:1079-1091.
Brunesi E, Nascimbene R (2014) Extreme response of reinforced concrete buildings through fiber force-based finite element analysis. Engineering Structures 69:206-215.
Brunesi E, Nascimbene R, Parisi F, et al. (2015) Progressive collapse fragility of reinforced concrete framed structures through incremental dynamic analysis. Engineering Structures 104:65-79.
CEN (2002) Eurocode 1: Actions on structures-Part 1-1: General actions-Densities, self-weight, imposed loads for buildings. European Committee for Standardization Brussels. EN 1991-1-1.
CEN (2004) Eurocode 2: Design of concrete structures—Part 1-1: General rules and rules for buildings. EN 1992-1-1.
Droogné D, Botte W, Caspeele R (2018) A multilevel calculation scheme for risk-based robustness quantification of reinforced concrete frames. Engineering Structures 160:56-70.
Faber MH, Kübler O, Fontana M, et al. (2004) Failure consequences and reliability acceptance criteria for exceptional building structures: A study taking basis in the failure of the World Trade Center Twin Towers. vdf Hochschulverlag AG.
Feng D, Wang Z, Wu G (2019a) Progressive collapse performance analysis of precast reinforced concrete structures. Structural Design of Tall and Special Buildings 28:e1588.
Feng D, Xie S, Deng W, et al. (2019b) Probabilistic failure analysis of reinforced concrete beam-column sub-assemblage under column removal scenario. Engineering Failure Analysis 100:381-392.
Feng D, Xie S, Xu J, et al. (2020) Robustness quantification of reinforced concrete structures subjected to progressive collapse via the probability density evolution method. Engineering Structures 202:109877.
fib (2013) Model code for concrete structures 2010.
Holický M, Sýkora M (2010) Stochastic models in analysis of structural reliability. The international symposium on stochastic models in reliability engineering, life sciences and operation management.

Izzuddin BA, Pereira MF, Kuhlmann U, et al. (2012) Application of probabilistic robustness framework: risk assessment of multi-storey buildings under extreme loading. Structural Engineering International 22:85-79.
Izzuddin BA, Vlassis AG, Elghazouli AY, et al. (2008) Progressive collapse of multi-storey buildings due to sudden column loss - Part I: Simplified assessment framework. Engineering Structures 30:1308-1318.
JCSS (2001) Probabilistic model code. Joint Committee on Structural Safety.
Jovanović B, Van Coile R, Hopkin D, et al. (2020) Review of current practice in probabilistic structural fire engineering: permanent and live load modelling. Fire Technology 57:1-30.
Kanda J (1996) Normalized failure cost as a measure of a structure importance. Nuclear engineering and design 160:299-305.
Kolay C, Ricles JM (2014) Development of a family of unconditionally stable explicit direct integration algorithms with controllable numerical energy dissipation. Earthquake engineering & structural dynamics 43:1361-1380.
Kolay C, Ricles JM (2016) Assessment of explicit and semi‐explicit classes of model‐based algorithms for direct integration in structural dynamics. International Journal for Numerical Methods in Engineering 107:49-73.
Li Y, Lu XZ, Guan H, et al. (2014) Progressive collapse resistance demand of reinforced concrete frames under catenary mechanism. ACI Structural Journal 111:1225-1234.
Mander JB, Priestley MJN, Park R (1988) Theoretical stress-strain model for confined concrete. Journal of Structural Engineering 114:1804-1826.
Mazzoni S, McKenna F, Scott MH, et al. (2006) OpenSees command language manual. Berkeley, California, United States.
Monti G, Petrone F (2015) Yield and ultimate moment and curvature closed-form equations for reinforced concrete sections. ACI Structural Journal 112:463.
OpenSees (2006) Open system for earthquake engineering simulation. University of California, Berkeley.
Stevens NJ, Uzumeri SM, Will GT (1991) Constitutive model for reinforced concrete finite element analysis. Structural Journal 88:49-59.
Tsai M-H (2012) A performance-based design approach for retrofitting regular building frames with steel braces against sudden column loss. Journal of Constructional Steel Research 77:1-11.
Tsai MH, Lin BH (2008) Investigation of progressive collapse resistance and inelastic response for an earthquake-resistant RC building subjected to column failure. Engineering Structures 30:3619-3628.
Wu JY, Li J, Faria R (2006) An energy release rate-based plastic-damage model for concrete. International Journal of Solids and Structures 43:583-612.

PART D

PROGRESSIVE COLLAPSE BEHAVIOUR OF EXISTING STRUCTURES

CHAPTER VIII

Progressive collapse behaviour of RC frames subjected to simulated reinforcement corrosion

VIII.1 Introduction

Civil engineering structures are also prone to ageing and deterioration processes from aggressive chemical attacks (Biondini and Vergani, 2014; Biondini and Frangopol, 2017; Cavaco *et al.*, 2018; Vereecken *et al.*, 2020a; Vereecken *et al.*, 2021). For instance, RC buildings may suffer from carbonation of the concrete cover and penetration of chloride ions, which may significantly reduce the performance of the structures. Consequently, the life-cycle performance assessment may become very important, but very limited information is available in literature with respect to its quantification in relation to membrane action effects and structural robustness (Botte *et al.*, 2016; Botte *et al.*, 2021). Botte *et al.* (2016) numerically investigated the influence of corrosion effects on the tensile membrane behaviour of RC slabs subjected to middle support removal scenarios. A significant influence on the ultimate load-bearing capacity of the slab was observed, even for a small corrosion level. Yu *et al.* (2017) studied the progressive collapse behaviour of ageing reinforced concrete structures subjected to middle column removal scenarios. The ageing structures with severe corrosion were observed to be much more vulnerable to progressive collapse than newly constructed ones. The ultimate deformation capacity was reduced by over 40% after 50 years of corrosion, while the ultimate load-bearing capacity was reduced almost by 20%-30%. Feng *et al.* (2021) numerically studied the time-dependent reliability and redundancy of a RC frame subjected to progressive collapse. Du *et al.* (2005a) indicated that corrosion in reinforcement used in structures subjected mainly to dynamic loads, e.g. in seismic zones, can significantly decrease their ductility and robustness, because the ultimate strain and elongation of bars are reduced. Hence, deterioration can significantly affect the progressive collapse resistance of RC structures.

The shear behaviour of both short (Vu and Li, 2018a) and slender (or flexural) (Vu and Li, 2018b) RC columns subjected to accelerated reinforcement corrosion has also been investigated in literature. The influence of the corrosion level of reinforcement in combination with the applied axial force ratio was investigated in these articles. The results showed that a significant reduction of shear capacity was observed due to the corrosion effects. The influence of stirrup corrosion on the shear strength of RC beams was investigated as well in (Ou and Chen, 2014; El-Sayed *et al.*, 2016), encompassing among others nine full-scale RC beams subjected to accelerated stirrup corrosion. Both the corrosion damage level and the spacing of stirrups were studied. The results of the four-point bending tests indicated that the corroded beams exhibited a reduced shear strength in comparison to the uncorroded beams.

Taking into account the above background, this chapter aims at numerically investigating the progressive collapse performance of deteriorated RC frame structures subjected to uniform reinforcement corrosion. The influence of different corrosion locations, different column removal scenarios as well as dynamic effects

are studied. The remaining parts of this chapter are arranged as follows: first, the implemented deterioration models for both reinforcement and concrete are presented in section VIII.2. Subsequently, an example RC frame is described in section VIII.3. Static pushdown analyses are performed to investigate the influence of different deterioration models (section VIII.4), different deterioration locations in the RC frame (section VIII.5), and different column removal scenarios (section VIII.6). Further, the influence of dynamic effects on the progressive collapse behaviour of the deteriorated RC frame is further studied in section VIII.7. Finally, conclusions are addressed in section VIII.8.

VIII.2 Corrosion modelling

The process of corrosion in RC buildings includes an initiation phase and a propagation phase (Botte *et al.*, 2016; Biondini and Frangopol, 2017; Yu *et al.*, 2017). The reinforcement becomes depassivated due to the ingress of chlorides or carbonation in the initiation phase. In the propagation phase the actual cross-sectional area of the reinforcements is reduced and the volume of the bars starts to expand due to the accumulation of corrosion products. Currently, only the propagation phase is considered in this chapter, as the duration of the initiation phase and the end of service life determination is not within the objectives of the investigations in this chapter. In general, damage modelling includes the following aspects (Biondini and Vergani, 2014; Botte *et al.*, 2016; Yu *et al.*, 2017):

- reduction of cross-sectional area of the corroded reinforcement;
- reduction of mechanical properties of the reinforcement;
- deterioration of concrete due to cracking and spalling (expansion of corrosion products); and
- reduction of bond behaviour between the reinforcing bars and the surrounding concrete. The reduction of bond behaviour is not taken into account in the present work and can be the subject of future further investigations.

VIII.2.1 Effect of corrosion on cross-sectional area of reinforcing steel

The reduction of the cross-sectional area of reinforcing bars is one of the most relevant effects of corrosion (Cairns *et al.*, 2005; Cavaco *et al.*, 2018). The corrosion mechanism can relate to uniform corrosion, pitting corrosion, or a mix of uniform and pitting corrosions, where the first two types are more suitable to represent a real case (Biondini and Vergani, 2014). Generally, the carbonation of the concrete cover (or the case of a low to moderate degree of chloride ingress) may produce uniform corrosion, while pitting corrosion is mainly developed in the presence of chloride ions (Du *et al.*, 2005a). In the following uniform corrosion is considered to investigate the progressive collapse behaviour of deteriorated RC

frames. However, the analysis could be also extended to take into account pitting corrosion, i.e. by incorporation of a pitting factor (Biondini and Vergani, 2014).

The average loss of cross-sectional area in case of uniform corrosion can be calculated if the corrosion penetration depth x is known, see Figure VIII.1. The original radius of the reinforcing bar is R_i, while the effective radius after corrosion is $R_{eff} = R_i - x$. Consequently, the percentage of cross-sectional area loss α (or corrosion level) can be calculated as follows:

$$\alpha = \frac{\Delta A_s}{A_s} \times 100\% \qquad \text{(VIII.1)}$$

where ΔA_s is the area reduction due to corrosion, and A_s is the nominal area of the non-corroded bar.

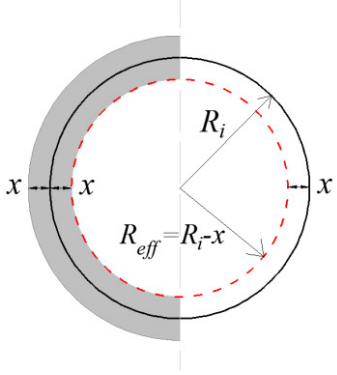

Figure VIII.1. Modelling of cross-section reduction of a corroded bar (Botte *et al.*, 2016).

An empirical model can be adopted to determine the time-dependent corrosion penetration depth x (Stewart and Suo, 2009). First the corrosion rate i_{corr} is calculated by:

$$i_{corr}(t) = 0.85 \cdot i_{corr}(0) \cdot t^{-0.29} \qquad \text{(VIII.2)}$$

$$i_{corr}(0) = \frac{2.7(1 - w/c)^{-1.64}}{d_c} \qquad \text{(VIII.3)}$$

where $i_{corr}(t)$ [$\mu A/cm^2$] is the corrosion rate at time t [year] since corrosion initiation; $i_{corr}(0)$ is the corrosion rate at the start of corrosion propagation; w/c is the water cement ratio; and d_c [cm] is the concrete cover. Consequently, the corrosion penetration depth x [mm] can be calculated using Eq. (VIII.4) as an integral of the corrosion rate:

$$x(t_n) = 0.0116 \int_0^{t_n} i_{corr}(t)dt \quad \text{(VIII.4)}$$

where 0.0116 is the unit conversion factor since 1 μA/cm^2 = 0.0116 mm/year.

VIII.2.2 Effect of corrosion on mechanical properties of reinforcing steel

The influence of corrosion on the strength of reinforcement steel, i.e. the yield stress and the ultimate strength, has been studied by many researchers (Almusallam, 2001; Cairns *et al.*, 2005; Du *et al.*, 2005b; Du *et al.*, 2005a; Apostolopoulos and Papadakis, 2008; Zhu and François, 2013; Yu *et al.*, 2017). However, contradictory conclusions were drawn. For example, Almusallam (2001) found that the tensile strength of steel bars was not influenced by the level of reinforcement corrosion when the actual (reduced) area of cross-section was adopted. Nonetheless, the tensile strength was significant reduced when the nominal diameter of the bars was utilized. Du *et al.* (2005b) found the residual strength of corroded reinforcement reduced significantly. A relatively modest strength loss of bars subjected to local or pitting corrosion was observed according to the results from accelerated corrosion tests (Cairns *et al.*, 2005; Apostolopoulos and Papadakis, 2008). Contrarily, both the effective yield stress and effective ultimate strength for reinforcements subjected to pitting corrosion were observed to be improved, according to the test results by Zhu and François (2013). Considering the above, the reduction of cross-section area (i.e. actual area of the corroded rebar) can be used to simulate the reduction of the capacity of the corroded rebar, and no reduction of the yield stress and the ultimate strength is considered in the current work.

Almost all experimental studies explicitly showed that corrosion may result in significant reduction of the ductility of reinforcement steel, especially with the presence of pitting attack (Coronelli and Gambarova, 2004; Yu *et al.*, 2015; Botte *et al.*, 2016). This is mainly due to the spatial variability of the attack penetration. Apostolopoulos and Papadakis (2008) found that the steel ductility significantly decreased for reinforcing steel subjected to accelerated corrosion, as well as for reinforcement bars embedded in real structures and exposed in natural corrosion for years. Moreover, they also reported that ductility reduction is a function of the cross-section loss, and an exponential reduction of the elongation to failure against the mass loss was observed. The study by Cairns et al. (2005) showed that the reduction in ductility is significant, where a bar with 8% cross-section reduction resulted in approximate 20% loss of its ductility. The significant reduction of the steel ductility was also reported by Almusallam (2001) and moreover the corrosion of reinforcing steel was found to increase its brittleness. Based on fitting of

available experimental data, different mathematical models for the ductility loss have been developed such as the following models:

1) Model 1: an exponential decrease of the ductility is considered as follows (Zhu and François, 2013; Yu *et al.*, 2015):

$$\frac{\varepsilon_{su,c}}{\varepsilon_{su}} = \mathrm{e}^{-0.1\alpha\%} \qquad \alpha \le 0.16 \tag{VIII.5}$$

$$\frac{\varepsilon_{su,c}}{\varepsilon_{su}} = 0.2 \qquad \alpha > 0.16 \tag{VIII.6}$$

where ε_{su} is the ultimate strain of the non-corroded reinforcement; $\varepsilon_{su,c}$ is the ultimate strain of the corroded reinforcement; and α is the percentage of steel cross-section loss (section VIII.2).

2) Model 2: a simple linear reduction model has been proposed by Coronelli and Gambarova (2004):

$$\frac{\varepsilon_{su,c}}{\varepsilon_{su}} = \frac{\varepsilon_{sy}}{\varepsilon_{su}} + \left(1 - \frac{\varepsilon_{sy}}{\varepsilon_{su}}\right)\left(1 - \frac{\alpha}{\alpha_{\max}}\right) \tag{VIII.7}$$

where ε_{sy} is the yield strain of the non-corroded reinforcement; and $\alpha_{\max}$ is the percentage of steel cross-sectional area loss with complete loss of ductility ($\varepsilon_{su,c} = \varepsilon_{sy}$). Therefore, the parameter $\alpha_{\max}$ is critical for the description of the linear reduction of bar ductility. Different values of $\alpha_{\max}$ have been found based on fitting different experimental results and a large variation from 0.1 to 0.5 for the value has been reported. According to the experimental results of Castel et al. (2000), a value of $\alpha_{\max} = 0.1$ is adopted for Model 2.

3) Model 3: Eq. (VIII.7) is applied to Model 3 as well, but with another value of $\alpha_{\max} = 0.5$. This value is according to the experimental results of Cairns and Millard (1999).

4) Model 4: the loss of steel ductility is expressed as an exponential reduction model (Biondini and Vergani, 2014; Feng *et al.*, 2021):

$$\varepsilon_{su,\mathrm{c}} = \begin{cases} \varepsilon_{su}, & 0 \le \alpha < 0.016 \\ 0.1521\alpha^{-0.4583}\varepsilon_{su}, & 0.016 \le \alpha \le 1 \end{cases} \tag{VIII.8}$$

VIII.2.3 Effect of corrosion on concrete properties

With increasing reinforcement corrosion level, considerable internal pressure can develop due to the formation of corrosion products (i.e. iron oxides) along the surface of reinforcing bars and this may lead to cracking and spalling of the concrete cover. The mechanical properties of both the cover concrete and the core concrete may be affected (Coronelli and Gambarova, 2004; Feng *et al.*, 2021). Regarding the cover concrete, the effect of cracking and spalling is considered by reducing the compressive strength of the concrete (Coronelli and Gambarova, 2004; Biondini and Vergani, 2014). The reduced concrete strength f_c^* is expressed as follows:

$$f_c^* = \frac{f_c}{1+\kappa(\varepsilon_{cr}/\varepsilon_{c1})} \tag{VIII.9}$$

where f_c is the concrete peak compressive strength with no reduction; κ is a coefficient related to bar roughness and diameter, where a value of 0.1 has been adopted for medium-diameter ribbed bars (Coronelli and Gambarova, 2004; Vereecken *et al.*, 2020b); ε_{c1} is the concrete peak strain; and ε_{cr} is the average (smeared) tensile strain in the cracked concrete and is calculated by (Coronelli and Gambarova, 2004):

$$\varepsilon_{cr} = n_{\text{bar}}\omega_{cr}/b_0 \tag{VIII.10}$$

$$\omega_{cr} = 2\pi(\gamma_{rs}-1)\cdot x \tag{VIII.11}$$

where b_0 is the initial section width (no corrosion cracks); n_{bar} is the number of the bars under compression; ω_{cr} is the total crack width for a given corrosion level; γ_{rs} is the ratio of volumetric expansion due to corrosion products (Figure VIII.1), which is set as 2 based on the assumption that all corrosion products accumulate around the corroded bar and are incompressible (Cairns *et al.*, 2005; Yu *et al.*, 2017); and x is the corrosion penetration depth.

In terms of the core concrete, the strength and ductility may decrease as well, since the confinement effect provided by the transverse bars decreases due to the corrosion. When updating the reduced properties of the core concrete, the reduced cross-sectional area of the corroded transverse bar is adopted. The modified Kent-Park model (Park *et al.*, 1982; Scott *et al.*, 1982) can be adopted to calculate the strength of the core concrete:

$$K = 1+\frac{\rho_{st}f_{yt}}{f_c} \tag{VIII.12}$$

$$f_{c,cor} = Kf_c \tag{VIII.13}$$

$$\varepsilon_{c,cor} = K\varepsilon_{c1} \quad \text{(VIII.14)}$$

where K is the confinement ratio; ρ_{st} is the volume ratio of corroded transverse reinforcement; f_{yt} is the yield stress of corroded transverse reinforcement; and $\varepsilon_{c,cor}$ is the peak strain corresponding to the confined core concrete strength $f_{c,cor}$.

VIII.3 Description and numerical modelling of an RC frame model

The RC frame presented in sections IV.4 (see Figure IV.16) is also adopted in this chapter to investigate the progressive collapse behaviour of RC frames subjected to simulated reinforcing corrosion. The 5-storey and 4-bay RC frame (Figure IV.16a) includes one first storey with the height of 4.5 m, while the height for the other four stories is 3.6 m each. The dimensions of the beams and the columns are 250 mm × 500 mm and 500 mm × 500 mm, respectively. The concrete cover is 30 mm in all elements. Concrete of type C20/25 (CEN, 2004) is used, i.e. the characteristic cylinder compressive strength is f_{ck} = 20 MPa, while the mean compressive strength of concrete is assumed to be $f_{cm} = f_{ck} + 8$ = 28 MPa and the mean tensile strength is $f_{ctm} = 0.3\ (f_{ck})^{2/3}$ = 2.2 MPa (fib, 2013). The aforementioned modified Kent-Park model is used to calculate the confinement effect on the core concrete (see section VIII.2.3). The characteristic yield stress and tensile strength of reinforcing steel are f_{yk} = 500 MPa and f_{uk} = 575 MPa (ductility class C), respectively (CEN, 2004). The mean yield stress of steel is assumed to be $f_{ym} = f_{yk} + 2\sigma_1$ = 560 MPa, where σ_1 = 30 MPa is the standard deviation (JCSS, 2001). The mean tensile strength is assumed to be $f_{um} = f_{uk} + 2\sigma_2$ = 655 MPa, where σ_2 = 40 MPa is the standard deviation (JCSS, 2001). The mechanical properties of both the concrete and the reinforcing steel are summarized in Table IV.3. The OpenSees FE model developed in sections IV.4 is used in this chapter as well. The RC frame subjected to the middle column removal scenario is shown in Figure VIII.2a. The column lines are labelled as A, B, C, D and E from left to right (Figure VIII.2a).

VIII.4 Influence of material deterioration

VIII.4.1 Corrosion of reinforcement

Figure VIII.2b shows the relationships of steel ultimate strain against corrosion level (from α = 0 to 60%) with regard to the four different models (see section VIII.2.2). Model 1 and Model 4 both show an exponential decrease and the difference between these two models is not too significant. The curve for Model 4 is more smooth, while the curve for Model 1 first decreases and then keeps constant after α = 16% (with $\varepsilon_{su,c}$ = 2.4%). Model 2 and Model 3 both show a linear decrease before the yield strain ε_{sy} is reached, i.e. until complete loss of steel ductility. The ultimate strain calculated by Model 2 decreases much faster than Model 3, since different parameters of $\alpha_{\max}$ = 0.1 (Model 2) and 0.5 (Model 3) are adopted.

Namely, the ultimate strain obtained by Model 2 decreases faster to the yield strain from α = 0 to 10%, while that from Model 3 linearly decreases to the yield strain from α = 0% to 50% with a much slower rate. Among all the four models, Model 2 almost always results in the smallest value of the reduced ultimate strain, while that for Model 3 is initially the largest but becomes smaller than Models 1 and 4 after α = 40%.

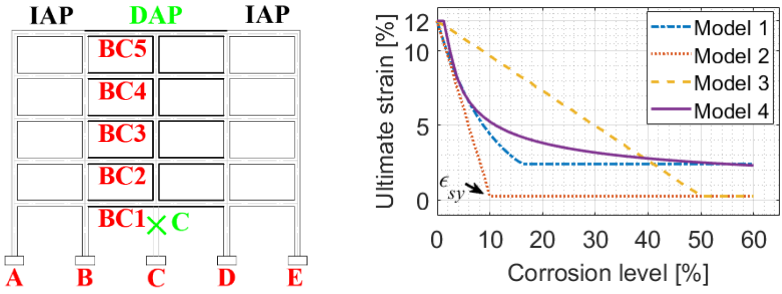

(a) (b)

Figure VIII.2. (a) Removal of the ground column C; and (b) steel ultimate strain vs. corrosion level α.

The four models are subsequently adopted to perform nonlinear static pushdown analyses, considering the RC frame subjected to the ground middle column C removal, see Figure VIII.2a. As a first step in the assessment of the influence of corrosion, it is assumed that all the beams and columns are exposed on four sides and all the reinforcements both in beams and column are subjected to uniform corrosion. Note that all the reinforcement is assumed to be subjected to the same corrosion level at a certain moment and no pitting corrosion is considered, i.e. a general influence of the corrosion degradation is investigated rather than localized (spatially variable) degradation phenomena. In the static pushdown analyses, uniformly distributed vertical loads are gradually increased in the entire structural system. A displacement-controlled analysis is carried out, where the displacement at the top of the removed column is controlled. The displacement at the control point is recorded, which results in the pushdown curves in Figure VIII.3. It can be observed that the maximum loads decrease with increasing corrosion level. This is as expected because a larger reduction of the reinforcement cross-sectional area is obtained under a higher corrosion level.

Figure VIII.3a shows the load-displacement curves (pushdown curves) for Model 1 under different corrosion levels α. The failure becomes more brittle with increasing corrosion level. The ultimate displacement corresponding to the ultimate load-bearing capacity first decreases significantly for corrosion levels up to α =

20% and then varies less significantly for higher corrosion levels. This is a direct result of the fact that the steel ultimate strain in Model 1 decreases significantly from α = 0% to 16% and then keeps constant (Figure VIII.2b). It is worth emphasizing that different failure modes may be observed with different corrosion levels. In general, the first failure in a system is important, as it can be considered as the onset of failure. The progressive collapse analysis beyond the first failure after column removal, is outside of the scope of investigations in this chapter. The first failure occurs at the left beam end in BC1 (Figure VIII.2a) due to concrete crushing when $\alpha \leq 10\%$. However, the first failure occurs at the left beam end in BC2 when α = 15% and 20%. When $\alpha > 30\%$, the beam ends of BC1 - BC5 fail (either concrete crushing or reinforcement rupture) almost simultaneously. The change of the failure modes may result from the load redistribution mechanism due to the Vierendeel action in the frame.

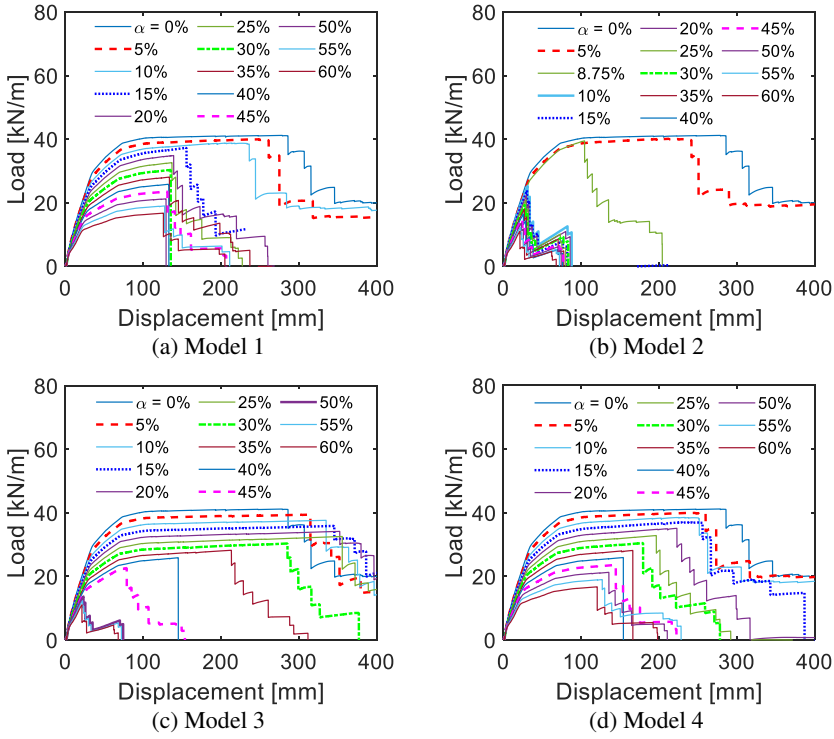

Figure VIII.3. Load-displacement relationships with different corrosion levels: (a) Model 1; (b) Model 2; (c) Model 3; and (d) Model 4.

Figure VIII.3b,c shows the load-displacement curves for Models 2 and 3, respectively. It can be observed that in case of Model 2, both the ultimate load-

bearing capacity and the corresponding displacement decreases significantly from $\alpha \geq 10\%$ onwards. This phenomenon is also found in case of Model 3 but after $\alpha \geq 50\%$. This can be explained as the reinforcement bars completely lose their ductility at $\alpha = 10\%$ and 50% respectively for Model 2 and Model 3, i.e. corresponding to the associated parameters α_{max} (Figure VIII.2b). The failure modes change with increasing corrosion level, i.e. the first failure location changes between different floors and at different beam ends of the bays immediately above the removed column (the change of failure mode was also observed for Model 1). However, the ultimate displacement (at first failure) is observed to significantly increase in case of Model 3 before $\alpha = 30\%$ (Figure VIII.3c), although the steel ultimate strain keeps on reducing. This may be due to the fact that the less reduction of the ultimate strain can still provide enough ductility (Figure VIII.2b).

Figure VIII.3d shows the load-displacement curves in case of Model 4. In general, both the ultimate load-bearing capacity corresponding to first failure and the corresponding displacement decrease with increasing corrosion level. Different failure modes (varying among the beam ends of BC1 – BC5) are observed under different corrosion levels. First failure always occurs in the bays directly above the removed column but varies at different beam ends (i.e. beam ends in different floors).

The ultimate load-bearing capacities (corresponding to first failure), obtained from the results in Figure VIII.3, against the corrosion levels are collected and presented in Figure VIII.4a. It is seen that almost identical results are obtained between Model 1 and Model 4, although the ultimate displacements and the failure modes may be different (Figure VIII.3). A sudden drop is observed at $\alpha = 10\%$ for Model 2, as the reduced ultimate strain of reinforcing steel reaches the yield strain of the steel at $\alpha = 10\%$. The curve for Model 3 is first almost identical to that of Model 1 and Model 4 and then an accelerated decrease is observed after $\alpha = 40\%$. Further, the curve becomes identical to Model 2 after $\alpha = 50\%$, since the steel ultimate strains of both Models 3 and 2 decease to the yield strain. Comparing the results from Models 2 and 3 to those from models 1 and 4, it can be observed that the load-bearing capacities will be much lower (or the results will be more conservative) if the yield strain of the reinforcing steel is reached (Figure VIII.4a).

The different models considered, result in different responses and failure modes, which emphasize the importance of adopting a proper model. It is difficult to say which model is more realistic and further experimental validations are required. Based on the previous results, the Models 2 and 3 may provide a too conservative estimation as no reinforcement ductility is left (i.e. $\varepsilon_{su,c} = \varepsilon_{sy}$), while this is not observed in Models 1 and 4. Excluding the extreme situation in which

reinforcement ductility is compeletely lost, Models 1 or 4 are adopted for illustration purpose in the following calculations.

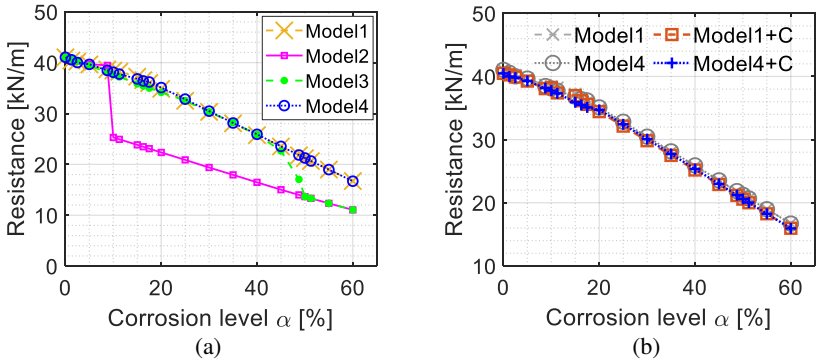

Figure VIII.4. Resistance vs. corrosion level: (a) only corrosion in reinforcement; and (b) corrosion including also the influence of deteriorated concrete.

VIII.4.2 Deterioration of concrete

Based on the model introduced in section VIII.2.3, the phenomenon of cracking and spalling in the compressed concrete is simulated by reducing its compressive strength in the cover concrete, while the confinement effect on the core concrete is determined by using the modified Kent-Park model (see section VIII.2.3) with the properties of the corroded transverse bars.

Again, the frame is assumed to be subjected to the loss of the ground middle column C (Figure VIII.2a) and pushdown analyses (identical to that in section VIII.4.1) are carried out. Model 1 and Model 4 (as discussed before) in relation to the steel ultimate strain are investigated. The obtained results of resistance against corrosion level are presented in Figure VIII.4b (designated as 'Model X + C'). The same tendency is observed compared to the corresponding response without considering the deterioration of concrete (see Figure VIII.4a). In both cases, it is clear that the effect of deterioration of concrete on the progressive collapse performance is very limited, i.e. resulting in only a slight reduction of the load-bearing capacity. This indicates that reinforcement corrosion is the predominant cause of the deterioration of the RC structural progressive collapse performance. Considering the above and the observations in section VIII.4.1, only the Model 4 for the steel ultimate strain is adopted in all the analyses in the remaining part of this chapter. Moreover, considering its limited influence observed in section VIII.4.2, the deterioration of concrete is not further taken into account.

VIII.5 Influence of corrosion at different locations

VIII.5.1 Corrosion in DAP and/or IAP

When the RC frame is subjected to the loss of ground column C (Figure VIII.2a), the bays immediately above the removed column can be regarded as the directly affected part (DAP), while the remaining part is the indirectly affected part (IAP) (Droogné *et al.*, 2018). The DAP will be the most affected part in the context of progressive collapse since large deformations are expected to occur there. Considering that corrosion may occur at specific locations in the frame, the (generalized) influence of having corrosion at different locations is investigated. In order to do so, the same column loss situation as that in section VIII.4 is considered, i.e. the removal of ground column C (Figure VIII.2a), and the static pushdown analysis is performed.

The first case which is considered is one in which all the beams from the first to fifth floors (designated as 'Beam-12345') are subjected to reinforcement corrosion. The curves of resistance against corrosion level are presented in Figure VIII.5. Note that the curve designated as 'entire' corresponds to the situation where the entire system, i.e. the reinforcement in all beams and columns, is subjected to corrosion as discussed in section VIII.4.1 (Figure VIII.4a). It is found that the curve 'Beam: 12345' is identical to the curve 'entire', which means corrosion in the beams completely governs the reduction of structural load-bearing capacity with increasing corrosion level.

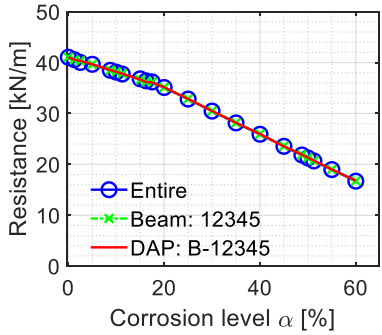

Figure VIII.5. Resistance vs. corrosion level with corrosion in beams and/or in columns.

Next, a situation is considered in which only the beams from the first to fifth floors in the DAP are subjected to reinforcement corrosion only (case designated as 'DAP: B-12345'). Hence, for this case no reinforcement corrosion is considered in the other beams in the IAP. Again, the curve 'DAP: B-12345' is almost identical

to the curves 'entire' and 'Beam-12345' (Figure VIII.5). This indicates that the load-bearing capacity for the RC frame subjected to reinforcement corrosion is determined by the capacities of the beams in the DAP for the particular case under investigation.

RC beams subjected to severe transverse reinforcement corrosion may encounter shear failures (Ou and Chen, 2014; El-Sayed *et al.*, 2016). As this cannot be automatically detected in the current FE model, the shear capacity of the beams is therefore checked separately. The following equations recommended in Eurocode (CEN, 2004) are adopted to calculate the shear capacity of RC beams subjected to stirrup corrosion:

$$V = V_c + V_s \tag{VIII.15}$$

$$V_c = \max\left[\left(C_c k(100\rho_l f_c)^{1/3} + k_1\sigma_{cp}\right)b_w d, \left(v_{\min} + k_1\sigma_{cp}\right)b_w d\right] \tag{VIII.16}$$

$$V_s = \min\left[\frac{A_{sw}}{s} z f_{yw} \cot\theta, \alpha_{cw} b_w z \nu_1 f_c / \left(\cot\theta + \tan\theta\right)\right] \tag{VIII.17}$$

where V is the shear capacity; V_c is the concrete contribution to the shear strength of the beam; V_s is stirrup contribution to the shear strength of the beam; C_c is a factor with a recommended value is 0.18; $k = 1 + \sqrt{200/d} \leq 2$; d is the effective depth; $\rho_l = A_{sl}/(b_w d) \leq 0.02$; A_{sl} is the area of the tensile reinforcement; b_w is the smallest width of the cross-section in the tensile area; f_c is concrete compressive strength; k_1 is a factor with a recommended value of 0.15; $\nu_{\min} = 0.035k^{3/2}f_c^{1/2}$; $\sigma_{cp} = N_E/A_c < 0.2f_c$; N_E is the axial force in the cross-section due to loading and a positive value for compression; A_c is the area of concrere cross section; A_{sw} is the cross-sectional area of the shear reinforcement; s is the spacing of the stirrups; f_{yw} is the yield stress of the shear reinforcement; $\nu_1 = 0.6(1 - f_c/250)$ is a strength reduction factor for concrete crack in shear; α_{cw} is a coefficient taking account of the state of the stress in the compression chord; $z = 0.9d$ is the inner lever arm; θ is the angle between the concrete compression strut and the beam axis perpendicular to the shear force, where cot θ = 1 is adopted (the recommended limits are $1 \leq \cot\theta \leq 2.5$).

The maximum shear forces in all the beams are compared to the shear capacity calculated according to the above equations. When corrosion level α = 0%, the maximum shear forces in the beams (from the first to the fifth floor) between column lines A and B (designated as 'Beams A-B', see Figure VIII.2a) are presented in Figure VIII.6a, as well as for the shear forces in the beams between column lines B and C (designated as 'Beams B-C'). Comparing to the shear capacity, the maximum shear forces are significant smaller. This indicates no shear

failures occur in the beams. Shear failure does not occur at corrosion level $\alpha = 60\%$ either (Figure VIII.6b). Note that the shear forces in case of $\alpha = 60\%$ are smaller than those in case of $\alpha = 0\%$, as the shear forces are related to situation corresponding to first failure (a lower ultimate load-carrying capacity in case of a higher corrosion level).

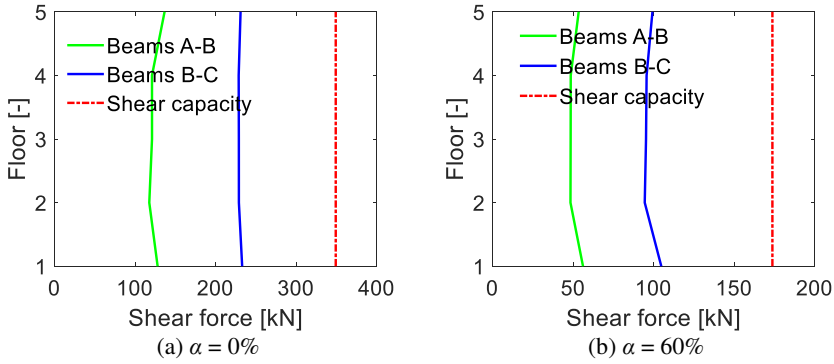

Figure VIII.6. Comparison between shear capacity and shear forces in beams (a) at corrosion level 0%; and (b) at corrosion level 60%.

RC columns subjected to severe transverse reinforcement corrosion may also encounter shear failures (Vu and Li, 2018a; Vu and Li, 2018b; Xu *et al.*, 2020). The shear capacities for the columns are also calculated. Based on the above equations in relation to the shear strength of RC cross sections, the shear capacities of the columns (Figure VIII.2a) can be calculated. Note that the shear capacity obtained by these formula is related to the applied axial force in the column, as shown in Eq. (VIII.16). Hence, the shear capacity in a column is a function of its axial load. First, the shear capacities of the entire system subjected to reinforcement corrosion is checked. The shear forces in the ground columns (columns A and B in the first floor) against the imposed loads (lager imposed loads result in larger axial forces) on the beams are presented in Figure VIII.7a when $\alpha = 60\%$. It is observed that the shear force is significantly lower than the shear capacities. Figure VIII.7b shows the maximum shear capacities and the corresponding maximum shear forces at different corrosion levels (e.g. Figure VIII.7a when $\alpha = 60\%$). The shear capacities remain larger than the shear forces for all cases considered. Both shear forces and shear capacities decrease with increasing corrosion level. It is observed that the shear forces decrease with increasing corrosion level, which is because of the reduced load-bearing capacity of the RC frame at a higher corrosion level (see Figure VIII.5). On the other hand, the reduced load-bearing capacity results in less axial forces in the columns, which results in less shear capacity of the columns (VIII.16). Moreover, the reduced rebar area also results in a smaller shear capacity.

No shear failures occur in the columns, as the beams fail earlier. This also demonstrates that the beams remain the most critical elements in the progressive collapse situation under investigation. This is in line with the study by Yu *et al.* (2017) in which only the corrosion effects in all the beams of the RC frame were taken into account in the context of progressive collapse.

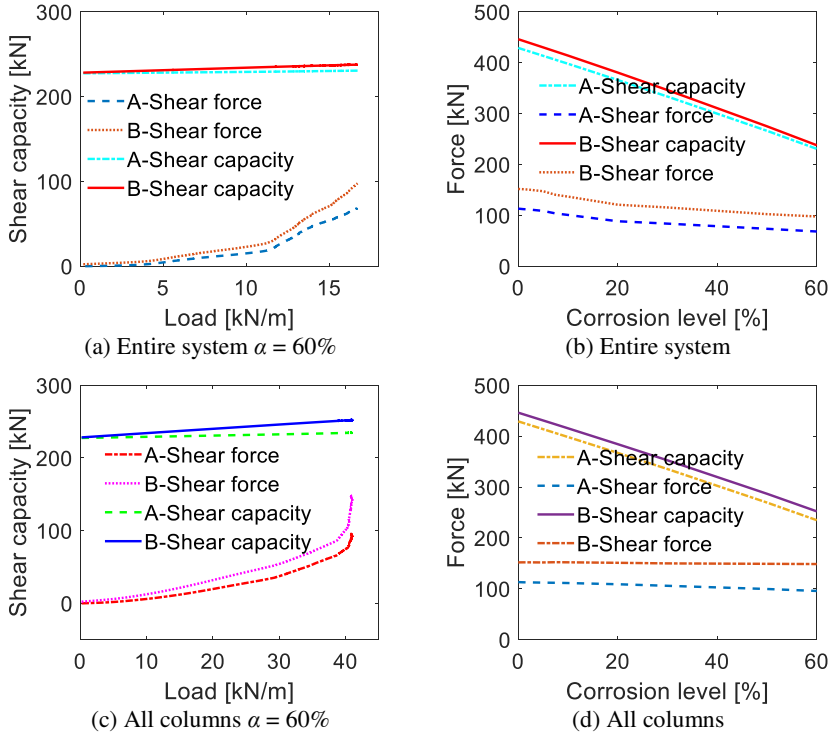

(a) Entire system α = 60% (b) Entire system

(c) All columns α = 60% (d) All columns

Figure VIII.7. Comparison of shear capacity and shear force in columns: (a) shear capacity vs. load (on beams); (b) shear capacity vs. shear force at different corrosion levels; (c) shear capacity vs. load; and (d) shear capacity vs. shear force at different corrosion levels.

Although no shear failures occur in the columns for the situation under investigation, the verification should always be performed, especially in case of severe deterioration. For example, shear failure was observed in one of the eight columns in an experimental test by (Vu and Li, 2018a), in which the column with shear failure was subjected to a transverse reinforcement corrosion level of 51.2% and a high axial load level. Hence, one more case is investigated, in which only the columns are subjected to reinforcement corrosion (no reinforcement corrosion in the beams). The results of the shear forces/shear capacities (in ground columns A and B) against the imposed loads on the beams are shown in Figure VIII.7c at the

corrosion level $\alpha = 60\%$. Although the shear capacities are still larger than the shear forces, less strength reserve is observed comparing to the former case (Figure VIII.7a). Further, also the shear capacities/shear forces in columns A and B at different corrosion levels are presented in Figure VIII.7d. The shear capacities decrease much faster than the shear forces in this case. If the corrosion level is further increased, shear failures are likely to occur in the columns before failure in the beams is triggered. For the remaining of this chapter, the shear failure for other cases have been checked in a similar way and no shear failures appears to occur. The shear failure criterion is hence not further discussed, but remains an important item of consideration in further investigations.

VIII.5.2 Corrosion in different floors of the DAP

In this section, four more cases with regard to different numbers of floor in the DAP subjected to reinforcement corrosion are investigated: only the beams in the first floor ('DAP: B-1'), in the first two floors ('DAP: B-12'), in the first three floors ('DAP: B-123'), in the first four floors ('DAP: B-1234'), and in all five floors (same to 'DAP: B-12345' in Figure VIII.5). The obtained resistance vs. corrosion level curves are presented in Figure VIII.8. It shows that the cases with more floors subjected to corrosion result in lower load-bearing capacities.

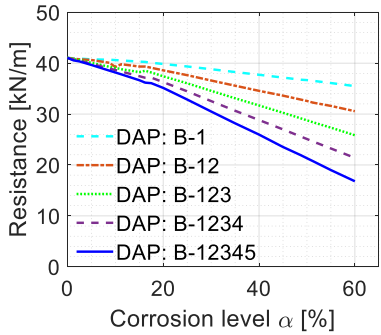

Figure VIII.8. Resistance vs. corrosion level when different floors of the DAP subjected to corrosion.

It should be noted that any one of the five floors in the DAP subjected to reinforcement corrosion results in almost identical results, e.g. see Figure VIII.9a ('DAP: B-1', 'DAP: B-3' and 'DAP: B-5'). This phenomenon can also be found in case of any two floors ('DAP: B-12', 'DAP: B-15' and 'DAP: B-24' in Figure VIII.9a), any three floors ('DAP: B-123', 'DAP: B-125' and 'DAP: B-245' in Figure VIII.9b), and four floors ('DAP: B-1234', 'DAP: B-1245' and 'DAP: B-2345' in Figure VIII.9b). Namely, every floor contributes almost evenly to the

reduction of the load-bearing capacity at a certain corrosion level. Note that 'DAP: B-XYZ' designates that the beams of the DAP in floor X, Y and Z are subjected to reinforcement corrosion.

VIII.6 Different column removal scenarios

The loss of a column of the ground floor is usually the critical case for a building structure. For the RC frame, different column loss scenarios may occur and are therefore investigated: loss of the ground column A (designated as 'Case A') and loss of ground column B (designated as 'Case B') as shown in Figure VIII.10. Note that the loss of ground column C (designated as 'Case C') has been analysed in previous sections. Static pushdown analyses are carried out for both Cases A and B. Uniformly downward loads are imposed on all the beams and displacement-controlled loading is adopted, where the controlled points are at the top of ground columns A and B for Cases A and B, respectively. The imposed load against the vertical displacement at the control point is recorded under different corrosion levels. Subsequently, the curves of ultimate load-bearing capacity (corresponding to first failure) vs. corrosion level are plotted in Figure VIII.11a for all the three column loss cases. Note that two situations are considered for every case, i.e. only the beams in the DAP (depending on different column loss cases) subjected to reinforcement corrosion, and the entire system subjected to reinforcement corrosion (in all beams and columns).

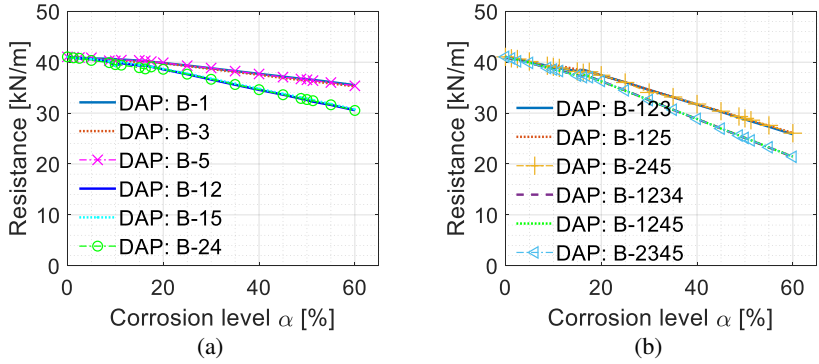

Figure VIII.9. Resistance vs. corrosion level: (a) any one or two floors in DAP subjected to reinforcement corrosion; and (b) any three or four floors in DAP subjected to reinforcement corrosion.

As shown in Figure VIII.11a, the curve of Case A (Case A – entire) is significantly lower than those of Cases B (Case B – entire) and C (Case C – entire). This attributes to that it is more difficult to redistribute the unbalanced force for an external column loss, i.e. less alternate load paths. The resistance vs. corrosion level

curves with regard to Cases B and C are almost identical, although slight deviation can be found when $\alpha < 15\%$. Moreover, as expected the responses from the situation only considering reinforcement corrosion in the DAP are identical to the corresponding results when all elements are subjected to corrosion for all the three column removal cases, e.g. curves 'Case A – entire' vs. 'Case A – DAP'. This confirms again that the load-bearing capacity of the deteriorated RC frame subjected to a column loss is mainly dominated by the reinforcement corrosion in the DAP. Note that the first failure always occurs at the beam ends in the DAP (Figure VIII.10).

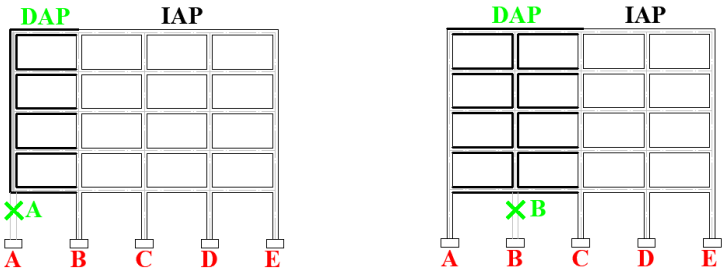

Figure VIII.10. Additional column removal scenarios: (a) loss of ground column A; and (b) loss of ground column B.

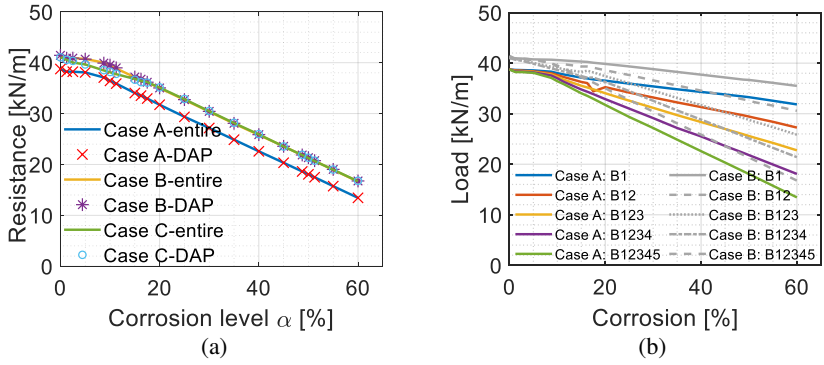

Figure VIII.11. Curves of resistance vs. corrosion level: (a) different column removal scenarios; and (b) different numbers of floor in DAP for Cases A and B.

The influence of different numbers of floor in the DAP subjected to reinforcement corrosion are also investigated for the Cases A and B, where five situations are taken into account, i.e. reinforcement corrosion in the first floor (B-1), the first two floors (B-12), the first three floors (B-123), the first four floors (B-1234), and all

five floors in DAP (B-12345). Only the results for Cases A and B are presented in Figure VIII.11b, as the results for Case C is similar to those of Case B. Again, more floors in DAP subjected to corrosion result in lower capacities. Case A is found to be more critical.

VIII.7 Influence of dynamic effects

VIII.7.1 Nonlinear dynamic analysis

Also incremental dynamic analysis (IDA) are performed to investigate the dynamic progressive collapse behaviour of the deteriorated RC frame. Rayleigh damping with damping ratio of 5% is adopted in all dynamic analyses (Tsai and Lin, 2008; Parisi and Scalvenzi, 2020; Liang *et al.*, 2021). To accurately determine the ultimate load-bearing capacity, a final load increment resolution of 0.1 kN/m is used.

The entire RC frame subjected to reinforcement corrosion (in all beams and columns) is investigated. The IDA are carried out for all the three column loss cases, i.e. the removals of column A, B and C. Moreover, an IDA is executed for each corrosion level with regard to each case. For instance, the time-history displacement responses when corrosion level α = 20% are presented in Figure VIII.12a,b for Cases A and C, respectively. The system oscillates around the equilibrium position and the oscillation decays due to damping effect after the sudden column removal. Moreover, the oscillation in Case A is irregular since the response or the redistribution mechanism for the unbalanced load is much more complex in case of an exterior column loss. Further, the peak values of the time-history displacement responses from IDA are collected to obtain the dynamic capacity curves (IDA curves).

The IDA curves with different corrosion levels obtained from the IDA are shown in Figure VIII.13a,b for Cases A and C, respectively. It can be seen that the ultimate load-bearing capacity and the ultimate displacement response decrease significantly with increasing corrosion levels from 0% to 60%. Note that the static load-displacement curves (i.e. pushdown curves) are also presented. The dynamic capacity curve (IDA) is significantly lower than the static capacity curve (pushdown) at a same corrosion level, which means the nonlinear static analysis overestimates the load-bearing capacity. Nonetheless, the maximum displacement in the IDA curve is almost identical to the displacement corresponding to the ultimate load-bearing capacity (corresponding to first failure) in the pushdown curve. Moreover, the failure mode of the dynamic analysis is similar to that in a static analysis at a same corrosion level.

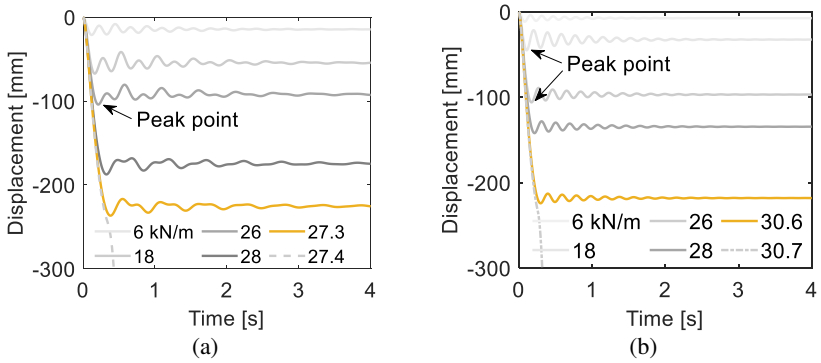

Figure VIII.12. Time-history displacement responses when α = 20%: (a) Case A; and (b) Case C.

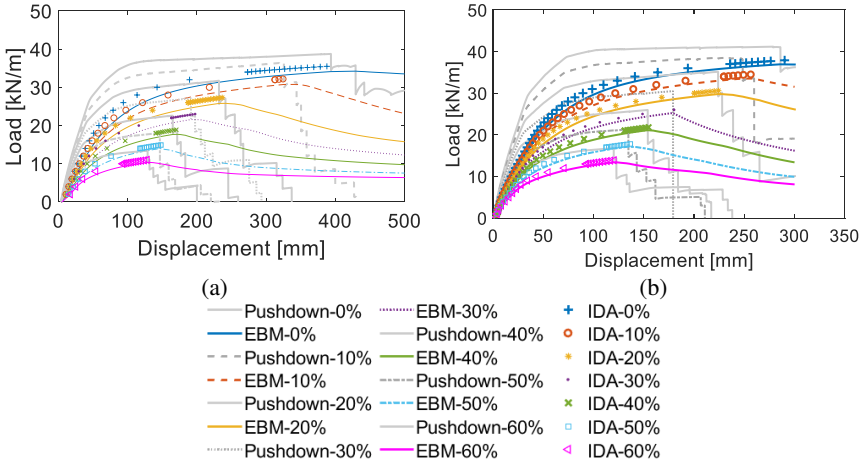

Figure VIII.13. Load - displacement relationship: (a) Case A; and (b) Case C.

Subsequently, the ultimate load-bearing capacities from the IDA are collected to plot the resistance vs. corrosion level curves for all the three cases. As expected, the curves from the IDA are markedly lower than the curves from the static pushdown analyses, as shown in Figure VIII.14a. Moreover, the exterior column removal case, i.e. Case A, is the most critical case since it has less alternate load paths. The curves of Cases B and C are almost identical. Almost a linear reduction tendency in relation to the ultimate load-bearing capacity curve can be observed with increasing corrosion level.

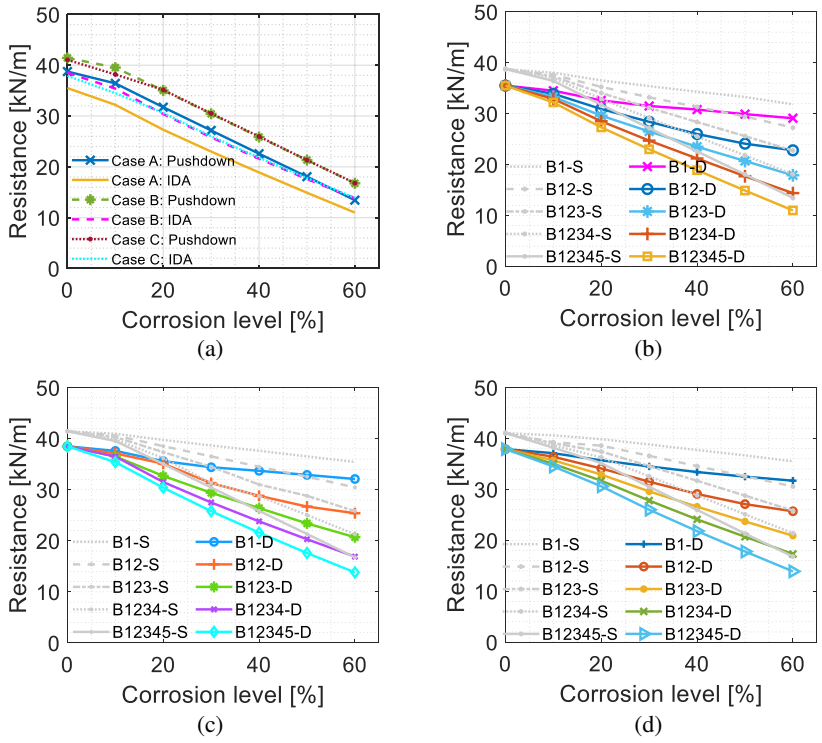

Figure VIII.14. Resistance vs. corrosion level: (a) all three cases; (b) Case A; (c) Case B; and (d) Case C.

Besides the entire RC frames subjected to corrosion, also the situation with different numbers of floor in the DAP subjected to reinforcement corrosion (only in beams) for Cases A, B and C are investigated and the results are presented in Figure VIII.14b,c,d, respectively. The following situations are presented here: only the first floor in the DAP subjected to reinforcement corrosion (B1), while 'B12', 'B123', 'B1234', and 'B12345' are respectively for the first two, three, four and five floors in the DAP subjected to corrosion. Moreover, 'S' means it is the static (pushdown) result, while 'D' indicates it is dynamic (IDA) result. Similarly to the static results, the dynamic resistances decrease significantly with larger numbers of floor in the DAP subjected to reinforcement corrosion.

Figure VIII.15a,b,c shows the percentages of the dynamic and static ultimate load-bearing capacities (R_α) with increasing corrosion level, relative to the corresponding values at $\alpha = 0\%$ (R_0) in Figure VIII.14b,c,d respectively, i.e. R_α/R_0. It can be seen that the dynamic resistances almost always decrease slightly faster

than the static capacities with increasing corrosion levels, resulting in larger dynamic amplification factors.

VIII.7.2 Energy-based method

Figure VIII.13a,b also shows the approximated dynamic capacity curves using the EBM based on the pushdown curves for Cases A and C (the entire RC frame subjected to reinforcement corrosion), respectively. It can be observed that the EBM curves are close to the IDA curves (EBM vs. IDA), which means the EBM can be used to approximately calculate the dynamic capacities also in case of reinforcement corrosion. The EBM curves are slightly lower, which means the EBM provides slightly conservative results. This is rational since dynamic effects, e.g. damping effect, cannot be taken into account in the EBM method but it is considered in the IDA. Note that the EBM curves are calculated up to the first peak (i.e. first failure) in the pushdown curve.

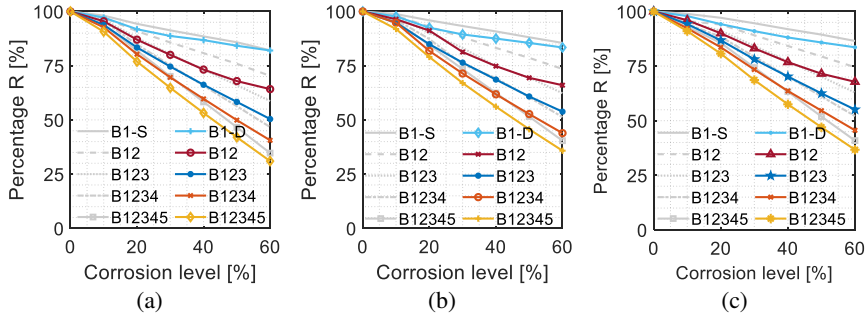

Figure VIII.15. Percentage of resistance vs. corrosion level: (a) Case A; (b) Case B; and (c) Case C.

The ultimate load-bearing capacities at different reinforcement corrosion levels for both EBM and IDA results (see Figure VIII.13a,b respectively for Cases A and C) are collected for all the three column loss cases. The collected ultimate load-bearing capacities are adopted to plot the resistance vs. corrosion level curves, as shown in Figure VIII.16. It can be observed that the results of EBM agree well with the IDA results, where the coefficients of determination R^2 are 0.98, 0.99 and 0.99 for Cases A, B and C respectively. Hence, the EBM has a good performance to approximate the dynamic ultimate load-bearing capacities under different corrosion levels.

VIII.8 Discussion and conclusions

In this chapter the progressive collapse performance of deteriorated RC frames subjected to column removal scenarios has been analysed in both static and dynamic situations, particularly with respect to the influences of different models

for the effect of reinforcement corrosion on the deterioriation of reinforcement and concrete mechanical properties, different corrosion locations, and different column removal scenarios. Both static and dynamic progressive collapse resistances of the deteriorated RC frame were found to significantly decrease with increasing corrosion level. Moreover, the EBM was employed to approximate the maximum dynamic response and a good performance was observed also for these situations.

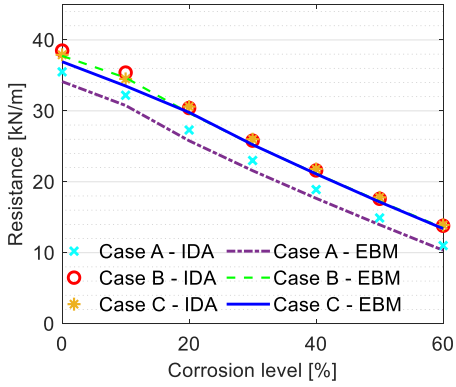

Figure VIII.16. Comparison between EBM and IDA.

The reinforcement corrosion was found to be the predominant cause of the deterioration of the progressive collapse performance with increasing corrosion level, while the effect of concrete deterioration had limited influence. Different deterioration models in relation to the steel ultimate strain gave different results and failure modes. The linear reduction models (Model 2 and Model 3) may give very conservative results, as the ultimate steel strain can reduce to the steel yield strain.

It was found that the reinforcement corrosion in the beams in DAP controlled the structural performance for all the three column loss cases. The reinforcement corrosion in other locations had little influence. As the shear failure could not be captured in the FE model, the shear capacities of both beams and columns were calculated according to the empirical equations proposed in literature. Comparing to the calculated shear capacities, the shear forces in both beams and columns were found to be smaller. This indicated that no shear failure occurred in the models for the cases under investigation, as the flexural failure occurred earlier in the beams. However, the shear failure in columns may occur if the columns are designed with a limited amount of shear reinforcement and/or subjected to severe shear reinforcement corrosion. This requires to be further studied.

Moreover, more floors in the DAP subjected to reinforcement corrosion resulted in significantly lower progressive collapse resistances. The progressive collapse resistances obtained by dynamic analyses were significantly lower than the static resistances. Moreover, the dynamic resistances were found to decrease slightly faster than those from static analyses with increasing corrosion level.

It must be emphasized that the obtained results are on the basis of some assumptions, e.g. uniform corrosion was assumed but pitting corrosion may be more realistic in real RC structures and the bond behaviour between reinforcing bars and concrete was not taken into account. Moreover, the shear failure mechanism in columns should be further investigated. Nevertheless, the above investigations provide a first stepping stone towards the further investigation of progressive collapse in case of degrading concrete structures.

VIII.9 References

Almusallam AA (2001) Effect of degree of corrosion on the properties of reinforcing steel bars. Construction and Building Materials 15:361-368.

Apostolopoulos CA, Papadakis VG (2008) Consequences of steel corrosion on the ductility properties of reinforcement bar. Construction and Building Materials 22:2316-2324.

Biondini F, Frangopol DM (2017) Time-variant redundancy and failure times of deteriorating concrete structures considering multiple limit states. Structure and Infrastructure Engineering 13:94-106.

Biondini F, Vergani M (2014) Deteriorating beam finite element for nonlinear analysis of concrete structures under corrosion. Structure and Infrastructure Engineering 11:519-532.

Botte W, Caspeele R, Taerwe L (2016) Membrane behavior in RC slabs subjected to simulated reinforcement corrosion. Engineering Structures 123:45-58.

Botte W, Vereecken E, Taerwe L, et al. (2021) Assessment of posttensioned concrete beams from the 1940s: Large-scale load testing, numerical analysis and Bayesian assessment of prestressing losses. Structural Concrete 22:1500-1522.

Cairns J, Millard S (1999) Reinforcement corrosion and its effect on residual strength of concrete structures. Proc 8th Int Conf on Structural Faults and Repair.

Cairns J, Plizzari GA, Du YG, et al. (2005) Mechanical properties of corrosion-damaged reinforcement. ACI Materials Journal 102:256-264.

Castel A, François R, Arliguie G (2000) Mechanical behaviour of corroded reinforced concrete beams—Part 2: Bond and notch effects. Materials and structures 33:545-551.

Cavaco ES, Neves LAC, Casas JR (2018) On the robustness to corrosion in the life cycle assessment of an existing reinforced concrete bridge. Structure and Infrastructure Engineering 14:137-150.
CEN (2004) Eurocode 2: Design of concrete structures—Part 1-1: General rules and rules for buildings. EN 1992-1-1.
Coronelli D, Gambarova P (2004) Structural assessment of corroded reinforced concrete beams: Modeling guidelines. Journal of Structural Engineering 130:1214-1224.
Droogné D, Botte W, Caspeele R (2018) A multilevel calculation scheme for risk-based robustness quantification of reinforced concrete frames. Engineering Structures 160:56-70.
Du YG, Clark LA, Chan AHC (2005a) Effect of corrosion on ductility of reinforcing bars. Magazine of Concrete Research 57:407-419.
Du YG, Clark LA, Chan AHC (2005b) Residual capacity of corroded reinforcing bars. Magazine of Concrete Research 57:135-147.
El-Sayed AK, Hussain RR, Shuraim AB (2016) Influence of stirrup corrosion on shear strength of reinforced concrete slender beams. ACI Structural Journal 113:1223-1232.
Feng DC, Xie SC, Li Y, et al. (2021) Time-dependent reliability-based redundancy assessment of deteriorated RC structures against progressive collapse considering corrosion effect. Structural safety 89:102061.
fib (2013) Model code for concrete structures 2010.
JCSS (2001) Probabilistic model code. Joint Committee on Structural Safety.
Liang CF, Xiao JZ, Wang YF, et al. (2021) Relationship between internal viscous damping and stiffness of concrete material and structure. Structural Concrete 22:1410-1428.
Ou Y-C, Chen H-H (2014) Cyclic behavior of reinforced concrete beams with corroded transverse steel reinforcement. Journal of Structural Engineering 140:04014050.
Parisi F, Scalvenzi M (2020) Progressive collapse assessment of gravity-load designed European RC buildings under multi-column loss scenarios. Engineering Structures 209:110001.
Park R, Priestley MJN, Gill WD (1982) Ductility of square-confined concrete columns. Journal of the structural division 108:929-950.
Scott B, Park R, Priestley M (1982) Stress-strain behavior of concrete confined by overlapping hoops at low and high strain rates. ACI Journal:13-27.
Stewart MG, Suo QH (2009) Extent of spatially variable corrosion damage as an indicator of strength and time-dependent reliability of RC beams. Engineering Structures 31:198-207.
Tsai MH, Lin BH (2008) Investigation of progressive collapse resistance and inelastic response for an earthquake-resistant RC building subjected to column failure. Engineering Structures 30:3619-3628.

Vereecken E, Botte W, Lombaert G, et al. (2020a) Bayesian decision analysis for the optimization of inspection and repair of spatially degrading concrete structures. Engineering Structures 220:111028.
Vereecken E, Botte W, Lombaert G, et al. (2020b) A Bayesian inference approach for the updating of spatially distributed corrosion model parameters based on heterogeneous measurement data. Structure and Infrastructure Engineering:1-17.
Vereecken E, Botte W, Lombaert G, et al. (2021) VoI-based optimization of structural assessment for spatially degrading RC structures. Applied Sciences-Basel 11:4994.
Vu NS, Li B (2018a) Seismic performance assessment of corroded reinforced concrete short columns. Journal of Structural Engineering 144:04018018.
Vu NS, Li B (2018b) Seismic performance of flexural reinforced concrete columns with corroded reinforcement. ACI Structural Journal 115:1253-1266.
Xu J-G, Feng D-C, Wu G, et al. (2020) Analytical modeling of corroded RC columns considering flexure-shear interaction for seismic performance assessment. Bulletin of Earthquake Engineering 18:2165-2190.
Yu L, François R, Dang VH, et al. (2015) Structural performance of RC beams damaged by natural corrosion under sustained loading in a chloride environment. Engineering Structures 96:30-40.
Yu XH, Qian K, Lu DG, et al. (2017) Progressive collapse behavior of aging reinforced concrete structures considering corrosion effects. Journal of Performance of Constructed Facilities 31:04017009.
Zhu W, François R (2013) Effect of corrosion pattern on the ductility of tensile reinforcement extracted from a 26-year-old corroded beam. Advances in concrete construction 1:121.

CHAPTER IX

General conclusions and recommendations

IX.1 Introduction

In this final chapter, the major findings of this PhD dissertation are summarized and recommendations with respect to practical applications of the investigated subjects are given. Finally, also some topics for further research are suggested and discussed.

IX.2 The performance of the energy-based method

IX.2.1 Evaluation of the performance of the energy-based method in a deterministic way

The threat-independent alternate load path method is widely used to perform numerical analyses in the context of progressive collapse or disproportional collapse. In such analyses, dynamic effects are required to be considered. However, the dynamic effects cannot be considered in the nonlinear static analysis approach and a dynamic amplification factor is required to consider the dynamic effects. The nonlinear dynamic analysis can give a more accurate response but the computational demand may be huge, especially in relation to structural stochastic analyses. The energy-based method (EBM) is able to approximately calculate the maximum dynamic responses on the basis of the principle of energy conservation, in which no nonlinear dynamic analyses and dynamic amplification factors are required. In general, the EBM is adopted after load-displacement results are obtained from the nonlinear static analysis. However, energy dissipated by the dynamic effects are not considered in the EBM. Consequently, the EBM always provides approximate (and conservative) results. In addition, the calculation time for the EBM is almost identical to that of the associated static pushdown analysis, which may be significantly less than that for direct dynamic analyses.

The simple energy-based method (EBM) is a promising approach to obtain an approximate evaluation of the maximum dynamic responses. The performance of the EBM has been evaluated in this dissertation. The dynamic effects that cannot be considered in the EBM are strain rate effects, damping effects, and column removal durations. Furthermore, the structure subjected to a column removal scenario is assumed to oscillate in a single deformation mode.

Comparing the results from the EBM to the results from the direct dynamic analysis, the effectiveness of the EBM has been proven. If no dynamic effects such as strain rate effects, damping or column removal durations are considered in the direct dynamic analysis, almost identical load-displacement capacity curves were obtained between the EBM and the direct dynamic analysis. Note that the EBM inherently cannot account for the dynamic effects, as the EBM results completely depend on results of the nonlinear static analysis. In this situation, the EBM is able to accurately predict the maximum dynamic responses since dynamic effects are

not considered in both approaches. The EBM approach also performs well in the highly nonlinear response stage or at severe damage states of the RC structures. For example, the EBM was still observed to work well after the rupture of one layer of the reinforcement in the RC slab investigated in this dissertation, as well as in the tensile membrane action stage (or large deformation state).

However, a deviation between EBM and the direct dynamic analysis can be observed when dynamic effects are considered in the dynamic analysis. Nonetheless, the deviation is not significant and can be considered acceptable for progressive collapse analyses. The strain rate dependency effects in large strain rate situations may influence material properties of RC structures and this may subsequently affect their responses. The strain energy storage capacities of a system for a given displacement in static and dynamic situations are different. In a small deformation situation (or flexural stage), overall the strain rate effects with regard to both the reinforcement and the concrete materials have been found to have limited influence on the dynamic response in sudden support removal scenarios. This can be attributed to the occurring strain rates of most finite elements being in general small and only localized elements experience large strain rates for a short duration. In this case, a good performance of the EBM was found, as the strain rate effects (which cannot be considered in the EBM) have little influence on the dynamic responses. In a large deformation situation (e.g. tensile membrane action stage), a slight influence from the strain rate effects has been observed, as a higher loading level resulted in a higher strain rate. Moreover, the influence of the strain rate effect of reinforcement was found to be slightly more significant than that of concrete, since the resistance in tensile membrane action stage is heavily influenced by the capacity of the reinforcing steel (i.e. tensile force in reinforcing bars). Overall, the influence of the strain rate effects was found to remain limited and hence the EBM can be considered to give a reasonably accurate prediction of the maximum dynamic response.

The damping effects are usually introduced in the dynamic analysis to reflect the energy dissipation. In the elastic stage, the influence of damping effects on the dynamic responses has been found to be insignificant and a good agreement between the EBM and the direct dynamic analysis was obtained. For larger deformations, the influence of damping effects are larger, as large damage in the RC structures occurs. A more significant influence on the dynamic response under a high load and large damping ratio was observed, since the energy dissipation by the damping is not accounted for in the EBM.

It is still a controversial issue how to model the damping mechanism for a sudden column removal scenario, e.g. viscous damping or Coulomb damping. Rayleigh damping mechanism (i.e. viscous damping) is more often used. The Rayleigh damping matrix is assumed to be proportional to the mass matrix and stiffness

matrix of the RC structures. Identified drawbacks associated with the use of Rayleigh damping based on initial stiffness have been found in literature, as well as in this dissertation. The stiffness matrix of a structural system will change in the inelastic stage. The assumption that the damping matrix is proportional to the initial stiffness matrix (the stiffness matrix and/or the associated coefficients are not updated in each step) may introduce unwanted artificial damping forces in the RC structural systems. This will overestimate the influence of the damping effects. Moreover, the reinforcement in the RC structures are usually subjected to strong tensile forces in tensile membrane action stage. This may significantly improve the stiffness of the RC structures and results in unwanted damping forces. On the other hand, this issue can be avoided or mitigated if the stiffness matrix in the damping matrix is updated accordingly for both the stiffness matrix and the associated coefficients. This is because the unwanted artificial damping forces are mitigated. In this case, a good performance was found for the EBM, in comparison with the direct dynamic analysis. Neglecting damping will always lead to a conservative estimation of the load-bearing capacities and the associated displacements by the simplified EBM calculations.

With regard to the modelling of sudden column removal scenarios in the context of progressive collapse or disproportional collapse, the guideline of the DoD stipulates that the removal duration must be less than one tenth of the first natural period (usually in the vertical direction). Different column removal durations may result in different responses. In general a more abrupt removal (shorter removal duration) could result in a larger peak displacement in the direct dynamic analysis. Moreover, the peak response is reached later. If the recommendation by the DoD (i.e. the removal duration must be less than one tenth of the first natural period in the dynamic analysis) is followed, cases with such short support removal time were found to still be accurately predicted by the EBM.

The EBM assumes that a structure subjected to a column removal scenario deforms in a single deformation mode. An exterior column removal scenario proves to affect the performance of the EBM, since its dynamic response may not be represented accurately by a single deformation mode according to the responses in the frequency domain. On the other hand, the response of a RC structure subjected to an interior column removal scenario usually behaves in a single deformation mode, for which the EBM overall has a very good performance. Hence, a better performance for the EBM could be observed for an interior column loss case than for an exterior column loss case.

IX.2.2 Evaluation of the performance of the energy-based method in a probabilistic way

When designing a structure with respect to robustness, it must also be taken into consideration that progressive collapses caused by extreme events are low-

probability high-consequence phenomena. In order to be able to accurately predict the structural response, it is important to study the progressive collapse behaviour using a probabilistic approach, as it has been found that there is a significant influence of many uncertainties, e.g. randomness from material properties, on the structural behaviour. Moreover, with regard to the three widely used approaches in relation to the quantification of the structural robustness, i.e. the deterministic-based method, the probabilistic or reliability-based method and the risk-based method, both the reliability-based method and the risk-based method require to perform a reliability analysis.

The EBM approach is a compromise between accuracy and complexity. An approximate result is obtained using the EBM in the context of RC building structures subjected to sudden column removal scenarios. Considering it is an approximate approach, it is therefore important to quantitatively assess the performance of the EBM, i.e. quantifying its model uncertainty through comparison to the more accurate direct dynamic analysis results. Moreover, the quantitative assessment of the model uncertainty associated to the EBM becomes important when the EBM is applied to quantify the reliability or robustness of a RC building structure following a sudden column removal scenario. To date there are insufficient experimental results to allow for a direct quantification of the EBM accuracy from experimental data. Therefore, the EBM accuracy can reasonably only be determined through comparison against nonlinear dynamic analyses and that has as such been investigated in this dissertation.

Comparing the results of EBM to the results of direct dynamic analyses, the model uncertainty of EBM has been calculated. Currently, two numerical examples have been investigated: one RC flat slab and one RC planner frame. For both numerical examples, a lognormal distribution was able to represent the model uncertainty well. The values of the model uncertainties associated with the resistances have been found to be close to unity and to have small standard deviations. This indicates that the EBM has a good accuracy in calculating the dynamic resistances. On the other hand, a slightly worse performance has been found for the EBM in relation to the computation of the corresponding displacements, as the mean values were slightly larger than one and the standard deviations were much larger.

IX.2.2.1 Numerical example A: the RC slab

For the one-way RC slab, the model uncertainty of the loads at the first load peaks (capacity at rupture of top layer reinforcement) obtained through the EBM compared to direct dynamic analysis has been found to be represented well by a lognormal distribution with mean of 0.95 and a standard deviation of 0.20, i.e. LN(0.95,0.20). With regard to the ultimate load-bearing capacities (regardless of whether this is occurring as a result of a post-peak behaviour associated with larger displacements and a complex stress redistribution), a lognormal distribution

LN(0.96,0.13) has been obtained. In terms of the model uncertainty for the loads of the second load peaks (i.e. final failure moment where both top and bottom layer reinforcement failed), a lognormal distribution LN(0.98, 0.13) has been found to fit the histogram.

When comparing the associated displacements, the model uncertainty for displacements at the first load peaks has been found to be represented well by a lognormal distribution with mean of 1.02 and a standard deviation of 0.38, while for the displacements at the ultimate load-bearing capacities, a lognormal distribution LN(1.00,0.15) has been found to be appropriate. With regard to the model uncertainty for the displacements of the second load peaks, a lognormal distribution LN(1.03,0.13) has been found to fit the histogram for the displacements.

IX.2.2.2 Numerical example B: the RC frame

In terms of the RC frame, three column removal cases has been investigated: one exterior column removal scenario, one penultimate column removal scenario, and one middle column removal scenario. Note that in the exterior column loss case the assumption of a single deformation model was not satisfied.

Probabilistic models have been proposed for the model uncertainty of EBM compared to IDA. For the three different removal scenarios considered together, a lognormal distribution with mean of 0.98 and a standard deviation of 0.02, i.e. LN(0.98,0.02), has been fitted for the resistances, while a lognormal distribution LN(1.07,0.08) has been obtained for the displacements.

IX.3 Different numerical modelling techniques in relation to the simulation of progressive collapse

The computational demand of numerical calculations sometimes are high, and an appropriate choice of modelling technique will mitigate this adverse issue. Usually, three kinds of numerical modelling techniques in relation to the modelling of RC structures subjected to column loss scenarios have been reported: the micro-based FE model, the macro-based FE model, and the hybrid FE model. The micro-based FE model (e.g. solid elements) and the macro-based FE model (e.g. beam elements and macro-based joints) are more often used. With the micro-based FE model, localized damage (e.g. concrete cracks) can be simulated adequately and detailed responses can be accurately reflected. However, the computation demand is very heavy, as a large number of solid elements are usually included in the FE model. Therefore, this approach is more suitable for the simulation of sub-structures, such as RC beam-column assemblies and RC slabs. On the other hand, much less elements are required in a macro-based FE model and the computational demand can be significantly reduced. Moreover, both local and global responses can be well

captured in case of RC building structures subjected to column removal scenarios. This means it has a great advantage in modelling entire RC structural systems. The application of a macro-based FE modelling technique is a good compromise between accuracy and computational efficiency. In order to reduce the computational demand, also the use of a hybrid FE modelling technique was investigated in relation to progressive collapse analyses. For example, a RC frame can be divided into a directly affected part and an indirectly affected part. The directly affected part, i.e. the bays immediately above the removed column, can be modelled with detailed FE models to take the nonlinearities into account, as large deformations are expected. The indirectly affected part is the remaining part of the frame, which can be modelled with a simple model with much less calculation demand, e.g. an empirical or analytical model.

IX.4 Quantification of structural robustness for RC structures

Comparing to the deterministic-based method, the reliability-based method can take the influence of uncertainties from both materials and loads into account. On the other hand, the reliability-based method is more objective than the risk-based method. Therefore, it is widely used in the structural robustness quantification cases. However, the risk-based method is more comprehensive as both the occurrence probability of the accidental events (and the probability of structural collapse) and the associated consequences are considered. Normally, the reliability-based method and the risk-based method have a high computational demand for RC building structures subjected to sudden column loss scenarios, as both nonlinearities and dynamic effects are involved.

As an alternative to the current way to consider dynamic effects using direct dynamic analyses in the context of structural robustness quantification for RC building structures subjected to sudden column loss scenarios, an EBM-based robustness or redundancy quantification approach was adopted. In this new proposed framework, the EBM method is adopted to replace the conventional direct dynamic analysis in order to reduce the computational effort. Comparing to the results from the traditional approach, a good performance of the EBM-based robustness or redundancy robustness calculation has been found, when in particular the proposed model uncertainty models are incorporated. The EBM-based robustness or redundancy robustness quantification approach requires less computational demand and proves to be a good option for structural robustness quantification when dynamic effects are to be considered.

The multilevel calculation scheme in combination with the risk-based robustness quantification approach for the structural robustness quantification of RC building structures subjected to sudden column removal scenarios is able to further reduce the computational demand. In this approach, a structural system is divided into a directly affected part and an indirectly affected part. The calculations on different

parts can be performed independently (as a hybrid model), i.e. with a detailed FE model for the directly affected part and for example an analytical model for the indirectly affected part. Hence, the robustness quantification is carried out at different levels of structural idealization in order to reduce the computational effort. Further, the directly affected part of a multi-storey RC frame is simplified as an equivalent directly affected part model in which only one floor is modelled. For the multi-storey RC frame, the average values of the stiffness from all the floors can be adopted as boundary condition (including both translational and rotational springs), which proved to result in an overall good performance. The boundary conditions can be determined through a nonlinear static analysis. Thereafter, the equivalent directly affected part model can be applied to replace the entire system model in dynamic analyses to reduce the calculating effort.

Comparing to the results from static analyses, the structural robustness indices from dynamic analyses have been found to be significantly smaller. Hence, it is concluded it is of paramount importance to include dynamic effects when assessing the performance of a structure subjected to progressive collapse.

IX.5 Progressive collapse behaviour of deteriorated RC building structures

The reinforcement corrosion in existing RC building structures can significantly reduce the performance of the structure. Reinforcement corrosion is the predominant cause of the deterioration of the progressive collapse performance, while the effect of concrete deterioration appears to have limited influence. To model the reinforcement corrosion effects, different models have been proposed. Moreover, different deterioration models in relation to the steel ultimate strain showed different results and failure modes. Hence, it appears important to pay more attention in future research to the selection of suitable deterioration models.

Reinforcement corrosion in the beams in DAP appears to dominate the structural performance. Moreover, when more floors in the DAP are subjected to reinforcement corrosion this results in a significantly lower progressive collapse resistance. The progressive collapse resistances obtained by dynamic analyses are significantly lower than the static resistances. Moreover, the dynamic resistances are found to decrease slightly faster with increasing corrosion level than those from static analyses.

IX.6 Recommendations for further research

IX.6.1 Performance of the energy-based method

The EBM is a promising approach to predict maximum dynamic responses with regard to RC buildings subjected to sudden column removal scenarios. However,

further evaluation of the performance of the EBM is still necessary. To evaluate the performance of the EBM, experimental tests are of particular importance as consistent validation in this regard is currently missing in literature. However, such kind of experimental tests have been rarely reported due to the huge cost associated to them. The experimental data can then be adopted to quantify the model uncertainty encompassing the numerical model uncertainty. The experimental test can also be used to investigate the damping mechanism in relation to RC structures subjected to sudden column removal scenarios, for which there also appears to be a lack of consistent data available in literature.

IX.6.2 Numerical modelling technique

The macro-based modelling technique requires less calculation demand. Therefore, it has a great advantage in the simulation of RC building structures subjected to column removal scenarios, especially in relation to probabilistic calculations. However, some empirical simplifications have been adopted. For example, the confinement effect for the core concrete provided by the transverse shear reinforcement and the bond-slip behaviour between concrete and reinforcement are considered by some empirical equations. Moreover, the shear failure of the structural members cannot be detected automatically through the fibre model and require to be checked separately. Therefore, further developments of the model in relation to those aspects is suggested.

The hybrid modelling technique is also an efficient way to reduce the computational effort. However, the accurate determination of boundary conditions for the DAP and the performance of the models in large deformation stages should be further refined and investigated. In particular also their adequacy in case of situations where degradation occurs is to be further investigated.

IX.6.3 Structural robustness

Although numerous investigations have been carried out in the field of structural robustness quantification, the observations and results here have again highlighted that some important issues and topics remain to be investigated in the future. A universally accepted framework to quantify the structural robustness of a design is still missing in currently available design codes and guidelines. For example, in the present thesis reliability-based robustness indices and the risk-based robustness indices were calculated, but quite different values for the structural robustness indices were obtained. Moreover, no target values for these indices are available. The structural robustness indices can only be used to a comparison purpose among different cases. Hence, the development of a codifiable reference framework would be advisable.

Further studies in relation to the structural robustness assessment of existing RC

structures are required. In this case, uncertainties from different sources may have a more significant influence on the structural robustness. Moreover, pitting corrosion is very common in existing RC structures and the influence on the overall progressive collapse mechanisms is to be further investigated.

Graphical schematization of structural systems.